

**UNIVERSITÀ DEGLI STUDI DI NAPOLI
FEDERICO II**



Dottorato di Ricerca in
INGEGNERIA DELLE COSTRUZIONI

22° CICLO

**HOMOGENIZATION TECHNIQUES
FOR POROUS SOLIDS**

GIANPAOLO PERRELLA

TABLE OF CONTENTS

INTRODUCTION

I. REMARKS ON THE THEORY OF ELASTICITY

1. Deformation Theory	1
1.1. Deformation in \mathbb{R}^3	1
1.2. Volume element in deformation configuration	6
1.3. The Piola transform; area element in the deformed configuration	7
1.4. Length element in the deformed configuration; Strain Tensor	10
2. The Equation of Equilibrium	16
2.1. Applied Forces	17
2.2. The stress principle of Euler and Cauchy	19
2.3. Cauchy's theorem; The Cauchy stress tensor	21
2.4. The equation of equilibrium and the principle of virtual work in the deformed configuration	23
2.5. The Piola-Kirchhoff stress tensor	24
2.6. The equation of equilibrium and the principle of virtual work in the reference configuration	26
3. Linear Anisotropic Elastic Media	29
3.1. Elastic Stiffnesses	30
3.2. Elastic Compliances	32
3.3. Contracted Notations	33
3.4. Material Symmetry	35
3.5. The Elasticity Tensor for Materials with Symmetry Planes	37
3.6. Restrictions on Elastic Constants	41

II. HETEROGENEOUS MATERIALS

1. Inhomogeneous solids: SAS/DAS theorems	43
1.1. Stress Associated Solution (SAS) Theorem for inhomogeneous Elasticity	43
1.1.a. Zero- eigenvalue stress and zero-eigenvalue strain fields	44
1.1.b. Stress Associated Solutions (SAS) Theorem	45
1.2. Generalization of the SAS theorem to piecewise defined inhomogeneities	50
1.2.a. Composite materials where φ is constant, but piecewise discontinuous	51
1.2.b. Composite materials where φ is piecewise continuous	53
1.3. Displacement Associated Solutions (DAS) Theorem for inhomogeneous elasticity	55

2. Anisotropic media: volume fraction and Fabric Tensors	63
2.1. Mean Intercept Length (MIL) Tensor	63
2.2. Orientation Distribution Function (ODF)	64
2.3. Fabric Tensor and Damage Distribution	67
2.4. Relationship between Fabric Tensor and Elasticity Tensor	72

III. THEORY OF HOMOGENIZATION

1. Thermodynamic framework and mathematically well-posed homogenization approaches	80
1.1. Representative Volume Element (RVE)	80
1.2. Localization Problem	81
1.3. The Hill-Mandel principle of macrohomogeneity	83
1.4. Example of pure elasticity	83
1.4.a. The localization problem	83
1.4.b. Case where \mathbf{E} is prescribed	84
1.4.c. Case where Σ is prescribed	85
1.4.d. Equivalence between ‘prescribed stress’ and ‘prescribed strain’	87
2. Composite heterogeneous materials: derivation of compliance and stiffness tensors	87
2.1. Direct Methods – Eshelby solution	88
2.2. Variational Methods – Hashin Shtrikman Variational Principle	92
3. Micro mechanics of porous materials: J-tensor and dilute distribution of voids cases	99
3.1. Average strain for prescribed macrostress	101
3.2. Overall compliance tensor for porous elastic solids	103
3.3. Average stress for prescribed macrostrain	105
3.4. Overall elasticity tensor for porous elastic solids	107

IV. ISOTROPIC AND CUBIC POROUS MEDIA

1. Evaluation of the elastic moduli for poroelastic solids: Randomly Arranged Microstructure.	110
2. Elastic moduli penalization law for Cubic/Isotropic porous Media	110
2.1. Finite Element Analyses	113
2.1.a. Geometry and Mesh	113
2.1.b. Boundary Conditions and Implementation	115
2.1.c. Model’s Accuracy	116
2.1.d. Cavities of Different Shapes	116
2.1.e. Homogenized Elastic Constants	117
2.1.f. Cavity’s Shape Influence	121
2.1.g. Algebraic Formulation	123

V. ORTHOTROPIC POROUS MEDIA

1. Micromechanical Approach to Inhomogeneous and Anisotropic Materials	131
1.1. Second Order Fabric Tensor	132
2. Compliance Penalization Law for Orthotropic Porous Media	134
2.1. Finite Element Analyses	134
2.1.a. Geometry and Mesh	134
2.1.b. Boundary Conditions and Implementation	135
2.1.c. Model's Accuracy	135
2.1.d. Homogenized Compliance Constants	136
2.1.e. Fitting Zisset Parameters	138

VI. TRANSVERSELY ISOTROPIC MEDIA

1. Homogenized Behaviour of Fibre Composite	142
1.1. Composite Cylinder Model	142
1.1.a. Uniaxial Modulus	144
1.1.b. Other Properties	144
1.1.c. A Model for the Transvers Shear of a Fibre System	145
1.2. Finite Length Fiber Effects	145
2. Design in Composite Materila	147
2.1. Materials: Fibers and Matrix	149
2.2. Chiralty in trigonal material	152
2.2.a. Chiral Materials and Locally Chiral Components in Globally Non-chiral Composites	154
2.3. Trigonal effects in Reinforcing Fibres	155
2.3.a. Numerical model	158
2.4. Axial-twisting effects on composite materials	175

APPENDIX

A.1. FE Test Boundary Conditions	180
A.1.1. Displacement FE Test Conditions	180
A.1.2. Traction FE Test Conditions	181
A.2. Elastic Constant Calculation	182
A.2.1. Voigt Calculation	183
A.2.2. Reuss Calculation	183
A.2.3. Isotropic Constants Unification	185

REFERNECES

INTRODUCTION

Motivated by a growing interest in material science and engineering, micromechanics and physical properties of heterogeneous materials have been intensely studied in the last decades.

Nature as well as synthetic materials offer a large number of examples of heterogeneous media. For example, if observed at different scale levels, many biological tissues exhibit a hierarchical microstructure whose architectural elements are constituted by collagen fibres, contractile elements, filaments and cell units, differently arranged to form structural networks aimed to guarantee optimal mechanical performances with respect to specific functions. On the other hand, synthetic materials such as composites, polymers, foams and porous media have been recently developed for applications in civil, mechanical and aerospace engineering fields, and special attention of the industry has been also registered for the manufacturing processes, design strategies and optimization techniques employed to create high-performance man-made material products.

From a mechanical standpoint, in order to derive macroscopic effective physical properties of heterogeneous materials from their microstructure, two main continuum theory-based approaches may be adopted: statistical and deterministic. Both engage averaging techniques and require the choice of the Representative Volume Element (RVE), that is the smallest statistically homogeneous material volume to which macroscopic constitutive relationships must be referred.

The statistical approach correlates the microstructure of the materials to their overall physical properties by introducing the statistical n -points probability function, that provides a mathematical representation of distribution and morphology of phases in heterogeneous materials. It is possible to show that the lowest order (one-point) probability function represents the volume fraction of the constituents, higher order probability functions being instead devoted to capture morphology features. Although a statistical approach may be successfully used for predicting physical properties of heterogeneous materials as well as in material design and processing optimization problems, the construction of reliable probability functions strongly depends on the possibility of exploring the material microstructure in detail. This entails to process a large amount of information, sometimes leading to overwhelming computational costs and intolerable calculation times.

The deterministic approach is instead based on a continuum theory where the micro-structural properties are incorporated in prescribed architectural variables, whose choice is generally suggested by analytical results or based on engineering assumptions that invoke phenomenological or heuristic arguments. Furthermore, in order to obey to some thermodynamic restrictions, these variables are usually introduced in the form of scalars or even-order tensors. Obviously, physically consistent and mathematically well-posed models constitute the premise for a good engineering analysis, but do not exhaust the subject of their practical applicability to real problems. In this sense, difficulties in the actual measurability of tensor variables representing the RVE architecture, unshared definitions of some morphological features and ambiguous geometrical interpretations of the RVE microstructure contribute to limit the applications of the deterministic approach.

In particular, in the framework of the mechanics of heterogeneous materials, great attention has been and is still reserved to *depleted media*, due to the fact that models based on them well interpret many different biological and man-made material behaviours.

Depleted media are materials whose overall stiffness and strength are reduced as a consequence of the presence of cavities in the solid matrix.

Two limit structural configurations can be identified in depleted matter. The first is characterized by the high density regions and can be visualized by means of a solid cube containing $n \in \mathbb{N}$ voids that do not touch one another or the surface. Examples are often met by studying some porous materials, damage or elastic solids weakened by non interacting penny-shaped micro-cracks. Complementarily, the second limit configuration is represented by material regions at lower density, where a structural ordered or randomly-arranged network of thin elements constituted by beams and plates generally is exhibited at the micro-scale level. Typical examples of this situation is offered by trabecular bone tissues, honeycomb materials or truss structures.

Overall mechanical properties of depleted media depend on the elasticity and strength of the solid matrix and upon some selected architectural variables inferred from the RVE micro-structural features.

From the experimental point of view, these features can be revealed by either destructive or non-destructive tests, making reference to direct surface observations (optical microscopy, scanning, atomic force electron microscopy, strain gauges, photo-elastic methods and interferometry techniques), direct three-dimensional

observations (X-ray radiography, dye penetrants, infrared techniques, ultrasounds, thermal wave imaging, MRI diffusivity, etc.) and indirect methods, based on compliance measurements.

From the mathematical standpoint, the architectural variables are usually established by making use of the theory of homogenization or by invoking micromechanical approaches that exploit heuristic and phenomenological arguments. Also, as already said above, to these variables is requested of obeying to some mechanical principles, so that they appear as mathematical objects in the form of scalars or even-order tensors.

A physical-geometrical interpretation of the architecture variables related to mechanical properties of depleted media allows to classify them by means of three main RVE microstructure features, namely *topology*, *density*, and *orientation*.

Topology

RVE topology refers about the micro-structural architecture of the material through two topological properties: *connection* and *integrity*.

Connection reveals the “skeleton” of the RVE solid matrix and then constitutes a measure of the amount of internal links which virtually form a dormant network, directly responsible of the effective stiffness and strength of the material. A scalar measure of connectivity can be represented by topological indexes of connectivity, such as the Euler Characteristic. A more complex tensor measures may be however obtained by averaging over the number of solid paths that interconnect any pair of arbitrary points belonging to the RVE matrix. Depleted media with RVEs characterized by solid skeletons in the form of three-dimensional truss structures constitute examples of micro-structures where the connection, say the number and the arrangement of bars, plays a crucial role in the overall stiffness of a selected cell.

Integrity is another important topological property of a depleted material. It refers the structural integrity of the solid network and then ascribes to the presence of interfaces (e.g., possible broken skeleton sections) the responsibility of a reducing in the overall RVE stiffness or strength. Truss structures where a geometrical interface is generated by fracturing one or more links, so interrupting the physical continuity, represents a case in which the RVE stiffness is reduced for a lack of integrity. Puzzle-like materials, where the presence of discontinuities at the interface between the tesserae significantly modifies the mechanical response of the ensemble, constitute another example of the influence of the integrity on the overall stiffness of a RVE.

Density

The main stereological measure of a depleted media is constituted by its density, whose architectural variable is usually identified with a dimensionless parameter named *volume fraction*, $\varphi \in]0, 1]$, or, equivalently, with the complementary *porosity* $\psi = 1 - \varphi$.

Orientation

In order to discover possible RVE mechanical anisotropies, the orientation of the microstructure plays a crucial role. Generally, it could be believed that orientation is a feature which can be detected intuitively, then recalling to a direct observation of the RVE microstructure. Actually, the cavities which weaken depleted media can be arranged inside the material domain so that the sole weapons of the direct observation result often inappropriate. On the contrary, how to detect and measure the microstructure orientation of a depleted RVE is still an open issue or – at least – a conflict matter.

In the framework depicted above, the present PhD dissertation is aimed to establish continuum-based micromechanical strategies for deriving constitutive laws for porous media, in absence of a fluid phase. The study is focused on depleted media where gradients and orientation of the voids can be recognized as the main responsible of the overall elastic response of the material, thus stiffness of the skeleton, solid matrix volume fraction and a second-order fabric tensor measuring the orientation of the RVE microstructure constitute the sole independent variables of the proposed model.

At the end, some numerical examples are illustrated to show the effectiveness of the method. In addition, further micromechanical in-progress results are shown, with reference to fibre-reinforced materials and to biomechanical applications.

CHAPTER I

REMARKS ON THE THEORY OF ELASTICITY

1. DEFORMATION THEORY

A central problem in nonlinear, three-dimensional elasticity consists in finding the equilibrium position of an elastic body that occupies a *reference configuration* $\bar{\Omega}$ in the absence of applied forces, where Ω is a bounded open connected subset of \mathbb{R}^3 with a Lipschitz-continuous boundary. When subjected to applied forces, the body occupies a *deformed configuration* $\varphi(\bar{\Omega})$, characterized by mapping $\varphi: \bar{\Omega} \rightarrow \mathbb{R}^3$ that must be in particular *orientation-preserving* in the set $\bar{\Omega}$ and *injective* on the set Ω , in order to be physically acceptable.

Such mapping φ are called *deformations*, and in the next sections their *geometrical properties* are studied. It is shown in particular that the changes in *volume*, *surfaces* and *lengths* associated with a deformation φ , are respectively governed by the scalar $\nabla \varphi$, the matrix $\mathbf{Cof} \nabla \varphi$ and the *right Cauchy-Green strain tensor* $\mathbf{C} = \nabla \varphi^T \nabla \varphi$.

1.1. Deformation in \mathbb{R}^3

We assume once and for all that an origin \mathbf{o} and an orthonormal basis $\{\mathbf{e}_1, \mathbf{e}_2, \mathbf{e}_3\}$ have been chosen in three-dimensional Euclidean space, which will therefore be identified with the space \mathbb{R}^3 . From the notational viewpoint, we identify the point \mathbf{x} with the vector $\mathbf{o}\mathbf{x}$. Whenever we consider components of vectors in \mathbb{R}^3 , or elements of matrices in \mathbb{M}^3 , we make the convention that Latin indices (i, j, p, ...) always take their values in the set $\{1, 2, 3\}$, and we combine this rule with the standard summation convention.

Let there be given a bounded, open, connected, subset Ω of \mathbb{R}^3 with a sufficiently smooth boundary (specific smoothness assumptions will be made subsequently). We shall think of the closure $\bar{\Omega}$ of the set Ω as representing the volume occupied by a body “before it is deformed”; for this reason, the set $\bar{\Omega}$ is called the *reference configuration*.

A deformation of the reference configuration $\bar{\Omega}$ is a vector field:

$$\varphi: \bar{\Omega} \rightarrow \mathbb{R}^3 \tag{1.1}$$

that is smooth enough, injective possibly on the boundary of the set Ω , and orientation-preserving.

Remarks.

1. The reason a deformation may lose its injectivity on the boundary of Ω is that “self-contact” must be allowed.
2. The expression “smooth enough” is simply a convenient way of saying that in a given definition, theorem, proof, etc. the smoothness of deformations involved is such that all arguments make sense. As a consequence, the underlying degree of smoothness varies from place to place. For instance, the existence of the deformation gradient (to be next introduced) implies that a deformation is differentiable at all points of the reference configuration; Theorem 1.1 relies on the Piola identity, which makes sense, at least in a classical setting, only for twice differentiable deformations; the characterization of rigid deformations is established for deformations that are continuously differentiable, etc.
3. Deformations are synonymously called configurations, or placements, by some authors.

We denote by \mathbf{x} a generic point in the set $\bar{\Omega}$, by x_i its components with respect to the basis $\{\mathbf{e}_i\}$, and by $\partial_i = \partial/\partial x_i$ the partial derivative with respect to variable x_i . Given a deformation $\boldsymbol{\varphi} = \varphi_i \mathbf{e}_i$, we define at each point of the set Ω the matrix

$$\nabla \boldsymbol{\varphi} := \begin{pmatrix} \partial_1 \varphi_1 & \partial_2 \varphi_1 & \partial_3 \varphi_1 \\ \partial_1 \varphi_2 & \partial_2 \varphi_2 & \partial_3 \varphi_2 \\ \partial_1 \varphi_3 & \partial_2 \varphi_3 & \partial_3 \varphi_3 \end{pmatrix}. \quad (1.2)$$

The matrix $\nabla \boldsymbol{\varphi}$ is called the **deformation gradient**. Since a deformation is orientation-preserving by definition, the determinant of the deformation gradient satisfies the **orientation-preserving condition**:

$$\det \nabla \boldsymbol{\varphi}(\mathbf{x}) > 0 \quad \text{for all } \mathbf{x} \in \bar{\Omega} \quad (1.3)$$

In particular, the matrix $\nabla \boldsymbol{\varphi}(\mathbf{x})$ is invertible at all points \mathbf{x} of the reference configuration $\bar{\Omega}$.

Remarks.

1. The notations $\mathbf{F} = \nabla \boldsymbol{\varphi}$ and $J = \det \nabla \boldsymbol{\varphi}$ are commonly used in the literature.
2. The notation $\nabla \boldsymbol{\varphi}$ is confusing, since the gradient of a real-valued function f is the column vector formed by the first partial derivative

$\partial_i f$, while $(\nabla \boldsymbol{\varphi})_{ij} = \partial_j \varphi_i$ (this explains why we used the notation **grad** f , and not ∇f). Indeed, the deformation gradient is simply the matrix representing the Fréchet derivative of the mapping $\boldsymbol{\varphi}$, which for real-valued functions, it is identified with the transpose of the gradient.

Together with a deformation $\boldsymbol{\varphi}$, it is often convenient to introduce the displacement \mathbf{u} , which is the vector field:

$$\mathbf{u} : \bar{\Omega} \rightarrow \mathbb{R}^3 \quad (1.4)$$

defined by the relation

$$\boldsymbol{\varphi} = \mathbf{id} + \mathbf{u}, \quad (1.5)$$

where \mathbf{id} denotes the (restriction to $\bar{\Omega}$ of the) identity map from \mathbb{R}^3 onto \mathbb{R}^3 . Notice that the displacement gradient

$$\nabla \mathbf{u} := \begin{pmatrix} \partial_1 u_1 & \partial_2 u_1 & \partial_3 u_1 \\ \partial_1 u_2 & \partial_2 u_2 & \partial_3 u_2 \\ \partial_1 u_3 & \partial_2 u_3 & \partial_3 u_3 \end{pmatrix} \quad (1.6)$$

and the deformation gradient are related by the equation

$$\nabla \boldsymbol{\varphi} = \mathbf{I} + \nabla \mathbf{u}. \quad (1.7)$$

Given a reference configuration $\bar{\Omega}$ and a deformation $\boldsymbol{\varphi} : \bar{\Omega} \rightarrow \mathbb{R}^3$, the set $\boldsymbol{\varphi}(\bar{\Omega})$ is called a **deformed configuration**. At each point

$$\mathbf{x}^\varphi := \boldsymbol{\varphi}(\mathbf{x}) \quad (1.8)$$

of a deformed configuration, we define the three vectors (Fig. 1.1)

$$\partial_j \boldsymbol{\varphi}(\mathbf{x}) = \partial_j \varphi_i(\mathbf{x}) \mathbf{e}_i. \quad (1.9)$$

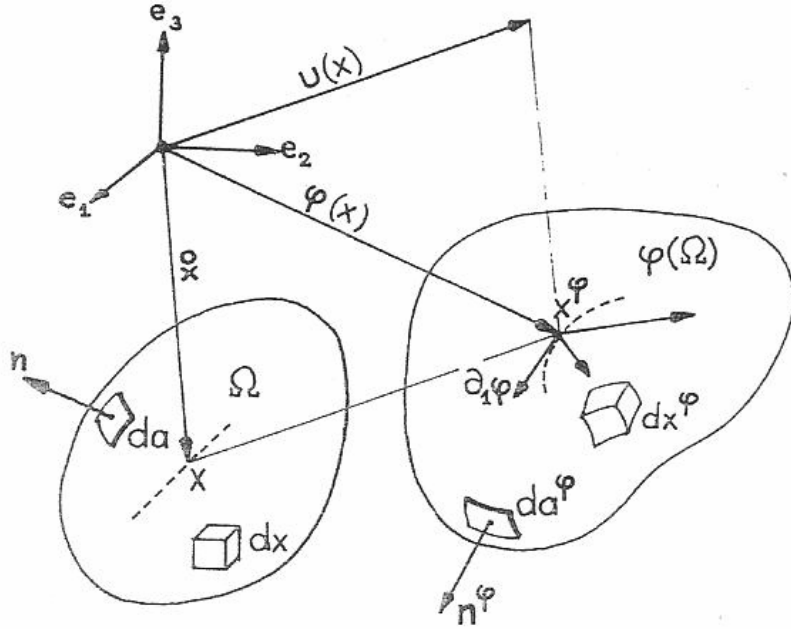
Each vector $\partial_j \boldsymbol{\varphi}(\mathbf{x})$ measures the “local deformation in the direction of the vector \mathbf{e}_j ” in the sense that, to within the first order with respect to dt , the vector $\mathbf{e}_j dt$ is transformed into the vector $\partial_j \boldsymbol{\varphi}(\mathbf{x}) dt$. Equivalently, the vector

$\partial_j \boldsymbol{\varphi}(\mathbf{x})$ is the tangent vector to the j th coordinate line passing through the point \mathbf{x}^φ (i.e. the image by the deformation $\boldsymbol{\varphi}$ of a segment parallel to the vector \mathbf{e}_j containing the point \mathbf{x} in its interior, and parametrized by t). Since the vector $\partial_j \boldsymbol{\varphi}(\mathbf{x})$ is precisely the j th column of the matrix $\nabla \boldsymbol{\varphi}$, the knowledge of the deformation gradient completely define the local deformation to within the first order.

Remarks.

1. While the deformation gradient $\nabla \boldsymbol{\varphi}$ clearly depends upon the basis \mathbf{e}_i , it is possible to exhibit the intrinsic geometrical character of the deformation at the point \mathbf{x} , by means of the polar factorization of the matrix $\nabla \boldsymbol{\varphi}(\mathbf{x})$, which then appears as the product of a “rotation tensor” by a “stretch tensor”. For details about this classical results, see for instance Germain (1972), Gurtin (1981), Truesdell&Noll (1965).
2. If the point $\mathbf{x}^\varphi = \boldsymbol{\varphi}(\mathbf{x})$ belongs to the interior of the deformed configuration $\boldsymbol{\varphi}(\bar{\Omega})$, the three vector $\partial_j \boldsymbol{\varphi}$ define in the terminology of differential geometry the tangent vector space at the point \mathbf{x} of the manifold $\boldsymbol{\varphi}(\bar{\Omega})$. This space is of dimension three since the matrix $\nabla \boldsymbol{\varphi}(\mathbf{x})$ is invertible (by definition of a deformation).
3. The points $x \in \Omega$ and the corresponding points $\mathbf{x}^\varphi \in \boldsymbol{\varphi}(\Omega)$ are often called material points and spatial points respectively, and they are often denoted X and \mathbf{x} respectively, in the continuum mechanics literature.

We next compute the volume, area, and length elements in the deformed configuration. In each case, the objective is, for a given deformation, to express quantities (volumes, surfaces, lengths) defined over the deformed configuration in terms of the same quantities, but defined over the reference configuration. To emphasize the crucial distinction between both types of quantities, we adopt the following notational device: the superscript “ φ ” is systematically attached to a quantity defined over the deformed configuration, while the related quantity over the reference configuration is designed by the same letter, but without the superscript “ φ ”; this rule has already been applied, for denoting a generic point $\mathbf{x} \in \bar{\Omega}$ and the corresponding point $\mathbf{x}^\varphi \in \boldsymbol{\varphi}(\mathbf{x}) \in \boldsymbol{\varphi}(\bar{\Omega})$.

**Fig. 1.1.**

Geometry of a deformation: the volume element, the area element, the unit outer normal, are denoted dx , da , \mathbf{n} in the reference configuration $\bar{\Omega}$, and dx^φ , da^φ , \mathbf{n}^φ in the deformed configuration $\varphi(\bar{\Omega})$. The vectors $\partial_j \varphi(\mathbf{x})$ define the deformation at a point $x \in \bar{\Omega}$ to within the first order.

This correspondence between a quantity defined as a function of the Lagrange variable \mathbf{x} , and a similar quantity defined as a function of the Euler variable $\mathbf{x}^\varphi \in \varphi(\mathbf{x})$, can be extended to other quantities than volume, surfaces, and lengths. As we shall see, it applies equally well to divergences of tensor fields and applied forces.

Remark.

1. This idea can be systematized through the notions of “pullback” and “push-forward”, familiar in differential geometry. In this respect, see for instance Choquet-Bruhat, Dewitt-Morette and Dillard-Bleick (1977), or Marsden and Hughes (1983).

1.2. Volume element in deformation configuration

Let φ be a deformation. If dx denotes the volume element at the point \mathbf{x} of the reference configuration, the volume element dx^φ at the point $\mathbf{x}^\varphi = \varphi(\mathbf{x})$ of the deformed configuration (Fig. 1.1) is given by

$$dx^\varphi = \det \nabla \varphi(x) dx, \quad (1.10)$$

since $|\det \nabla \varphi(x)| = \det \nabla \varphi(x) > 0$ by assumption.

The volume element dx^φ is used for computing volumes in the deformed configuration: If A denotes a measurable subset of the reference configuration $\bar{\Omega}$, the volume of the set A and the volume of the deformed set $A^\varphi := \varphi(A)$ are respectively given by:

$$\text{vol } A := \int_A dx, \quad \text{vol } A^\varphi := \int_{A^\varphi} dx^\varphi = \int_A \det \nabla \varphi(x) dx. \quad (1.11)$$

Notice that the last equality is nothing but a special case of the formula for changes of variables in multiple integrals: Let $\varphi: A \rightarrow \varphi(A) = A^\varphi$ be an injective, continuously differentiable mapping with a continuous inverse $\varphi^{-1}: A^\varphi \rightarrow A$. Then a function $u: x^\varphi \in A^\varphi \rightarrow \mathbf{R}$ is dx^φ -integrable over the set A^φ if and only if the function

$$x \in A \rightarrow (u \circ \varphi)(x) |\det \nabla \varphi(x)| \quad (1.12)$$

is dx -integrable over the set A and if this is the case,

$$\int_{A^\varphi = \varphi(A)} u(x^\varphi) dx^\varphi = \int_A (u \circ \varphi)(x) |\det \nabla \varphi(x)| dx. \quad (1.13)$$

It should be remembered that the validity of this formula hinges critically on the assumption that the mapping φ is injective. Otherwise, it must be replaced by the more general relation:

$$\int_{\varphi(A)} u(x') \text{card} \varphi^{-1}(x') dx' = \int_A (u \circ \varphi)(x) |\det \nabla \varphi(x)| dx \quad (1.14)$$

where $\text{card } B$ denote in general the number of elements in a set B . For details, see Schwartz (1967), Rado & Reichelderfer (1955), Federer (1969), Smith

(1983), Bojarski & Iwaniec (1983), Marcus & Mizel (1973), Vodopyanov, Goldshtein & Reshetnyak (1979) for its extension to Sobolev space-valued mappings.

These properties hold in \mathbb{R}^n , for arbitrary n . The volume $\int_A dx$ of a dx -measurable subset of \mathbb{R}^n is denoted dx -means A .

1.3. The Piola transform; area element in the deformed configuration

As a preparation for computing the area element in the deformed configuration in terms of the area element in the reference configuration, it is convenient to introduce a particular transformation between tensors defined over the reference configuration $\bar{\Omega}$ and tensors defined over the deformed configuration $\bar{\Omega}^\varphi$. Besides, this transform plays a crucial role in the definition of the first Piola-Kirchhoff tensor, following introduced.

Let us first review some definitions and results pertaining to tensor fields defined over either sets $\bar{\Omega}$ or $\bar{\Omega}^\varphi$. By a tensor, we mean here a second-order tensor

$$\mathbf{T} = (T_{ij}), \quad i: \text{row index}, j: \text{column index}.$$

Since we ignore the distinction between covariant and contravariant components, the set of all such tensors will be identified with the set \mathbb{M}^3 of all square matrices of order three.

Given a smooth enough tensor field $\mathbf{T}: \bar{\Omega} \rightarrow \mathbb{M}^3$ defined over the reference configuration $\bar{\Omega}$, we define at each point of $\bar{\Omega}$ its divergence $\mathbf{div} \mathbf{T}$ as the vector whose components are the divergences of the transposes of the row vectors of the matrix \mathbf{T} . More explicitly,

$$\mathbf{T} = T_{ij} = \begin{pmatrix} T_{11} & T_{12} & T_{13} \\ T_{21} & T_{22} & T_{23} \\ T_{31} & T_{32} & T_{33} \end{pmatrix} \Rightarrow \mathbf{div} \mathbf{T} := \begin{pmatrix} \partial_1 T_{11} + \partial_2 T_{12} + \partial_3 T_{13} \\ \partial_1 T_{21} + \partial_2 T_{22} + \partial_3 T_{23} \\ \partial_1 T_{31} + \partial_2 T_{32} + \partial_3 T_{33} \end{pmatrix} = \partial_j T_{ij} \mathbf{e}_i. \quad (1.15)$$

Of course, a similar definition holds for the divergence $\mathbf{div}^\varphi \mathbf{T}^\varphi$ of tensor fields $\mathbf{T}^\varphi: \mathbf{B}^\varphi \rightarrow \mathbb{M}^3$ defined over the deformed configuration:

$$\mathbf{T}^\varphi = (T_{ij}^\varphi) \Rightarrow \mathbf{div}^\varphi \mathbf{T}^\varphi := \partial_j^\varphi T_{ij}^\varphi \mathbf{e}_i \quad (1.16)$$

where $\partial_j^\varphi := \partial / \partial x_j^\varphi$ denote the partial derivatives with respect to the variables x_j^φ .

A Simple application of the fundamental Green's formula over the set $\bar{\Omega}$ shows that the divergence of a tensor field satisfies:

$$\int_{\Omega} \mathbf{div} \mathbf{T} dX = \left(\int_{\Omega} \partial_j T_{ij} dx \right) \mathbf{e}_i = \left(\int_{\partial\Omega} T_{ij} n_j da \right) \mathbf{e}_i \quad (1.17)$$

or equivalently in matrix form:

$$\int_{\Omega} \mathbf{div} \mathbf{T} dx = \int_{\partial\Omega} \mathbf{T} \mathbf{n} da \quad (1.18)$$

Recall that a vector is always understood as a column vector when viewed as a matrix; thus the notation $\mathbf{T} \mathbf{n}$ in the previous formula represents the column vector obtained by applying the matrix \mathbf{T} to the column vector \mathbf{n} . This Green formula is called the divergence theorem for tensor fields. A tensor field $\mathbf{T}^\varphi = \bar{\Omega}^\varphi \rightarrow \mathbb{M}^3$ likewise satisfies:

$$\int_{\Omega^\varphi} \mathbf{div}^\varphi \mathbf{T}^\varphi dx^\varphi = \int_{\partial\Omega^\varphi} \mathbf{T}^\varphi \mathbf{n}^\varphi da^\varphi, \quad (1.19)$$

where \mathbf{n}^φ denotes the unit outer normal vector along the boundary of the deformed configuration.

We now come to an important definition. Let φ be a deformation that is injective on $\bar{\Omega}$, so that the matrix $\nabla \varphi$ is invertible at all points of the reference configuration. Then if $\mathbf{T}^\varphi(\mathbf{x}^\varphi)$ is a tensor defined at the point $\mathbf{x}^\varphi = \varphi(\mathbf{x})$ of the deformed configuration, we associate with $\mathbf{T}^\varphi(\mathbf{x}^\varphi)$ a tensor $\mathbf{T}(\mathbf{x})$ defined at the point \mathbf{x} of the reference configuration by:

$$\mathbf{T}(\mathbf{x}) := (\det \nabla \varphi(x)) \mathbf{T}^\varphi(\mathbf{x}^\varphi) \nabla \varphi(x)^{-T} = \mathbf{T}^\varphi(\mathbf{x}^\varphi) \mathbf{Cof}(\nabla \varphi(x)), \quad (1.20)$$

$$\mathbf{x}^\varphi = \varphi(\mathbf{x}).$$

In this fashion, a correspondence, called the Piola transform, is established between tensor fields defined over the deformed and reference configurations, respectively.

Remark.

1. It would be equally conceivable, and somehow more natural, to start with a tensor field $\mathbf{T} : \bar{\Omega} \rightarrow \mathbb{M}^3$ and to associate with it its “inverse Piola transform” $\mathbf{T}^\varphi : \bar{\Omega}^\varphi \rightarrow \mathbb{M}^3$ defined by

$$\mathbf{T}^\varphi(\mathbf{x}^\varphi) := (\det \nabla \boldsymbol{\varphi}(x))^{-1} \mathbf{T}(\mathbf{x}) \nabla \boldsymbol{\varphi}(x)^T, \quad x \in \bar{\Omega}.$$

The reason we proceed the other way is that the starting point in elasticity is a tensor field defined over the deformed configuration (the Cauchy stress tensor field), and it is its Piola transform over three reference configuration (the first Piola –Kirchhoff stress tensor field) that subsequently plays a key role.

As shown in the next theorem, the main interest of the Piola transform is that it yields a simple relation between the divergences of the tensors \mathbf{T}^φ and \mathbf{T} and (as a corollary) the desired relation between corresponding area elements da^φ and da .

Theorem 1.1. (properties of the Piola transform). Let $\mathbf{T} : \bar{\Omega} \rightarrow \mathbb{M}^3$ denote the Piola transform of $\mathbf{T}^\varphi : \bar{\Omega}^\varphi \rightarrow \mathbb{M}^3$. Then

$$\operatorname{div} \mathbf{T}(\mathbf{x}) = (\det \nabla \boldsymbol{\varphi}(x)) \operatorname{div}^\varphi \mathbf{T}^\varphi(\mathbf{x}^\varphi) \quad \text{for all } \mathbf{x}^\varphi = \boldsymbol{\varphi}(\mathbf{x}), \quad x \in \bar{\Omega}, \quad (1.21)$$

$$\mathbf{T}(\mathbf{x}) \mathbf{n} da = \mathbf{T}^\varphi(\mathbf{x}^\varphi) \mathbf{n}^\varphi da^\varphi \quad \text{for all } \mathbf{x}^\varphi = \boldsymbol{\varphi}(\mathbf{x}), \quad x \in \bar{\Omega}. \quad (1.22)$$

The area elements da and da^φ at the points $x \in \partial\Omega$ and $\mathbf{x}^\varphi = \boldsymbol{\varphi}(x) \in \partial\Omega^\varphi$, with unit outer normal vectors \mathbf{n} and \mathbf{n}^φ respectively, are related by

$$\det \nabla \boldsymbol{\varphi}(x) \left| \nabla \boldsymbol{\varphi}(x)^{-T} \mathbf{n} \right| da = \left| \operatorname{Cof} \nabla \boldsymbol{\varphi}(x) \mathbf{n} \right| da = da^\varphi. \quad (1.23)$$

Remarks.

1. Of course, the conclusions of Theorem 1.1 still hold if we replace the set Ω by any sub-domain A of Ω , in which case the corresponding area elements and outer normal vectors are to be understood as being defined along the corresponding boundaries ∂A and $\partial A^\varphi = \boldsymbol{\varphi}(\partial A)$.
2. While the relation between the vectors $\operatorname{div} \mathbf{T}$ and $\operatorname{div}^\varphi \mathbf{T}^\varphi$ has been established here for deformations $\boldsymbol{\varphi}$ that are twice differentiable, the relations between the area elements established in Theorem (1.1) still hold under weaker regularity assumptions on the deformation.

3. The last equation in Theorem 1.1 shows that the unit outer normal vectors at the points $x^\varphi = \varphi(x)$ and x are related by

$$\mathbf{n}^\varphi = \frac{\mathbf{Cof} \nabla \varphi(x) \mathbf{n}}{|\mathbf{Cof} \nabla \varphi(x) \mathbf{n}|}.$$

We now have everything at our disposal to specify how areas are transformed: If Δ is a measurable subset of the boundary ∂A of a sub-domain A , the area of the deformed set $\Delta^\varphi = \varphi(\Delta)$ is given by

$$\text{area } \Delta^\varphi := \int_{\Delta^\varphi} da^\varphi = \int_{\Delta} (\det \nabla \varphi) |\nabla \varphi^{-T} \mathbf{n}| da \quad (1.24)$$

1.4. Length element in the deformed configuration; Strain Tensor

If a deformation φ is differentiable at a point $x \in \bar{\Omega}$, then (by definition of differentiability) we can write, for all points $x + \delta \mathbf{x} \in \bar{\Omega}$:

$$\varphi(x + \delta \mathbf{x}) - \varphi(x) = \nabla \varphi(x) \delta \mathbf{x} + o(|\delta \mathbf{x}|) \quad (1.25)$$

and whence

$$|\varphi(x + \delta \mathbf{x}) - \varphi(x)|^2 = \delta \mathbf{x}^T \nabla \varphi^T(x) \nabla \varphi(x) \delta \mathbf{x} + o(|\delta \mathbf{x}|^2) \quad (1.26)$$

The symmetric tensor

$$\mathbf{C} := \nabla \varphi^T \nabla \varphi \quad (1.27)$$

found in the above expression is called in elasticity the **right Cauchy-Green strain tensor**. Notice that the associated quadratic form:

$$(\xi, \xi) \in \mathbf{R}^3 \times \mathbf{R}^3 \rightarrow \xi^T \mathbf{C}(x) \xi = |\nabla \varphi(x) \xi|^2 \quad (1.28)$$

is positive definite at all points $x \in \bar{\Omega}$, since the deformation gradient $\nabla \varphi$ is everywhere invertible by assumption. As expected, this quadratic form is used for computing lengths: Let

$$\gamma = f(I), \quad f: I \rightarrow \bar{\Omega}, \quad I: \text{compact interval of } \mathbb{R} \quad (1.29)$$

be a curve in the reference configuration (Fig. 1.2). Denoting by f_i the components of the mapping \mathbf{f} , the length of the curve γ is given by ($f' = df/dt$):

$$\text{length } \gamma := \int_L |f'(t)| dt = \int_L \left\{ f'(t) f'(t) \right\}^{1/2} dt, \quad (1.30)$$

while the length of the deformed curve $\gamma^\varphi : \varphi(\gamma)$ is given by

$$\text{length } \gamma^\varphi := \int_L |\varphi \circ f'(t)| dt = \int_L \left\{ C_{ij}(f(t)) f'(t) f'(t) \right\}^{1/2} dt \quad (1.31)$$

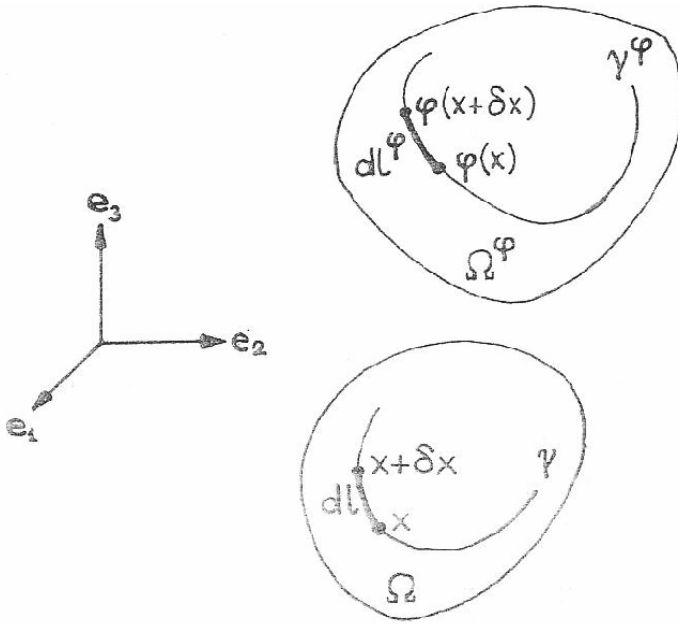
Consequently, the length elements dl and dl^φ in the reference and deformed configurations may be symbolically written as:

$$dl = \left\{ \mathbf{dx}^T \mathbf{dx} \right\}^{1/2}, \quad dl^\varphi = \left\{ \mathbf{dx}^T \mathbf{C} \mathbf{dx} \right\}^{1/2}. \quad (1.32)$$

If in particular $\mathbf{dx} = dt \mathbf{e}_j$, the corresponding length element in the deformed configuration is $\left\{ C_{jj} \right\}^{1/2} dt = |\partial_j \varphi| dt$.

Remark.

1. In the language of differential geometry, the manifold $\bar{\Omega}$ is equipped with a Riemannian structure through the data of the metric tensor $\mathbf{C} = (C_{ij})$, often denoted $\mathbf{g} = g_{ij}$ in differential geometry, whose associated quadratic form, often denoted ds^2 , is called the first fundamental form of the manifold. For details, see e.g. Lelong Ferrand(1963), Malliavin (1972).

**Fig. 1.2.**

The length elements $dl = \{\mathbf{dx}^T \mathbf{dx}\}^{1/2}$ and $dl^\varphi = \{\mathbf{dx}^T \mathbf{C} \mathbf{dx}\}^{1/2}$ in the reference and deformed configurations. The tensor $\mathbf{C} = \nabla \varphi^T \nabla \varphi$ is the right Cauchy-Green tensor.

Although it has no immediate geometric interpretation, the left Cauchy-Green strain tensor

$$\mathbf{B} : \nabla \varphi \nabla \varphi^T \quad (1.33)$$

which is also symmetric, is equally important; in particular, it plays an essential role in the representation theorem for the response function of the Cauchy stress tensor. For the time being, we simply notice that the two matrices $\mathbf{C} = \mathbf{F}^T \mathbf{F}$ and $\mathbf{B} = \mathbf{F} \mathbf{F}^T$ have the same characteristic polynomial, since this is true in general of the products $\mathbf{F} \mathbf{G}$ and $\mathbf{G} \mathbf{F}$ of two arbitrary matrices \mathbf{F} and \mathbf{G} of the same order. When $\mathbf{G} = \mathbf{F}^T$, this result is a direct consequence of the polar factorization theorem.

In view of showing that the tensor \mathbf{C} is indeed a good measure of “strain”, understood here in its intuitive sense of “change in form or size”, let us first consider a class of deformations that induce no “strain”: A deformation is called a rigid deformation if it is of the form

$$\varphi(x) = \mathbf{a} + \mathbf{Q} \circ x, \quad \mathbf{a} \in \mathbf{R}, \quad \mathbf{Q} \in \mathbf{O}_+^3, \quad \text{for all } x \in \bar{\Omega}, \quad (1.34)$$

where \mathbb{O}_+^3 denotes the set of rotations in \mathbb{R}^3 , i.e., the set of orthogonal matrices of order 3 whose determinant is +1. In other words, the corresponding deformed configuration is obtained by rotating the reference configuration around the origin by the rotation \mathbf{Q} and by translating it by the vector \mathbf{a} : this indeed corresponds to the idea of a “rigid” deformation, where the reference configuration is “moved”, but without any “strain” (Fig. 1.3). Observe that the rotation \mathbf{Q} may be performed around any point $\tilde{\mathbf{x}} \in \mathbb{R}^3$ (Fig. 1.3), since we can also write

$$\boldsymbol{\varphi}(\mathbf{x}) = \boldsymbol{\varphi}(\tilde{\mathbf{x}}) + \mathbf{Q} \tilde{\mathbf{x}} \mathbf{x} \quad (1.35)$$

If $\boldsymbol{\varphi}$ is a rigid deformation, then $\nabla \boldsymbol{\varphi}(\mathbf{x}) = \mathbf{Q} \in \mathbb{O}_+^3$ at all points $\mathbf{x} \in \bar{\Omega}$, and therefore

$$\mathbf{C} = \mathbf{I} \quad \text{in } \bar{\Omega}, \quad \text{i.e.,} \quad \nabla \boldsymbol{\varphi}(\mathbf{x})^T \nabla \boldsymbol{\varphi}(\mathbf{x}) = \mathbf{I} \quad \text{for all } \mathbf{x} \in \bar{\Omega}. \quad (1.36)$$

It is remarkable that conversely, if $\mathbf{C} = \mathbf{I}$ in $\bar{\Omega}$ and $\det \nabla \boldsymbol{\varphi} > 0$, the corresponding deformation is necessarily rigid.

Theorem 1.2. (characterization of rigid deformations). Let Ω be an open connected subset of \mathbb{R}^n , and let there be given a mapping

$$\boldsymbol{\varphi} \in C^1(\Omega, \mathbb{R}^n) \quad (1.37)$$

that satisfies

$$\nabla \boldsymbol{\varphi}(\mathbf{x})^T \nabla \boldsymbol{\varphi}(\mathbf{x}) = \mathbf{I} \quad \text{for all } \mathbf{x} \in \Omega \quad (1.38)$$

then there exists a vector $\mathbf{a} \in \mathbb{R}^n$ and an orthogonal matrix $\mathbf{Q} \in \mathbf{O}^n$ such that

$$\boldsymbol{\varphi}(\mathbf{x}) = \mathbf{a} + \mathbf{Q} \circ \mathbf{x} \quad \text{for all } \mathbf{x} \in \Omega. \quad (1.39)$$

The result of theorem 1.2 can be viewed as a special case (let $\boldsymbol{\psi}$ be any rigid deformation in the theorem 1.3) of the following result, which shows that two deformations corresponding to the same tensor \mathbf{C} can be obtained from one another by composition with a rigid deformation.

Theorem 1.3. Let Ω be an open connected subset of \mathbb{R}^n , and let here be given two mappings

$$\boldsymbol{\varphi}, \boldsymbol{\psi} \in C^1(\Omega, \mathbb{R}^n) \quad (1.40)$$

such that

$$\nabla \boldsymbol{\varphi}(\mathbf{x})^T \cdot \nabla \boldsymbol{\varphi}(\mathbf{x}) = \nabla \boldsymbol{\psi}(\mathbf{x})^T \cdot \nabla \boldsymbol{\psi}(\mathbf{x}) \text{ for all } \mathbf{x} \in \Omega \quad (1.41)$$

$\boldsymbol{\psi} : \Omega \rightarrow \mathbb{R}^n$ is injective, and let $\nabla \boldsymbol{\psi}(\mathbf{x}) \neq 0$ for all $\mathbf{x} \in \Omega$.

Then here exist a vector $\mathbf{a} \in \mathbb{R}^n$ and an orthogonal matrix $\mathbf{Q} \in O^n$ such that :

$$\boldsymbol{\varphi}(\mathbf{x}) = \mathbf{a} + \mathbf{Q}\boldsymbol{\psi}(\mathbf{x}) \text{ for all } \mathbf{x} \in \Omega. \quad (1.42)$$

The previous two theorems are useful for understanding the role played by the tensor \mathbf{C} . First, theorem 1.2. shows that the difference

$$2\mathbf{E} := \mathbf{C} - \mathbf{I} \quad (1.43)$$

is a measure of the “deviation” between a given deformation and a rigid deformation, since $\mathbf{C} = \mathbf{I}$ if and only if the deformation is rigid. Secondly, theorem 1.3. shows that the knowledge of the tensor field $\mathbf{C} : \Omega \rightarrow \mathbb{S}_{>}^3$ completely determines the deformation, up to composition with rigid deformations (the question of proving the existence of deformations for which the associated tensor field $\mathbf{C} : \Omega \rightarrow \mathbb{S}_{>}^3$ is equal to a given tensor field is quite another matter). These considerations are illustrated in figure 1.3.

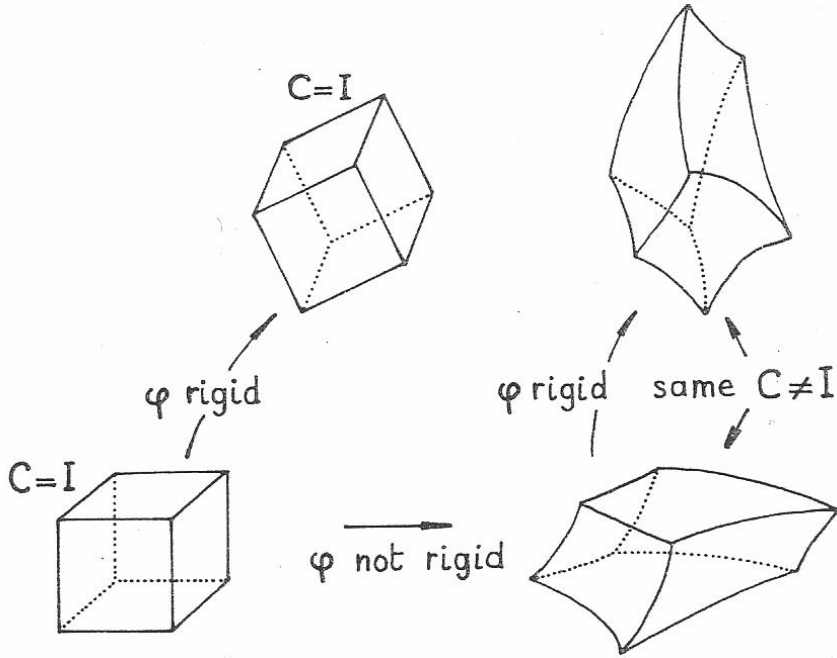


Fig. 1.3.

*The right Cauchy-Green tensor C is equal to I if and only if the deformation is rigid.
Two deformations corresponding to the same tensor C differ by a rigid deformation.*

The tensor E is called the Green-St Venant strain tensor. Expressed in terms of the displacement gradient $\nabla \mathbf{u}$, in lieu of the deformation gradient $\nabla \boldsymbol{\varphi} = I + \nabla \mathbf{u}$ (recall that $\boldsymbol{\varphi} = \mathbf{id} + \mathbf{u}$), the strain tensor C becomes

$$C = \nabla \boldsymbol{\varphi}^T \nabla \boldsymbol{\varphi} = I + \nabla \mathbf{u}^T + \nabla \mathbf{u} + \nabla \mathbf{u}^T \nabla \mathbf{u} = I + 2E \quad (1.44)$$

with

$$E(\mathbf{u}) := E = \frac{1}{2}(\nabla \mathbf{u}^T + \nabla \mathbf{u} + \nabla \mathbf{u}^T \nabla \mathbf{u}) \quad (1.45)$$

whose “first order” part $\frac{1}{2}(\nabla \mathbf{u}^T + \nabla \mathbf{u})$ coincide with the *linearized strain tensor*, which played a key role in the earlier linearized theories that prevailed in elasticity.

2. THE EQUATION OF EQUILIBRIUM

A body occupying a deformed configuration $\bar{\Omega}^\varphi$, and subjected to applied body forces in its interior Ω^φ and to applied surface forces on a portion $\Gamma_1^\varphi = \varphi(\Gamma_1)$ of its boundary, is in static equilibrium if the fundamental stress principle of Euler and Cauchy is satisfied. This axiom, which is the basis of continuum mechanics, implies the celebrated Cauchy theorem, according to which there exists a symmetric tensor field $\mathbf{T}^\varphi : \bar{\Omega}^\varphi \rightarrow \mathbb{S}^3$ such that

$$\begin{cases} -\text{div}^\varphi \mathbf{T}^\varphi = \mathbf{f}^\varphi & \text{in } \Omega^\varphi \\ \mathbf{T}^\varphi \mathbf{n}^\varphi = \mathbf{g}^\varphi & \text{on } \Gamma_1^\varphi \end{cases} \quad (1.46)$$

where \mathbf{f}^φ and \mathbf{g}^φ denote the densities of the applied body and surface forces respectively, and \mathbf{n}^φ is the unit outer normal vector along Γ_1^φ . These equations are called the equilibrium over the deformed configuration, and the tensor \mathbf{T}^φ is called the Cauchy stress tensor.

A remarkable feature of these equations is their “divergence structure”, which makes them amenable to a variational formulation; a disadvantage is that they are expressed in terms of the unknown $\mathbf{x}^\varphi = \varphi(\mathbf{x})$. In order to obviate this difficulty while retaining the divergence structure of the equations, we use the Piola transform $\mathbf{T} : \bar{\Omega} \rightarrow \mathbb{M}^3$ of the Cauchy stress tensor field, which is defined by $\mathbf{T}(\mathbf{x}) = \mathbf{T}^\varphi(\mathbf{x}^\varphi) \text{Cof } \nabla \varphi(\mathbf{x})$. In this fashion, it is found that the equilibrium equations over $\bar{\Omega}^\varphi$ are equivalent to the equilibrium equations over the reference configuration $\bar{\Omega}$,

$$\begin{cases} -\text{div} \mathbf{T} = \mathbf{f} & \text{in } \Omega \\ \mathbf{T} \mathbf{n} = \mathbf{g} & \text{on } \Gamma_1 \end{cases} \quad (1.47)$$

where \mathbf{n} denotes the unit outer normal vector along Γ_1 , and the fields $\mathbf{f} : \Omega \rightarrow \mathbb{R}^3$ and $\mathbf{g} : \Gamma_1 \rightarrow \mathbb{R}^3$ are related to the fields $\mathbf{f}^\varphi : \Omega^\varphi \rightarrow \mathbb{R}^3$ and $\mathbf{g}^\varphi : \Gamma_1^\varphi \rightarrow \mathbb{R}^3$ by the simple formulas $\mathbf{f} dx = \mathbf{f}^\varphi dx^\varphi$ and $\mathbf{g} dx = \mathbf{g}^\varphi dx^\varphi$. Because they are still in divergence form, these equations can be given a variational formulation, known as the principle of virtual work. This principle plays a key role as the starting point of the theory of hyperelastic materials, as well in the asymptotic theory of two-dimensional plate models.

The tensor \mathbf{T} is called the first Piola-Kirchhoff stress tensor. We also introduce the symmetric second Piola-Kirchhoff stress tensor $\boldsymbol{\Sigma} = \nabla \varphi^{-1} \mathbf{T}$, which naturally arises in the expression of the constitutive equations of elastic materials.

2.1. Applied Forces

We assume that in the deformed configuration $\bar{\Omega}^\varphi$ associated with an arbitrary deformation φ , the body is subjected to applied forces of two types:

- (i) applied **body forces**, defined by a vector field

$$\mathbf{f}^\varphi : \Omega^\varphi \rightarrow \mathbb{R}^3, \quad (1.48)$$

called the density of the applied body forces per unit volume in the deformed configuration;

- (ii) applied **surface forces**, defined by a vector field

$$\mathbf{g}^\varphi : \Gamma_1^\varphi \rightarrow \mathbb{R}^3 \quad (1.49)$$

on a da^φ -measurable subset Γ_1^φ of the boundary

$$\Gamma^\varphi := \partial\Omega^\varphi \quad (1.50)$$

called the density of the applied surface force per unit area in the deformed configuration.

Let $\rho^\varphi : \Omega^\varphi \rightarrow \mathbb{R}$ denote the mass density in the deformed configuration, so that the mass of every dx^φ -measurable subset A^φ of $\bar{\Omega}^\varphi$ is given by the integral $\int_{A^\varphi} \rho^\varphi(x^\varphi) dx^\varphi$. We assume that

$$\rho^\varphi(x^\varphi) > 0 \quad \text{for all } x^\varphi \in \Omega \quad (1.51)$$

The applied body forces can be equivalently defined by their density $\mathbf{b}^\varphi : \Omega^\varphi \rightarrow \mathbb{R}^3$ per unit mass in the deformed configuration, which is related to the density \mathbf{f}^φ by the equation

$$\mathbf{f}^\varphi = \rho^\varphi \mathbf{b}^\varphi \quad (1.52)$$

The applied forces describe the action of the outside world on the body: An elementary force $\mathbf{f}^\varphi(x^\varphi) dx^\varphi$ is exerted on the elementary volume dx^φ at each point x^φ of the deformed configuration. For example, this is the case of the gravity field, for which $\mathbf{f}(x^\varphi) = -g\rho^\varphi(x^\varphi)\mathbf{e}_3$ for all $x^\varphi \in \Omega^\varphi$ (assuming that

the vector \mathbf{e}_3 is vertical and oriented “upward”), where g is the gravitational constant. Another example is given by the action of electrostatic forces.

Likewise, an elementary force $\mathbf{g}^\varphi(x^\varphi)dx^\varphi$ is exerted on the elementary area da^φ at each point x^φ of the subset Γ_1^φ of the boundary of the deformed configuration (Fig. 1.3). Such forces generally represent the action of another body (whatever its nature it may be) along the portion Γ_1^φ of the boundary.

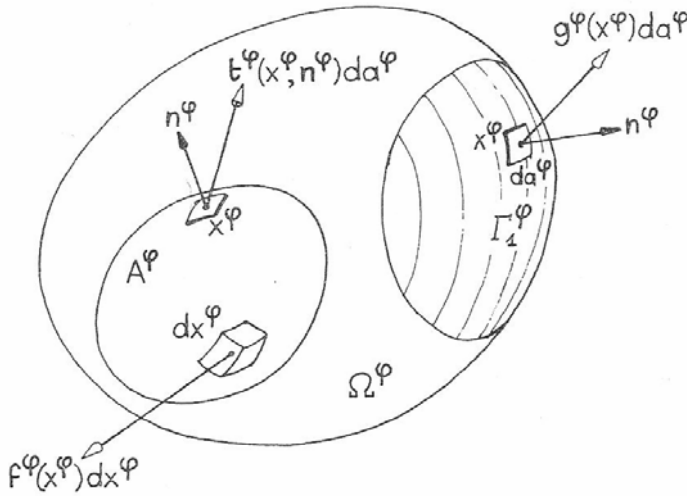


Fig. 1.3.

Applied forces comprise applied body forces $\mathbf{f}^\varphi(x)dx^\varphi$, $x^\varphi \in \Omega^\varphi$ and applied surface forces $\mathbf{g}^\varphi(x)dx^\varphi$, $x^\varphi \in \Gamma_1^\varphi$. The stress principle of Euler and Cauchy asserts in addition the existence of elementary surface forces $\mathbf{t}^\varphi(\mathbf{x}^\varphi, \mathbf{n}^\varphi)da^\varphi$, $x^\varphi \in \partial A^\varphi$, along the boundary ∂A^φ , with unit outer normal vector \mathbf{n}^φ , of any sub-domain A^φ of the deformed configuration $\bar{\Omega}^\varphi$.

Remark.

1. In order to avoid introducing too many notations, we use the same symbol to denote distinct quantities in the same figure. For instance in Fig. 1.3. the symbol x^φ stands for three different points, and the symbols da^φ and \mathbf{n}^φ stand for two different area elements and normal vectors.

Applied surface forces that are only “partially” specified (for instance, only the normal component $\mathbf{g}^\varphi(x) \cdot \mathbf{n}^\varphi$ could be prescribed along Γ_1^φ) are not excluded from our analysis; but in order to simplify the exposition, we solely considered

at this stage the “extreme” cases where either the density \mathbf{g}^φ is fully known on Γ_1^φ , or is left completely unspecified, as on the remaining portion

$$\Gamma_0^\varphi := \Gamma^\varphi - \Gamma_1^\varphi \quad (1.53)$$

of the boundary of the deformed configuration. This being the case, we shall see that it is the deformation itself that should be specified on the corresponding portion $\Gamma_0 := \varphi^{-1}(\Gamma_0^\varphi)$ of the boundary of the reference configuration, in order that the problem be well posed.

2.2. The stress principle of Euler and Cauchy

Continuum mechanics for static problems is founded on the following axiom, named after the fundamental contributions of Euler (1757,1771) and Cauchy (1823,1827a). Note that the exterior product in \mathbb{R}^3 is denoted \wedge .

Axiom 1. (stress principle of Euler and Cauchy). Consider a body occupying a deformed configuration $\bar{\Omega}^\varphi$, and subjected to applied forces represented by densities $\mathbf{f}^\varphi := \Omega^\varphi \rightarrow \mathbb{R}^3$ and $\mathbf{g}^\varphi := \Omega^\varphi \rightarrow \mathbb{R}^3$. Then there exists a vector field

$$\mathbf{t}^\varphi : \Omega^\varphi \times S_1 \rightarrow \mathbb{R}^3, \quad \text{where} \quad S_1 = \{v \in \mathbb{R}^3; |v| = 1\}, \quad (1.54)$$

such that:

- (a) For any sub-domain A^φ of $\bar{\Omega}^\varphi$, and at any point $\mathbf{x}^\varphi \in \Gamma_1^\varphi \cap \partial A^\varphi$ where the unit outer normal vector \mathbf{n}^φ to $\Gamma_1^\varphi \cap \partial A^\varphi$ exists:
 $\mathbf{t}^\varphi(\mathbf{x}^\varphi, \mathbf{n}^\varphi) = \mathbf{g}^\varphi(\mathbf{x}^\varphi)$.

- (b) Axiom of **force balance**: For any sub-domain A^φ of $\bar{\Omega}^\varphi$,

$$\int_{A^\varphi} \mathbf{f}^\varphi(\mathbf{x}^\varphi) dx^\varphi + \int_{\partial A^\varphi} \mathbf{t}^\varphi(\mathbf{x}^\varphi, \mathbf{n}^\varphi) dx^\varphi = \mathbf{0} \quad (1.55)$$

where \mathbf{n}^φ denotes the unit outer normal vector along ∂A^φ .

- (c) Axiom of **moment balance**: For any sub-domain A^φ of $\bar{\Omega}^\varphi$,

$$\int_{A^\varphi} \mathbf{ox}^\varphi \wedge \mathbf{f}^\varphi(\mathbf{x}^\varphi) dx^\varphi + \int_{\partial A^\varphi} \mathbf{ox}^\varphi \wedge \mathbf{t}^\varphi(\mathbf{x}^\varphi, \mathbf{n}^\varphi) dx^\varphi = \mathbf{0}. \quad (1.56)$$

The stress principle thus first asserts the existence of elementary **surface forces** $\mathbf{t}^\varphi(\mathbf{x}^\varphi, \mathbf{n}^\varphi) da^\varphi$ along the boundaries of all domains of the reference configuration (Fig. 1.3.).

Secondly, the stress principle asserts that at a point \mathbf{x}^φ of the boundary ∂A^φ of a sub-domain A^φ , the elementary surface force depends on the sub-domain A^φ , only via the normal vector \mathbf{n}^φ to ∂A^φ at \mathbf{x}^φ . While it would be equally conceivable a priori that the elementary surface force at \mathbf{x}^φ be also dependent on other geometrical properties of the sub-domain A^φ , for instance the curvature of ∂A^φ at \mathbf{x}^φ , etc., it is possible to rigorously rule out such further geometrical dependences by constructing a general theory of surfaces forces, as shown by Noll (1959).

Thirdly, the stress principle asserts that any sub-domain A^φ of the deformed configuration $\bar{\Omega}^\varphi$, including $\bar{\Omega}^\varphi$ itself, is in static equilibrium, in the sense that the torsor formed by the elementary forces $\mathbf{t}^\varphi(\mathbf{x}^\varphi, \mathbf{n}^\varphi) da^\varphi$, $\mathbf{x}^\varphi \in \partial A^\varphi$, \mathbf{n}^φ normal to ∂A^φ at \mathbf{x}^φ , and the body forces $\mathbf{f}^\varphi(\mathbf{x}^\varphi) d\mathbf{x}^\varphi$, $\mathbf{x}^\varphi \in A^\varphi$, is equivalent to zero.

This means that its resultant vector vanishes (axiom of force balance) and that its resulting moment with respect to the origin (and thus with respect to any other point, by a classical property of torsos) vanishes (axiom of moment balance).

Hence the stress principle mathematically express, in the form of an axiom, the intuitive idea that the static equilibrium of any sub-domain A^φ of $\bar{\Omega}^\varphi$, already subjected to given applied body forces $\mathbf{f}^\varphi(\mathbf{x}^\varphi) d\mathbf{x}^\varphi$, $\mathbf{x}^\varphi \in A^\varphi$, and (possibly) to given applied surface forces $\mathbf{g}^\varphi(\mathbf{x}^\varphi) da^\varphi$ at those points $\mathbf{x}^\varphi \in \Gamma_1^\varphi \cap \partial A^\varphi$ where the outer normal vector to $\Gamma_1^\varphi \cap \partial A^\varphi$ exists, is made possible by the added effect of elementary surfaces forces of the specific form indicated, acting on the remaining part of the boundary ∂A^φ .

Remark.

1. Gurtin (1981a, 1981b) calls system of forces the set formed by the applied body forces, corresponding to the vector field $\mathbf{f}^\varphi := \Omega^\varphi \rightarrow \mathbb{R}^3$ and by the surface forces, corresponding to the vector field $\mathbf{t}^\varphi := \Omega^\varphi \times S_1 \rightarrow \mathbb{R}^3$.

Let \mathbf{x}^φ be a point of the deformed configuration. The vector $\mathbf{t}^\varphi(\mathbf{x}^\varphi, \mathbf{n}^\varphi)$ is called the Cauchy stress vector across an oriented surface element with normal \mathbf{n}^φ , or the density of the surface force per unit area in the deformed configuration.

2.3. Cauchy's theorem; The Cauchy stress tensor

We now derive consequences of paramount importance from the stress principle. The first one, due to Cauchy (1823, 1827a), is one of the most important results in continuum mechanics. It asserts that the dependence of the Cauchy stress vector $\mathbf{t}^\varphi(\mathbf{x}^\varphi, \mathbf{n}^\varphi)$ with respect to its second argument $\mathbf{n} \in S_1$ is linear, i.e., at each point $\mathbf{x}^\varphi \in \Omega^\varphi$, there exists a tensor $\mathbf{T}^\varphi(\mathbf{x}^\varphi) \in \mathbb{M}^3$ such that $\mathbf{t}^\varphi(\mathbf{x}^\varphi, \mathbf{n}^\varphi) = \mathbf{T}^\varphi(\mathbf{x}^\varphi) \mathbf{n}$ for all $\mathbf{n} \in S_1$; the second one asserts that at each point $\mathbf{x}^\varphi \in \Omega^\varphi$, the tensor $\mathbf{T}^\varphi(\mathbf{x}^\varphi)$ is symmetric; the third one, again due to Cauchy (1827b, 1828), is that the tensor field $\mathbf{T}^\varphi : \Omega^\varphi \rightarrow \mathbb{M}^3$ and the vector fields $\mathbf{f}^\varphi : \Omega^\varphi \rightarrow \mathbb{R}^3$ and $\mathbf{g}^\varphi := \Gamma_1^\varphi \rightarrow \mathbb{R}^3$ are related by a partial differential equation in Ω^φ , and by a boundary condition on Γ_1^φ , respectively.

Theorem 1.2. (Cauchy's theorem). Assume that the applied body force density $\mathbf{f}^\varphi : \Omega^\varphi \rightarrow \mathbb{R}^3$ is continuous, and that the Cauchy stress vector field

$$\mathbf{t}^\varphi : (\mathbf{x}^\varphi, \mathbf{n}^\varphi) \in \bar{\Omega}^\varphi \times S_1 \rightarrow \mathbf{t}^\varphi(\mathbf{x}^\varphi, \mathbf{n}) \in \mathbb{R}^3 \quad (1.57)$$

is continuously differentiable with respect to the variable $\mathbf{x}^\varphi \in \bar{\Omega}^\varphi$ for each $\mathbf{n} \in S_1$ and continuous with respect to the variable $\mathbf{n} \in S_1$ for each $\mathbf{x}^\varphi \in \bar{\Omega}^\varphi$. Then the axioms of force and moment balance imply that there exists a continuously differentiable tensor field

$$\mathbf{T}^\varphi : \mathbf{x}^\varphi \in \bar{\Omega}^\varphi \rightarrow \mathbf{T}^\varphi(\mathbf{x}^\varphi) \in \mathbb{M}^3, \quad (1.58)$$

such that the Cauchy stress vector satisfies

$$\mathbf{t}^\varphi(\mathbf{x}^\varphi, \mathbf{n}) = \mathbf{T}^\varphi(\mathbf{x}^\varphi) \mathbf{n} \quad \text{for all } \mathbf{x}^\varphi \in \bar{\Omega}^\varphi \quad \text{and all } \mathbf{n} \in S_1, \quad (1.59)$$

and such that

$$-\operatorname{div}^\varphi \mathbf{T}^\varphi(\mathbf{x}^\varphi) = \mathbf{f}^\varphi(\mathbf{x}^\varphi) \quad \text{for all } \mathbf{x}^\varphi \in \Omega^\varphi, \quad (1.60)$$

$$\mathbf{T}^\varphi(\mathbf{x}^\varphi) = \mathbf{T}^\varphi(\mathbf{x}^\varphi)^T \quad \text{for all } \mathbf{x}^\varphi \in \bar{\Omega}^\varphi, \quad (1.61)$$

$$\mathbf{T}^\varphi(\mathbf{x}^\varphi) \mathbf{n}^\varphi = \mathbf{g}^\varphi(\mathbf{x}^\varphi) \quad \text{for all } \mathbf{x}^\varphi \in \Gamma_1^\varphi \quad (1.62)$$

where \mathbf{n}^φ is the unit outer normal vector along Γ_1^φ .

The symmetry tensor \mathbf{T}^φ is called the Cauchy stress tensor at the point $\mathbf{x}^\varphi \in \bar{\Omega}^\varphi$. It is helpful to keep in mind the interpretation of its elements $\mathbf{T}_{ij}^\varphi(\mathbf{x}^\varphi)$: Since $\mathbf{t}^\varphi(x^\varphi, \mathbf{e}_j) = \mathbf{T}_{ij}^\varphi(\mathbf{x}^\varphi) \cdot \mathbf{e}_i$, the elements of the j -th row of the tensor $\mathbf{T}^\varphi(x^\varphi)$ represent the components of the Cauchy stress vector $\mathbf{t}^\varphi(x^\varphi, \mathbf{n})$ at the point \mathbf{x}^φ corresponding to the particular choice $\mathbf{n} = \mathbf{e}_j$ (Fig. 1.4. where the case $j=1$ is considered). The knowledge of the three vectors $\mathbf{t}^\varphi(x^\varphi, \mathbf{e}_j)$ in turn completely determines the Cauchy stress vector $\mathbf{t}^\varphi(x^\varphi, \mathbf{n})$ for an arbitrary vector $\mathbf{n} = n_i \mathbf{e}_i \in S_1$, since

$$\mathbf{t}^\varphi(x^\varphi, \mathbf{n}) = n_j \mathbf{t}^\varphi(x^\varphi, \mathbf{e}_j) \quad (1.63)$$

This observation is used in the drawing of figures, where the Cauchy stress vector is often represented on three mutually perpendicular faces of a rectangular parallelepiped.

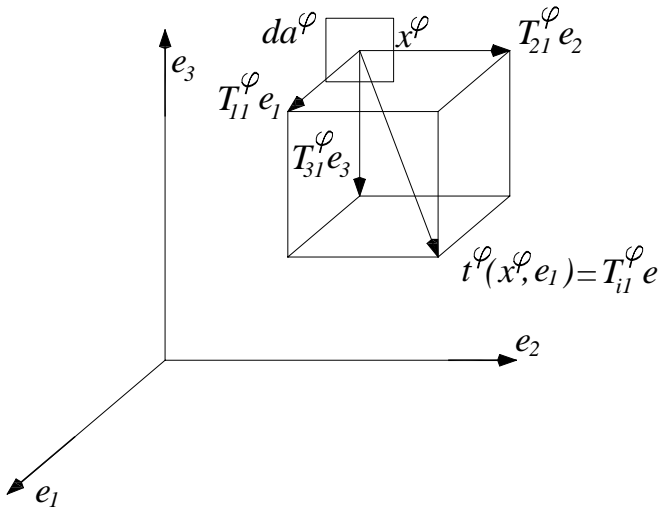


Fig. 1.4.

Interpretation of the elements \mathbf{T}_{i1}^φ of the Cauchy stress tensor $\mathbf{T}^\varphi = (T_{ij}^\varphi)$.

2.4. The equation of equilibrium and the principle of virtual work in the deformed configuration

As shown in Theorem 1.2., the axioms of force and moment balance imply that the Cauchy stress tensor field $\mathbf{T}^\varphi : \bar{\Omega}^\varphi \rightarrow \mathbb{S}^3$ satisfies a boundary value problem expressed in terms of the Euler variable x^φ over the deformed configuration, comprising the partial differential equation $-\text{div}^\varphi \mathbf{T}^\varphi = \mathbf{f}^\varphi$ in Ω^φ and the boundary condition $\mathbf{T}^\varphi \mathbf{n}^\varphi = \mathbf{g}^\varphi$ on Γ_1^φ . A remarkable property of this boundary value problem, due to its “divergence form”, is that it can be given a variational formulation, as we now show. In what follows, $\mathbf{u} \cdot \mathbf{v} = u_i v_i$ denotes the Euclidean vector inner product, $\mathbf{A} : \mathbf{B} = A_{ij} B_{ji} = \text{tr } \mathbf{A}^T \mathbf{B}$ denotes the matrix inner product, and $\nabla^\varphi \boldsymbol{\theta}^\varphi$ denotes the matrix $(\partial_j^\varphi \theta_i^\varphi)$.

Theorem 1.3. The boundary value problem:

$$\begin{aligned} -\text{div}^\varphi \mathbf{T}^\varphi &= \mathbf{f}^\varphi & \text{in } \Omega^\varphi \\ \mathbf{T}^\varphi \mathbf{n}^\varphi &= \mathbf{g}^\varphi & \text{on } \Gamma_1^\varphi \end{aligned} \quad (1.64)$$

Is formally equivalent to the variational equations:

$$\int_{\Omega^\varphi} \mathbf{T}^\varphi : \nabla^\varphi \boldsymbol{\theta}^\varphi dx^\varphi = \int_{\Omega^\varphi} \mathbf{f}^\varphi \cdot \boldsymbol{\theta}^\varphi dx^\varphi + \int_{\Gamma_1^\varphi} \mathbf{g}^\varphi \cdot \boldsymbol{\theta}^\varphi dx^\varphi \quad (1.65)$$

valid for all smooth enough vector fields: $\boldsymbol{\theta}^\varphi : \Omega^\varphi \rightarrow \mathbb{R}^3$ that satisfy

$$\boldsymbol{\theta}^\varphi = \mathbf{0} \quad \text{on } \Gamma_o^\varphi := \Gamma^\varphi - \Gamma_1^\varphi. \quad (1.66)$$

The equation

$$\begin{aligned} -\text{div}^\varphi \mathbf{T}^\varphi &= \mathbf{f}^\varphi & \text{in } \Omega^\varphi, \\ \mathbf{T}^\varphi &= (\mathbf{T}^\varphi)^T & \text{in } \Omega^\varphi, \\ \mathbf{T}^\varphi \mathbf{n}^\varphi &= \mathbf{g}^\varphi & \text{on } \Gamma_1^\varphi, \end{aligned} \quad (1.67)$$

are called the equations of equilibrium in the deformed configuration, while the associated variational equations (1.65) of Theorem 1.3. constitute the principle of virtual work in the deformed configuration.

2.5. The Piola-Kirchhoff stress tensors

Our final objective is to determine the deformation field and the Cauchy stress tensor field that arise in a body subjected to a given system of applied forces. In this respect, the equations of equilibrium in the deformed configuration are of not much avail, since they are expressed in terms of the Euler variable $\mathbf{x}^\varphi = \varphi(x)$, which is precisely one of the unknowns. To obviate this difficulty, we shall rewrite these equations in terms of the Lagrange variable x that is attached to the reference configuration, which is considered as being given once and for all. More specifically, we shall transform the left-hand sides $\operatorname{div}^\varphi \mathbf{T}^\varphi$ and $\mathbf{T}^\varphi \mathbf{n}^\varphi$ and the right-hand sides \mathbf{f}^φ and \mathbf{g}^φ appearing in the equations of equilibrium over $\bar{\Omega}^\varphi$ into similar expressions over $\bar{\Omega}$.

We defined the Piola transform: $\mathbf{T} : \bar{\Omega} \rightarrow \mathbb{M}^3$ of a tensor field $\mathbf{T}^\varphi : \bar{\Omega}^\varphi = \varphi(\bar{\Omega}) \rightarrow \mathbb{M}^3$ by letting

$$\mathbf{T}(x) = (\det \nabla \varphi(x)) \mathbf{T}^\varphi(x^\varphi) \nabla \varphi(x)^{-T}, \quad x^\varphi = \varphi(x). \quad (1.68)$$

We shall therefore apply this transform to the Cauchy stress tensor \mathbf{T}^φ , in which case its Piola transform \mathbf{T} is called the first Piola-Kirchhoff stress tensor. As shown in theorem 1 (chapter 1a), the main advantage of this transform is to induce a particularly simple relation between the divergences of both tensors:

$$\operatorname{div} \mathbf{T}(x) = (\det \nabla \varphi(x)) \operatorname{div}^\varphi \mathbf{T}^\varphi(x^\varphi), \quad x^\varphi = \varphi(x). \quad (1.69)$$

As a consequence, the equations of equilibrium over the deformed configuration will be transformed into equations over the reference configuration that have a similar divergence structure. This property in turn makes it possible to write these partial differential equations in variational form.

One can likewise transform the Cauchy stress vector $\mathbf{t}^\varphi(x^\varphi, \mathbf{n}) = \mathbf{T}^\varphi(x^\varphi) \mathbf{n}^\varphi$ into a vector $\mathbf{t}(x, \mathbf{n})$ in such a way that the relation

$$\mathbf{t}(x, \mathbf{n}) = \mathbf{T}(x) \mathbf{n}, \quad (1.70)$$

holds, where $\mathbf{T}(x)$ is the first Piola-Kirchhoff stress tensor and where \mathbf{n} and \mathbf{n}^φ are the corresponding normal vectors at the points x and $x^\varphi = \varphi(x)$ of the boundaries of corresponding sub-domains A and $A^\varphi = \varphi(A)$. Notice that there is no ambiguity in this process since the normal vector \mathbf{n}^φ at the point

$\mathbf{x}^\varphi = \varphi(x)$ is the same for all sub-domains whose boundary passes through the point x with \mathbf{n} as the normal vector there. In view of the relation $\mathbf{T}(x)\mathbf{n}da = \mathbf{T}^\varphi(x^\varphi)\mathbf{n}^\varphi da^\varphi$ established in Theorem 1.1., it suffices to define the vector $\mathbf{t}(x, \mathbf{n})$ by the relation:

$$\mathbf{t}(x, \mathbf{n})da = \mathbf{t}^\varphi(x^\varphi, \mathbf{n}^\varphi)da^\varphi. \quad (1.71)$$

Since $\mathbf{t}^\varphi(x^\varphi, \mathbf{n}) = \mathbf{T}^\varphi(x^\varphi)\mathbf{n}^\varphi$ by Cauchy's theorem, the desired relation $\mathbf{t}(x, \mathbf{n}) = \mathbf{T}(x)\mathbf{n}$ holds.

The vector $\mathbf{t}(x, \mathbf{n})$ is called the **first Piola-Kirchhoff stress vector** at the point x of the reference configuration, across the oriented surface element with normal \mathbf{n} . The vector field $\mathbf{t} : \bar{\Omega} \times S_1 \rightarrow \mathbb{R}^3$ defined in this fashion thus measures the density of the surface force per unit area in the reference configuration.

While the Cauchy stress tensor $\mathbf{T}^\varphi(x^\varphi)$ is symmetric (Theorem 1.2.) the first Piola-Kirchhoff stress tensor $\mathbf{T}(x)$ is not symmetric in general; instead one has:

$$\mathbf{T}(x)^T = \nabla \varphi(x)^{-1} \mathbf{T}(x) \nabla \varphi(x)^{-T}. \quad (1.72)$$

It is nevertheless desirable to define a symmetric stress tensor in the reference configuration, essentially because the constitutive equation in the reference configuration then takes a simpler form. More specifically, we define the **second Piola-Kirchhoff stress tensor** $\Sigma(x)$ by letting

$$\Sigma(x) = \nabla \varphi(x)^{-1} \mathbf{T}(x) = (\det \nabla \varphi(x)) \nabla \varphi(x)^{-1} \mathbf{T}^\varphi(x^\varphi) \nabla \varphi(x)^{-T}, \quad (1.73)$$

$$x^\varphi = \varphi(x)$$

Remarks.

- (1) In fact, the question of whether or not the matrix $\mathbf{T}(x)$ is symmetric does not make sense for, as a tensor, it has one index attached to the reference configuration and one index attached to the deformed configuration. A complete discussion of these aspect can be found in Marsden & Hughes (1983)-
- (2) Historical reference on the Piola-Kirchhoff stress tensors are given in Truesdell & Toupin (1960).

The Piola-Kirchhoff stress tensor $\mathbf{T}(x)$ and $\Sigma(\mathbf{x})$ both depend on the deformation $\boldsymbol{\varphi}$, first through the Piola transform itself, secondly because the Cauchy stress tensor also dependent on $\boldsymbol{\varphi}$.

2.6. The equation of equilibrium and the principle of virtual work in the reference configuration

It remains to transform the applied forces densities that appear in the equilibrium equations over the deformed configuration. First, with the density $\mathbf{f}^\varphi : \Omega^\varphi \rightarrow \mathbb{R}^3$ of the applied force per unit volume in the deformed configuration, we associate a vector field $\mathbf{f} : \Omega \rightarrow \mathbb{R}^3$ in such a way that

$$\mathbf{f}(x)dx = \mathbf{f}^\varphi(x^\varphi)dx^\varphi \text{ for all } x^\varphi = \varphi(x) \in \Omega^\varphi \quad (1.74)$$

where dx and dx^φ denote the corresponding volume elements. Since

$$dx^\varphi = (\det \nabla \boldsymbol{\varphi}(x)) \mathbf{f}^\varphi(x^\varphi), \quad x^\varphi = \varphi(x), \quad (1.75)$$

so that the vector $\mathbf{f}(x)$ depends on the deformation $\boldsymbol{\varphi}$, via the factor $\det \nabla \boldsymbol{\varphi}(x)$ on the one hand, and via the possible dependence of the density \mathbf{f}^φ on the deformation $\boldsymbol{\varphi}$ on the other hand. Notice that this relation displays the same factor $\det \nabla \boldsymbol{\varphi}(x)$ as the relation between the vectors $\mathbf{div} \mathbf{T}(x)$ and $\mathbf{div}^\varphi \mathbf{T}^\varphi(x^\varphi)$.

The vector field $\mathbf{f} : \Omega \rightarrow \mathbb{R}^3$ measures the density of the applied body force per unit volume in the reference configuration; the vector $\mathbf{f}(x)$ is defined in such a way that the elementary vector $\mathbf{f}(x)dx$ is equal to the elementary body force $\mathbf{f}(x^\varphi)dx^\varphi$ acting on the corresponding volume element dx^φ at the point $x^\varphi = \varphi(x)$ (Figure 1.5.).

Let: $\rho : \Omega \rightarrow \mathbb{R}$ denote the mass density in the reference configuration. Expressing that the mass of the elementary volumes dx and $dx^\varphi = \det \nabla \boldsymbol{\varphi}(x)dx$ is the same, we find the mass densities $\rho : \Omega \rightarrow \mathbb{R}$ and $\rho^\varphi : \Omega^\varphi \rightarrow \mathbb{R}$ are related by the equation

$$\rho(x) = \det \nabla \boldsymbol{\varphi}(x) \rho^\varphi(x^\varphi), \quad x^\varphi = \varphi(x). \quad (1.76)$$

Incidentally, this relation also shows that, regardless of any consideration concerning the preservation of orientation, the Jacobian $\det \nabla \boldsymbol{\varphi}(x)$ should not vanish in an actual deformation, since mass density is always > 0 , at least macroscopically.

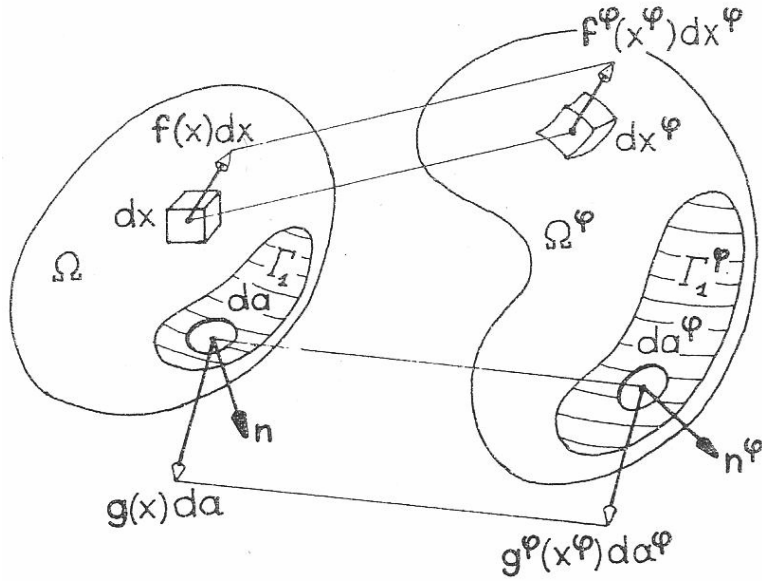


Fig. 1.5.

The applied body force and surface force densities in the deformed configuration and in the reference configuration

Then if we define the density $\mathbf{b} : \Omega \rightarrow \mathbb{R}^3$ of the applied body forces per unit mass in the reference configuration by letting

$$\mathbf{f}(x) = \rho(x)\mathbf{b}(x) \text{ for all } x \in \Omega \quad (1.77)$$

it follows that the densities of the applied force per unit mass are related by

$$\mathbf{b}(x) = \mathbf{b}^\varphi(x^\varphi), \quad x^\varphi = \varphi(x). \quad (1.78)$$

Secondly, in order to transform the boundary condition $\mathbf{T}^\varphi \mathbf{n}^\varphi = \mathbf{g}^\varphi$ over $\Gamma_1^\varphi = \varphi(\Gamma_1)$ into a similar condition over Γ_1 , it suffices to use the first Piola-Kirchhoff stress vector, which was precisely defined for this purpose: With the

density $\mathbf{g}^\varphi : \Gamma_1^\varphi \rightarrow \mathbb{R}^3$ of the applied surface force per unit area in the deformed configuration, we associate the vector field $\mathbf{g} : \Gamma_1 \rightarrow \mathbb{R}^3$ defined by

$$\mathbf{g}(x) da = \mathbf{g}^\varphi(x^\varphi) da^\varphi \text{ for all } x^\varphi = \varphi(x) \in \Gamma_1^\varphi \quad (1.79)$$

where da and da^φ are the corresponding area elements. Hence by Theorem 1.1 (Properties of the Piola transform), the vector $\mathbf{g}(x)$ is given by

$$\mathbf{g}(x) = \det \nabla \varphi(x) \left| \nabla \varphi(x)^{-T} \mathbf{n} \right| \mathbf{g}^\varphi(x^\varphi). \quad (1.80)$$

Notice that the vector $\mathbf{g}(x)$ depends on the deformation φ , via the formula relating the corresponding area elements on the one hand and via the possible dependence of the density, \mathbf{g}^φ on the deformation φ on the other hand. The vector field $\mathbf{g} : \Gamma_1 \rightarrow \mathbb{R}^3$ measures the density of the applied surface force per unit area in the reference configuration; it is defined in such a way that the elementary vector $\mathbf{g}(x) da$ is equal to the elementary surface force $\mathbf{g}^\varphi(x^\varphi) da^\varphi$ acting on the corresponding area element da^φ at the point $x^\varphi = \varphi(x)$ (Fig. 1.5).

We can now establish the analogous of Theorem 1.3 over the reference configuration:

Theorem 1.4. The first Piola-Kirchhoff stress tensor

$$\mathbf{T}(x) = (\det \nabla \varphi(x)) \mathbf{T}^\varphi(x^\varphi) \nabla \varphi(x)^{-T} \quad (1.81)$$

satisfies the following equations in the reference configuration $\bar{\Omega}$:

$$\begin{aligned} -\operatorname{div} \mathbf{T}(x) &= \mathbf{f}(x), \quad x \in \Omega, \\ \nabla \varphi(x) \mathbf{T}(x)^T &= \mathbf{T}(x) \nabla \varphi(x)^T, \quad x \in \Omega, \\ \mathbf{T}(x) \mathbf{n} &= \mathbf{g}(x), \quad x \in \Gamma_1 \end{aligned} \quad (1.82)$$

where $\mathbf{f} dx = \mathbf{f}^\varphi dx^\varphi$, $\mathbf{g} da = \mathbf{g}^\varphi da^\varphi$. The first and third equations are together equivalent to the variational equations:

$$\int_{\Omega} \mathbf{T} : \nabla \boldsymbol{\theta} dx = \int_{\Omega} \mathbf{f} \cdot \boldsymbol{\theta} dx + \int_{\Gamma_1} \mathbf{g} \cdot \boldsymbol{\theta} da, \quad (1.83)$$

valid for all smooth enough vector fields $\boldsymbol{\theta} : \bar{\Omega} \rightarrow \mathbb{R}^3$ that satisfy

$$\boldsymbol{\theta} = \mathbf{0} \quad \text{on} \quad \Gamma_0 = \Gamma - \Gamma_1. \quad (1.84)$$

In terms of the second Piola-Kirchhoff stress tensor, the above result becomes:

Theorem 1.5. The second Piola-Kirchhoff stress tensor

$$\boldsymbol{\Sigma}(x) = (\det \nabla \boldsymbol{\varphi}(x)) \nabla \boldsymbol{\varphi}(x)^{-1} \mathbf{T}^\varphi(x^\varphi) \nabla \boldsymbol{\varphi}(x)^{-T} \quad (1.85)$$

satisfies the following equations in the reference configuration $\bar{\Omega}$:

$$\begin{aligned} -\operatorname{div}(\nabla \boldsymbol{\varphi}(x) \boldsymbol{\Sigma}(x)) &= \mathbf{f}(x), \quad x \in \bar{\Omega}, \\ \boldsymbol{\Sigma}(x) &= \boldsymbol{\Sigma}(x)^T, \quad x \in \Omega, \\ \nabla \boldsymbol{\varphi}(x) \boldsymbol{\Sigma}(x) \mathbf{n} &= \mathbf{g}(x), \quad x \in \Gamma_1 \end{aligned} \quad (1.86)$$

The first and third equations are together equivalent to the variational equations

$$\int_{\Omega} \nabla \boldsymbol{\varphi} \boldsymbol{\Sigma} : \nabla \boldsymbol{\theta} dx = \int_{\Omega} \mathbf{f} \cdot \boldsymbol{\theta} dx + \int_{\Gamma_1} \mathbf{g} \cdot \boldsymbol{\theta} da \quad (1.87)$$

valid for all smooth enough maps $\boldsymbol{\theta} : \bar{\Omega} \rightarrow \mathbb{R}^3$ that satisfy

$$\boldsymbol{\theta} = \mathbf{0} \quad \text{on} \quad \Gamma_0 = \Gamma - \Gamma_1 \quad (1.88)$$

The equations satisfied over Ω and Γ_1 by either stress tensor are called the equations of equilibrium in the reference configuration, and their associated variational equations constitute the principal of virtual work in the reference configuration. The equation on Γ_1 is called a boundary condition of traction.

3. LINEAR ANISOTROPIC ELASTIC MEDIA

The relation between stress and strain in an anisotropic elastic material are presented in this section. A linear anisotropic elastic material can have as many as 21 elastic constants. This number is reduced when the material possesses a certain material symmetry. The number of elastic constants is also reduced, in most cases, when a two-dimensional deformation is considered. An important condition on elastic constants is that the strain energy must be positive. This condition implies that the 6x6 matrices of elastic constants presented herein must be positive definite.

3.1. Elastic Stiffnesses

Referring to a fixed rectangular coordinate system x_1, x_2, x_3 , let σ_{ij} and ε_{ij} be the stress and strain, respectively, in an anisotropic elastic material. The stress-strain law can be written as

$$\sigma_{ij} = C_{ijkl} \varepsilon_{kl} \quad (1.89)$$

in which C_{ijkl} , are the *elastic stiffnesses* which are components of a fourth rank tensor. They satisfy the full symmetry conditions

$$C_{ijkl} = C_{jikl}, \quad C_{ijkl} = C_{ijlk}, \quad C_{ijkl} = C_{klij}. \quad (1.90)$$

Before we present justifications for the three conditions in (1.90), we show that $(1.90)_1$ and $(1.90)_3$ imply $(1.90)_2$. Using $(1.90)_3$, $(1.90)_1$ and $(1.90)_3$ in that order we have

$$C_{ijkl} = C_{klij} = C_{lkij} = C_{ijlk}$$

which proves $(1.90)_2$. Therefore the three conditions in (1.90) are written as

$$C_{ijkl} = C_{jikl} = C_{klij}. \quad (1.91)$$

One can also show that $(1.90)_2$ and $(1.90)_3$ imply $(1.90)_1$.

The first equation of (1.90) follows directly from the symmetry of the stress tensor $\sigma_{ij} = \sigma_{ji}$. The second equation of (1.90) does *not* follow directly from the symmetry of the strain tensor $\varepsilon_{ij} = \varepsilon_{ji}$. However, if the C_{ijkl} in (1.90) do not satisfy $(1.90)_2$, we rewrite (1.90) as

$$\sigma_{ij} = \frac{1}{2} C_{ijkl} \varepsilon_{kl} + \frac{1}{2} C_{ijlk} \varepsilon_{kl} = \frac{1}{2} C_{ijkl} \varepsilon_{kl} + \frac{1}{2} C_{ijlk} \varepsilon_{lk}$$

or since $\varepsilon_{lk} = \varepsilon_{kl}$,

$$\sigma_{ij} = \frac{1}{2} (C_{ijkl} + C_{ijlk}) \varepsilon_{kl}. \quad (1.92)$$

The coefficients of ε_{kl} are symmetric with the subscripts kl . We can therefore redefine the coefficients of ε_{kl} in (1.92) as the new C_{ijkl} which satisfy $(1.90)_2$.

The third equation follows from the consideration of strain energy. The strain energy W per unit volume of the material is

$$W = \int_0^{\varepsilon_{pq}} \sigma_{ij} d\varepsilon_{ij} = \int_0^{\varepsilon_{pq}} C_{ijkl} \varepsilon_{kl} d\varepsilon_{ij} . \quad (1.93)$$

We demand that the integral be independent of the path ε_{ij} takes from 0 to ε_{pq} .

If not, say path 1 yields a larger integral than path 2, one can consider loading the material from 0 to ε_{pq} through path 1, and unloading from ε_{pq} to 0 through the reverse of path 2. The energy gained is the difference between the W 's for path 1 and path 2. If we repeat the process we can extract unlimited amount of energy from the material, which is physically impossible for a real material. Therefore the integral in (1.93) must be independent of the path taken by ε_{ij} , and W depends on the final strain ε_{pq} only. This implies that the integrand must be the total differential dW , i.e.,

$$C_{ijkl} \varepsilon_{kl} d\varepsilon_{ij} = dW = \frac{\partial W}{\partial \varepsilon_{ij}} d\varepsilon_{ij} . \quad (1.94)$$

Since $d\varepsilon_{ij}$ is arbitrary we must have

$$\sigma_{ij} = C_{ijkl} \varepsilon_{kl} = \frac{\partial W}{\partial \varepsilon_{ij}} \quad (1.95)$$

in which the first equality follows from (1.89). Differentiation of (1.95) with ε_{kl} leads to

$$C_{ijkl} = \frac{\partial^2 W}{\partial \varepsilon_{kl} \partial \varepsilon_{ij}}$$

The double differentiations on the right are interchangeable. Therefore

$$C_{ijkl} = C_{klij}$$

is the condition for the integral in (1.93) to be Independent of the loading path.

This proves (1.90)₃. With (1.90)₃, (1.94) is written as

$$dW = C_{ijkl} \varepsilon_{kl} d\varepsilon_{ij} = \frac{1}{2} d(C_{ijkl} \varepsilon_{ij} \varepsilon_{kl}).$$

Hence

$$W = \frac{1}{2} C_{ijkl} \varepsilon_{ij} \varepsilon_{kl} = \frac{1}{2} \sigma_{ij} \varepsilon_{ij}. \quad (1.96)$$

and since the strain energy must be positive, it results

$$C_{ijkl} \varepsilon_{ij} \varepsilon_{kl} > 0 \quad (1.97)$$

for any real, nonzero, symmetric tensor ε_{kl} .

3.2. Elastic Compliances

The inverse of (1.89) is written as

$$\varepsilon_{ij} = S_{ijkl} \sigma_{kl} \quad (1.98)$$

where S_{ijkl} are the elastic compliance which are components of a four rank tensor. They also possess the full symmetry

$$S_{ijkl} = S_{jikl}, \quad S_{ijkl} = S_{ijlk}, \quad S_{ijkl} = S_{klij} \quad (1.99)$$

or, as in (1.91)

$$S_{ijkl} = S_{jikl} = S_{klij}. \quad (1.100)$$

The justifications of the first and second equations in (1.101) are similar to their counterparts in (1.102). The justification of (1.103)₃ also follows from the energy consideration. Integration by parts of (1.104)₁ leads to

$$W = \sigma_{pq} \varepsilon_{pq} - \int_0^{\sigma_{pq}} \varepsilon_{ij} d\sigma_{ij} = \sigma_{pq} \varepsilon_{pq} - \int_0^{\sigma_{pq}} S_{ijkl} \sigma_{kl} d\sigma_{ij}.$$

If W depends on the final strain ε_{pq} it depends on the final stress σ_{pq} . The last integral which represents the *complementary energy* must be independent of the path σ_{ij} takes from 0 to the final stress σ_{pq} . Following a similar argument for

C_{ijkl} , we deduce that (1.105)₃ must hold for the integral to be path independent. Since the strain energy must be positive, the substitution of the (1.98) into the (1.96) yields

$$S_{ijkl}\sigma_{ij}\sigma_{kl} > 0 \quad (1.106)$$

3.3. Contracted Notations

Introducing the contracted notation (Voigt, 1928; Lekhnitskii, 1963; Christensen, 1979)

$$\sigma_{11} = \sigma_1, \quad \sigma_{22} = \sigma_2, \quad \sigma_{33} = \sigma_3, \quad (1.107)$$

$$\sigma_{32} = \sigma_4, \quad \sigma_{31} = \sigma_5, \quad \sigma_{12} = \sigma_6,$$

$$\varepsilon_{11} = \varepsilon_1, \quad \varepsilon_{22} = \varepsilon_2, \quad \varepsilon_{33} = \varepsilon_3, \quad (1.108)$$

$$2\varepsilon_{32} = \varepsilon_4, \quad 2\varepsilon_{31} = \varepsilon_5, \quad 2\varepsilon_{12} = \varepsilon_6,$$

the stress-strain law (1.89) and (1.90) can be written as

$$\sigma_\alpha = C_{\alpha\beta}\varepsilon_\beta, \quad C_{\alpha\beta} = C_{\beta\alpha}, \quad (1.109)$$

or, in matrix notation,

$$\mathbf{T} = \mathcal{C}\mathbf{E}, \quad \mathcal{C} = \mathcal{C}^T. \quad (1.110)$$

In the above \mathbf{T} and \mathbf{E} are 6×1 column matrices and \mathcal{C} is the 6×6 symmetric matrix given by

$$\mathcal{C} = \begin{bmatrix} C_{11} & C_{12} & C_{13} & C_{14} & C_{15} & C_{16} \\ C_{12} & C_{22} & C_{23} & C_{24} & C_{25} & C_{26} \\ C_{13} & C_{23} & C_{33} & C_{34} & C_{35} & C_{36} \\ C_{14} & C_{24} & C_{34} & C_{44} & C_{45} & C_{46} \\ C_{15} & C_{25} & C_{35} & C_{45} & C_{55} & C_{56} \\ C_{16} & C_{26} & C_{36} & C_{46} & C_{56} & C_{66} \end{bmatrix} \quad (1.111)$$

The transformation between C_{ijkl} and $C_{\alpha\beta}$ is accomplished by replacing the subscripts ij (or kl) by α (or β) using the following rules:

$$\begin{aligned}
 ij(\text{or } kl) &\leftrightarrow \alpha(\text{or } \beta) \\
 11 &\leftrightarrow 1 \\
 22 &\leftrightarrow 2 \\
 33 &\leftrightarrow 3 \\
 32 \text{ or } 23 &\leftrightarrow 4 \\
 31 \text{ or } 13 &\leftrightarrow 5 \\
 12 \text{ or } 21 &\leftrightarrow 6
 \end{aligned} \tag{1.112}$$

The presence of the factor 2 in (1.108)₄₋₅₋₆ but not in (1.107)₄₋₅₋₆ is necessary for the symmetry of \mathcal{C} .

Analogously, with reference to the equation (1.107) and (1.108), the stress-strain law in the form (1.98) may be expressed in a matrix form, as it follows:

$$\mathbf{E} = \mathcal{S} \mathbf{T}, \quad \mathcal{S} = \mathcal{S}^T \tag{1.113}$$

where the compliance tensor \mathcal{S} is expressed in form of the 6×6 symmetric matrix, given by:

$$\mathcal{S} = \begin{bmatrix} S_{11} & S_{12} & S_{13} & S_{14} & S_{15} & S_{16} \\ S_{12} & S_{22} & S_{23} & S_{24} & S_{25} & S_{26} \\ S_{13} & S_{23} & S_{33} & S_{34} & S_{35} & S_{36} \\ S_{14} & S_{24} & S_{34} & S_{44} & S_{45} & S_{46} \\ S_{15} & S_{25} & S_{35} & S_{45} & S_{55} & S_{56} \\ S_{16} & S_{26} & S_{36} & S_{46} & S_{56} & S_{66} \end{bmatrix} \tag{1.114}$$

Note that the transformation between S_{ijkl} and $S_{\alpha\beta}$ is similar to that one between C_{ijkl} and $C_{\alpha\beta}$ except the following:

$$\begin{aligned}
 S_{ijhk} &= S_{\alpha\beta} \quad \text{if both } \alpha, \beta \leq 3 \\
 2S_{ijhk} &= S_{\alpha\beta} \quad \text{if either } \alpha \text{ or } \beta \leq 3 \\
 4S_{ijhk} &= S_{\alpha\beta} \quad \text{if both } \alpha, \beta > 3.
 \end{aligned} \tag{1.115}$$

From (1.110)₁ and (1.113)₁, it is obtained the expression of the strain energy, the strain energy W becomes:

$$W = \frac{1}{2} \mathbf{T}^T \mathbf{E} = \frac{1}{2} \mathbf{E}^T \mathcal{C} \mathbf{E} = \mathbf{T}^T \mathcal{S} \mathbf{T} \quad (1.116)$$

and, for the positiveness of W , it must be:

$$\begin{aligned} \mathbf{E}^T \mathcal{C} \mathbf{E} &> 0 \\ \mathbf{T}^T \mathcal{S} \mathbf{T} &> 0 \end{aligned} \quad (1.117)$$

This implies that the matrices \mathcal{C} and \mathcal{S} are both positive definite. Moreover, the substitution of the (1.113)₁ into the (1.110)₁ yields:

$$\mathcal{C} \mathcal{S} = \mathbb{I} = \mathcal{S} \mathcal{C} \quad (1.118)$$

where the second equality follows from the first one which says that \mathcal{C} and \mathcal{S} are the inverses of each other and, hence their product commute.

3.4. Material Symmetry

The 6×6 matrices \mathcal{C} and \mathcal{S} contain 21 independent elastic constants. The number of independent constants is reduced when the material possesses a certain material symmetry.

Under an orthogonal transformation

$$x_i^* = Q_{ij} x_j \quad \text{or} \quad \mathbf{x}^* = \mathbf{Q} \mathbf{x} \quad (1.119)$$

in which \mathbf{Q} is an orthogonal matrix that satisfies the that satisfies the relations:

$$\mathbf{Q} \cdot \mathbf{Q}^T = \mathbf{I} = \mathbf{Q}^T \mathbf{Q}, \quad (1.120)$$

the four rank elasticity tensor C_{ijkl}^* , referred to the x_i^* coordinate system becomes

$$C_{ijkl}^* = Q_{ip} Q_{jq} Q_{kr} Q_{ls} C_{pqrs} \quad (1.121)$$

If it results $C_{ijkl}^* = C_{ijkl}$, i.e.,

$$C_{ijkl} = Q_{ip} Q_{jq} Q_{kr} Q_{ls} C_{pqrs} \quad (1.122)$$

material is said to possess a *symmetry* with respect to \mathbf{Q} .

An anisotropic material possesses the symmetry of *central inversion* if (1.122) is satisfied for

$$\mathbf{Q} = \begin{bmatrix} -1 & 0 & 0 \\ 0 & -1 & 0 \\ 0 & 0 & -1 \end{bmatrix} = -\mathbf{I}. \quad (1.123)$$

It is obvious that the (1.122) is satisfied by the \mathbf{Q} given in the (1.123) for any C_{ijkl} . Therefore, all the anisotropic materials have the symmetry of central inversion.

If \mathbf{Q} is a proper orthogonal matrix, the transformation (1.119) represents a rigid body rotation about an axis. So, an anisotropic material is said to possess a *rotational symmetry* if the (1.122) is satisfied for:

$$\mathbf{Q}^r(\theta) = \begin{bmatrix} \cos \theta & \sin \theta & 0 \\ -\sin \theta & \cos \theta & 0 \\ 0 & 0 & 1 \end{bmatrix} \quad (1.124)$$

which represents, for example, a rotation about the x_3 -axis an angle θ .

An orthogonal transformation \mathbf{Q} is a *reflection* if

$$\mathbf{Q} = \mathbf{I} - 2\mathbf{n} \otimes \mathbf{n}^T \quad (1.125)$$

where \mathbf{n} is a unit vector normal to the reflection plane. If \mathbf{m} is any vector on the plane,

$$\mathbf{Q}\mathbf{n} = -\mathbf{n}, \quad \mathbf{Q}\mathbf{m} = \mathbf{m}. \quad (1.126)$$

Thus a vector normal to the reflection plane reverses its direction after the transformation while a vector on the reflection plane remains unchanged. When (1.122) is satisfied by the \mathbf{Q} of (1.125), the material is said to possess a *symmetry plane*. For example, let

$$\mathbf{n}^T = [\cos \theta, \sin \theta, 0] \quad (1.127)$$

the symmetry plane. In this case, the orthogonal matrix \mathbf{Q} of the (1.125) has the following expression

$$\mathbf{Q}(\theta) = \begin{bmatrix} 2 + \cos 2\theta & \sin 2\theta & 0 \\ \sin 2\theta & 2 - \cos 2\theta & 0 \\ 0 & 0 & 1 \end{bmatrix}, \quad -\frac{\pi}{2} < \theta \leq \frac{\pi}{2}, \quad (1.128)$$

which is an improper orthogonal matrix. Since θ and $\theta + \pi$ represent the same plane, θ is limited to the range shown in (1.128)₂.

When $\theta = 0$, \mathbf{Q} becomes:

$$\mathbf{Q}(0) = \begin{bmatrix} -1 & 0 & 0 \\ 0 & 1 & 0 \\ 0 & 0 & 1 \end{bmatrix} \quad (1.129)$$

which represents a reflection about the plane $x_1 = 0$. When (1.122) is satisfied by (1.129), the material has a symmetry plane at $x_1 = 0$. If (1.122) is satisfied by (1.128) for any θ , the material is *transversely isotropic*. The x_3 -axis is the *axis of symmetry*. Two extreme cases of anisotropic elastic materials are *triclinic materials* and *isotropic materials*. A triclinic material possesses no rotational symmetry or a plane of reflection symmetry. An isotropic material possesses infinitely many rotational symmetries and planes of reflection symmetry.

3.5. The Elasticity Tensor for Materials with Symmetry Planes

Depending on the number of rotations and/or reflection symmetry a crystal possesses, Voigt (1928) has classified crystals into 32 classes. (See also Gurtin, 1972; Cowin and Mehrabadi, 1987; and Mehrabadi and Cowin, 1990). In terms of the 6×6 matrix \mathcal{C} however there are only 8 basic groups. For a non-crystalline material the structure of \mathcal{C} can also be represented by one of the 8 basic groups. We list below the 8 basic groups for \mathcal{C} according to the number of symmetry planes that each group has. Consideration of rotational symmetry does not change the structure of \mathcal{C} in each group. Without loss in generality we choose the symmetry plane (or planes) to coincide with the coordinate planes whenever possible. We will therefore employ the orthogonal matrix \mathbf{Q} (1.128) which represents a reflection with respect to a plane whose normal is on the

(x_1, x_2) plane making an angle θ with the x_1 -axis. We will also employ the orthogonal matrix

$$\hat{\mathbf{Q}}(\psi) = \begin{bmatrix} 1 & 0 & 0 \\ 0 & -\cos 2\psi & -\sin 2\psi \\ 0 & -\sin 2\psi & \cos 2\psi \end{bmatrix}, \quad -\frac{\pi}{2} < \psi \leq \frac{\pi}{2} \quad (1.130)$$

which represents a reflection with respect to a plane whose normal is on the (x_2, x_3) plane making an angle ψ with the x_2 -axis, (Fig. 1.6.). The plane $x_2 = 0$ can be represented by either $\theta = \pi/2$ or $\psi = 0$.

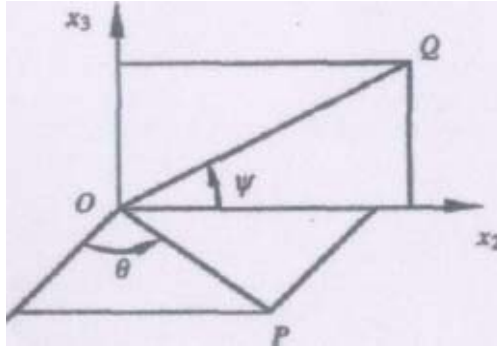


Fig. 1.6.

I. *Triclinic Materials.* No symmetry planes exist.

$$\mathbb{C} = \begin{bmatrix} C_{11} & C_{12} & C_{13} & C_{14} & C_{15} & C_{16} \\ C_{12} & C_{22} & C_{23} & C_{24} & C_{25} & C_{26} \\ C_{13} & C_{23} & C_{33} & C_{34} & C_{35} & C_{36} \\ C_{14} & C_{24} & C_{34} & C_{44} & C_{45} & C_{46} \\ C_{15} & C_{25} & C_{35} & C_{45} & C_{55} & C_{56} \\ C_{16} & C_{26} & C_{36} & C_{46} & C_{56} & C_{66} \end{bmatrix} \quad n = 21 \quad (1.131)$$

II. *Monoclinic Materials*. One symmetry plane.(a) Symmetry plane at $x_1 = 0$, i.e., $\theta = 0$.

$$\mathbb{C} = \begin{bmatrix} C_{11} & C_{12} & C_{13} & C_{14} & 0 & 0 \\ C_{12} & C_{22} & C_{23} & C_{24} & 0 & 0 \\ C_{13} & C_{23} & C_{33} & C_{34} & 0 & 0 \\ C_{14} & C_{24} & C_{34} & C_{44} & 0 & 0 \\ 0 & 0 & 0 & 0 & C_{55} & C_{56} \\ 0 & 0 & 0 & 0 & C_{56} & C_{66} \end{bmatrix} \quad n=13 \quad (1.132)$$

(b) Symmetry plane at $x_2 = 0$, i.e., $\theta = \pi/2$ or $\psi = 0$.

$$\mathbb{C} = \begin{bmatrix} C_{11} & C_{12} & C_{13} & 0 & C_{15} & 0 \\ C_{12} & C_{22} & C_{23} & 0 & C_{25} & 0 \\ C_{13} & C_{23} & C_{33} & 0 & C_{35} & 0 \\ 0 & 0 & 0 & C_{44} & 0 & C_{46} \\ C_{15} & C_{25} & C_{35} & 0 & C_{55} & 0 \\ 0 & 0 & 0 & C_{46} & 0 & C_{66} \end{bmatrix} \quad n=13 \quad (1.133)$$

(c) Symmetry plane at $x_3 = 0$, i.e., $\psi = \pi/2$.

$$\mathbb{C} = \begin{bmatrix} C_{11} & C_{12} & C_{13} & 0 & 0 & C_{16} \\ C_{12} & C_{22} & C_{23} & 0 & 0 & C_{26} \\ C_{13} & C_{23} & C_{33} & 0 & 0 & C_{36} \\ 0 & 0 & 0 & C_{44} & C_{45} & 0 \\ 0 & 0 & 0 & C_{45} & C_{55} & 0 \\ C_{16} & C_{26} & C_{36} & 0 & 0 & C_{66} \end{bmatrix} \quad n=13 \quad (1.134)$$

II. *Orthotropic (or Rhombic) Materials*. The three coordinate planes $\theta = 0$, $\pi/2$, and $\psi = \pi/2$ are the symmetry planes.

$$\mathbb{C} = \begin{bmatrix} C_{11} & C_{12} & C_{13} & 0 & 0 & 0 \\ C_{12} & C_{22} & C_{23} & 0 & 0 & 0 \\ C_{13} & C_{23} & C_{33} & 0 & 0 & 0 \\ 0 & 0 & 0 & C_{44} & 0 & 0 \\ 0 & 0 & 0 & 0 & C_{55} & 0 \\ 0 & 0 & 0 & 0 & 0 & C_{66} \end{bmatrix} \quad n=9 \quad (1.135)$$

III. *Trigonal Materials.* Three symmetry planes at $\theta = 0$ and $\pm\pi/3$.

$$\mathbb{C} = \begin{bmatrix} C_{11} & C_{12} & C_{13} & C_{14} & 0 & 0 \\ C_{12} & C_{11} & C_{13} & -C_{14} & 0 & 0 \\ C_{13} & C_{13} & C_{33} & 0 & 0 & 0 \\ C_{14} & -C_{14} & 0 & C_{44} & 0 & 0 \\ 0 & 0 & 0 & 0 & C_{44} & C_{14} \\ 0 & 0 & 0 & 0 & C_{14} & \frac{C_{11}-C_{12}}{2} \end{bmatrix} \quad n=6 \quad (1.136)$$

IV. *Tetragonal Materials.* Five symmetry planes at $\theta = 0, \pm\pi/4, \pi/2$ and $\psi = \pi/2$.

$$\mathbb{C} = \begin{bmatrix} C_{11} & C_{12} & C_{13} & 0 & 0 & 0 \\ C_{12} & C_{11} & C_{13} & 0 & 0 & 0 \\ C_{13} & C_{13} & C_{33} & 0 & 0 & 0 \\ 0 & 0 & 0 & C_{44} & 0 & 0 \\ 0 & 0 & 0 & 0 & C_{44} & 0 \\ 0 & 0 & 0 & 0 & 0 & C_{66} \end{bmatrix} \quad n=6 \quad (1.137)$$

V. *Transversely Isotropic (or Hexagonal) Materials.* The symmetry planes are the $x_3 = 0$ plane and any plane that contains the x_3 -axis. The x_3 -axis is the axis of symmetry.

$$\mathcal{C} = \begin{bmatrix} C_{11} & C_{12} & C_{13} & 0 & 0 & 0 \\ C_{12} & C_{11} & C_{13} & 0 & 0 & 0 \\ C_{13} & C_{13} & C_{33} & 0 & 0 & 0 \\ 0 & 0 & 0 & C_{44} & 0 & 0 \\ 0 & 0 & 0 & 0 & C_{44} & 0 \\ 0 & 0 & 0 & 0 & 0 & \frac{C_{11}-C_{12}}{2} \end{bmatrix} \quad n=5 \quad (1.138)$$

- VI. *Cubic Materials.* Nine planes of symmetry whose normals are on the three coordinate axes and on the coordinate planes making an angle $\pi/4$ with the coordinate axes.

$$\mathcal{C} = \begin{bmatrix} C_{11} & C_{12} & C_{12} & 0 & 0 & 0 \\ C_{12} & C_{11} & C_{12} & 0 & 0 & 0 \\ C_{12} & C_{12} & C_{11} & 0 & 0 & 0 \\ 0 & 0 & 0 & C_{44} & 0 & 0 \\ 0 & 0 & 0 & 0 & C_{44} & 0 \\ 0 & 0 & 0 & 0 & 0 & C_{44} \end{bmatrix} \quad n=3 \quad (1.139)$$

- VII. *Isotropic Materials.* Any plane is a symmetry plane.

$$\mathcal{C} = \begin{bmatrix} C_{11} & C_{12} & C_{12} & 0 & 0 & 0 \\ C_{12} & C_{11} & C_{12} & 0 & 0 & 0 \\ C_{12} & C_{12} & C_{11} & 0 & 0 & 0 \\ 0 & 0 & 0 & \frac{C_{11}-C_{12}}{2} & 0 & 0 \\ 0 & 0 & 0 & 0 & \frac{C_{11}-C_{12}}{2} & 0 \\ 0 & 0 & 0 & 0 & 0 & \frac{C_{11}-C_{12}}{2} \end{bmatrix} \quad n=2 \quad (1.140)$$

Note that while the number of nonzero elements in \mathcal{C} may increase when different coordinate system are employed, the number of independent elastic constants n does not depend on the choice of the coordinate systems.

3.6. Restrictions on Elastic Constants

As shown above, the positiveness of the strain energy, yields that the stiffness tensor \mathcal{C} is positive defined, as well as, the positive definiteness of the stress energy, yields that the compliance tensor \mathcal{S} is defined positive. In particular, in the contracted notation, the (1.97) is equivalent to the (1.117)₁ which implies that the 6×6 matrix \mathcal{C} is also positive definite and, therefore, all its principal minors are positive, i.e.:

$$\begin{aligned}
 & C_{ii} > 0 \quad (i \text{ not summed}), \\
 & \begin{vmatrix} C_{ii} & C_{ij} \\ C_{ij} & C_{jj} \end{vmatrix} > 0 \quad (i, j \text{ not summed}), \\
 & \begin{vmatrix} C_{ii} & C_{ij} & C_{ih} \\ C_{ij} & C_{jj} & C_{jh} \\ C_{ih} & C_{jh} & C_{hh} \end{vmatrix} > 0 \quad (i, j, k \text{ not summed}), \\
 & \vdots
 \end{aligned}$$

where i, j, h are distinct integers which can have any value from 1 to 6. In particular, according to the theorem which states that a real symmetric matrix is positive definite if and only if its *leading* principal minors are positive, the *necessary and sufficient conditions* for the 6×6 matrix \mathcal{C} to be positive definite are the positivity of its 6 *leading* principal minors. Same considerations may be applied to the compliance tensor \mathcal{S} . By imposing these conditions of positivity on the minors of the matrices, some restrictions on the elastic coefficients can be found.

CHAPTER II

HETEROGENEOUS MATERIALS

1. INHOMOGENEOUS SOLIDS: SAS/DAS THEOREMS

It is well known the difficulty to find solutions to anisotropic inhomogeneous material problems. A very few restricted classes of these problems are solved in a general way.

One example of these solutions is for cylinders subjected to pure torsion and possessing cylindrical orthotropy, with a variation of the shear moduli with the local normal direction to the family of curves of which the lateral boundary is a member (Cowin, 1987). This solution is a generalization, to a set of arbitrary cross-sectional shapes, of a problem solved by Voigt (Voigt, 1928) for a circular cross-section with radial variation of its cylindrical anisotropy. These cylinders are said to possess *shape intrinsic orthotropy* since it is the boundary of the cylinder that establishes the possible directional variation of the elastic moduli. A second example was given by Chung & Ting (Chung & Ting, 1995) who presented an exact solution for the case of an anisotropic half-space with elastic moduli dependent upon one coordinate, the angle θ , when the loads on the half-space are represented by a straight line of force. These kinds of problems were called *angularly inhomogeneous problems* by the authors. Closely related to these solutions is a third example called *radially inhomogeneous problems* (Alshits and Kirchner, 2001). As the name suggests, the variation of the elastic constants is in the radial direction in this case.

In spite of this difficulty, in the last years, it has been a growing interest about the mechanical behaviour of anisotropic and inhomogeneous solids, above all in biomechanics. Moreover, the necessity to build thermodynamically consistent theories for this kind of materials, by means the employment of the mathematical theory of the *homogenization*, has determined the necessity to find exact analytical solutions in the ambit of this more complex section of the theory of elasticity, (Lions, 1985), (Maugin, 1993).

In the next sections, it is presented a useful method enables one to find solutions for inhomogeneous, anisotropic elastostatic problems under particular conditions by means of the use of two theorems, *S.A.S. theorem* and *D.A.S. theorem* (Fraldi and Cowin, 2004).

1.1. Stress Associated Solutions (SAS) Theorem for inhomogeneous elasticity

The Stress Associated Solution Theorem lets to find solutions for inhomogeneous, anisotropic elastostatic problems if two conditions are satisfied:

(1) a knowledge of the solution for a homogeneous elastic *reference* problem (the *associated problem*) whose solution has a stress state with a zero eigenvalue everywhere in the domain of the problem, and (2) an inhomogeneous anisotropic elastic tensor related to the homogeneous anisotropic elastic tensor of (1) by

$$\mathcal{C}^I = \varphi(\mathbf{x})\mathcal{C}^H, \quad \varphi(\mathbf{x})| \quad \forall \mathbf{x} \in B, \quad \varphi(\mathbf{x}) > \alpha > 0, \quad \alpha \in \mathbb{R}^+ \quad (2.1)$$

where $\mathcal{C}^H = \mathcal{C}^{H^T}$ is the elasticity tensor of a generic anisotropic homogeneous elastic material of the *reference problem*, \mathcal{C}^I is the elasticity tensor of the corresponding anisotropic inhomogeneous elastic problem, B is the domain occupied by both the homogeneous object B^H and the inhomogeneous one B^I , $\alpha \in \mathbb{R}^+$ is an arbitrary positive real number, while $\varphi(\mathbf{x})$ is a $C^2(B)$ scalar function. The assumption (2.1) means that the inhomogeneous character of the material is due to the presence of a scalar parameter producing the inhomogeneity in the elastic coefficients.

This method makes it possible to find analytical solutions for an *inhomogeneous* anisotropic elastic problem if the elastic solution of the corresponding *homogeneous* anisotropic *reference* problem is known and characterized everywhere by a stress state with a zero eigenvalue. The solutions to the *inhomogeneous* anisotropic elastic problem are called the *associated solutions* of the *homogeneous problem*.

1.1.a. Zero-eigenvalue stress and zero-eigenvalue strain fields

A zero-eigenvalue stress state (zero-eigenvalue strain state) is characterized by the condition that the determinant of the stress (strain) is zero

$$\det \mathbf{T} = 0, \quad (\det \mathbf{E} = 0). \quad (2.2)$$

It is easy to show that a zero-eigenvalue stress (strain) state is a necessary condition for a plane stress (strain) state. The components of the stress tensor \mathbf{T} (strain tensor \mathbf{E}) are denoted by σ_{ij} (ε_{ij}). The strain tensor \mathbf{E} is related to the displacement field \mathbf{u} by

$$\mathbf{E} = \frac{1}{2}[(\nabla \otimes \mathbf{u}) + (\nabla \otimes \mathbf{u})^T] = \text{sym} \nabla \otimes \mathbf{u} \quad \forall \mathbf{x} \in B \quad (2.3)$$

in which $\text{grad } \mathbf{u} = (\nabla \otimes \mathbf{u})$ and the symbol \otimes represents the *tensor product*. In components we have

$$\varepsilon_{ij} = \frac{1}{2}(u_{i,j} + u_{j,i}), \quad (2.4)$$

where the comma denotes differentiation and \mathbf{u} is the displacement field.

1.1.b. Stress Associated Solutions (SAS) Theorem

Consider the following mixed boundary-value elastostatic homogeneous and anisotropic problem P^H in the absence of action-at-a-distance forces

$$\nabla \cdot \mathbf{T}(\mathbf{u}) = \mathbf{0} \quad \text{in } B^H, \quad \mathbf{T}(\mathbf{u}) \cdot \mathbf{n} = \mathbf{t} \quad \text{on } \partial B_t^H, \quad \mathbf{u} = \mathbf{u}_0 \quad \text{on } \partial B_u^H \quad (2.5)$$

where B^H is the domain occupied by the homogeneous elastic object, $\partial B^H = \{\partial B_t^H \cup \partial B_u^H\}$ is its boundary and \mathbf{t} and \mathbf{u}_0 are the traction field and the displacements assigned on the corresponding partition of the boundary, respectively (Barber, 1992; Gurtin, 1972). The notation for the divergence of the stress tensor is $\nabla \cdot \mathbf{T}(\mathbf{u}) = \text{div} \mathbf{T}(\mathbf{u})$, where the *del operator* is a vectorial differential operator defined by $\nabla \equiv \partial_i \mathbf{e}_i$, $\partial_i \equiv \partial / \partial x_i = (*)_{,i}$ is the partial differential operator and \mathbf{e}_i is the base unit vector of the i -axis.

The anisotropic Hooke's law is written

$$\mathbf{T}(\mathbf{u}) = \mathbb{C}^H : \mathbf{E}(\mathbf{u}) = \mathbb{C}^H : \text{sym}(\nabla \otimes \mathbf{u}) = \mathbb{C}^H : (\nabla \otimes \mathbf{u}) \quad (2.6)$$

or, in components

$$\sigma_{ij} = C_{ijhk}^H \varepsilon_{hk} = C_{ijhk}^H u_{h,k}. \quad (2.7)$$

Let $\mathfrak{S}^H = \{\mathbf{u}^H, \mathbf{E}^H, \mathbf{T}^H\}$ be the solution of the homogeneous problem (2.5).

Consider now an associated anisotropic elastic inhomogeneous problem P^I , described by modifying the system (2.5), with $\mathbf{t}^I = \varphi \mathbf{t}$ representing the traction field applied on ∂B_t^I and the inhomogeneous anisotropic elasticity tensor given by (2.1), thus

$$\nabla \cdot \mathbf{T}(\mathbf{u}) = \mathbf{0} \quad \text{in } B^I, \quad \mathbf{T}(\mathbf{u}) \cdot \mathbf{n} = \mathbf{t}^I \quad \text{on } \partial B_t^I, \quad \mathbf{u} = \mathbf{u}_0 \quad \text{on } \partial B_u^I \quad (2.8)$$

The solid domains B^H and B^I , as well as their corresponding boundary partitions made on ∂B^H and ∂B^I , are geometrically the same in the homogeneous and inhomogeneous problems. Then, if we expand the equation (2.8)₁ it is possible to write

$$\begin{aligned}
\nabla \cdot \mathbf{T}(\mathbf{u}) &= \nabla \cdot [\varphi(\mathbf{x}) \mathbb{C}^H : \mathbf{E}(\mathbf{u})] = \\
&= \varphi(\mathbf{x}) \nabla \cdot [\mathbb{C}^H : \mathbf{E}(\mathbf{u})] + [\mathbb{C}^H : \mathbf{E}(\mathbf{u})] \cdot \nabla \varphi(\mathbf{x}) = \mathbf{0}
\end{aligned} \tag{2.9}$$

where $\nabla(*) = \text{grad}(*)$ is the gradient operator applied on a generic scalar-valued function $(*)$. Consider now the situation in which the displacements are equal for the homogeneous and inhomogeneous problems. Then, by substituting the displacement solution \mathbf{u}^H obtained for the homogeneous problem P^H in (2.9) in place of the displacement vector \mathbf{u} , we have that

$$\nabla \cdot \mathbf{T}(\mathbf{u}^H) = \varphi(\mathbf{x}) [\nabla \cdot \mathbf{T}^H(\mathbf{u}^H)] + [\mathbf{T}^H(\mathbf{u}^H)] \cdot \nabla \varphi(\mathbf{x}) = \mathbf{0} \tag{2.10}$$

But, since $\nabla \cdot [\mathbf{T}^H(\mathbf{u}^H)] = \nabla \cdot [\mathbb{C}^H : \mathbf{E}(\mathbf{u}^H)] = \mathbf{0}$, it follows that

$$[\mathbf{T}^H(\mathbf{u}^H)] \cdot \nabla \varphi(\mathbf{x}) = \mathbf{0} \quad \forall \mathbf{x} \in B^I \tag{2.11}$$

By excluding the trivial case in which $\varphi(\mathbf{x}) = \text{constant}$, it follows that

$$\det \mathbf{T}^H = 0, \quad \forall \mathbf{x} \in B^H \tag{2.12}$$

This means that the stress state at \mathbf{x} of the *reference* homogeneous problem is required to be a zero eigenvalue stress state everywhere in the domain. To investigate the geometrical meaning of the equation (2.11), since (2.11) must be true everywhere in B^I , we consider, without loss of generality, the *local principal stress reference system* $\{\xi_1, \xi_2, \xi_3\}$, in which the stress tensor \mathbf{T}^H takes the component form

$$\mathbf{T}^H = \begin{bmatrix} \sigma_{\xi_1}^H & 0 & 0 \\ 0 & \sigma_{\xi_2}^H & 0 \\ 0 & 0 & \sigma_{\xi_3}^H \end{bmatrix}. \tag{2.13}$$

Representing the gradient of the scalar function φ as

$$\nabla \varphi(\boldsymbol{\xi})^T = [\varphi_{,\xi_1} \quad \varphi_{,\xi_2} \quad \varphi_{,\xi_3}], \tag{2.14}$$

the three scalar equations implied by (2.11) are written as

$$\sigma_{\xi_1}^H \varphi_{,\xi_1} = 0, \quad \sigma_{\xi_2}^H \varphi_{,\xi_2} = 0, \quad \sigma_{\xi_3}^H \varphi_{,\xi_3} = 0. \tag{2.15}$$

The system (2.15) is satisfied if the stress tensor \mathbf{T}^H for the reference homogeneous problem P^H is, at each internal point $\mathbf{x} \in B^H$, a locally variable *zero eigenvalue stress* state. If there is only one zero eigenvalue, say in the ξ_3 -direction, the only non-zero component of the vector $\nabla \varphi$, is $\varphi_{,\xi_3}$ at the corresponding points $\mathbf{x} \in B^I$. If there are two zero eigenvalues there can be two non-zero components of $\nabla \varphi$. The case of three zero eigenvalues of the stress tensor \mathbf{T}^H is trivial and will not be mentioned further. It follows that, at each internal point, the equipotential surfaces of φ admit as a tangent plane the plane whose normal is coaxial with the eigenvector associated with the zero stress eigenvalue (or a direction, in the case of two zero stress eigenvalues). This is illustrated in Figure 2.1. for the case of one zero eigenvalue of stress.

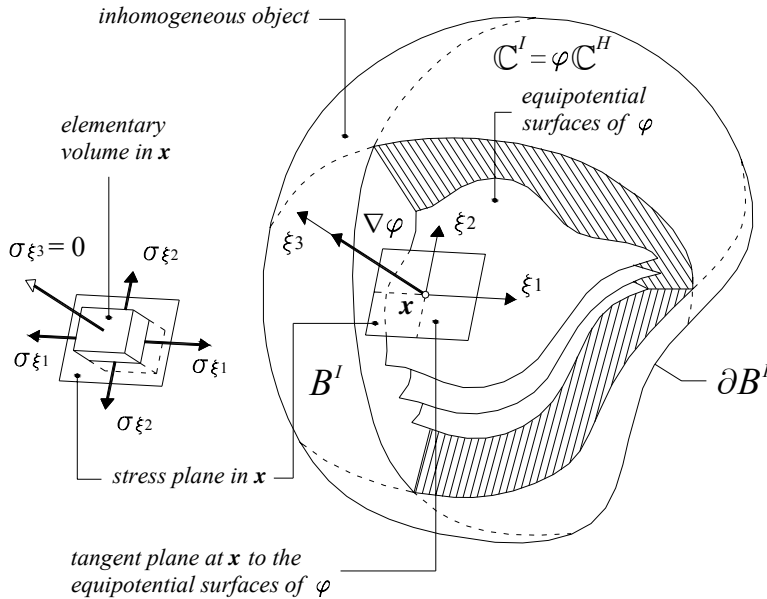


Fig. 2.1.

Geometrical interpretation of the relationship between the equipotential surfaces of φ and the distribution of the planes of stresses in the associated anisotropic problem

The geometrical relationship (2.11) between the stress tensor \mathbf{T}^H and the vector $\nabla \varphi$ may be rewritten in the form

$$\{\mathbf{T}^H \cdot \nabla \varphi = \mathbf{0}\} \Leftrightarrow \{\forall \mathbf{v} \in V, \quad \mathbf{T}^H : (\nabla \varphi \otimes \mathbf{v}) = \mathbf{0}\} \quad (2.16)$$

where \mathbf{v} is any unit vector defined in the three-dimensional Euclidean space \mathbb{E}^3 and V represents the corresponding vector space. It follows that the stress vector on the plane whose normal is \mathbf{v} is always orthogonal to the vector $\nabla\varphi$.

Then, it is possible to establish the following theorem:

Stress Associated Solution (SAS) Theorem. *Consider two geometrically identical elastic objects B^H and B^I , one homogeneous and the other inhomogeneous, respectively. Let \mathcal{C}^H and $\mathcal{C}^I = \varphi(\mathbf{x})\mathcal{C}^H$ be the corresponding elasticity tensors (Figure 2.2.). The two elastostatic problems associated with the two objects are*

$$\begin{aligned} P^H : \quad & \{\nabla \cdot \mathbf{T}(\mathbf{u}) = \mathbf{0} \text{ in } B^H, \mathbf{T}(\mathbf{u}) \cdot \mathbf{n} = \mathbf{t} \text{ on } \partial B_t^H, \mathbf{u} = \mathbf{u}^0 \text{ on } \partial B_u^H\}, \\ P^I : \quad & \{\nabla \cdot \mathbf{T}(\mathbf{u}) = \mathbf{0} \text{ in } B^I, \mathbf{T}(\mathbf{u}) \cdot \mathbf{n} = \varphi \mathbf{t} \text{ on } \partial B_t^I, \mathbf{u} = \mathbf{u}^0 \text{ on } \partial B_u^I\}, \end{aligned}$$

where

$$\varphi(\mathbf{x}) \in C^2(B) \mid \forall \mathbf{x} \in B, \varphi(\mathbf{x}) > \alpha > 0, \quad \alpha \in \mathbb{R}^+.$$

If \mathbf{u}^H is the solution of the homogeneous problem P^H , then $\mathbf{u}^I = \mathbf{u}^H$ if and only if $\{\mathbf{T}^H : (\nabla\varphi \otimes \mathbf{v}) = \mathbf{0}, \quad \forall \mathbf{v} \in V\}$, i.e.

$$\{\forall \mathbf{x} \in B^I, \forall \mathbf{v} \in V, \mathbf{T}^H : (\nabla\varphi \otimes \mathbf{v}) = \mathbf{0}\} \Leftrightarrow \mathbf{u}^I = \mathbf{u}^H.$$

Proof. The necessary condition has been established in the preamble. To prove the sufficient condition:

$$\{\forall \mathbf{v} \in V, \mathbf{T}^H : (\nabla\varphi \otimes \mathbf{v}) = \mathbf{0}\} \Rightarrow \mathbf{u}^I = \mathbf{u}^H,$$

we first recall (2.16). Consequently, if \mathbf{u}^H is the displacement solution of the homogeneous problem P^H , we can write

$$\begin{aligned} & \{\nabla \cdot [\mathbf{T}^H(\mathbf{u}^H)] = \mathbf{0}, [\mathbf{T}^H(\mathbf{u}^H)] \cdot \nabla\varphi = \mathbf{0}\} \Rightarrow \\ & \Rightarrow \{\nabla \cdot [\mathcal{C}^H : (\nabla \otimes \mathbf{u}^H)] = \mathbf{0}, [\mathcal{C}^H : (\nabla \otimes \mathbf{u}^H)] \cdot \nabla\varphi = \mathbf{0}\} \Rightarrow \\ & \Rightarrow \varphi \nabla \cdot [\mathcal{C}^H : (\nabla \otimes \mathbf{u}^H)] + [\mathcal{C}^H : (\nabla \otimes \mathbf{u}^H)] \cdot \nabla\varphi = \mathbf{0}, \end{aligned}$$

from which it follows that

$$\nabla \cdot [\mathcal{C}^I : (\nabla \otimes \mathbf{u}^H)] = \mathbf{0},$$

when (2.1) is considered. Then, if we rewrite the inhomogeneous elastostatic problem P^I in terms of displacements, that is

$$P^I : \{\nabla \cdot [\mathbb{C}^I : (\nabla \otimes \mathbf{u}^I)] = \mathbf{0} \text{ in } B^I, [\mathbb{C}^I : (\nabla \otimes \mathbf{u}^I)] \cdot \mathbf{n} = \boldsymbol{\varphi} \mathbf{t} \text{ on } \partial B_t^I, \mathbf{u}^I = \mathbf{u}^0 \text{ on } \partial B_u^I\}$$

we can observe that \mathbf{u}^H satisfies all these field and boundary equations. Therefore, from the uniqueness theorem, it follows that $\mathbf{u}^I = \mathbf{u}^H$ and, consequently, $\mathbf{T}^I = \boldsymbol{\varphi} \mathbb{C}^H : (\nabla \otimes \mathbf{u}^H) = \boldsymbol{\varphi} \mathbf{T}^H$. This proves the sufficiency condition.

It is convenient to increase the similarity between the elastic problems for the homogeneous and the inhomogeneous materials by writing the boundary conditions in the same way. Thus we substitute for the prescribed boundary tractions a corresponding prescribed displacement field; this converts the portion of the boundary upon which the surface tractions are prescribed to a portion of the boundary upon which the displacements are prescribed. Due to uniqueness of solution, this is always possible in a linear elastic problem. Then, the two problems may be written in the equivalent forms as

$$\begin{aligned} P^H : \quad & \{\nabla \cdot \mathbf{T}(\mathbf{u}) = \mathbf{0} \text{ in } B^H, \mathbf{u} = \mathbf{u}^t \text{ on } \partial B_t^H, \mathbf{u} = \mathbf{u}^0 \text{ on } \partial B_u^H\}, \\ P^I : \quad & \{\nabla \cdot \mathbf{T}(\mathbf{u}) = \mathbf{0} \text{ in } B^I, \mathbf{u} = \mathbf{u}^t \text{ on } \partial B_t^I, \mathbf{u} = \mathbf{u}^0 \text{ on } \partial B_u^I\}, \end{aligned}$$

where \mathbf{u}^t represents the prescribed displacement on ∂B_t and where, now, the tractions \mathbf{t} and $\boldsymbol{\varphi} \mathbf{t}$ represent the reactions of the constraints on ∂B_t specified by \mathbf{u}^t . It follows that, when a solution $\mathfrak{S}^H = \{\mathbf{u}^H, \mathbf{E}^H, \mathbf{T}^H\}$ for an anisotropic homogeneous elastic problem P^H is known, the *Stress Associated Solution Theorem* yields the corresponding solution for an inhomogeneous problem P^I as $\mathfrak{S}^I = \{\mathbf{u}^H, \mathbf{E}^H, \boldsymbol{\varphi} \mathbf{T}^H\}$, if and only if $\mathbf{T}^H \cdot \nabla \boldsymbol{\varphi} = \mathbf{0}$ everywhere in the object and the displacement boundary conditions are the same for both the homogeneous and the inhomogeneous objects. Thus the solution $\mathfrak{S}^H = \{\mathbf{u}^H, \mathbf{E}^H, \mathbf{T}^H\}$ is used to construct a solution of the associated inhomogeneous problem.

Finally we note that the restriction (2.1) may be relaxed in many different ways. For example the *Associated Solutions* could involve only some selected elastic moduli of the homogeneous elasticity tensor, so that the solutions do not depend on all stiffness coefficients. This means that it is possible to extend the validity of the proposed theorem by rewriting the assumption (2.1) in the weaker form

$$\hat{C}_{ijhk}^I = \boldsymbol{\varphi} \hat{C}_{ijhk}^H,$$

where \hat{C}_{ijhk}^H represents only those elastic coefficients explicitly involved in the specific anisotropic homogeneous problem used to construct the associated solution. In the next section it is shown that components of the elasticity tensor not involved in the solution of the homogeneous problem will not be involved in the solution of the associated inhomogeneous problem.

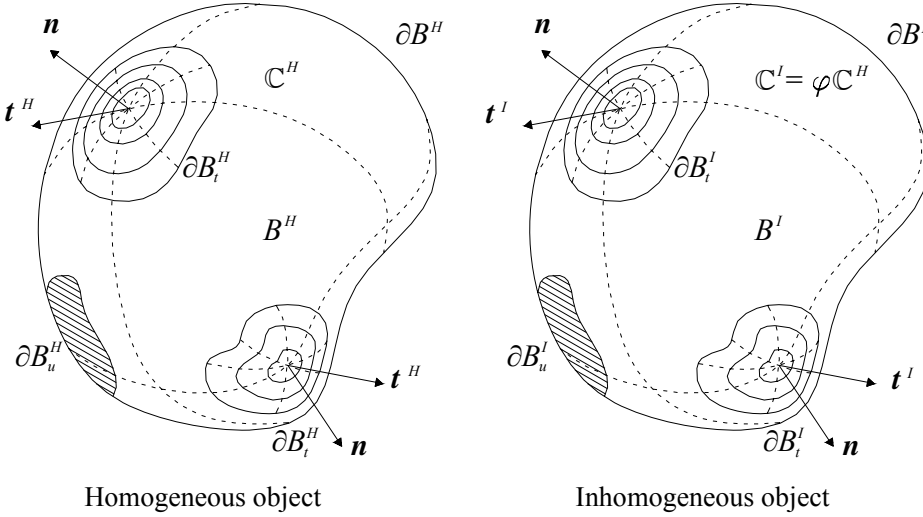


Fig. 2.2.

The homogeneous and inhomogeneous bodies with their boundary conditions

1.2. Generalization of the SAS theorem to piecewise defined inhomogeneities

Two types of composite materials are considered in this section, one in which φ is *constant*, but piecewise *discontinuous* and another in which φ is a *piecewise continuous function*. These two cases extend the domain of applicability of the condition (2.1), and therefore the domain of applicability of the SAS theorem. In the first case the extension is to composite materials for which each phase is characterized by elastic moduli that are constant within their own phase, but are different from the constant elastic moduli of the other phases. In the second case

the extension is to composite materials for which each phase is characterized by the possibility of each phase having variable elastic coefficients inside the phase domain and discontinuous elastic coefficients across phase boundaries.

1.2.a. Composite materials where φ is constant, but piecewise discontinuous

In the following two sections we extend the SAS theorem to heterogeneous materials where there is not a smooth variation of the elastic moduli. To achieve this, we will make reference to some results obtained previously and formulate new hypotheses about the features of composite inhomogeneous bodies considered. In particular, for each phase p present of a composite material, we will assume here that the elasticity tensor can be written as

$$\mathbb{C}_p^H = \varphi_p \mathbb{C}^H, \quad p = \{1, 2, \dots, n\} \subset \mathbb{N} \quad (2.17)$$

where \mathbb{C}^H is the elasticity tensor of a reference isotropic or anisotropic homogeneous material and φ_p is a positive scalar parameter. This hypothesis does not constitute the most general case for describing the relation between the elastic tensors of the different phases for a composite material, but it is widely utilized in literature because many artificial and natural composites exhibit mechanical properties that are well represented by the proposed assumption (Lekhnitskii, 1963; Ting, 1996; Fraldi and Guarracino, 2001; Nemat-Nasser and Hori, 1993).

Let us consider a partition of the inhomogeneous body $\{\Omega_p(B) \mid B \equiv \bigcup_{p=1}^n \Omega_p(B)\}$,

where $\partial\Omega_{(p,q)}$ represents the interface boundary between two generic sub-domains Ω_p and Ω_q of the partition, with elasticity tensors \mathbb{C}_p^H and \mathbb{C}_q^H , respectively.

If we assume that the solution for the anisotropic homogeneous reference problem is known, and the geometries of the homogeneous and composite material objects are the same, we can study the conditions under which the stress tensor for the inhomogeneous material (multi-phase material) assumes the form

$$\mathbf{T}_p^H = \varphi_p \mathbf{T}^H, \quad \forall \mathbf{x} \in \Omega_p(B) \quad (2.18)$$

required by the SAS theorem. Note that the stress (2.18) satisfies the equilibrium equations in each sub-domain of the partition,

$$\nabla \cdot \mathbf{T}_p^H = \varphi_p \nabla \cdot \mathbf{T}^H = \mathbf{0}, \quad \forall \mathbf{x} \in \Omega_p(B). \quad (2.19)$$

Moreover, by virtue of the assumed constitutive relationships,

$$\mathbf{E}_p^H = \mathbb{C}_p^{H-1} \mathbf{T}_p^H = \mathbb{C}^{H-1} \mathbf{T}^H = \mathbf{E}^H, \quad \{\forall p \in \mathbf{N}, \forall \mathbf{x} \in \Omega_p\} \quad (2.20)$$

the satisfaction of the compatibility condition on the surfaces of discontinuity between the different materials of the composite object is automatic. From the force equilibrium on the interfaces between two adjacent phases, it follows that

$$\mathbf{T}_p^H \cdot \mathbf{n}_{(p,q)} = \mathbf{T}_q^H \cdot \mathbf{n}_{(p,q)}, \quad \{\forall \{p, q\} \in \mathbf{N}, \forall \mathbf{x} \in \partial\Omega_{(p,q)}\} \quad (2.21)$$

where $\mathbf{n}_{(p,q)}$ is the unit normal vector to the interface between the phases p and q . By virtue of (2.18), the equation (2.21) is satisfied if

$$\mathbf{T}^H \cdot \mathbf{n}_{(p,q)} = \mathbf{0}, \quad \forall \mathbf{x} \in \partial\Omega_{(p,q)}. \quad (2.22)$$

Equation (2.22) requires that for each point belonging to the interface surfaces between two phases, the stress tensor \mathbf{T}^H must possess at least one zero-eigenvalue, that is $\{\det \mathbf{T}^H = 0, \forall \mathbf{x} \in \partial\Omega_{(p,q)}\}$. This hypothesis is necessary in order to orient the plane of the stress on the interface surfaces such that the eigenvector associated with a zero eigenvalue of the stress tensor is coaxial with the unit normal vector to the tangent plane to the interface. For structures sometimes consistent with this hypothesis one can consider the interfaces between layers of certain plant structures, for example, onions and leeks. In the literature of this subject examples that conform to this hypothesis include the piece-wise angularly inhomogeneous elastic wedges considered by Ting (Ting, 1996a), the intrinsically orthotropic layered cylinders under torsion, described by Cowin (Cowin, 1987), as well as in other examples analyzed by Lekhnitskii (Lekhnitskii, 1963).

To complete the elastic solution for the composite material (2.17) using the known solution of a homogeneous reference problem, we note the satisfaction of the compatibility and equilibrium conditions on the external boundary. The satisfaction of the compatibility conditions is easily verified by virtue of (2.20). The equilibrium equation on the part of the external boundary where the tractions are prescribed is given by

$$\mathbf{T}_e^H \cdot \mathbf{n} = \mathbf{t}_e^H = \varphi_e \mathbf{t}^H, \quad \forall \mathbf{x} \in \partial B_{t(e)} \quad (2.23)$$

where $\partial B_{t(e)}$ represents a typical element of the partition of the external boundary on which the tractions \mathbf{t}^H are prescribed in the homogeneous reference problem. The total stress boundary is the sum over all the typical

distinct boundaries, $\partial B_i = \bigcup_{e=1}^k \partial B_{i(e)}$, where k represents the total number of

phases that have a projection of their boundary on the external boundary on which the tractions are assigned. Then, if the conditions (2.22) and (2.23) are satisfied, we can build the elastic solution of composite multi-phase materials from a knowledge of the displacements and the stresses for a homogeneous object with analogous geometry using the extension of the SAS theorem.

Note that, in order to utilize the results of the proposed theorem for inhomogeneous materials in which φ was assumed to be a continuous scalar function, the stress tensor \mathbf{T}^H had to exhibit a zero-eigenvalue at each point of the body. However, in order to generalize the SAS theorem to composite materials where φ is constant, but piecewise discontinuous, it is sufficient that the stress tensor \mathbf{T}^H related to the associated homogeneous problem possesses a zero-eigenvalue ($\det \mathbf{T}^H = 0$) only in the points belonging to the internal interfaces between the different phases. This means that, in the case of materials where φ is a constant, but piecewise discontinuous, \mathbf{T}^H can be a three-dimensional stress field in any other point of the solid domain.

1.2.b. Composite materials where φ is piecewise continuous

In this subsection we consider the new and more general situation in which each phase p of the heterogeneous solid (composite material) can be represented by the following elasticity tensor

$$\mathcal{C}_p^H = \varphi_p(\mathbf{x}_p) \mathcal{C}^H, \quad \forall \mathbf{x}_p \in \Omega_p \subset B \quad (2.24)$$

where \mathcal{C}^H is the elasticity tensor of a homogeneous reference material, while φ_p is now a positive scalar function, not necessarily constant, but continuous inside each phase (or sub-domain defined by the partition described above). We relax some of the hypotheses for the situation when φ is constant, but retain the

previous notation; $\{\Omega_p(B) \mid B \equiv \bigcup_{p=1}^n \Omega_p(B)\}$ is again the partition of the

inhomogeneous object, with $\partial\Omega_{(p,q)}$ representing the interface boundary between two generic adjacent sub-domains Ω_p and Ω_q of the partition whose elasticity tensors are \mathcal{C}_p^H and \mathcal{C}_q^H , respectively, see Figure 2.3.. The representation of the stress tensor of the phase p required by the SAS theorem is

$$\mathbf{T}_p^H = \varphi_p(\mathbf{x}_p) \mathbf{T}^H, \quad \forall \mathbf{x}_p \in \Omega_p(B). \quad (2.25)$$

Equilibrium is satisfied if the divergence of the stress for each phase is zero;

$$\nabla \cdot \mathbf{T}_p^H = \varphi_p \nabla \cdot \mathbf{T}^H + \mathbf{T}^H \cdot \nabla \varphi_p = \mathbf{0} \Rightarrow \mathbf{T}^H \cdot \nabla \varphi_p = \mathbf{0}, \quad \forall \mathbf{x}_p \in \Omega_p(B) \quad (2.26)$$

From this result it follows, using (2.17) and (2.20), that $\mathbf{E}_p^H = \mathbf{E}^H$, $\{\forall p \in \mathbf{N}, \forall \mathbf{x}_p \in \Omega_p\}$. The equilibrium conditions (2.21)-(2.22) across the interface between two phases are then satisfied as well the external boundary conditions (2.23) considered previously. This means that, in order to extend the SAS theorem to piecewise continuous composite materials, one has to first establish two facts about the stress tensor \mathbf{T}^H , namely: 1) at each internal point of each phase p , the stress tensor \mathbf{T}^H possesses at least one zero-eigenvalue and 2) at every point in the interface between two adjacent phases the normal to the tangent plane has to be coincident with the direction of the eigenvector associated with the zero eigenvalue.

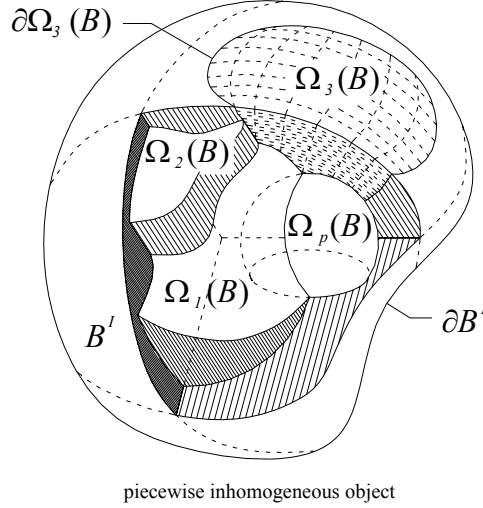


Fig. 2.3.

A representation of a possible spatial distribution of the phases inside a piecewise inhomogeneous material.

1.3. Displacement Associated Solutions (DAS) Theorem for inhomogeneous elasticity

Analogously to the SAS theorem, the *Displacement Associated Solution* (D.A.S.) theorem lets to find solutions for inhomogeneous anisotropic elastostatic problems, if two conditions are satisfied, (Fraldi, Cowin, 2004): (3) the solution of the homogeneous elastic *reference problem* (*the associated one*) is known and it has a local plane strain state, with a zero eigenvalue everywhere in the domain of the problem and (4) the inhomogeneous anisotropic compliance tensor is in relation with the homogeneous associated one according to the following equation:

$$\mathcal{S}^I = \frac{1}{\varphi(\mathbf{x})} \mathcal{C}^{H^{-1}} = \lambda(\mathbf{x}) \mathcal{S}^H, \quad \lambda(\mathbf{x})| \quad \forall \mathbf{x} \in B, \quad \lambda(\mathbf{x}) > \beta > 0, \quad \beta \in \mathbb{R}^+ \quad (2.27)$$

where $\mathcal{S}^H = \mathcal{S}^{H^*}$ is the compliance tensor of the anisotropic homogeneous elastic *reference problem*, \mathcal{S}^I is the compliance tensor of the corresponding anisotropic inhomogeneous elastic problem, B is the domain occupied by both the homogeneous object B^H and the inhomogeneous one B^I , $\beta \in \mathbb{R}^+$ is an arbitrary positive real number, while $\lambda(\mathbf{x})$ is a $C^2(B)$ scalar function.

The second condition implies that the inhomogeneous character of the material is due to the presence of a scalar parameter, $\lambda(\mathbf{x})$, producing the inhomogeneity in the compliance coefficients. It can be also relaxed and, so, written in a weaker form:

$$\hat{\mathcal{S}}_{ijhk}^I = \lambda \hat{\mathcal{S}}_{ijhk}^H \quad (2.28)$$

where $\hat{\mathcal{S}}_{ijhk}^H$ represents only those compliance coefficients explicitly involved in the specific anisotropic homogeneous problem used to construct the associated solution.

This means that components of the compliance tensor not involved in the solution of the homogeneous problem will not be involved in that one of the associated inhomogeneous problem.

If the conditions (3) and (4) are satisfied, starting from the known solution of the homogeneous problem, the *associated solution*, that is the solution to the inhomogeneous problem, is derived.

In particular, the stress field solution is identical with the stress field of the homogeneous reference solution, while the strain field of the inhomogeneous problem is equal to $\lambda(\mathbf{x})$ times the strain field of the homogeneous problem.

The advantage of this method is in the fact that its use yields exact solutions for several new interesting inhomogeneous and anisotropic problems.

More in detail, let us to consider an anisotropic homogeneous elastic object, that occupies a volume B^H , with mixed boundary-value (see Figure 2.2.a).

In presence of action-at-a-distance forces and taking into account the compatibility of the solution by writing the equilibrium equations in terms of displacements, the following equilibrium equations can be written

$$\begin{aligned}\nabla \cdot \mathbf{T}(\mathbf{u}) &= \mathbf{0} & \text{in } B^H \\ \mathbf{T}(\mathbf{u}) \cdot \mathbf{n} &= \mathbf{t} & \text{on } \partial B_t^H \\ \mathbf{T}(\mathbf{u}) \cdot \mathbf{n} &= \mathbf{0} & \text{on } \partial B_0^H\end{aligned}\tag{2.29}$$

where $\nabla = \partial_i \mathbf{e}_i$ is a vectorial differential operator, ∂B_t^H is the boundary partition of the homogeneous continuum on which the traction field is assigned, ∂B_0^H is the boundary partition of the homogeneous continuum in absence of both traction and displacements fields.

On the boundary partition on which the displacements field is assigned, the following relation has to be satisfied

$$\mathbf{u} = \mathbf{0} \quad \text{on } \partial B_u^H\tag{2.30}$$

where ∂B_u^H is the boundary partition of the homogeneous continuum on which the displacements field is assigned.

The anisotropic Hooke's law, in a linear elastic stress-strain relation, is written in the form

$$\mathbf{T}(\mathbf{u}) = \mathbb{C}^H : \mathbf{E}(\mathbf{u}) = \mathbb{C}^H : \text{sym}(\nabla \otimes \mathbf{u}) = \mathbb{C}^H : (\nabla \otimes \mathbf{u})\tag{2.31}$$

or

$$\text{sym}(\nabla \otimes \mathbf{u}) = \mathbf{E}(\mathbf{u}) = \mathbb{S}^H : \mathbf{T}(\mathbf{u})\tag{2.32}$$

in components

$$\sigma_{ij} = C_{ijhk}^H \varepsilon_{hk} = C_{ijhk}^H u_{h,k}\tag{2.33}$$

or

$$\varepsilon_{ij} = S_{ijhk}^H \sigma_{hk}.\tag{2.34}$$

Let us to consider, now, an anisotropic inhomogeneous elastic object, that occupies a volume B^I , geometrically the same of B^H , with mixed boundary-value (see Figure 2.2.b).

In presence of action-at-a-distance forces and taking into account the compatibility of the solution by writing the equilibrium equations in terms of displacements, in an analogous manner to what has been done before, the following equilibrium equations can be written

$$\begin{aligned}\nabla \cdot \mathbf{T}(\mathbf{u}) &= -\mathbf{b} & \text{in } B^I \\ \mathbf{T}(\mathbf{u}) \cdot \mathbf{n} &= \mathbf{t} & \text{on } \partial B_t^I \\ \mathbf{T}(\mathbf{u}) \cdot \mathbf{n} &= \mathbf{0} & \text{on } \partial B_0^I\end{aligned}\tag{2.35}$$

where ∂B_t^I is the boundary partition of the inhomogeneous continuum on which the traction field is assigned. It is geometrically the same of that one in the homogeneous problem and ∂B_0^I is the boundary partition of the inhomogeneous continuum in absence of both traction and displacements fields. It is geometrically the same of that one in the homogeneous problem.

On the boundary partition on which the displacements field is assigned, the following relation has to be satisfied

$$\mathbf{u} = \mathbf{0} \quad \text{on } \partial B_u^I\tag{2.36}$$

where ∂B_u^I is the boundary partition of the inhomogeneous continuum on which the displacements field is assigned. It is geometrically the same of that one in the homogeneous problem.

Let us to assume the stress tensor \mathbf{T}^H as the solution for the homogeneous problem, and let us to assume, also, the hypothesis that

$$\mathbf{T}^I = \mathbf{T}^H.\tag{2.37}$$

In this way, the equations in the differential system (2.29) are automatically satisfied. Moreover, if \mathbf{T}^H is the solution of the first anisotropic and homogeneous problem, we have that the compatibility condition

$$\nabla \times \left[\nabla \times (\mathcal{S}^H : \mathbf{T}^H) \right] = \mathbf{0}\tag{2.38}$$

have to be also satisfied. As well-known, this ensures that a displacement field \mathbf{u}^H exists. So, it is possible to write the strain-displacement relationship

$$\mathbf{E}^H = \mathcal{S}^H : \mathbf{T}^H = \text{sym}(\nabla \otimes \mathbf{u}^H) \quad (2.39)$$

where \mathbf{u}^H is displacements field, solution of the homogeneous problem. Then, in order to accept the hypothesis (2.37), the following equation

$$\nabla \times [\nabla \times (\mathcal{S}^I : \mathbf{T}^I)] = \nabla \times [\nabla \times (\lambda \mathcal{S}^H : \mathbf{T}^H)] = \mathbf{0} \quad (2.40)$$

becomes necessary and sufficient condition for the existence of a displacement field \mathbf{u}^I , where \mathbf{u}^I is the displacements field, solution of the inhomogeneous problem, and it is given by

$$\text{sym}(\nabla \otimes \mathbf{u}^I) = \mathbf{E}^I = \mathcal{S}^I : \mathbf{T}^I = \lambda \mathcal{S}^H : \mathbf{T}^H. \quad (2.41)$$

The compatibility condition (2.40), in general, is not satisfied. Therefore, it is necessary to find the conditions under whose it becomes true, (Fraldi, Cowin, 2004). Without loss of generality, let us consider

$$\lambda = \lambda(\mathbf{x}_3) \quad (2.42)$$

that means that the \mathbf{x}_3 is the direction locally coaxial with the gradient of λ , i.e.,

$$\nabla \lambda^T = [0, 0, \partial \lambda / \partial x_3]. \quad (2.43)$$

So, by recalling that \mathbf{u}^H is the solution of the homogeneous problem, and by operating some algebraic manipulations, the set of compatibility equations (2.40) can be reduced to five differential equations as it is shown

$$\begin{cases} \lambda_{,33} u_{1,1}^H + \lambda_{,3} (u_{1,3}^H - u_{3,1}^H)_{,1} = 0 \\ \lambda_{,33} u_{2,2}^H + \lambda_{,3} (u_{2,3}^H - u_{3,2}^H)_{,2} = 0 \\ \lambda_{,3} (u_{1,2}^H - u_{2,1}^H)_{,1} = 0 \\ \lambda_{,3} (u_{1,2}^H - u_{2,1}^H)_{,2} = 0 \\ \lambda_{,33} (u_{1,2}^H + u_{2,1}^H) + \lambda_{,3} [(u_{1,3}^H - u_{3,1}^H)_{,2} + (u_{2,3}^H - u_{3,2}^H)_{,1}] = 0 \end{cases} \quad (2.44)$$

where, obviously, is absent any prescribed constrain about the relation between the first and the second derivatives of the parameter λ .

It can be noted that the terms in the parentheses represent the skew components of the $\nabla \otimes \mathbf{u}^H$, that are local rotations, while the only present strain components are $(1 - \delta_{i3})(1 - \delta_{j3})\mathbf{u}_{i,j}^H$, having indicated with δ_{hk} the standard Kronecker operator.

It has to be noted that:

1. the displacement field for the reference homogeneous problem has to be related, at each internal point $\mathbf{x} \in B^H$, with a local plane strain field, where any plane with support the axis \mathbf{x}_3 can be the plane of the strains

2.

$$\det \mathbf{E}^H = 0 ; \quad (2.45)$$

3. the vector $\nabla \lambda$, the corresponding points $\mathbf{x} \in B^I$, has to be coaxial with the support axis \mathbf{x}_3 of plane of the strains in the homogeneous problem;
4. $\text{curl}(\mathbf{u}^H)$ must be independent from \mathbf{x}_3 -direction, i.e. the $\nabla \lambda$ -direction.

In the previous statements, analogously to what has been done with the stress state, it has been implicitly considered the definition about the "*plane strain*": a strain state will be *said plane* if, in a fixed point \mathbf{x} of the solid, there is a *plane of the strains* to which all the strain components ε_{ij} belong. It is easy to demonstrate that this plane exists if the strain tensor \mathbf{E} has a zero eigenvalue. So, if $\{\xi_1, \xi_2, \xi_3\}$ is the orthogonal *principal* reference frame of the strain tensor \mathbf{E} and if ξ_3 is assumed, for example, as the eigenvector associated to the zero eigenvalue of \mathbf{E} , the *plane of the strains* must coincide with $\xi_1 - \xi_3$ plane.

It follows that a necessary and sufficient condition for the existence of a *plane strain* is given by

$$\det \mathbf{E} = 0 . \quad (2.46)$$

It has to be noted that the satisfaction of the compatibility condition (2.40) yields that the displacements field of the homogeneous problem has to satisfy the equations (2.44).

This compatibility condition (2.40), therefore, may be rewritten in the form

$$\left\{ \text{curl} \left[\text{curl} \left(\lambda \mathcal{S}^H : \mathbf{T}^H \right) \right] = \mathbf{0} \right\} \Leftrightarrow \left\{ \forall \mathbf{h} \in V : \nabla \lambda \cdot \mathbf{h} = 0, \left(\nabla \otimes \text{curl} \mathbf{u}^H \right) \mathbf{h} = \mathbf{0}, \text{sym} \left(\nabla \otimes \mathbf{u}^H \right) \mathbf{h} \cdot \mathbf{h} = 0 \right\} \quad (2.47)$$

where $\lambda(\mathbf{x}) \in C^2(B) \mid \forall \mathbf{x} \in B, \lambda(\mathbf{x}) > \alpha > 0, \alpha \in \mathbb{R}^+, \mathbf{h}$ is any unit vector defined in the three-dimensional Euclidean space \mathbb{E}^3 and V is the corresponding vector space.

Moreover, it is worth to note that the assumed position (2.27) and the hypothesis (2.37), that is true if the equation (2.40) is satisfied, imply

$$\mathbf{E}^I = \lambda \mathbf{E}^H. \quad (2.48)$$

So, at this point, it can be stated that any anisotropic and homogeneous elastic problem that possesses a solution represented by the displacement equations can be considered a *Displacement Auxiliary Solution* for the corresponding dual inhomogeneous elastic problem.

In other words, it can be possible to demonstrate the following theorem:

Displacement Associated Solution (DAS) Theorem

Consider two geometrically identical anisotropic elastic objects, one homogeneous, B^H , and the other inhomogeneous, B^I , respectively. Let be \mathcal{S}^H and $\mathcal{S}^I = \lambda(\mathbf{x})\mathcal{S}^H$ the corresponding compliance tensors. The two elastostatic Cauchy problems associated with the two objects, in presence of the body forces and of mixed boundary-value, are

$$\begin{aligned} P^H : \{ \nabla \cdot \mathbf{T}(\mathbf{u}) = -\mathbf{b} \text{ in } B^H, \mathbf{T}(\mathbf{u}) \cdot \mathbf{n} = \mathbf{t} \text{ on } \partial B_t^H, \mathbf{T}(\mathbf{u}) \cdot \mathbf{n} = \mathbf{0} \text{ on } \partial B_0^H, \mathbf{u} = \mathbf{0} \text{ on } \partial B_u^H \}, \\ P^I : \{ \nabla \cdot \mathbf{T}(\mathbf{u}) = -\mathbf{b} \text{ in } B^I, \mathbf{T}(\mathbf{u}) \cdot \mathbf{n} = \mathbf{t} \text{ on } \partial B_t^I, \mathbf{T}(\mathbf{u}) \cdot \mathbf{n} = \mathbf{0} \text{ on } \partial B_0^H, \mathbf{u} = \mathbf{0} \text{ on } \partial B_u^H \}. \end{aligned} \quad (2.49)$$

If \mathbf{T}^H is the solution of the homogeneous problem p^H , then $\mathbf{T}^I = \mathbf{T}^H$ if and only if the second part of the equation (2.47) is verified, i.e. if

$$\mathbf{w}^H = \text{curl} \mathbf{u}^H \mid \forall \mathbf{v}, \text{skew}(\nabla \otimes \mathbf{u}^H) \mathbf{v} = \mathbf{w}^H \wedge \mathbf{v}$$

we have that

$$\forall \mathbf{h} \in V \mid \nabla \lambda \cdot \mathbf{h} = 0, \{ (\nabla \otimes \text{curl} \mathbf{u}^H) \mathbf{h} = \mathbf{0}, \text{sym}(\nabla \otimes \mathbf{u}^H) \mathbf{h} \cdot \mathbf{h} = 0 \} \Leftrightarrow \{ \mathbf{T}^I = \mathbf{T}^H \}. \quad (2.50)$$

In other words, when a solution $\mathbf{B}_\varepsilon^H = \{ \mathbf{u}^H, \mathbf{E}^H, \mathbf{T}^H \}$ for an anisotropic homogeneous elastic problem p^H is known, the DAS theorem yields the

corresponding solution for an inhomogeneous elastic problem p^I as $B_\varepsilon^I = \{\lambda E^H, T^H\}$, if and only if the anisotropic and homogeneous elastic problem possesses, everywhere in the object, a displacement solution satisfying the equations (2.44) and if the displacements boundary conditions are the same for both the homogeneous and inhomogeneous objects.

The solution u^I , for the inhomogeneous problem, in general, have to be integrated with reference to the specific case.

It is worth to underline that in the case where displacement boundary-value u is not equal to zero, the elastic mixed problem can be rewritten as the corresponding first type one, in which only the traction and reaction fields are considered.

For more details on D.A.S. demonstration, see (Fraldi, Cowin, 2004).

It is useful to underline, now and again, the geometrical interpretation of the result of the theorem, constituted by the observation that, in order to find an analytical solution for a given elastic inhomogeneous and anisotropic body in the form $B_\varepsilon^I = \{\lambda E^H, T^H\}$, a necessary and sufficient condition is that the displacement solution for the corresponding anisotropic and homogeneous problem is related with a local plane strain field that has as plane of the strains any plane with support an axis coaxial with the gradient of λ , with rotational part depending on this gradient direction, only.

The D.A.S. theorem can be generalized to comprise different types of composite materials. For example, it is possible to consider the case of a multi-linear law for λ , i.e.:

$$\lambda = \lambda_0 + \lambda_1 x_1 + \lambda_2 x_2 + \lambda_3 x_3 \quad (2.51)$$

with λ_i , $i = \{0, \dots, 3\}$ arbitrary constants.

In this case, it is obtained that the second derivatives of the differential system (2.44) go to zero, therefore, the compatibility equation system becomes as it follows

$$\begin{cases}
\lambda_1 (u_{1,2}^* - u_{2,1}^*)_{,2} = \lambda_2 (u_{1,2}^* - u_{2,1}^*)_{,1} \\
\lambda_2 (u_{2,3}^* - u_{3,2}^*)_{,3} = \lambda_3 (u_{2,3}^* - u_{3,2}^*)_{,2} \\
\lambda_3 (u_{1,3}^* - u_{3,1}^*)_{,1} = \lambda_1 (u_{1,3}^* - u_{3,1}^*)_{,3} \\
\lambda_1 \left[(u_{1,2}^* - u_{2,1}^*)_{,3} + (u_{1,3}^* - u_{3,1}^*)_{,2} \right] = \lambda_2 (u_{1,3}^* - u_{3,1}^*)_{,1} + \lambda_3 (u_{1,2}^* - u_{2,1}^*)_{,1} \\
\lambda_2 \left[(u_{2,1}^* - u_{1,2}^*)_{,3} + (u_{1,3}^* - u_{3,1}^*)_{,1} \right] = \lambda_1 (u_{2,3}^* - u_{3,2}^*)_{,2} + \lambda_3 (u_{2,1}^* - u_{1,2}^*)_{,2} \\
\lambda_3 \left[(u_{3,1}^* - u_{1,3}^*)_{,2} + (u_{3,2}^* - u_{2,3}^*)_{,1} \right] = \lambda_1 (u_{3,2}^* - u_{2,3}^*)_{,3} + \lambda_2 (u_{3,1}^* - u_{1,3}^*)_{,3}
\end{cases} \quad (2.52)$$

Because of the arbitrariness of the assumption about the constants in the λ law, by setting to zero all skew components of $\nabla \otimes \mathbf{u}^H$, a very closed solution of the system can be found in the classical *strain potential* form, (Barber, 1992), that is

$$\mathbf{u}^H = \nabla \phi \quad (2.53)$$

where $\phi = \phi(\mathbf{x})$ is a scalar function. The displacement in the form of the equation (2.52) produces, as well-known, an irrotational deformation field and constitutes the irrotational part of the Papkovitch-neuber representation in the isotropic elasticity, (Barber, 1992). The reason for which this particular case could result very useful is related to the fact that many fundamental solutions in isotropic and anisotropic elasticity have a representation as described in (2.52), as the axisymmetric, thermoelastic and heat-conduction problems.

It is, also, interesting to observe that, for the case of multi-linear law of λ , not any prescription on the form of the strain tensor \mathbf{E}^H is necessary and, so, it is possible to use as *Displacement Associated Solutions* all the three dimensional solutions about anisotropic elasticity, satisfying the equation (2.52), that is, all the three dimensional solutions that satisfy the equation

$$\text{curl } \mathbf{u}^H = \mathbf{0} \quad (2.54)$$

For the examples of applicability of the DAS theorem and for more details on its formulation, let us to send to the references being in literature, (Fraldi, Cowin, 2004).

It is worth to note that the DAS theorem, like the SAS one, yields the possibility to find a closed-form solution for some inhomogeneous materials and it evidences that this possibility depends, in general, on the relation between the geometry of the strain distribution in the homogeneous material and the structural gradient, $\nabla \lambda$, of the inhomogeneous material.

2. ANISOTROPIC MEDIA: VOLUME FRACTION AND FABRIC TENSORS

In multiphase or damage materials, mechanical properties are closely related to the underlying microstructure or crack distribution. Although the volume fraction is the primary parameter in the geometric characterization of the microstructure of such materials, it does not provide information about the arrangement and the orientation of the microstructure. It is therefore necessary to introduce further parameters able to describe such orientations. The approach commonly use to modelling the material microstructure consists on introducing tensors of higher rank which characterize the microstructural architecture. In particular, in many application, microstructural anisotropy seems to be sufficiently well described by a scalar and a symmetric second rank fabric tensor, which restricts the material symmetry to orthotropy.

Fabric tensors may be defined in a wide number of ways but it is required to be a positive define tensor that is a quantitative stereological measure of the microstructural architecture, a measure whose principal axes are coincident with the principal microstructural direction and whose eigenvalues are proportional to the distribution of the microstructure in the associated principal direction. The fabric tensor may be measure on a finite test volume and it is considered a continuous function of the position in the material. It should be highlight that since the fabric tensor is a continuum point property, its applicability to solve real problem is really difficult because would require a wide number of measures. In other words it would be necessary evaluate the fabric tensor in each point of the material.

In the next sections, some way to construct fabric tensors proposed in scientific literature are illustrate.

2.1. Mean Intercept Length (MIL) Tensor

In order to characterize the microstructural anisotropy in orthotropic materials, Harrigan and Mann (1984) proposed a particular second order tensor – the so-called mean intercept length (MIL) tensor – related to the stereological measurement of the microstructural arrangement. In particular, the MIL in a material is define as the average distance, measured along a particular straight line, between two interfaces of the two different constituents. The value of the MIL is a function of the slope θ of the line along which the measurement is made in a specific plane. If, by plotting in a polar diagram the MIL – measured in the selected plane passing through a particular point in the specimen – as function of θ , the polar diagram produced ellipses (see Figure 2.4), than the values of all MILs in the plane may be represented by a second-order tensor in two dimension. By extending these consideration to a three-dimensional case, the MILs in all direction would be represented by an ellipsoid that is by a positive define second rank tensor \mathbf{M} which is commonly related to the mean

intercept length $L(\mathbf{n})$ by the relationship $1/L^2(\mathbf{n}) = \mathbf{n} \cdot \mathbf{M} \mathbf{n}$, where \mathbf{n} is the unit vector in the direction of the mean intercept length measurement.

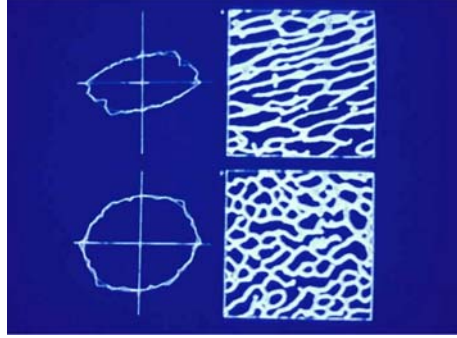


Fig. 2.4.

Polar diagram of the Mean Intercept Length function of a cancellous bone

The MIL approach as well as other stereological methods – e.g. the volume orientation method, the star volume distribution method – were proposed to construct the fabric tensor for biphasic materials, with particular reference to a specific porous material, the cancellous bone (Odgaard *et al.*, 1997). However, it is worth to highlight that for particular microstructure – e.g. planar fibre networks or materials made of a set of plates – the MIL distribution is not in general elliptic and so it may not be analytically expressed in terms of a second-order tensor (Tözeren and Skalak, 1989).

Cowin (Cowin, 1986) defined a fabric tensor \mathbf{H} related to the MIL tensor \mathbf{M} by $\mathbf{H} = \mathbf{M}^{-1/2}$. Such tensor is well defined being the positive square root of the inverse of the positive definite symmetric tensor \mathbf{M} . The difference between \mathbf{H} and \mathbf{M} is in the shape of ellipsoid while the principal axes coincide.

2.2. Orientation Distribution Function (ODF)

Let φ be some macroscopic scalar property of a material. At a given instant, φ generally depends on the material point, identified with the reference position vector \mathbf{x} , and on the orientation, specified by the unit vector \mathbf{n} ; that is, $\varphi = \varphi(\mathbf{x}, \mathbf{n})$. Since only the dependence of φ on \mathbf{n} is concerned in subsequent investigations, it is convenient to consider \mathbf{x} as fixed and drop the dependence of φ on \mathbf{x} . Then we write

$$\varphi = f(\mathbf{n}), \quad f: L \rightarrow R \quad (2.55)$$

and call f , the scalar-valued function defined on the unit sphere L , the *orientation distribution function* (ODF) of the property φ . Concretely φ may be the effective surface density of the microdefects, Young's modulus, the wave speed, the electrical resistivity, the fatigue limit, etc. (Lemaitre *et al.*, 1987).

The function $f(\mathbf{n})$ must satisfy the condition

$$f(\mathbf{n}) = f(-\mathbf{n}), \quad \forall \mathbf{n} \in L, \quad (2.56)$$

because any material property φ in a direction is independent of the geometrical choice made between \mathbf{n} and $-\mathbf{n}$ for defining that direction. It is possible to prove that the invariance requirement (2.56) is satisfied if and only if there exists a function \hat{f} from $N = L \otimes L$ to \mathbb{R} such that

$$f(\mathbf{n}) = \hat{f}(\mathbf{n} \otimes \mathbf{n}) = \hat{f}(N), \quad \forall \mathbf{n} \in L. \quad (2.57)$$

In the following we only consider the function $\hat{f}(N)$ for which the condition (2.56) is verified.

Assume $\hat{f}(N)$ to be square-integrable:

$$\int_L |\hat{f}(N)|^2 da < +\infty, \quad (2.58)$$

where $da = \sin \theta d\theta d\phi$ is an infinitesimal surface element of the unit sphere L . It is that known (Vilenkin, 1969; Bunge, 1982; Jones, 1985) that $\hat{f}(N)$ can be expanded in the following Fourier series:

$$\begin{aligned} \hat{f}(N) &= f_0(N) + f_1(N) + f_2(N) + \dots \\ &= g + \mathbf{G}' : \mathbf{F}(N) + \mathcal{G}' :: \mathbb{F}(N) + \dots, \quad \forall N \in N, \end{aligned} \quad (2.59)$$

which is convergent in mean, i.e.

$$\lim_{n \rightarrow \infty} \int_L |\hat{f}(N) - s_n(N)|^2 da = 0, \quad s_n(N) := f_0(N) + f_1(N) + \dots + f_n(N). \quad (2.60)$$

In the equation (2.59), $\{\mathbf{I}, \mathbf{F}(N), \mathbb{F}(N), \dots\}$ are generalized spherical harmonics (Kanatani, 1984; Onat, 1984; Jones, 1985) and form a complete orthogonal basis for the square-integrable functions on L .

The first two tensor spherical harmonics $\mathbf{F}(\mathbf{N})$ and $\mathbb{F}(\mathbf{N})$ are of particular interest. In view of the tensor products of Kronecker-type, they may be written in the coordinate-free forms:

$$\mathbf{F}(\mathbf{N}) = \mathbf{N} - \frac{1}{3}\mathbf{I} \quad (2.61)$$

$$\begin{aligned} \mathbb{F}(\mathbf{N}) = & \mathbf{N} \otimes \mathbf{N} - \frac{1}{7}(\mathbf{I} \otimes \mathbf{N} + \mathbf{N} \otimes \mathbf{I} + \mathbf{I} \underline{\otimes} \mathbf{N} + \mathbf{N} \underline{\otimes} \mathbf{I} + \mathbf{I} \overline{\otimes} \mathbf{N} + \mathbf{N} \overline{\otimes} \mathbf{I}) + \\ & \frac{1}{35}(\mathbf{I} \otimes \mathbf{I} + \mathbf{I} \underline{\otimes} \mathbf{I} + \mathbf{I} \overline{\otimes} \mathbf{I}) \end{aligned} \quad (2.62)$$

The orthogonality of the basis functions $\{\mathbf{I}, \mathbf{F}(\mathbf{N}), \mathbb{F}(\mathbf{N}), \dots\}$ means that

$$\begin{aligned} \int_L \mathbf{F}(\mathbf{N}) da &= \mathbf{0}, & \int_L \mathbb{F}(\mathbf{N}) da &= \mathbf{0} \\ \int_L \mathbf{F}(\mathbf{N}) \otimes \mathbb{F}(\mathbf{N}) da &= \int_L \mathbb{F}(\mathbf{N}) \otimes \mathbf{F}(\mathbf{N}) da = \mathbb{O}_{6, \dots} \end{aligned} \quad (2.63)$$

where \mathbb{O}_6 denotes the sixth-order zero tensor. It is important to remark that $\mathbf{F}(\mathbf{N})$ is symmetric and traceless:

$$\mathbf{F}^T = \mathbf{F}; \quad \mathbf{I} : \mathbf{F} = 0, \quad (2.64)$$

and that $\mathbb{F}(\mathbf{N})$ is completely symmetric and traceless:

$$\mathbb{F} = (\mathbf{I} \overline{\otimes} \mathbf{I}) \mathbb{F} = \mathbb{F}^T; \quad (\mathbf{Y} \overline{\otimes} \mathbf{X}) :: \mathbb{F} = (\mathbf{Y} \overline{\otimes} \mathbf{X}^T) :: \mathbb{F}, \quad \forall \mathbf{X}, \mathbf{Y} \in L; \quad \mathbb{F} \mathbf{I} = \mathbf{0}. \quad (2.65)$$

The first three expansion coefficients of equation (2.59) can be determined from $f(\mathbf{n})$ via the integrals (Kanatani, 1984):

$$\begin{aligned} g &= \frac{1}{4\pi} \int_L \hat{f}(\mathbf{N}) da, & \mathbf{G}' &= \frac{15}{8\pi} \int_L \hat{f}(\mathbf{N}) \mathbf{F}(\mathbf{N}) da, \\ \mathbb{G}' &= \frac{315}{32\pi} \int_L \hat{f}(\mathbf{N}) \mathbb{F}(\mathbf{N}) da. \end{aligned} \quad (2.66)$$

Due to equations (2.64) and (2.65), \mathbf{G}' turns out to be symmetric and traceless and \mathbb{G}' to be completely symmetric and traceless. With these properties, in the most general case, \mathbf{G}' and \mathbb{G}' contain five and nine independent components, respectively.

It is readily seen from equations (2.59) and (2.60) that any square-integrable ODF $\hat{f}(N)$ is fully characterized by its scalar and tensor expansion coefficients $\{g, \mathbf{G}', \mathbb{G}', \dots\}$. If only the leading terms (for example, the first three ones) of the series expansion, (2.59), are retained, a finite or discrete description is then obtained for $\hat{f}(N)$. Theoretically speaking, the accuracy of such a description increases with the number of the leading terms being employed; in practice, the maximum value of this number is determined by the degree of accuracy with which the directional data of the property φ are experimentally acquired.

The importance of this result resides in the fact that only the tensors of zero or even orders are usable for a finite description of the ODF of a scalar-valued physical or mechanical property φ .

2.3. Fabric Tensor and Microcrack Distribution

In the characterization of mechanical response of damaged materials, a central problem is represented by the development of the formalism which enables a traditional continuum representation of the statistical distribution of microcracks compiled from the stereological data measured on a statistically homogeneous volume of damaged microstructure. The selection of the damage parameter approximating the measured data is not unique due to the contradictory requirements of accuracy and simplicity.

In the framework of damage mechanics, the effective continuum theories (Krajcinovic, 1996) are based on the assumption that the exact location of a microcrack within a representative volume element is not very important for the determination of the effective properties. This statement is, rigorously speaking, valid only in the dilute concentration limit. In other case, it is necessary to determine the distribution of crack surface densities as a function, for example, of the orientation of their bedding planes. For this purpose, the damage at a material point x is defined by a finite set of doublets $[\rho_i, n_i]$ ($i = 1, 2, \dots, m$) where ρ_i is the microcrack density in a plane with normal n_i . Geometrically this set of doublets represents a binned histogram. Each bin defines the microcrack density in planes with orientations belonging to a particular range of angles. To determine the density of microcracks sharing a particular orientation (defined by a normal \mathbf{n} to their bedding plane) it is necessary to make a large number of parallel cuts through a representative volume element of the actual material which maps on the observed material point in the effective continuum. In the limit of a very large number of orientations the density function $\rho(\mathbf{n})$ tends to a continuous distribution of the densities of microcracks in planes with normals \mathbf{n} passing through the material point \mathbf{x}_0 (Ilankamban and Krajcinovic 1987, Curran, *et al.* 1987).

The principal problem in the formulation of an analytical representation of the experimental data is related to the representation of the raw statistical data in a frame indifferent (objective) manner. This question was explored and answered by Kanatani (1984) and later elaborated upon in connection to the damage distribution by Budiansky and O'Connell (1976), Onat and Leckie (1984), Wong (1985) and Lubarda and Krajcinovic (1993). The central task is to establish a procedure relating a measured distribution of microcrack densities as a function of their orientation $\rho(\mathbf{n})$ to an appropriate damage measure in form of a tensor invariant to coordinate transformations. This procedure must provide a criterion needed to measure the fit between the experimental data and various analytical descriptions of the microcrack distributions. The empirical function $\rho(\mathbf{n})$, typically determined for a limited number of bedding planes and samples, is seldom smooth. Depending on the heterogeneity of the material, size of the representative volume element, experimental technique, available equipment and finally the chance itself the function $\rho(\mathbf{n})$ may substantially change from one sample to the other. A large number of samples and sections may be needed for a statistically valid characterization of the function $\rho(\mathbf{n})$. In most cases a task like this is not cheap enough to be feasible. It is possible to utilize the measured or conjectured directional dependence of the crack surface area density $\rho(\mathbf{n})$ directly into an appropriately formulated computational model (Ilankamban and Krajcinovic 1987, Curran, *et al.* 1987). For the present purposes it is obviously advantageous to use a tensor function which approximates the distribution $\rho(\mathbf{n})$ with sufficient accuracy. The procedure, shown in the previous section, is developed in order to derive a tensor approximation of the raw data arranged into the histogram, expanding the function $\rho(\mathbf{n})$ into a Fourier-type series of certain families of Laplace spherical harmonics (Kanatani 1984, Onat and Leckie 1988) which represent the dyadic products of the unit vector \mathbf{n} and the Kronecker delta tensor δ . Since a surface is defined by an axial vector the analytical expression for the distribution $\rho(\mathbf{n})$ can involve only even order tensors. A rigorous approximation of an empirical or actually measured function $\rho(\mathbf{n})$ involves an infinite series of tensors of even order. In many cases the details of this distribution may not have a discernible effect on the macro properties and may not be reproducible when testing "identical" specimens under "identical" circumstances. For purely practical purposes this series must be truncated to a rather moderate number of terms limited to the lowest order tensors. The truncation introduces inevitable errors into the selected representation and some non-physical effects which were not noticed until recently.

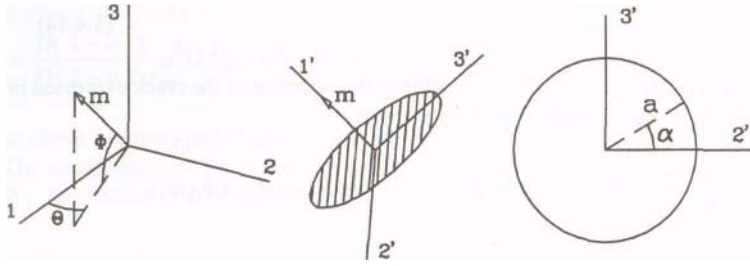


Fig. 2.5.
Geometry of a penny-shaped crack

With reference to penny-shaped cracks defined by their radii a and two Euler angles (θ, ϕ) , shown in Figure 2.5., it is possible to write (Krajcinovic, 1996) the average crack density within a selected unit sphere centered at a material point as

$$\begin{aligned} \bar{w} &= \frac{1}{4\pi} \int_{a^-}^{a^+} a^3 \mathcal{G}(a) da \int_0^{2\pi} \int_{-\pi/2}^{\pi/2} \rho(\phi, \theta) \cos \phi \, d\theta d\phi = \\ &= \frac{1}{4\pi} N \langle a^3 \rangle \int_0^{2\pi} \int_{-\pi/2}^{\pi/2} \rho(\phi, \theta) \cos \phi \, d\theta d\phi = N \langle a^3 \rangle \bar{\rho}(\mathbf{n}) \end{aligned} \quad (2.67)$$

where $N \langle a^3 \rangle = \int_{a^-}^{a^+} a^3 \mathcal{G}(a) da$ is the non-dimensional microcracks density. To be able to compare different microcrack distributions with respect to the orientations $w(\mathbf{n}) = N \langle a^3 \rangle \rho(\mathbf{n}) = N \langle a^3 \rangle \rho(\phi, \theta)$ the product $N \langle a^3 \rangle = 1$ will be fixed in the sequel.

Scalar Representation of the Damage Variable. The microcrack distribution can be assumed to be approximately isotropic when the microcrack density is a weak function of the plane orientation (defined by the normal \mathbf{n} to the bedding plane through the material point). In this special case (which is preferred primarily by analysts if not by the geometry, nature and the physics of defect nucleation and growth) the microcrack distribution is fully defined by a single scalar ρ_0 which represents the total microcrack density or by the density $\bar{\rho}$ averaged over the solid angle. These two scalar measures of the crack distribution are related by the well known formula

$$\rho^0 \equiv D^0 = \int_{\Omega} \rho(\mathbf{n}) d\Omega = 4\pi \bar{\rho}. \quad (2.68)$$

The integration in (2.68) is extended over all orientations within the solid angle $\Omega = 4\pi$. In this, simplest of all cases, the damage is defined by a single parameter ρ^0 (microcrack density). All symmetries of the original solid are preserved. The scalar damage variable (2.68) is introduced for the sake of consistency and uniformity. Due to its simplicity the scalar damage variable representation has been extensively utilized in the past (see, for example, Lemaitre and Chaboche 1978, Lemaitre 1986, 1992).

Second Order Tensor Representation of the Damage Variable. The isotropic distribution of microcracks is a relatively rare phenomenon which may occur in rocks in crustal conditions (i.e. well confined in all directions) which are exposed to large temperatures and internal pressures and/or expansive exothermic reactions. In a general case the microcracks distribution is characterized by a varying degree of anisotropy. In a frequently encountered class of problems and tests the microcrack distribution may render the specimen statistically (macro) orthotropic. The orthotropy may also be a function of the variations of strength and stiffness with direction. This may happen in sedimentary rocks characterized by a strong dependence of the cohesive strength on the primary depositional petrofabric and also in laminate composites made of fiber reinforced laminae. The microcrack induced orthotropy can also be stress induced. The damage density in an initially isotropic solid subjected to proportional loading will reach maximum densities in the planes perpendicular to the largest principal stress. Similarly, the microcrack densities will be minimal in planes which are orthogonal to the minimum principal stress. The principal planes of the damage density will often be perpendicular assuming that the state of stress is simple and the loads proportional. This class of microcrack distributions may be adequately represented by a second order tensor. The microcrack density in planes with a normal \mathbf{n} can be in this case defined by the expression

$$\rho(\mathbf{n}) = \rho_{ij} n_i n_j \quad (2.69)$$

(Lubarda, Krajcinovic 1993) where ρ_{ij} is a symmetric second order tensor. Integrating (2.69) over the entire solid angle, and using the identity

$$\int_{\Omega} n_i n_j d\Omega = \frac{4\pi}{3} \delta_{ij} \quad (2.70)$$

where δ_{ij} is the Kronecker (identity) delta tensor, it follows that the first invariant (trace) of the second order tensor ρ_{ij} is

$$\rho_{kk} = \frac{3}{4\pi} \rho^0 \quad (2.71)$$

The scalar damage variable ρ^0 in (2.71) is defined by (2.68). Multiplying both sides of (2.69) by $n_m n_n$ and integrating the product over the solid angle while making use of the identity

$$\int_{\Omega} n_i n_j n_m n_n d\Omega = \frac{4\pi}{5} I_{ijmn} \quad (2.72)$$

leads to the following expression

$$\frac{8\pi}{15} \left(\rho_{ij} + \frac{1}{2} \rho_{kk} \delta_{ij} \right) = \int_{\Omega} \rho(n) n_i n_j d\Omega. \quad (2.73)$$

The fourth order tensor I in (2.72) is defined by the tensor products of two delta second order tensors as

$$I_{ijmn} = \frac{1}{3} (\delta_{ij} \delta_{mn} + \delta_{im} \delta_{jn} + \delta_{in} \delta_{jm}) \quad (2.74)$$

The microcrack density tensor can now be derived by substituting (2.71) into (2.73)

$$\rho_{ij} = \frac{15}{8\pi} \left(D_{ij} - \frac{\rho^0}{5} \delta_{ij} \right) \quad (2.75)$$

where

$$D_{ij} = \int_{\Omega} \rho(n) n_i n_j d\Omega \quad (2.76)$$

is referred to as the second order damage tensor. The microcrack density distribution (2.69) is, in view of (2.75), a function of the scalar and second order tensor damage parameters

$$\rho(n) = \frac{15}{8\pi} n_i n_j D_{ij} - \frac{3}{8\pi} D^0. \quad (2.77)$$

2.4. Relationship between Fabric Tensor and Elasticity Tensor

From a mathematical point of view, identifying the dependence of the elastic behaviour of the material on its microstructure consists in analyzing the formal relationship between the fabric tensor and the elasticity tensor.

The main attempt to relate a fabric tensor describing microstructure to a fourth rank elasticity tensor – with specific reference to porous materials – is due to Cowin (Cowin, 1985). He proposed a model based on a normalized second rank fabric tensor and developed a general representation of $\bar{\mathbf{C}}$ as a function of the solid volume fraction γ and of the invariants of the fabric tensor \mathbf{H} based on the notion that the matrix material of the porous elastic solid is isotropic and that the anisotropy of the porous elastic solid itself is due only to the geometry of microstructure represented by the fabric tensor. The mathematical statement of this notion is that the stress tensor \mathbf{T} is an isotropic function of the strain tensor \mathbf{E} and the fabric tensor \mathbf{H} as well as the solid volume fraction γ . Thus, the tensor valued function

$$\mathbf{T} = \mathbf{T}(\gamma, \mathbf{E}, \mathbf{H}) \quad (2.78)$$

has the property that

$$\mathbf{Q}\mathbf{T}\mathbf{Q}^T = \mathbf{T}(\gamma, \mathbf{Q}\mathbf{E}\mathbf{Q}^T, \mathbf{Q}\mathbf{H}\mathbf{Q}^T) \quad (2.79)$$

for all orthogonal tensors \mathbf{Q} . This definition of an isotropic tensor valued function is given, for example, by Truesdell and Noll (1965). In accord with the isotropy assumption, the stress tensor \mathbf{T} has the representation

$$\begin{aligned} \mathbf{T} = & f_1 \mathbf{I} + f_2 \mathbf{H} + f_3 \mathbf{H}^2 + f_4 \mathbf{E} + f_5 \mathbf{E}^2 + f_6 (\mathbf{H}\mathbf{E} + \mathbf{E}\mathbf{H}) \\ & + f_7 (\mathbf{H}^2 \mathbf{E} + \mathbf{E}\mathbf{H}^2) + f_8 (\mathbf{H}\mathbf{E}^2 + \mathbf{E}^2 \mathbf{H}) + f_9 (\mathbf{H}^2 \mathbf{E}^2 + \mathbf{E}^2 \mathbf{H}^2) \end{aligned} \quad (2.80)$$

where f_1 through f_9 are function of the ten invariants $\text{Tr}\mathbf{H}$, $\text{Tr}\mathbf{H}^2$, $\text{Tr}\mathbf{H}^3$, $\text{Tr}\mathbf{E}$, $\text{Tr}\mathbf{E}^2$, $\text{Tr}\mathbf{E}^3$, $\text{Tr}\mathbf{H}\mathbf{E}$, $\text{Tr}\mathbf{H}^2 \mathbf{E}$, $\text{Tr}\mathbf{H}\mathbf{E}^2$, $\text{Tr}\mathbf{E}^2 \mathbf{H}^2$. This representation is reduced by the requirement that \mathbf{T} be linear in \mathbf{E} and that \mathbf{T} vanish when \mathbf{E} vanishes, thus

$$\mathbf{T} = f_1 \mathbf{I} + f_2 \mathbf{H} + f_3 \mathbf{H}^2 + f_4 \mathbf{E} + f_6 (\mathbf{H}\mathbf{E} + \mathbf{E}\mathbf{H}) + f_7 (\mathbf{H}^2 \mathbf{E} + \mathbf{E}\mathbf{H}^2) \quad (2.81)$$

where f_1, f_2, f_3 must be of the form

$$\begin{aligned} f_1 &= a_1 Tr\mathbf{E} + a_2 Tr\mathbf{HE} + a_3 Tr\mathbf{H}^2\mathbf{E}, \\ f_2 &= d_1 Tr\mathbf{E} + b_1 Tr\mathbf{HE} + b_2 Tr\mathbf{H}^2\mathbf{E}, \\ f_3 &= d_2 Tr\mathbf{E} + d_3 Tr\mathbf{HE} + b_3 Tr\mathbf{H}^2\mathbf{E}, \end{aligned} \quad (2.82)$$

and where $a_1, a_2, a_3, b_1, b_2, b_3, d_1, d_2$ and d_3 , are function of $Tr\mathbf{H}$, $Tr\mathbf{H}^2$ and $Tr\mathbf{H}^3$. It follows then that

$$\begin{aligned} \mathbf{T} &= \mathbf{I} \left(a_1 Tr\mathbf{E} + a_2 Tr\mathbf{HE} + a_3 Tr\mathbf{H}^2\mathbf{E} \right) + \mathbf{H} \left(d_1 Tr\mathbf{E} + b_1 Tr\mathbf{HE} + b_2 Tr\mathbf{H}^2\mathbf{E} \right) \\ &\quad + \mathbf{H}^2 \left(d_2 Tr\mathbf{E} + d_3 Tr\mathbf{HE} + b_3 Tr\mathbf{H}^2\mathbf{E} \right) + 2c_1\mathbf{E} + 2c_2(\mathbf{HE} + \mathbf{EH}) \\ &\quad + 2c_3(\mathbf{H}^2\mathbf{E} + \mathbf{EH}^2) \end{aligned} \quad (2.83)$$

where we have set $f_4 = 2c_1$, $f_6 = 2c_2$ and $f_7 = 2c_3$. This result may be expressed in indicial notation as

$$\begin{aligned} T_{ij} &= \delta_{ij} \left(a_1 E_{kk} + a_2 H_{rp} E_{pr} + a_3 H_{rq} H_{qp} E_{pr} \right) + H_{ij} \left(d_1 E_{kk} + b_1 H_{rp} E_{pr} + b_2 H_{rq} H_{qp} E_{pr} \right) \\ &\quad + H_{is} H_{sj} \left(d_2 E_{kk} + d_3 H_{rp} E_{pr} + b_3 H_{rq} H_{qp} E_{pr} \right) + 2c_1 E_{ij} + 2c_2 (H_{ir} E_{rj} + E_{ir} H_{rj}) \\ &\quad + 2c_3 (H_{ip} H_{pr} E_{rj} + E_{ir} H_{rp} H_{pj}) \end{aligned} \quad (2.84)$$

Comparison of this result with the constitutive equation $T_{ij} = C_{ijhk} E_{hk}$ suggests that C_{ijhk} should be of the form

$$\begin{aligned} C_{ijhk} &= \left(a_1 \delta_{ij} + d_1 H_{ij} + d_2 H_{is} H_{sj} \right) \delta_{hk} + \left(a_2 \delta_{ij} + b_1 H_{ij} + d_3 H_{is} H_{sj} \right) H_{hk} \\ &\quad + \left(a_3 \delta_{ij} + b_2 H_{ij} + b_3 H_{is} H_{sj} \right) H_{hq} H_{qk} + 2c_1 \delta_{hi} \delta_{kj} \\ &\quad + 2c_2 (H_{ih} \delta_{kj} + \delta_{ih} H_{kj}) + 2c_3 (H_{ip} H_{pk} \delta_{hj} + \delta_{ih} H_{kp} H_{ps}). \end{aligned} \quad (2.85)$$

In order to satisfy the symmetry conditions (1.90) we must set $d_1 = a_2$, $d_2 = a_3$, and $d_3 = b_2$ and take the symmetric parts of the terms multiplied by $2c_1$, $2c_2$, and $2c_3$ with respect to hk and ij . The final results may be express as follow

$$\begin{aligned}
C_{ijhk} = & a_1 \delta_{ij} \delta_{hk} + a_2 (H_{ij} \delta_{ij} + H_{hk} \delta_{hk}) + a_3 (\delta_{ij} H_{hq} H_{qk} + \delta_{hk} H_{iq} H_{qj}) + \\
& + b_1 H_{ij} H_{hk} + b_2 (H_{ij} H_{hq} H_{qk} + H_{is} H_{sj} H_{hk}) + b_3 H_{is} H_{sj} H_{hq} H_{qk} + \\
& + c_1 (\delta_{hi} \delta_{kj} + \delta_{ki} \delta_{hj}) + c_2 (H_{ih} \delta_{kj} + H_{hj} \delta_{ki} + H_{ik} \delta_{hj} + H_{kj} \delta_{hi}) + \\
& + c_3 (H_{ir} H_{rh} \delta_{kj} + H_{rj} H_{hr} \delta_{ki} + H_{ir} H_{rk} \delta_{hj} + H_{kr} H_{rj} \delta_{ih})
\end{aligned} \quad (2.86)$$

where $a_1, a_2, a_3, b_1, b_2, b_3, c_1, c_2$ and c_3 are functions of γ and $Tr\mathbf{H}$, $Tr\mathbf{H}^2$ and $Tr\mathbf{H}^3$.

It is possible to show that the representation (2.86) for the fourth rank elasticity tensor is not capable of representing all possible elastic material symmetry. The last material symmetry that may be represented by is orthotropy. In fact, expanding in indicial notation in the coordinate system that diagonalized the fabric tensor ($H_{12} = H_{13} = H_{23} = 0$), only the following nine components of the elastic tensor are non-zero and are function of the nine coefficient $a_1, a_2, a_3, b_1, b_2, b_3, c_1, c_2, c_3$ and of the three eigenvalues of \mathbf{H} , H_{11}, H_{22} and H_{33}

$$\begin{aligned}
C_{1111} &= a_1 + 2c_1 + 2(a_2 + 2c_2)H_{11} + (2a_3 + b_1 + 4c_3)H_{11}^2 + 2b_2H_{11}^3 + b_3H_{11}^4 \\
C_{2222} &= a_1 + 2c_1 + 2(a_2 + 2c_2)H_{22} + (2a_3 + b_1 + 4c_3)H_{22}^2 + 2b_2H_{22}^3 + b_3H_{22}^4 \\
C_{3333} &= a_1 + 2c_1 + 2(a_2 + 2c_2)H_{33} + (2a_3 + b_1 + 4c_3)H_{33}^2 + 2b_2H_{33}^3 + b_3H_{33}^4 \\
C_{1122} &= a_1 + a_2(H_{11} + H_{22}) + a_3(H_{11}^2 + H_{22}^2) + b_1H_{11}H_{22} + b_2(H_{11}H_{22}^2 + H_{22}H_{11}^2) \\
&+ b_3H_{11}^2H_{22}^2 \\
C_{1133} &= a_1 + a_2(H_{11} + H_{33}) + a_3(H_{11}^2 + H_{33}^2) + b_1H_{11}H_{33} + b_2(H_{11}H_{33}^2 + H_{33}H_{11}^2) \\
&+ b_3H_{11}^2H_{33}^2 \\
C_{3322} &= a_1 + a_2(H_{33} + H_{22}) + a_3(H_{33}^2 + H_{22}^2) + b_1H_{33}H_{22} + b_2(H_{33}H_{22}^2 + H_{22}H_{33}^2) \\
&+ b_3H_{33}^2H_{22}^2 \\
C_{1212} &= c_1 + c_2(H_{11} + H_{22}) + c_3(H_{11}^2 + H_{22}^2) \\
C_{1313} &= c_1 + c_2(H_{11} + H_{33}) + c_3(H_{11}^2 + H_{33}^2) \\
C_{3232} &= c_1 + c_2(H_{33} + H_{22}) + c_3(H_{33}^2 + H_{22}^2)
\end{aligned} \quad (2.87)$$

Note that these nine components of the elasticity tensor are distinct if and only if the eigenvalues of \mathbf{H} are distinct. In fact, it is easy to see that by setting $H_{22} = H_{33}$ in the (2.87), only the following six constants are different

$$\begin{aligned}
C_{1111} &= a_1 + 2c_1 + 2(a_2 + 2c_2)H_{11} + (2a_3 + b_1 + 4c_3)H_{11}^2 + 2b_2H_{11}^3 + b_3H_{11}^4 \\
C_{2222} &= C_{3333} = a_1 + 2c_1 + 2(a_2 + 2c_2)H_{22} + (2a_3 + b_1 + 4c_3)H_{22}^2 + 2b_2H_{22}^3 + b_3H_{22}^4 \\
C_{1122} &= C_{1133} = a_1 + a_2(H_{11} + H_{22}) + a_3(H_{11}^2 + H_{22}^2) + b_1H_{11}H_{22} + b_2(H_{11}H_{22}^2 + H_{22}H_{11}^2) \\
&\quad + b_3H_{11}^2H_{22}^2 \\
C_{3322} &= a_1 + a_2(H_{33} + H_{22}) + a_3(H_{33}^2 + H_{22}^2) + b_1H_{33}H_{22} + b_2(H_{33}H_{22}^2 + H_{22}H_{33}^2) \\
&\quad + b_3H_{33}^2H_{22}^2 \\
C_{1212} &= C_{1313} = c_1 + c_2(H_{11} + H_{22}) + c_3(H_{11}^2 + H_{22}^2) \\
C_{3232} &= c_1 + c_2(H_{33} + H_{22}) + c_3(H_{33}^2 + H_{22}^2)
\end{aligned} \tag{2.88}$$

and only five of which are independent being $C_{2222} = C_{2233} + 2C_{2323}$. Thus, the represented material symmetry is the transversely isotropy. In the same way, if the eigenvalues of \mathbf{H} are all equal the represented material symmetry is the isotropy, being only the following three constant different

$$\begin{aligned}
C_{1111} &= C_{2222} = C_{3333} = a_1 + 2c_1 + 2(a_2 + 2c_2)H_{11} + (2a_3 + b_1 + 4c_3)H_{11}^2 \\
&\quad + 2b_2H_{11}^3 + b_3H_{11}^4 \\
C_{1122} &= C_{1133} = C_{2233} = a_1 + a_2(H_{11} + H_{22}) + a_3(H_{11}^2 + H_{22}^2) + b_1H_{11}H_{22} \\
&\quad + b_2(H_{11}H_{22}^2 + H_{22}H_{11}^2) + b_3H_{11}^2H_{22}^2 \\
C_{1212} &= C_{1313} = C_{3232} = c_1 + c_2(H_{11} + H_{22}) + c_3(H_{11}^2 + H_{22}^2)
\end{aligned} \tag{2.89}$$

and only two of which are independent, being $C_{1111} = C_{1122} + 2C_{1212}$.

The nine functions $a_1, a_2, a_3, b_1, b_2, b_3, c_1, c_2$ and c_3 depending upon γ , $Tr\mathbf{H}$, $Tr\mathbf{H}^2$ and $Tr\mathbf{H}^3$, can be determine by means of experimental tests.

Following this method, Zysset and Curnier (1995) introduce a general approach for relating the material microstructure to the four rank elasticity tensor. In particular, they describe the microstructure by means of a scalar and a symmetric, traceless second rank fabric tensor. By using a representation theorem for anisotropic function with tensorial arguments, they derive a general expression for the elastic free energy and discuss the resulting material symmetry in terms of the fabric tensor.

Specifically, they hypothesize that the mechanical anisotropy of the material is identical to that of a single microstructural property $f = f(\mathbf{N}) > 0$, where $\mathbf{N} = \mathbf{n} \otimes \mathbf{n}$ is the dyadic product of the unit vector \mathbf{n} specifying the orientation (He *et al.*, 1995). By following the procedure shown in section 2.2, assuming

that the function f to be square integrable, it can be expanded in a convergent Fourier series

$$f(N) = g \cdot I + G : F(N) + \mathcal{G} :: \mathbb{F}(N) + \dots, \quad \forall N \quad (2.90)$$

where I , $F(N)$ and $\mathbb{F}(N)$ are even ranked tensorial basis functions – in particular I is the second order unit tensor, while $F(N)$ and $\mathbb{F}(N)$ are given by the (2.61) and (2.62), respectively – and g , G and \mathcal{G} are the corresponding even ranked tensorial coefficients, called fabric tensor and given by the equations (2.66). As highlight in section 2.2., the accuracy of the series expansion improves with the number of retained leading terms. However, in most applications, the first and second terms provide a sufficient description of material anisotropy. So, the orientation distribution function f is approximate with

$$f(N) = g \cdot I + G : F(N) \quad (2.91)$$

which implies a restriction on material symmetry – that can be orthotropy if all three eigenvalues of G are distinct, transverse isotropy if only two eigenvalues of G are distinct or isotropy if the tensor G vanishes.

By using the second rank tensor representation Q of the orthogonal group *Orth*, the material symmetry group G can be characterized by the fabric tensors:

$$Q \in G \Leftrightarrow \begin{cases} Q^T g I Q = g I \\ Q^T G Q = G \\ (Q \otimes Q)^T \mathcal{G} (Q \otimes Q) = \mathcal{G} \\ \dots \end{cases} \quad (2.92)$$

Following this hypothesis, a scalar valued function $\psi(E)$ invariant with respect to the elements of the symmetry group G can be identified with an isotropic function $\hat{\psi}(E, g, G, \mathcal{G}, \dots)$ of the same argument and the corresponding fabric tensor (Boehler, 1987)

$$\psi(E) = \psi(Q^T E Q), \quad \forall Q \in G,$$

$$\hat{\psi}(E, g, G, \mathcal{G}, \dots) = \hat{\psi}(Q^T E Q, g, Q^T G Q, (Q \otimes Q)^T \mathcal{G} (Q \otimes Q)), \quad \forall Q \in \text{Orth}.$$

Representation theorems then provide the most general form of the isotropic scalar function $\hat{\psi}(E, g, G, \mathcal{G}, \dots)$ in terms of invariants of the arguments.

For a scalar g and two second rank tensor arguments \mathbf{E} and \mathbf{G} , with \mathbf{G} being traceless, a set of irreducible invariants is given by (Boehler, 1987) $Tr(\mathbf{E})$, $Tr(\mathbf{E}^2)$, $Tr(\mathbf{E}^3)$, g , $Tr(\mathbf{G}^2)$, $Tr(\mathbf{G}^3)$, $Tr(\mathbf{EG})$, $Tr(\mathbf{E}^2\mathbf{G})$, $Tr(\mathbf{EG}^2)$, $Tr((\mathbf{EG})^2)$. Retaining only quadratic terms in \mathbf{E} to come up with linear elasticity, general form of the elastic free energy is

$$\begin{aligned}\psi = \psi(\mathbf{E}, g, \mathbf{G}) &= \frac{c_1}{2} Tr^2(\mathbf{E}) + \frac{c_2}{2} Tr(\mathbf{E}^2) + \frac{c_3}{2} Tr^2(\mathbf{EG}) \\ &+ c_4 Tr(\mathbf{E}^2\mathbf{G}) + \frac{c_5}{2} Tr^2(\mathbf{EG}^2) + \frac{c_6}{2} Tr((\mathbf{EG})^2) + c_7 Tr(\mathbf{E}) Tr(\mathbf{EG}) \\ &+ c_8 Tr(\mathbf{EG}) Tr(\mathbf{EG}^2) + c_9 Tr(\mathbf{E}) Tr(\mathbf{EG}^2)\end{aligned}\quad (2.93)$$

where c_i are functions of g and the two invariants of \mathbf{G} .

The constitutive equation for the stress tensor is obtained by derivation of the free energy potential ψ with respect to the strain \mathbf{E}

$$\begin{aligned}\mathbf{T} = \frac{\partial \psi}{\partial \mathbf{E}}(\mathbf{E}, g, \mathbf{G}) &= c_1 Tr(\mathbf{E}) \mathbf{I} + c_2 \mathbf{E} + c_3 Tr(\mathbf{EG}) \mathbf{G} + c_4 (\mathbf{EG} + \mathbf{GE}) \\ &+ c_5 Tr(\mathbf{EG}^2) \mathbf{G}^2 + c_6 (\mathbf{GEG}) + c_7 (Tr(\mathbf{EG}) \mathbf{I} + Tr(\mathbf{E}) \mathbf{G}) \\ &+ c_8 (Tr(\mathbf{EG}^2) \mathbf{G} + Tr(\mathbf{EG}) \mathbf{G}^2) + c_9 (Tr(\mathbf{EG}^2) \mathbf{I} + Tr(\mathbf{E}) \mathbf{G}^2).\end{aligned}\quad (2.94)$$

The elasticity tensor is obtained by further derivation

$$\begin{aligned}\mathbb{C} &= \frac{\partial^2 \psi}{\partial \mathbf{E}^2}(\mathbf{E}, g, \mathbf{G}) \\ &= c_1 \mathbf{I} \otimes \mathbf{I} + c_2 \mathbf{I} \bar{\otimes} \mathbf{I} + c_3 \mathbf{G} \bar{\otimes} \mathbf{G} + c_4 (\mathbf{G} \bar{\otimes} \mathbf{I} + \mathbf{I} \bar{\otimes} \mathbf{G}) + c_5 \mathbf{G}^2 \otimes \mathbf{G}^2 + c_6 \mathbf{G} \bar{\otimes} \mathbf{G} \\ &+ c_7 (\mathbf{I} \otimes \mathbf{G} + \mathbf{G} \otimes \mathbf{I}) + c_8 (\mathbf{G} \otimes \mathbf{G}^2 + \mathbf{G}^2 \otimes \mathbf{G}) + c_9 (\mathbf{I} \otimes \mathbf{G}^2 + \mathbf{G}^2 \otimes \mathbf{I}).\end{aligned}\quad (2.95)$$

The material symmetry represented by the elasticity tensor in the form (2.95), like which one in (2.86), is at least the orthotropy that may degenerate into transverse isotropy when two eigenvalues of \mathbf{G} are identical and into isotropy when the fabric tensor \mathbf{G} vanishes.

By using the spectral decomposition of \mathbf{G} :

$$\mathbf{G} = g_i \mathbf{G}_i, \quad \mathbf{G}_i = \mathbf{g}_i \otimes \mathbf{g}_i,$$

where g_i are the eigenvalues and \mathbf{g}_i are the unit orthogonal eigenvectors of \mathbf{G} , and the property $\mathbf{G}_1 + \mathbf{G}_2 + \mathbf{G}_3 = \mathbf{I}$, the elasticity tensor (2.95) may be translated in the general orthotropic form

$$\mathcal{S} = \lambda_{ii} \mathbf{G}_i \otimes \mathbf{G}_i + \lambda_{ij}^* (\mathbf{G}_i \otimes \mathbf{G}_j + \mathbf{G}_j \otimes \mathbf{G}_i) + 2\mu_{ij} (\mathbf{G}_i \underline{\otimes} \mathbf{G}_j + \mathbf{G}_j \underline{\otimes} \mathbf{G}_i), \quad (2.96)$$

where summation is performed for $i < j$ due to symmetrization of tensor products. The identification of the coefficients leads

$$\begin{aligned} \lambda_{ii} &= c_1 + c_2 + c_3 g_i^2 + 2c_4 g_i + c_5 g_i^4 + c_6 g_i^2 + 2c_7 g_i + c_8 g_i^3 + 2c_9 g_i^2, \\ \lambda_{ij}^* &= c_1 + c_3 g_i g_j + c_5 g_i^2 g_j^2 + c_7 (g_i + g_j) + c_8 (g_i g_j^2 + g_j g_i^2) + c_9 (g_i^2 + g_j^2), \\ \mu_{ij} &= \frac{1}{2} c_2 + \frac{1}{2} c_4 (g_i + g_j) + \frac{1}{2} c_6 g_i g_j. \end{aligned} \quad (2.97)$$

At this stage, additional assumption are necessary to guide the choice of the nine function c_i . The hypothesis they made, consists in introducing a homogeneity property for the set of fabric tensor $\{g, \mathbf{G}\}$, which means that anisotropy of the elastic constitutive law is independent of the size or physical units of the microstructural properties $\mathcal{S}(\lambda \mathbf{G}) = \lambda^k \mathcal{S}(g, \mathbf{G})$, $\forall \lambda > 0$, where $k \neq 0$ is the degree of the homogeneity property.

By considering the isotropic elasticity tensor, $\mathcal{S} = \lambda_c \mathbf{I} \otimes \mathbf{I} + 2\mu_c \mathbf{I} \underline{\otimes} \mathbf{I}$, and substituting the identity tensor \mathbf{I} by the tensor $g\mathbf{I} + \mathbf{G}$:

$$\mathcal{S} = \lambda_c (g\mathbf{I} + \mathbf{G}) \otimes (g\mathbf{I} + \mathbf{G}) + 2\mu_c (g\mathbf{I} + \mathbf{G}) \underline{\otimes} (g\mathbf{I} + \mathbf{G}) \quad (2.98)$$

where λ_c and μ_c are Lamé like constants, a particular form of the previous model is provided:

$$\begin{aligned} c_1 &= \lambda_c g^2, & c_2 &= 2\mu_c g^2, & c_3 &= \lambda_c, \\ c_4 &= 2\mu_c g, & c_5 &= 0, & c_6 &= 2\mu_c, \\ c_7 &= \lambda_c g, & c_8 &= 0, & c_9 &= 0. \end{aligned} \quad (2.99)$$

In the principal reference frame of \mathbf{G} :

$$\begin{aligned} \mathcal{S}(g, \mathbf{G}) &= (\lambda_c + 2\mu_c) (g + g_i)^2 (\mathbf{G}_i \otimes \mathbf{G}_i) \\ &\quad + \lambda_c (g + g_i) (g + g_j) (\mathbf{G}_i \otimes \mathbf{G}_j + \mathbf{G}_j \otimes \mathbf{G}_i) \\ &\quad + 2\mu_c (g + g_i) (g + g_j) (\mathbf{G}_i \underline{\otimes} \mathbf{G}_j + \mathbf{G}_j \underline{\otimes} \mathbf{G}_i) \end{aligned} \quad (2.100)$$

Comparison with the general orthotropic form gives

$$\begin{aligned}\lambda_{ii} &= (\lambda_c + 2\mu_c)(g + g_i)^2, \quad \forall i, \\ \lambda_{ij}^* &= \lambda_c(g + g_i)(g + g_j), \quad \forall i, j \ (i < j), \\ \mu_{ij} &= \mu_c(g + g_i)(g + g_j), \quad \forall i, j \ (i < j).\end{aligned}\quad (2.101)$$

Sufficient but not necessary to satisfy the homogeneity condition, the substitution (2.98) provides the most simple orthotropic model that degenerates into transverse isotropy if two eigenvalues of \mathbf{G} are identical and into isotropy if $\mathbf{G} = \mathbf{0}$.

In order to generalize the previous approach, it is considered now the substitution (2.98) for an arbitrary strictly positive power k of the tensor $g\mathbf{I} + \mathbf{G}$. In the principal reference frame of \mathbf{G} , the elasticity tensor becomes:

$$\begin{aligned}\mathcal{S}(g, \mathbf{G}) &= (\lambda_c + 2\mu_c)m_i^{2k}(\mathbf{G}_i \otimes \mathbf{G}_i) \\ &\quad + \lambda_c m_i^k m_j^k (\mathbf{G}_i \otimes \mathbf{G}_j + \mathbf{G}_j \otimes \mathbf{G}_i) \\ &\quad + 2\mu_c m_i^k m_j^k (\mathbf{G}_i \underline{\otimes} \mathbf{G}_j + \mathbf{G}_j \underline{\otimes} \mathbf{G}_i)\end{aligned}\quad (2.102)$$

where $m_i = g + g_i$. The coefficient exhibit the more general form:

$$\begin{aligned}\lambda_{ii} &= (\lambda_c + 2\mu_c)m_i^{2k}, \quad \forall i, \\ \lambda_{ij}^* &= \lambda_c m_i^k m_j^k, \quad \forall i, j \ (i < j), \\ \mu_{ij} &= \mu_c m_i^k m_j^k, \quad \forall i, j \ (i < j).\end{aligned}\quad (2.103)$$

In this case, the anisotropic elastic behaviour of the material is completely described by the two constants λ_c and μ_c , the exponent k and the fabric tensor $\{g, \mathbf{G}\}$ and the overall elasticity tensor assumes the form:

$$\mathcal{S} = \begin{pmatrix} (\lambda_c + 2\mu_c)m_1^{2k} & \lambda_c m_1^k m_2^k & \lambda_c m_1^k m_3^k & 0 & 0 & 0 \\ \lambda_c m_2^k m_1^k & (\lambda_c + 2\mu_c)m_2^{2k} & \lambda_c m_2^k m_3^k & 0 & 0 & 0 \\ \lambda_c m_3^k m_1^k & \lambda_c m_3^k m_2^k & (\lambda_c + 2\mu_c)m_3^{2k} & 0 & 0 & 0 \\ 0 & 0 & 0 & 2\mu_c m_2^k m_3^k & 0 & 0 \\ 0 & 0 & 0 & 0 & 2\mu_c m_3^k m_1^k & 0 \\ 0 & 0 & 0 & 0 & 0 & 2\mu_c m_1^k m_2^k \end{pmatrix}.\quad (2.104)$$

CHAPTER III

THEORY OF HOMOGENIZATION

1. THERMODYNAMIC FRAMEWORK AND MATHEMATICALLY WELL-POSED HOMOGENIZATION APPROACHES

Homogenization is the modelling of a heterogeneous medium by means of a *unique* continuous medium. A heterogeneous medium is a medium of which material properties (e. g., elasticity coefficients) vary pointwise in a continuous or discontinuous manner, in a periodic or nonperiodic way, deterministically or randomly. While, obviously, homogenization is a modelling technique that applies to all fields of macroscopic physics governed by nice partial differential equations, we focus more particularly on the mechanics of deformable bodies.

1.1. Representative Volume Element (RVE)

Two different scales are used in the description of heterogeneous media. One of these is a **macroscopic** (x) scale at which homogeneities are weak. The other one is the scale of inhomogeneities and is referred to as the **microscopic** (y) scale. The latter defines the size of the representative volume element (Fig. 3.1). The basic cell of a periodic composite is an example of RVE.

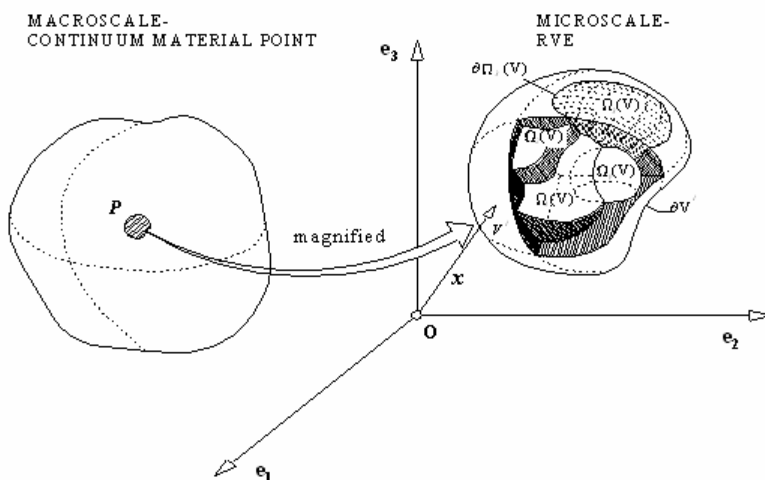


Fig. 3.1.
Representative Volume Element

From the experimental point of view, we can say that there exists a kind of statistical homogeneity in the sense that any RVE at a specific point looks very much like any other RVE taken at random at another point.

The mathematical problem presents itself in the following manner. Let $\sigma(y)$ and $\varepsilon(y)$ be the stress and strain at the micro scale in the framework of small-perturbation hypothesis. We denote by Σ and \mathbf{E} the same notion at the macro scale. Let $\langle \dots \rangle$ indicate the *averaging operator*. For a volume averaging we have

$$\begin{aligned}\Sigma(x) &= \langle \sigma \rangle = \frac{1}{|V|} \int_V \sigma(x, y) dy \\ \mathbf{E}(x) &= \langle \varepsilon \rangle = \frac{1}{|V|} \int_V \varepsilon(x, y) dy\end{aligned}\tag{3.1}$$

where V is the volume of the RVE.

It is important to notice that any quantity that is an additive function is averaged in the micro-macro transition. Thus, if $\bar{\rho} = \langle \rho \rangle$ denotes the averaged density, then we have

$$\begin{aligned}\bar{\rho}E &= \langle \rho e \rangle, & \text{internal energy,} \\ \bar{\rho}S &= \langle \rho \eta \rangle, & \text{entropy,} \\ \Phi &= \langle \phi \rangle, & \text{dissipation.}\end{aligned}\tag{3.2}$$

1.2. Localization Problem

We can state the following

- the process that relates (Σ, \mathbf{E}) by means of equations (3.1) and (3.2) and the microscopic constitutive equations is called **homogenization**;
- the inverse process that consists in determining $\sigma(y)$ and $\varepsilon(y)$ from Σ and \mathbf{E} is called **localization**.

Therefore, the data are Σ and \mathbf{E} in the localization process which corresponds to the following problem:

$$(P \ L) \left\{ \begin{array}{l} \langle \sigma \rangle = \Sigma \\ \langle \varepsilon \rangle = \mathbf{E} \\ \text{div } \sigma = \mathbf{0} \end{array} \right. \tag{3.3}$$

This problem is original, because of the following two reasons:

- i. the load is the averaged value of a field and not a prescription at points in the bulk or at a limiting surface;
- ii. there are *no* boundary conditions.

It follows from (ii) that the problem (3.3) is *ill-posed*. The missing boundary condition must, in some way, reproduce the internal state of the RVE in the most satisfactory manner. They therefore depend on the choice of RVE, more specifically on its size. As a rule, different choices of RVE will provide different macroscopic laws.

The following give some examples of boundary conditions:

$$\boldsymbol{\sigma} \cdot \mathbf{n} = \boldsymbol{\Sigma} \cdot \mathbf{n} \quad \text{on } \partial V \quad - \quad \text{uniform traction on } \partial V ; \quad (3.4)$$

$$\mathbf{u} = \mathbf{E} \cdot \mathbf{y} \quad \text{on } \partial V \quad - \quad \text{uniform traction on } \partial V . \quad (3.5)$$

With this and $\text{div } \boldsymbol{\sigma} = \mathbf{0}$, in V , it is verified that (3.1) holds good. Indeed, for (3.5) we have

$$\frac{1}{2} \int_V \left(\frac{\partial u_i}{\partial y_j} + \frac{\partial u_j}{\partial y_i} \right) dv = \frac{1}{2} \int_{\partial V} (u_i n_j + u_j n_i) ds = \frac{1}{2} \int_{\partial V} (E_{ik} y_k n_j + E_{jk} y_k n_i) ds \quad (3.6)$$

or

$$\langle \boldsymbol{\varepsilon}(\mathbf{u}) \rangle = \mathbf{E} \quad (3.7)$$

The proof for (3.4) is self-evident.

The above reasoning does not apply to the case of a periodic structure. In that case, $\boldsymbol{\sigma}$ and $\boldsymbol{\varepsilon}$ are locally periodic (they are only quasi-periodic for a large sample) and the periodicity condition read as follows:

- the traction $\boldsymbol{\sigma} \cdot \mathbf{n}$ are opposite on opposite faces of ∂V (where \mathbf{n} corresponds to $-\mathbf{n}$);
- the local strain $\boldsymbol{\varepsilon}(\mathbf{u})$ is made of two part, the mean \mathbf{E} and the fluctuation part $\boldsymbol{\varepsilon}(\mathbf{u}^*)$ such that

$$\boldsymbol{\varepsilon}(\mathbf{u}) = \mathbf{E} + \boldsymbol{\varepsilon}(\mathbf{u}^*), \quad \langle \boldsymbol{\varepsilon}(\mathbf{u}^*) \rangle = 0, \quad (3.8)$$

where \mathbf{u}^* can be shown to be periodic. Therefore, the condition are

$$\begin{cases} \boldsymbol{\sigma} \cdot \mathbf{n} & \text{is antiperiodic,} \\ \mathbf{u} = \mathbf{E} \cdot \mathbf{y} + \mathbf{u}^*, \mathbf{u}^* & \text{periodic.} \end{cases} \quad (3.9)$$

On account of (3.4), (3.5) and (3.9), the problem (3.3) now is theoretically well-posed, but this must be verified for each constitutive behaviour.

1.3. The Hill-Mandel principle of macrohomogeneity

Let $\bar{\sigma}$ and \bar{u} be, respectively, a statistically admissible (SA) stress field and a kinematically admissible (KA) displacement field. Then it is possible to prove that

$$\langle \bar{\sigma} : \varepsilon(\bar{u}) \rangle = \bar{\Sigma} : \bar{E}. \quad (3.10)$$

The remarkable expression (3.10) is called the *principle of macrohomogeneity of Hill and Mandel* (Hill, 1965a, Mandel 1971) or the *Hill-Mandel* relation between micro and macro scales. In statistical theories this condition is viewed as an ergodic hypothesis. This condition, in fact, plays in the end a much more important role than the boundary conditions applied at the RVE.

1.4. The example of pure elasticity

In this section the localization problem in the case of *anisotropic linear elastic* components are examined.

1.4.a. The localization problem

This problem is written in the following form (here $\mathcal{C}(y)$ is the tensor of elasticity coefficient at the micro scale):

$$\begin{cases} \sigma(y) = \mathcal{C}(y) : \varepsilon(y) = \mathcal{C}(y) : [\mathbf{E} + \varepsilon(\mathbf{u}^*(y))] \\ \text{div } \sigma = \mathbf{0} \\ \text{boundary conditions} \end{cases} \quad (3.11)$$

where \mathbf{E} or Σ is prescribed. Accordingly, the fluctuation displacement \mathbf{u}^* is the solution of the following problem:

$$\begin{cases} \text{div}(\mathcal{C} : \varepsilon(\mathbf{u}^*)) = -\text{div}(\mathcal{C} : \mathbf{E}) \\ \text{boundary conditions} \end{cases} \quad (3.12)$$

Whenever \mathbf{E} is constant for each constituent component, it can be shown that

$$\text{div}(\mathcal{C} : \mathbf{E}) = (\llbracket \mathcal{C} \rrbracket : \mathbf{E}) \mathbf{n} \delta(S), \quad (3.13)$$

where $[[\mathcal{C}]] = \mathcal{C}^+ - \mathcal{C}^-$, $\delta(S)$ is Dirac's distribution, and \mathbf{n} is the unit normal oriented from the '−' to the '+' side of the surface S separating components. Then we can state the following:

Proposition. Under classical working hypotheses applying to \mathcal{C} (symmetry and positivity), the problem (3.12) admits a unique solution for all three types of boundary condition.

To prove this we must distinguish whether it is \mathbf{E} or Σ which is prescribed.

1.4.b. Case where \mathbf{E} is prescribed

For the existence and uniqueness proofs one can see Suquet (1981b). We shall only give the representation of the solution. As the problem is linear, the solution $\boldsymbol{\varepsilon}(\mathbf{u}^*)$ depends linearly on the prescribed field \mathbf{E} . The latter can be decomposed into six elementary states of macroscopic strains (stretch in three directions and three shears). Let $\boldsymbol{\varepsilon}(\chi_{kl})$ be the fluctuation strain field induced by these six elementary states at the microscopic level. The solution $\boldsymbol{\varepsilon}(\mathbf{u}^*)$ for a general macrostrain \mathbf{E} is the superposition of the six elementary solutions, so that we can write (summation over k and l)

$$\boldsymbol{\varepsilon}(\mathbf{u}^*) = \mathbf{E}_{kl} \boldsymbol{\varepsilon}(\chi_{kl}). \quad (3.14)$$

In all we have

$$\boldsymbol{\varepsilon}(\mathbf{u}) = \mathbf{E} + \boldsymbol{\varepsilon}(\mathbf{u}^*) = \mathbf{E}(\mathbf{I} + \boldsymbol{\varepsilon}(\chi)) \quad (3.15)$$

or, in components,

$$\varepsilon_{ij}(\mathbf{u}) = D_{ijkl} \mathbf{E}_{kl} = (\mathbf{D} : \mathbf{E})_{ij} \quad (3.16)$$

where

$$D_{ijkl} = I_{ijkl} + \varepsilon_{ij}(\chi_{kl}) \quad (3.17)$$

Here $I_{ijkl} = \frac{1}{2}(\delta_{ik}\delta_{jl} + \delta_{il}\delta_{jk})$ is the tensorial representation in \mathbb{R}^3 of the unity of \mathbb{R}^6 and D_{ijkl} is called, depending on the author, the **tensor of strain localization**, or **tensor of concentrations** (Mandel, 1971) or the **tensor of influence** (Hill, 1967).

Homogenization

We can write in an obvious manner

$$\boldsymbol{\Sigma} = \langle \boldsymbol{\sigma} \rangle = \langle \mathcal{C} : \boldsymbol{\varepsilon}(\mathbf{u}) \rangle = \langle \mathcal{C} : \mathbf{D} : \mathbf{E} \rangle = \langle \mathcal{C} : \mathbf{D} \rangle : \mathbf{E} \quad (3.18)$$

so that

$$\boldsymbol{\Sigma} = \mathcal{C}^{\text{hom}} : \mathbf{E}, \quad \mathcal{C}^{\text{hom}} = \langle \mathcal{C} : \mathbf{D} \rangle. \quad (3.19)$$

We note that

$$\langle \mathbf{D} \rangle = \mathbf{I}, \quad \langle \mathbf{D}^T \rangle = \mathbf{I}.$$

Equation (3.19)₂ shows that the tensor of ‘macro’ elasticity coefficients is obtained by taking the average of ‘micro’ elasticity coefficients, the latter being *weighted* by the tensor of strain localization. It is possible to prove that the tensor \mathcal{C}^{hom} is symmetric. For a direct proof we compute $\langle \mathbf{D}^T : \bar{\boldsymbol{\sigma}} \rangle$ for an admissible field $\bar{\boldsymbol{\sigma}}$, obtaining thus

$$\langle \mathbf{D}^T : \bar{\boldsymbol{\sigma}} \rangle_{ij} = \langle D_{ijkl}^T : \bar{\sigma}_{kl} \rangle = \left\langle \left[I_{ijkl} + \varepsilon_{kl}(\chi_{ij}) \right] \bar{\sigma}_{kl} \right\rangle = \bar{\Sigma}_{ij}$$

i.e.,

$$\boldsymbol{\Sigma} = \langle \mathbf{D}^T : \boldsymbol{\sigma} \rangle = \langle \mathbf{D}^T : \mathcal{C} : \boldsymbol{\varepsilon}(\mathbf{u}) \rangle = \langle \mathbf{D}^T : \mathcal{C} : \mathbf{D} \rangle : \mathbf{E},$$

so that

$$\mathcal{C}^{\text{hom}} = \langle \mathbf{D}^T : \mathcal{C} : \mathbf{D} \rangle, \quad (3.20)$$

which is symmetric.

1.4.c. Case where $\boldsymbol{\Sigma}$ is prescribed

The localization problem then reads

$$\begin{cases} \boldsymbol{\varepsilon}(\mathbf{u}) = \boldsymbol{\varepsilon}(\mathbf{u}^*) + \mathbf{E} = \mathcal{S} : \boldsymbol{\sigma} \\ \operatorname{div} \boldsymbol{\sigma} = \mathbf{0} \\ \langle \boldsymbol{\sigma} \rangle = \boldsymbol{\Sigma} \\ \text{boundary conditions} \end{cases} \quad (3.21)$$

where \mathcal{S} is the tensor of the ‘micro’ elastic compliance and \mathbf{E} is an unknown. The existence and uniqueness of the solution may be proved (Suquet, 1981b). Thus, here, we assume that a unique solution $\boldsymbol{\sigma}$ exists. This solution depends linearly on data by virtue of the linearity of the problem. Let us call S_{kl} the solution of the problem (3.21) for the datum $\boldsymbol{\Sigma} = \mathbf{I}_{kl}$ - note that $I_{ijkl} = (\mathbf{I}_{kl})_{ij}$.

Then the general solution, obtained by superposition, is written

$$\begin{aligned} \boldsymbol{\sigma} &= \mathbf{A} : \boldsymbol{\Sigma}, \quad \text{i.e.,} \quad \boldsymbol{\sigma}(y) = \Sigma_{kl} A_{kl}(y), \\ \text{or} \quad \sigma_{ij} &= A_{ijkl} \Sigma_{kl}, \quad A_{ijkl} = (\mathbf{A}_{kl})_{ij}, \end{aligned} \quad (3.22)$$

where \mathbf{A} is the *tensor of stress localization*.

The homogenized compliance tensor \mathcal{S}^{hom} is evaluated thus. We have directly

$$\mathbf{E} = \langle \boldsymbol{\varepsilon}(\mathbf{u}) \rangle = \langle \mathcal{S} : \boldsymbol{\sigma} \rangle = \langle \mathcal{S} : \mathbf{A} \rangle : \boldsymbol{\Sigma} = \mathcal{S}^{\text{hom}} : \boldsymbol{\Sigma}, \quad (3.23)$$

whence

$$\mathcal{S}^{\text{hom}} = \langle \mathcal{S} : \mathbf{A} \rangle. \quad (3.24)$$

We note that

$$\langle \mathbf{A}^T \rangle = \mathbf{I}, \quad (3.25)$$

and for any admissible field $\langle \boldsymbol{\varepsilon}(\bar{\mathbf{u}}) \rangle$ we can write

$$\langle \mathbf{A}^T : \boldsymbol{\varepsilon}(\bar{\mathbf{u}}) \rangle_{ij} = \langle A_{ijkl}^T \varepsilon_{kl}(\bar{\mathbf{u}}) \rangle = \langle (A_{ij})_{kl} \varepsilon_{kl}(\bar{\mathbf{u}}) \rangle = \langle (A_{ij})_{kl} \rangle \langle \varepsilon_{kl}(\bar{\mathbf{u}}) \rangle = \bar{E}_{ij}$$

so that

$$\mathbf{E} = \langle \mathbf{A}^T : \boldsymbol{\varepsilon}(\mathbf{u}) \rangle = \langle \mathbf{A}^T : \mathcal{S} : \boldsymbol{\sigma} \rangle = \langle \mathbf{A}^T : \mathcal{S} : \mathbf{A} \rangle : \boldsymbol{\Sigma},$$

whence

$$\mathcal{S}^{\text{hom}} = \langle \mathbf{A}^T : \mathcal{S} : \mathbf{A} \rangle \quad (3.26)$$

and thus \mathcal{S}^{hom} is symmetric.

1.4.d. Equivalence between ‘prescribed stress’ and ‘prescribed strain’

First we note that \mathcal{C}^{hom} and \mathcal{S}^{hom} are *inverse* tensors (in \mathbb{R}^6) of one another if they correspond to the *same* choice of boundary conditions in the localization problem. Indeed, using the symmetry of \mathcal{C}^{hom} we can write

$$\mathcal{C}^{\text{hom}} : \mathcal{S}^{\text{hom}} = \left(\mathcal{C}^{\text{hom}} \right)^T : \mathcal{S}^{\text{hom}} = \langle \mathbf{D}^T : \mathcal{C} \rangle : \langle \mathcal{S} : \mathbf{A} \rangle \quad (3.27)$$

in which the first factor is an admissible stress field (from the definition of \mathbf{D} and \mathbf{A}) and the second factor is an admissible strain field. The principle (3.10) therefore applies and we can write ($\mathcal{C} : \mathcal{S} = \mathbb{I}$)

$$\mathcal{C}^{\text{hom}} : \mathcal{S}^{\text{hom}} = \langle \mathbf{D}^T : \mathcal{C} : \mathcal{S} : \mathbf{A} \rangle = \langle \mathbf{D}^T : \mathbf{A} \rangle = \langle \mathbf{D}^T \rangle : \langle \mathbf{A} \rangle = \mathbf{I}. \quad (3.28)$$

However, if *different* boundary conditions are used, one then has the estimate of Hill (1967) and Mandel (1971),

$$\mathcal{C}^{\text{hom}} : \mathcal{S}^{\text{hom}} = \mathbb{I} + O\left((d/l)^3\right), \quad (3.29)$$

where \mathcal{C}^{hom} is evaluated by using the condition (3.5), while \mathcal{S}^{hom} is computed through use of the condition (3.4), d is a characteristic size of an inhomogeneity and l is the typical size of the RVE. If $l \gg d$, then the choice of boundary condition is hardly important. For *periodic* media where $d/l = O(1)$, this choice is most important.

2. COMPOSITE HETEROGENEOUS MATERIALS: DERIVATION OF COMPLIANCE AND STIFFNESS TENSORS

The overall properties of a composite material depends not only upon the constitutive properties of each phases, but also on the microstructural

architecture and define a relationship between the overall field variables – such as the deformation and the stress. The determination of the overall deformation and stress obviously needs of the preventive determination of the deformation and stress, and than the solution of an elastic PDE problem which involves the equilibrium, compatibility and constitutive equations of each phase, as well as the continuity conditions of the interphase. In other words, between two different phases – called here (1) and (2) – it must results

$$\mathbf{u}^{(1)} = \mathbf{u}^{(2)}, \quad \boldsymbol{\sigma}^{(1)} \mathbf{n} = \boldsymbol{\sigma}^{(2)} \mathbf{n} \quad (3.30)$$

being $\mathbf{u}^{(i)}$ the displacement field of the i -phase, $\boldsymbol{\sigma}^{(i)}$ the stress field of the i -phase and \mathbf{n} is the outer normal vector of a point on the interphase. From such procedure – which may be see as a direct approach to the homogenization problem – seems clear that the homogenized properties depend upon the microstructure architecture. Consequently, this procedure is often extremely difficult to apply because of the equations (3.30), and may be developed only in vary particular – and often ideal – cases.

In the following section, alternative approaches to determine the overall properties of composite materials are presented. In particular, the **direct approach** requires the exact evaluation of the microscopic fields for some specific geometries, and so it is the more efficient, the more the microstructural geometry is similar to that one used in the model.

The **variational approaches** are always able to furnish upper and lower bounds of the overall properties of the composite materials. In particular, such approaches are the only ones that may solve the homogenization problem when the microstructural geometries are particular irregular or not completely known. Obviously, the wider the range defined by the upper and lower bounds gets, the less the practical utility of these methods is.

2.1. Direct Methods – Eshelby solution

Let consider an homogeneous, linearly elastic and infinitely extended medium, subjected to a uniform prescribed strain \mathbf{E}^* on the domain Ω . Generally, the resulting strain \mathbf{E} is variable on Ω , but Eshelby proved that if Ω is an ellipsoid then the resulting strain \mathbf{E} and hence the stress \mathbf{T} , are also uniform in Ω , the former being given by

$$\mathbf{E} = \mathbb{P} \mathbf{E}^* \quad (3.31)$$

where the four-order tensor \mathbb{P} is called Eshelby's tensor and it shows the following propeties:

- it is symmetric with respect to the first two indices and the second two indices, $P_{ijkl} = P_{jikl} = P_{ijlk}$, while, in general, it is not symmetric with respect to the exchange of ij and kl , i. e., in general, $P_{ijkl} \neq P_{klij}$;
- it is independent of the material properties of the inclusion Ω ;
- it is completely defined in terms of the aspect ratios of the ellipsoidal inclusion Ω , and the elastic parameters of the surrounding matrix;
- when the surrounding matrix is isotropic, then \mathbb{P} depends only on the Poisson's ratio of the matrix and the aspect ratios of Ω .

In the following this results is proving in the case of isotropic matrix with Poisson's ratio ν and shear modulus μ .

Let

$$u_i(\mathbf{x}) = -C_{jkmn} \varepsilon_{mn}^* \int_{\Omega} G_{ij/k}(\mathbf{x} - \mathbf{x}') d\mathbf{x}' \quad (3.32)$$

be the solution of the PDE problem of the considered problem, where the Green function $\mathbf{G}(\mathbf{x} - \mathbf{x}')$ for the homogeneous and isotropic medium is

$$\mathbf{G}(\mathbf{x} - \mathbf{x}') = \frac{1}{16\pi\mu(1-\nu)} \left[\frac{(3-4\nu)\mathbf{I}}{|\mathbf{x} - \mathbf{x}'|} + \frac{(\mathbf{x} - \mathbf{x}') \otimes (\mathbf{x} - \mathbf{x}')}{|\mathbf{x} - \mathbf{x}'|^3} \right] \quad (3.33)$$

where \mathbf{I} is the second order identity tensor. Being Ω an ellipsoid of equation

$$\frac{x_1^2}{a_1^2} + \frac{x_2^2}{a_2^2} + \frac{x_3^2}{a_3^2} \leq 1 \quad (3.34)$$

through simple algebraic manipulation it result

$$u_i(\mathbf{x}) = \frac{-\varepsilon_{jk}^*}{8\pi(1-\nu)} \int_{\Omega} g_{ijk}(\mathbf{l}) \frac{d\mathbf{x}'}{|\mathbf{x} - \mathbf{x}'|^2} \quad (3.35)$$

where

$$g_{ijk}(\mathbf{l}) = (1-2\nu) (\delta_{ij} l_k + \delta_{ik} l_j - \delta_{jk} l_i) + 3l_i l_j l_k \quad (3.36)$$

being \mathbf{l} the versor of $(\mathbf{x}' - \mathbf{x})/|\mathbf{x}' - \mathbf{x}|$.

By assuming that the point \mathbf{x} is inside the region Ω , the integral into the (3.35) may be explicitly calculated. To achieve this goal, the volume element $d\mathbf{x}'$ may

be written as $r^2 dr d\omega$, being $r = |\mathbf{x} - \mathbf{x}'|$ and $d\omega$ the superficial element of a unit sphere centred in \mathbf{x} . The integration of the (3.35) with respect to r , yields

$$u_i(\mathbf{x}) = \frac{-\mathcal{E}_{jk}^*}{8\pi(1-\nu)} \int_{\Sigma} r(\mathbf{l}) g_{ijk}(\mathbf{l}) d\omega, \quad (3.37)$$

where $r(\mathbf{l})$ is the positive root of

$$(x_1 + rl_1)^2/a_1^2 + (x_2 + rl_2)^2/a_2^2 + (x_3 + rl_3)^2/a_3^2 = 1, \quad (3.38)$$

that is

$$r(\mathbf{l}) = -f/g + \sqrt{f^2/g^2 + e/g} \quad (3.39)$$

with

$$\begin{aligned} g &= l_1^2/a_1^2 + l_2^2/a_2^2 + l_3^2/a_3^2 \\ f &= l_1 x_1/a_1^2 + l_2 x_2/a_2^2 + l_3 x_3/a_3^2 \\ e &= 1 - x_1^2/a_1^2 - x_2^2/a_2^2 - x_3^2/a_3^2. \end{aligned} \quad (3.40)$$

By posing $\lambda_i = l_i/a_i^2$, the (3.37) becomes

$$u_i(\mathbf{x}) = \frac{x_m \mathcal{E}_{jk}^*}{8\pi(1-\nu)} \int_{\Sigma} \frac{\lambda_m g_{ijk}}{g} d\omega \quad (3.41)$$

from which the strain inside Ω may be calculated

$$\varepsilon_{ij}(\mathbf{x}) = \frac{\mathcal{E}_{mn}^*}{16\pi(1-\nu)} \int_{\Sigma} \frac{\lambda_i g_{jmn} + \lambda_j g_{imn}}{g} d\omega \quad (3.42)$$

which depends upon $\mathbf{x} \in \Omega$.

So, the components of Eshelby's tensor \mathbb{P} introduced in the equation (3.31) are:

$$\begin{aligned}
P_{1111} &= \frac{3}{8\pi(1-\nu)} a_1^2 I_{11} + \frac{1-2\nu}{8\pi(1-\nu)} I_1 \\
P_{1122} &= \frac{1}{8\pi(1-\nu)} a_2^2 I_{12} - \frac{1-2\nu}{8\pi(1-\nu)} I_1 \\
P_{1133} &= \frac{1}{8\pi(1-\nu)} a_3^2 I_{13} - \frac{1-2\nu}{8\pi(1-\nu)} I_1 \\
P_{1212} &= \frac{a_1^2 + a_2^2}{16\pi(1-\nu)} I_{12} + \frac{1-2\nu}{16\pi(1-\nu)} (I_1 + I_2)
\end{aligned} \tag{3.43}$$

with

$$\begin{aligned}
I_1 &= \int_{\Sigma} \frac{l_1^2}{a_1^2 g} d\omega \\
I_{11} &= \int_{\Sigma} \frac{l_1^4}{a_1^4 g} d\omega \\
I_{12} &= 3 \int_{\Sigma} \frac{l_1^2 l_2^2}{a_1^2 a_2^2 g} d\omega.
\end{aligned} \tag{3.44}$$

All the other non-zero components may be obtained through a cyclic permutation of the indexes (1, 2, 3).

Such solution may be particularized for many cases of practical interest. By means of the solution (3.43), it is possible to determine the concentration strain tensor in an ellipsoidal inclusion of elasticity tensor $\mathbb{C}^{(2)}$ embedded in a homogeneous, isotropic and infinitely extended medium of elasticity tensor $\mathbb{C}^{(1)}$. Then, under the uniform strain field \mathbf{E}^0 , the medium, supposed homogeneous, would be subjected to a uniform stress $\mathbf{T} = \mathbb{C}^{(1)} \mathbf{E}^0$. This uniform stress field is perturbed by the presence of the inclusion. But the stress field $\mathbf{T}^{(2)} = \mathbb{C}^{(2)} \mathbf{E}^{(2)}$ in a generic point of the inclusion is the same that we would have in the inclusion imagining to substitute the inclusion with the matrix subjected to \mathbf{E}^0 as well as to the strain \mathbf{E}^* , such as

$$\mathbb{C}^{(2)} \mathbf{E}^{(2)} = \mathbb{C}^{(1)} (\mathbf{E}^{(2)} - \mathbf{E}^*). \tag{3.45}$$

As proved by Eshelby, a uniform strain \mathbf{E}^* applied on an ellipsoidal region yields – as unique equilibrated and compatible solution – a uniform strain in the region given by the equation (3.31). In this case, being also \mathbf{E}^0 , it results

$$\mathbf{E}^{(2)} = \bar{\mathbf{E}}^{(2)} = \mathbf{E}^0 + \mathbb{P} \mathbf{E}^*. \tag{3.46}$$

The (3.46) and (3.45), yield

$$\mathbf{E}^{(2)} = \left[\mathbb{I} + \mathbb{P} \left(\mathbb{C}^{(1)} \right)^{(-1)} \left[\mathbb{C}^{(2)} - \mathbb{C}^{(1)} \right] \right]^{-1} \mathbf{E}^0. \quad (3.47)$$

Being $\mathbf{E}^{(2)}$ uniform in Ω , the concentration strain tensor into the inclusion is

$$\mathbb{A}^{(2)} = \left[\mathbb{I} + \mathbb{P} \left(\mathbb{C}^{(1)} \right)^{(-1)} \left[\mathbb{C}^{(2)} - \mathbb{C}^{(1)} \right] \right]^{-1}. \quad (3.48)$$

2.2. Variational Methods – Hashin Shtrikman Variational Principle

The homogenization problem of an heterogeneous RVE is equivalent to solve one of the following variational problems:

$$\begin{aligned} \frac{1}{2} \bar{\mathcal{C}} \bar{\mathbf{E}} \cdot \bar{\mathbf{E}} &= \inf_{\mathbf{E}^d \in E} \frac{1}{V} \int_V \frac{1}{2} \mathcal{C} (\bar{\mathbf{E}} + \mathbf{E}^d) \cdot (\bar{\mathbf{E}} + \mathbf{E}^d) dV \\ \frac{1}{2} \bar{\mathcal{S}} \bar{\mathbf{T}} \cdot \bar{\mathbf{T}} &= \inf_{\mathbf{T}^d \in T} \frac{1}{V} \int_V \frac{1}{2} \mathcal{S} (\bar{\mathbf{T}} + \mathbf{T}^d) \cdot (\bar{\mathbf{T}} + \mathbf{T}^d) dV \end{aligned} \quad (3.49)$$

where: \mathbf{E} is compatible periodic strain field space, whose average value is equal to zero, \mathbf{T} is equilibrated periodic stress field space, whose average value is equal to zero, $\bar{\mathcal{C}}$ is homogenized stiffness tensor, $\bar{\mathcal{S}}$ is homogenized compliance tensor, $\bar{\mathbf{T}}$ is the generic symmetric stress field, and $\bar{\mathbf{E}}$ is the generic symmetric strain field.

The first members of the (3.49)₁ and (3.49)₂ represent the elastic energy density and the complementary energy density of the homogenized material. In particular, solving the first problem of the (3.49)₁ is equivalent to determine, among the compatible strain fields, whose prescribed average value is $\bar{\mathbf{E}}$, the sole one that is also equilibrated. On the contrary, solving the (3.49)₂ is equivalent of determining, among the equilibrated stress fields, whose prescribed average value is $\bar{\mathbf{T}}$, the sole one that is also compatible.

It is possible to demonstrate that, if the stiffness tensor \mathcal{C} and the compliance one \mathcal{S} have, uniformly in V , all the eigenvalues lower down bounded by a positive constant, then the equations (3.49) admit one and only one solution.

Since the functionals in the first members of the (3.49) are conjugate each other, (Giangreco, 2003), it follows that the homogenized properties of the material are well defined, hence:

$$\bar{\mathcal{S}} = \bar{\mathcal{C}}^{-1}. \quad (3.50)$$

In this framework, the basic physic idea of the Hashin and Shtrikman's principles is to substitute the heterogeneous medium with a reference homogeneous one, having a stiffness tensor, \mathcal{C}^H , and a compliance tensor, \mathcal{S}^H . In order to simulate the actual micro-structure, eigenstress and eigenstrain fields are prescribed on the reference homogeneous medium, as already seen in the previous section. So, the Hashin and Shtrikman's variational principles are characterized from two tumbled variational problems:

- the first problem, defined as auxiliary problem, is related to the elastostatic response of the reference homogeneous solid, subjected to a prescribed field of polarization (eigenstress or eigenstrain);
- the second problem, defined as optimization problem, has the objective to found the unknown field of polarization.

In the follows, the four classic Hashin and Shtrikman's variational principles are reported. It is worth to underline that two of these are minimum principles, while the other two are saddle principles. Obviously, the minimum principles are particularly useful, because each numeric approximation of them, for example by using the Finite Element Method, represents an upper estimation of the solution.

In particular, consider a reference homogeneous material which is more deformable than each phase included in the heterogeneous RVE, such that $\mathcal{C} - \mathcal{C}^H$ is positive definite everywhere in V . Hence, the following identity is verified:

$$\int_V \left(\frac{1}{2} \mathcal{C} \mathbf{E} \cdot \mathbf{E} - \frac{1}{2} \mathcal{C}^H \mathbf{E} \cdot \mathbf{E} \right) dV = \sup_{\mathbf{T}^* \in \mathbf{H}} \left\{ \int_V \mathbf{T}^* \cdot \mathbf{E} - \frac{1}{2} (\mathcal{C} - \mathcal{C}^H) \mathbf{T}^* \cdot \mathbf{T}^* dV \right\} \quad (3.51)$$

where \mathbf{H} is the space of symmetric second-order periodic tensors, \mathbf{T}^* is polarization field (eigenstress) prescribed on the reference homogeneous medium in order to simulate the actual micro-structure of the heterogeneous RVE.

In particular, by taking:

$$\mathbf{E} = \bar{\mathbf{E}} + \hat{\mathbf{E}} \quad (3.52)$$

where $\bar{\mathbf{E}} \in \text{Sym}$ and $\hat{\mathbf{E}} \in \mathbf{E}$, and by remembering that \mathcal{C}^H is constant in V , the (3.51) assumes the following form:

$$\begin{aligned}
& \int_V \left[\frac{1}{2} \mathcal{C} (\bar{\mathbf{E}} + \hat{\mathbf{E}}) (\bar{\mathbf{E}} + \hat{\mathbf{E}}) - \frac{1}{2} \mathcal{C}^H \bar{\mathbf{E}} \cdot \bar{\mathbf{E}} \right] dV = \\
& = \sup_{\mathbf{T}^* \in \mathbf{H}} \left\{ \int_V \left[\langle \mathbf{T}^* \rangle \cdot \bar{\mathbf{E}} - \frac{1}{2} (\mathcal{C} - \mathcal{C}^H)^{-1} \mathbf{T}^* \cdot \mathbf{T}^* \right] dV \right\} + \int_V \left(\mathbf{T}^* \cdot \hat{\mathbf{E}} + \frac{1}{2} \mathcal{C}^H \hat{\mathbf{E}} \cdot \hat{\mathbf{E}} \right) dV
\end{aligned} \tag{3.53}$$

where $\langle \mathbf{T}^* \rangle$ denotes the average value of \mathbf{T}^* in V .

Therefore, by considering the lower bound with respect to $\hat{\mathbf{E}}$, changing the minimization with the maximization and by dividing for V , it is obtained:

$$\frac{1}{2} \bar{\mathcal{C}} \bar{\mathbf{E}} \cdot \bar{\mathbf{E}} - \frac{1}{2} \mathcal{C}^H \bar{\mathbf{E}} \cdot \bar{\mathbf{E}} = \frac{1}{V} \sup_{\mathbf{T}^* \in \mathbf{H}} \left\{ \int_V \left(\langle \mathbf{T}^* \rangle \cdot \bar{\mathbf{E}} - \frac{1}{2} (\mathcal{C} - \mathcal{C}^H)^{-1} \mathbf{T}^* \cdot \mathbf{T}^* \right) dV + \inf_{\hat{\mathbf{E}} \in \mathbf{E}} F_{\mathcal{C}''}^{\mathbf{T}^*} \right\} \tag{3.54}$$

where the quadratic functional $F_{\mathcal{C}''}^{\mathbf{T}^*}$ is defined by:

$$F_{\mathcal{C}''}^{\mathbf{T}^*} = \hat{\mathbf{E}} \in E \rightarrow \int_V \left(\mathbf{T}^* \cdot \hat{\mathbf{E}} + \frac{1}{2} \mathcal{C}^H \hat{\mathbf{E}} \cdot \hat{\mathbf{E}} \right) dV. \tag{3.55}$$

Consider, now, a reference homogeneous material which is stiffer than each phase included in the heterogeneous RVE, such that $\mathcal{C} - \mathcal{C}^H$ is negative definite everywhere in V . Hence, in analogous manner, it is obtained the following equation:

$$\frac{1}{2} \bar{\mathcal{C}} \bar{\mathbf{E}} \cdot \bar{\mathbf{E}} - \frac{1}{2} \mathcal{C}^H \bar{\mathbf{E}} \cdot \bar{\mathbf{E}} = \frac{1}{V} \inf_{\mathbf{T}^* \in \mathbf{H}} \left\{ \int_V \left(\langle \mathbf{T}^* \rangle \cdot \bar{\mathbf{E}} - \frac{1}{2} (\mathcal{C} - \mathcal{C}^H)^{-1} \mathbf{T}^* \cdot \mathbf{T}^* \right) dV + \inf_{\hat{\mathbf{E}} \in \mathbf{E}} F_{\mathcal{C}''}^{\mathbf{T}^*} \right\} \tag{3.56}$$

The equations (3.54) and (3.56) represent the Hashin and Shtrikman's variational principles, based on the eigenstress. In particular, the (3.54) is a saddle principle, while the (3.56) is a minimum principle. From them, by imposing stationariness principles with respect to \mathbf{T}^* , it is obtained:

$$(\mathcal{C} - \mathcal{C}^H)^{-1} \mathbf{T}^* = \hat{\mathbf{E}} + \bar{\mathbf{E}} \tag{3.57}$$

that confirms that stress field \mathbf{T}^* is the correction which has to be prescribed to the reference homogeneous material stress field $\mathcal{C}^H(\hat{\mathbf{E}} + \bar{\mathbf{E}})$ in order to obtain the stress field in the actual material $\mathcal{C}(\hat{\mathbf{E}} + \bar{\mathbf{E}})$.

It is possible to obtain other two variational principles, having similar expressions to the (3.54) and the (3.56) and involving the overall compliance tensor \mathcal{S} . About them, the sole results will be shown, directly, since they are reached with similar considerations to those ones already done.

Therefore, consider a reference homogeneous material which is stiffer than each phase included in the heterogeneous RVE, such that $\mathcal{S} - \mathcal{S}^H$ is positive definite everywhere in V . Hence, in analogous manner, it is obtained the following equation:

$$\frac{1}{2}\bar{\mathcal{S}}\bar{\mathbf{T}}\cdot\bar{\mathbf{T}} - \frac{1}{2}\bar{\mathcal{S}}^H\bar{\mathbf{T}}\cdot\bar{\mathbf{T}} = \frac{1}{V}\sup_{\mathbf{E}^* \in \mathbf{H}} \left\{ \int_V \left(\langle \mathbf{E}^* \rangle \cdot \bar{\mathbf{T}} - \frac{1}{2}(\mathcal{S} - \mathcal{S}^H)^{-1} \mathbf{E}^* \cdot \mathbf{E}^* \right) dV + \inf_{\hat{\mathbf{T}} \in T} F_{\mathcal{S}''}^{\mathbf{E}^*} \right\} \quad (3.58)$$

where the quadratic functional $F_{\mathcal{S}''}^{\mathbf{E}^*}$ is defined by:

$$F_{\mathcal{S}''}^{\mathbf{E}^*} = \hat{\mathbf{T}} \in T \rightarrow \int_V \left(\mathbf{E}^* \cdot \hat{\mathbf{T}} + \frac{1}{2}\mathcal{S}^H \hat{\mathbf{T}} \cdot \hat{\mathbf{T}} \right) dV \quad (3.59)$$

and where \mathbf{H} is the space of symmetric second-order periodic tensors, \mathbf{E}^* is polarization field (eigenstrain) prescribed on the reference homogeneous medium in order to simulate the actual micro-structure of the heterogeneous RVE.

Consider, on the contrary, a reference homogeneous material which is more deformable than each phase included in the heterogeneous RVE, such that $\mathcal{S} - \mathcal{S}^H$ is positive definite everywhere in V . Hence, in similar form, it is obtained the following equation:

$$\frac{1}{2}\bar{\mathcal{S}}\bar{\mathbf{T}}\cdot\bar{\mathbf{T}} - \frac{1}{2}\bar{\mathcal{S}}^H\bar{\mathbf{T}}\cdot\bar{\mathbf{T}} = \frac{1}{V}\inf_{\mathbf{E}^* \in \mathbf{H}} \left\{ \int_V \left(\langle \mathbf{E}^* \rangle \cdot \bar{\mathbf{T}} - \frac{1}{2}(\mathcal{S} - \mathcal{S}^H)^{-1} \mathbf{E}^* \cdot \mathbf{E}^* \right) dV + \inf_{\hat{\mathbf{T}} \in T} F_{\mathcal{S}''}^{\mathbf{E}^*} \right\} \quad (3.60)$$

The equations (3.58) and (3.60) represent the Hashin and Shtrikman's variational principles, based on the eigenstrain. In particular, the (3.58) is a

saddle principle, while the (3.60) is a minimum principle. From them, by imposing stationariness principles with respect to \mathbf{E}^* , it is obtained:

$$(\mathcal{S} - \mathcal{S}^H)^{-1} \mathbf{E}^* = \hat{\mathbf{T}} + \bar{\mathbf{T}} \quad (3.61)$$

that confirms that strain field \mathbf{E}^* is the correction which has to be prescribed to the reference homogeneous material strain field $\mathcal{S}^H(\hat{\mathbf{T}} + \bar{\mathbf{T}})$ in order to obtain the strain field in the actual material $\mathcal{S}(\hat{\mathbf{T}} + \bar{\mathbf{T}})$.

It has to be considered that the Hashin and Shtrikman's variational principles involve auxiliary problems, consisting in the minimization of the functionals, $F_{C^m}^{\mathbf{T}^*}$ (or $F_{S^m}^{\mathbf{E}^*}$). The goal is to solve an equilibrium (or a compatibility) problem, for the reference homogeneous solid, subject to a prescribed eigenstress, \mathbf{T}^* , (or an eigenstrain \mathbf{E}^*). For such problem, however, only few particular cases has a solution.

In particular, it can be remembered the Eshelby's solution for the case in which the polarization field is constant and different from zero, only in an ellipsoidal region. This solution lets to use the Hashin and Shtrikman's variational principles for determining the homogenized properties of a biphasic composite, with a low concentration of inclusions. In order to do it, the same matrix or the inclusions can be chosen as reference homogeneous material, but the matrix and the inclusions have to be well ordered, that means, $\mathcal{C}^M - \mathcal{C}^\Omega$ has to be defined in sign.

In case of periodic composite, the auxiliary problem is easier to solve, because it is possible to transform the RVE domain into a Fourier domain. It is not our interest to expose this procedure, so the interested reader is referred to (Giangreco, 2003).

The calculation of the elastic energy density and of the complementary one, according to the two equations (3.49), requires the execution of very difficult minimization with respect of functionals, that are defined on unbounded space. Operating such minimizations is equivalent to solve the elastostatic problem for the RVE, in the cases of displacements approach and tractions approach, respectively. A numeric minimization, obtained, for example, by using the Element Finite Method, can be employed on finite subspaces, E_f and T_f , of the above mentioned spaces, \mathbf{E} and \mathbf{T} .

Consequently, numeric minimization will yield the following expressions of the tensors, \mathcal{C}^+ and \mathcal{S}^+ :

$$\begin{aligned}
\frac{1}{2} \mathcal{C}^+ \bar{\mathbf{E}} \cdot \bar{\mathbf{E}} &= \inf_{\mathbf{E}^d \in E_f} \frac{1}{V} \int_V \frac{1}{2} \mathcal{C}(\bar{\mathbf{E}} + \mathbf{E}^d)(\bar{\mathbf{E}} + \mathbf{E}^d) dV \\
\frac{1}{2} \mathcal{S}^+ \bar{\mathbf{T}} \cdot \bar{\mathbf{T}} &= \inf_{\mathbf{T}^d \in T_f} \frac{1}{V} \int_V \frac{1}{2} \mathcal{S}(\bar{\mathbf{T}} + \mathbf{T}^d)(\bar{\mathbf{T}} + \mathbf{T}^d) dV
\end{aligned} \tag{3.62}$$

which, for constructions, satisfy the following inequalities:

$$\begin{aligned}
\frac{1}{2} \bar{\mathcal{C}} \bar{\mathbf{E}} \cdot \bar{\mathbf{E}} &\leq \frac{1}{2} \mathcal{C}^+ \bar{\mathbf{E}} \cdot \bar{\mathbf{E}} \\
\frac{1}{2} \bar{\mathcal{S}} \bar{\mathbf{T}} \cdot \bar{\mathbf{T}} &\leq \frac{1}{2} \mathcal{S}^+ \bar{\mathbf{T}} \cdot \bar{\mathbf{T}}.
\end{aligned} \tag{3.63}$$

By naming with \mathcal{C}^- and \mathcal{S}^- , respectively, the inverse of the tensors \mathcal{S}^+ and \mathcal{C}^+ , the upper and lower limitations for the elastic energy, and the complementary one, of the homogenized material are obtained, as given by:

$$\begin{aligned}
\frac{1}{2} \mathcal{C}^- \bar{\mathbf{E}} \cdot \bar{\mathbf{E}} &\leq \frac{1}{2} \bar{\mathcal{C}} \bar{\mathbf{E}} \cdot \bar{\mathbf{E}} \leq \frac{1}{2} \mathcal{C}^+ \bar{\mathbf{E}} \cdot \bar{\mathbf{E}} \\
\frac{1}{2} \mathcal{S}^- \bar{\mathbf{T}} \cdot \bar{\mathbf{T}} &\leq \frac{1}{2} \bar{\mathcal{S}} \bar{\mathbf{T}} \cdot \bar{\mathbf{T}} \leq \frac{1}{2} \mathcal{S}^+ \bar{\mathbf{T}} \cdot \bar{\mathbf{T}}.
\end{aligned} \tag{3.64}$$

Elementary estimations on $\bar{\mathcal{C}}$ and $\bar{\mathcal{S}}$ are obtained by choosing the simplest E_f and T_f , i.e., coinciding with the space constituted by the sole null tensor. In this way, the well known Voigt and Reuss' estimations are reached; in particular, for a biphasic composite, they are:

$$\begin{aligned}
(f_M \mathbb{S}_M + f_\Omega \mathbb{S}_\Omega)^{-1} &\leq \bar{\mathcal{C}} \leq f_M \mathbb{C}_M + f_\Omega \mathbb{C}_\Omega \\
(f_M \mathbb{C}_M + f_\Omega \mathbb{C}_\Omega)^{-1} &\leq \bar{\mathcal{S}} \leq f_M \mathbb{S}_M + f_\Omega \mathbb{S}_\Omega
\end{aligned} \tag{3.65}$$

with:

$$\begin{aligned}
(f_M \mathbb{C}_M + f_\Omega \mathbb{C}_\Omega)^{-1} &= (\mathbb{C}^+)^V, \quad (f_M \mathbb{C}_M + f_\Omega \mathbb{C}_\Omega)^{-1} = (\mathbb{S}^-)^V \\
(f_M \mathbb{S}_M + f_\Omega \mathbb{S}_\Omega)^{-1} &= (\mathbb{C}^-)^R, \quad (f_M \mathbb{S}_M + f_\Omega \mathbb{S}_\Omega)^{-1} = (\mathbb{S}^+)^R
\end{aligned} \tag{3.66}$$

where the superscript V and R stands for Voigt and Reuss.

At the same manner, the Hashin and Shtrikman's variational principles (3.54), (3.56), (3.58) and (3.60) yield estimations on the stiffness and compliance

tensors, if the optimization with regard to the polarization fields is employed above a finite underspace H_f , of the above unbounded mentioned space H of all possible polarization fields.

In particular, it results

$$\frac{1}{2}\bar{\mathcal{C}}\bar{\mathbf{E}}\cdot\bar{\mathbf{E}}-\frac{1}{2}\mathcal{C}^H\bar{\mathbf{E}}\cdot\bar{\mathbf{E}}\geq\frac{1}{V}\sup_{\mathbf{T}^*\in H_f}\left\{\int_V\left(\langle\mathbf{T}^*\rangle\cdot\bar{\mathbf{E}}-\frac{1}{2}(\mathcal{C}-\mathcal{C}^H)^{-1}\mathbf{T}^*\cdot\mathbf{T}^*\right)dV+\inf_{\hat{\mathbf{E}}\in E}F_{\mathcal{C}''}^{\mathbf{T}^*}\right\}\quad (3.67)$$

and

$$\frac{1}{2}\bar{\mathcal{S}}\bar{\mathbf{T}}\cdot\bar{\mathbf{T}}-\frac{1}{2}\mathcal{S}^H\bar{\mathbf{T}}\cdot\bar{\mathbf{T}}\leq\frac{1}{V}\inf_{\mathbf{E}^*\in H_f}\left\{\int_V\left(\langle\mathbf{E}^*\rangle\cdot\bar{\mathbf{T}}-\frac{1}{2}(\mathcal{S}-\mathcal{S}^H)^{-1}\mathbf{E}^*\cdot\mathbf{E}^*\right)dV+\inf_{\hat{\mathbf{T}}\in T}F_{\mathcal{S}''}^{\mathbf{E}^*}\right\}\quad (3.68)$$

if the reference homogeneous material is more deformable than each phase included in the heterogeneous RVE; on the contrary, it results

$$\frac{1}{2}\bar{\mathcal{C}}\bar{\mathbf{E}}\cdot\bar{\mathbf{E}}-\frac{1}{2}\mathcal{C}^H\bar{\mathbf{E}}\cdot\bar{\mathbf{E}}\leq\frac{1}{V}\inf_{\mathbf{T}^*\in H}\left\{\int_V\left(\langle\mathbf{T}^*\rangle\cdot\bar{\mathbf{E}}-\frac{1}{2}(\mathcal{C}-\mathcal{C}^H)^{-1}\mathbf{T}^*\cdot\mathbf{T}^*\right)dV+\inf_{\hat{\mathbf{E}}\in E}F_{\mathcal{C}''}^{\mathbf{T}^*}\right\}\quad (3.69)$$

and

$$\frac{1}{2}\bar{\mathcal{S}}\bar{\mathbf{T}}\cdot\bar{\mathbf{T}}-\frac{1}{2}\mathcal{S}^H\bar{\mathbf{T}}\cdot\bar{\mathbf{T}}\geq\frac{1}{V}\sup_{\mathbf{E}^*\in H_f}\left\{\int_V\left(\langle\mathbf{E}^*\rangle\cdot\bar{\mathbf{T}}-\frac{1}{2}(\mathcal{S}-\mathcal{S}^H)^{-1}\mathbf{E}^*\cdot\mathbf{E}^*\right)dV+\inf_{\hat{\mathbf{T}}\in T}F_{\mathcal{S}''}^{\mathbf{E}^*}\right\}\quad (3.70)$$

if the reference homogeneous material is stiffer than each phase included in the heterogeneous RVE.

A numeric estimation of the inferior extreme of $F_{\mathcal{C}''}^{\mathbf{T}^*}$ and of $F_{\mathcal{S}''}^{\mathbf{E}^*}$ implies that only the minimum principles (3.68) and (3.69) yield upper estimations for the density of the elastic complementary energy and for the elastic one, respectively,

for the homogenized material. The saddle principles (3.67) and (3.70), instead, are able to yield an estimation that cannot be read as an upper or lower estimation.

3. MICROMECHANICS OF POROUS MATERIALS: J-TENSOR AND DILUTE DISTRIBUTION OF VOIDS CASES

In this section, the overall stress-strain/strain stress relations are developed with reference to an RVE consisting of a linearly elastic material which contains stress-free cavities.

Consider an RVE with total volume V , bounded *externally* by surface ∂V . On this surface, either uniform tractions,

$$\mathbf{t}^0 = \mathbf{n} \cdot \boldsymbol{\sigma}^0 \quad \text{on } \partial V, \quad (3.71)$$

or linear displacements,

$$\mathbf{u}^0 = \mathbf{x} \cdot \boldsymbol{\varepsilon}^0 \quad \text{on } \partial V, \quad (3.72)$$

are assumed to be prescribed, where $\boldsymbol{\sigma}^0$ and $\boldsymbol{\varepsilon}^0$ are second-order symmetric *constant* stress and strain tensors for the macro-element. It is emphasized that either (3.71) or (3.72) (4.1.1 a), but not both, can be prescribed. In other words, if the traction boundary data (3.71) corresponding to the constant macrostress $\boldsymbol{\Sigma} = \boldsymbol{\sigma}^0$, are prescribed, then the surface displacements on ∂V , corresponding to these tractions, in general, are *not* spatially linear, being affected by the microstructure of the RVE. Similarly, if the linear displacement boundary data (3.72) corresponding to the constant macrostrain $\mathbf{E} = \boldsymbol{\varepsilon}^0$, are prescribed, then the surface tractions on ∂V , produced by these displacements, are *not*, in general, spatially uniform. In the sequel, therefore, the two cases are treated separately and independently, and then the relation between the results is discussed.

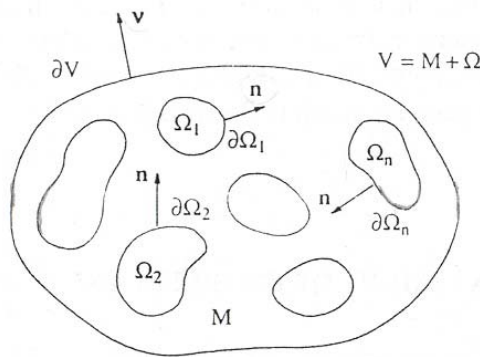


Fig. 3.2.
Matrix M and microcavities Ω_α

Assume that the material of the RVE is linearly elastic and *homogeneous* (but not necessarily isotropic). The inhomogeneity, therefore, stems solely from the presence of cavities. Denote a typical cavity by Ω_α , with the boundary $\partial\Omega_\alpha$ ($\alpha = 1, 2, \dots, n$), so that there are a total of n individual cavities in V . The union of these cavities is denoted by Ω , having the boundary $\partial\Omega$ which is the union of all $\partial\Omega_\alpha$, i.e.,

$$\Omega \equiv \bigcup_{\alpha=1}^n \Omega_\alpha \quad \partial\Omega \equiv \bigcup_{\alpha=1}^n \partial\Omega_\alpha \quad (3.73)$$

The remainder of the RVE (i.e, when Ω is excluded) is called the *matrix*. The matrix is denoted by M . The boundary of M is the sum of ∂V and $\partial\Omega$, Figure 3.2.,

$$M \equiv V - \Omega \quad \partial M \equiv \partial V - \partial\Omega. \quad (3.74)$$

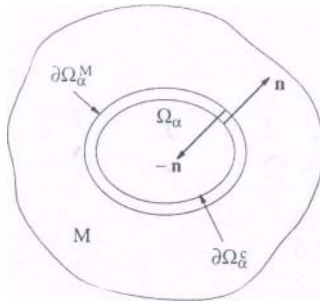


Fig. 3.3.
 $\partial\Omega_\alpha^M$ and $\partial\Omega_\alpha^c$

The total boundary surface of the RVE can include some portion of $\partial\Omega$. For simplicity, however, exclude this possibility. Thus, all cavities are within the RVE, each being fully surrounded by the matrix material. For a typical cavity, Ω_α , two faces of its surface boundary, $\partial\Omega_\alpha$, may be distinguished, as follows:

- the *exterior* face of the cavity, denoted by $\partial\Omega_\alpha^c$ which is the face toward the matrix material, denoted by the direction of the exterior unit normal \mathbf{n} of the cavity;

- the *exterior* face of the *surrounding matrix*, denoted by $\partial\Omega_\alpha^M$, which is the face toward the interior of the cavity, denned by the direction of the exterior unit normal $(-\mathbf{n})$ of the matrix (i.e., the interior unit normal of the cavity). $\partial\Omega_\alpha$ coincides with $\partial\Omega_\alpha^c$, for the cavity Ω_α , while ∂M at the cavity Ω_α coincides with $\partial\Omega_\alpha^M$ (Fig. 3.3). In view of this convention, the integral of a surface quantity taken over ∂M can always be decomposed as

$$\begin{aligned} \int_{\partial M} (\cdot) dS &= \int_{\partial V} (\cdot) dS + \sum_{\alpha=1}^n \int_{\partial\Omega_\alpha^M} (\cdot) dS = \\ &= \int_{\partial V} (\cdot) dS - \sum_{\alpha=1}^n \int_{\partial\Omega_\alpha^c} (\cdot) dS = \int_{\partial V} (\cdot) dS - \int_{\partial\Omega} (\cdot) dS. \end{aligned} \quad (3.75)$$

Thus $\partial\Omega$ always stands for the union of $\partial\Omega_\alpha^c$ ($\alpha = 1, 2, \dots, n$).

To distinguish the boundary of M at the cavities from that at the exterior of the RVE, which is ∂V , the exterior unit normal on ∂V is systematically denoted by \mathbf{n} (as before), and the *exterior* unit normal on the surface $\partial\Omega_\alpha$ for a typical cavity Ω_α , by \mathbf{n} , *pointing from the inside of the cavity toward the matrix M*.

The matrix material is linearly elastic and homogeneous. Denote the corresponding constant elasticity tensor by \mathcal{C} and the compliance tensor by \mathcal{S} .

3.1. Average strain for prescribed macrostress

Suppose that uniform tractions $\mathbf{t}^0 = \mathbf{n} \cdot \boldsymbol{\sigma}^0$ are prescribed on ∂V , associated with the constant symmetric macrostress $\boldsymbol{\Sigma} = \boldsymbol{\sigma}^0$. If the RVE is homogeneous, having *no* cavities, then the corresponding average strain associated with the average stress $\boldsymbol{\sigma}^0$ would be

$$\boldsymbol{\varepsilon}^0 = \mathcal{S} : \boldsymbol{\sigma}^0, \quad (3.76)$$

and hence, in conjunction with $\bar{\boldsymbol{\sigma}} = \boldsymbol{\sigma}^0$, the average strain would be $\boldsymbol{\varepsilon}^0$. The presence of cavities disturbs the uniform stress and strain fields, producing the variable stress field $\boldsymbol{\sigma} = \boldsymbol{\sigma}(\mathbf{x})$ and strain field $\boldsymbol{\varepsilon} = \boldsymbol{\varepsilon}(\mathbf{x})$, in M, with $\boldsymbol{\sigma} = \mathbf{0}$ in Ω . Nevertheless, from the (3.1)

$$\bar{\boldsymbol{\sigma}} = \langle \boldsymbol{\sigma} \rangle = \frac{1}{V} \int_V \boldsymbol{\sigma} dv = \frac{1}{V} \int_M \boldsymbol{\sigma} dv = \boldsymbol{\sigma}^0. \quad (3.77)$$

On the other hand, the average strain is *not*, in general, equal to $\boldsymbol{\varepsilon}^0$. Instead,

$$\bar{\boldsymbol{\varepsilon}} = \langle \boldsymbol{\varepsilon} \rangle = \boldsymbol{\varepsilon}^0 + \bar{\boldsymbol{\varepsilon}}^c, \quad (3.78)$$

where $\boldsymbol{\varepsilon}^0$ is defined by (3.76), and $\bar{\boldsymbol{\varepsilon}}^c$ is the additional strain due to the presence of cavities.

To calculate the additional strain $\bar{\boldsymbol{\varepsilon}}^c$ due to cavities, one may apply the reciprocal theorem, as follows. Consider two sets of loads, one defined by

$$\mathbf{t}^{(1)} = \begin{cases} \mathbf{n} \cdot \delta \boldsymbol{\sigma}^0 & \text{on } \partial V \\ -\mathbf{n} \cdot \delta \boldsymbol{\sigma}^0 & \text{on } \partial \Omega \end{cases} \quad (3.79)$$

which corresponds to uniform *virtual* stress $\delta \boldsymbol{\sigma}^0$ and strain $\delta \boldsymbol{\varepsilon}^0 = \mathcal{S} : \delta \boldsymbol{\sigma}^0$ within the entire RVE (as illustrated in Figure 3.3, $-\mathbf{n}$ is the *interior* unit normal on the *cavity* surface $\partial \Omega$, or the *exterior* unit normal to the boundary of the *matrix*), and the other defined by

$$\mathbf{t}^{(2)} = \begin{cases} \mathbf{n} \cdot \boldsymbol{\sigma}^0 & \text{on } \partial V \\ \mathbf{0} & \text{on } \partial \Omega \end{cases} \quad (3.80)$$

which is the actual loading considered for the RVE.

Denote the displacement, strain, and stress fields associated with the first loading (3.79) by

$$\{\mathbf{u}^{(1)}, \boldsymbol{\varepsilon}^{(1)}, \boldsymbol{\sigma}^{(1)}\} = \{(\mathbf{x} \cdot \delta \boldsymbol{\varepsilon}^0), \delta \boldsymbol{\varepsilon}^0, \delta \boldsymbol{\sigma}^0\} \quad (3.81)$$

which follows from the fact that, for loading (3.79), the strain and stress fields are both uniform throughout the matrix M. And denote the fields associated with the second (i.e., the actual) loading (3.80) by

$$\{\mathbf{u}^{(2)}, \boldsymbol{\varepsilon}^{(2)}, \boldsymbol{\sigma}^{(2)}\} = \{\mathbf{u}, \boldsymbol{\varepsilon}, \boldsymbol{\sigma}\}. \quad (3.82)$$

From the reciprocal theorem, it follows that

$$\int_{\partial V} (\mathbf{n} \cdot \boldsymbol{\sigma}^0) \cdot (\mathbf{x} \cdot \delta \boldsymbol{\varepsilon}^0) ds = \int_{\partial V} (\mathbf{n} \cdot \delta \boldsymbol{\sigma}^0) \cdot \mathbf{u} ds - \int_{\partial \Omega} (\mathbf{n} \cdot \delta \boldsymbol{\sigma}^0) \cdot \mathbf{u} ds \quad (3.83)$$

which can be written as

$$\delta \boldsymbol{\sigma}^0 : \left\{ \int_{\partial V} \mathcal{S} : \{(\mathbf{x} \otimes \mathbf{n}) \cdot \boldsymbol{\sigma}^0\} ds - \int_{\partial V} \mathbf{n} \otimes \mathbf{u} ds + \int_{\partial \Omega} \mathbf{n} \otimes \mathbf{u} ds \right\} = 0. \quad (3.84)$$

Since $\delta\boldsymbol{\sigma}^0$ is an arbitrary symmetric tensor, the symmetric part of the quantity within the braces must vanish identically. Noting that the first integral within the braces yields

$$\frac{1}{V} \int_{\partial V} \mathcal{S} : \{(\mathbf{x} \otimes \mathbf{n}) \cdot \boldsymbol{\sigma}^0\} ds = \mathcal{S} : \{I \cdot \boldsymbol{\sigma}^0\} = \boldsymbol{\varepsilon}^0, \quad (3.85)$$

and using the averaging scheme, it follows that

$$\bar{\boldsymbol{\varepsilon}} = \frac{1}{V} \int_V \frac{1}{2} \{ \nabla \otimes \mathbf{u} + (\nabla \otimes \mathbf{u})^T \} dv = \boldsymbol{\varepsilon}^0 + \frac{1}{V} \int_{\partial\Omega} \frac{1}{2} (\mathbf{n} \otimes \mathbf{u} + \mathbf{u} \otimes \mathbf{n}) ds. \quad (3.86)$$

Comparison with (3.78) shows that the additional strain $\bar{\boldsymbol{\varepsilon}}^c$ due to cavities, is given by

$$\bar{\boldsymbol{\varepsilon}}^c = \frac{1}{V} \int_{\partial\Omega} \frac{1}{2} (\mathbf{n} \otimes \mathbf{u} + \mathbf{u} \otimes \mathbf{n}) ds. \quad (3.87)$$

3.2. Overall compliance tensor for porous elastic solids

Define *the overall compliance* $\bar{\mathcal{S}}$ of the porous RVE with a linearly elastic homogeneous matrix, through

$$\bar{\boldsymbol{\varepsilon}} = \bar{\mathcal{S}} : \bar{\boldsymbol{\sigma}} = \bar{\mathcal{S}} : \boldsymbol{\sigma}^0, \quad (3.88)$$

where the macrostress, $\boldsymbol{\Sigma} = \boldsymbol{\sigma}^0$, is regarded prescribed, and the average strain is given by (3.78). To obtain the overall compliance in an explicit form, the strain $\bar{\boldsymbol{\varepsilon}}^c$ due to cavities will now be expressed in terms of the applied stress $\boldsymbol{\sigma}^0$. Since the matrix of the RVE is linearly elastic, for a given microstructure the displacement $\mathbf{u}(\mathbf{x})$ at a point \mathbf{x} on $\partial\Omega$ is linearly dependent on the uniform overall stress $\boldsymbol{\sigma}^0$, as show following. By remembering that the displacement field may be expressed in terms of Green function as

$$\mathbf{u}(\mathbf{x}) = \int_{\partial V} \mathbf{G}(\mathbf{x}, \mathbf{y}) \cdot \mathbf{t}(\mathbf{y}) ds \quad (3.89)$$

where $\mathbf{t}(\mathbf{y})$ are the self-equilibrating surface traction prescribed on the boundary ∂V of the RVE, if the applied tractions (3.71) are substituting into (3.89), to arrive at

$$\mathbf{u}(\mathbf{x}) = \int_{\partial V} \mathbf{G}(\mathbf{x}, \mathbf{y}) \cdot \{\mathbf{n}(\mathbf{y}) \cdot \boldsymbol{\sigma}^0\} dS, \quad (3.90)$$

where the integration is taken with respect to \mathbf{y} over the boundary ∂V of the RVE. Since $\boldsymbol{\sigma}^0$ is a symmetric constant tensor, (3.90) can be expressed as

$$u_i(\mathbf{x}) = K_{ijk}(\mathbf{x}) \sigma_{jk}^0 \quad (3.91)$$

where the third-order tensor,

$$K_{ijk}(\mathbf{x}) = K_{jik}(\mathbf{x}) = \int_{\partial V} \frac{1}{2} \{G_{ij}(\mathbf{x}, \mathbf{y}) n_k(\mathbf{y}) + G_{ik}(\mathbf{x}, \mathbf{y}) n_j(\mathbf{y})\} dS, \quad (3.92)$$

depends on the geometry and the elastic properties of the matrix of the RVE. To obtain the additional overall strain, $\bar{\boldsymbol{\varepsilon}}^c$, due to the presence of cavities in terms of the prescribed overall stress, $\boldsymbol{\sigma}^0$, substitute from (3.92) into (3.87), to arrive at

$$\bar{\boldsymbol{\varepsilon}}_{ij}^c = H_{ijkl} \sigma_{kl}^0, \quad (3.93)$$

where the *constant* fourth-order tensor, \mathbb{H} , is given by

$$H_{ijkl} \equiv H_{jikl} \equiv H_{ijlk} \equiv \frac{1}{V} \int_{\partial \Omega} \frac{1}{2} \{n_i(\mathbf{x}) K_{jkl}(\mathbf{x}) + n_j(\mathbf{x}) K_{ikl}(\mathbf{x})\} dS. \quad (3.94)$$

Hence, for an RVE with a linearly elastic matrix containing cavities of *arbitrary shapes and sizes*, the following general result is obtained, when the overall macrostress is regarded prescribed (Hori and Nemat-Nasser, 1983):

$$\bar{\boldsymbol{\varepsilon}}^c = \mathbb{H} : \boldsymbol{\sigma}^0. \quad (3.95)$$

It should be noted that this exact result is valid whether or not the linearly elastic constituent of the RVE is homogeneous. The requirements are:

- the matrix of the RVE is linearly elastic;
- the microstructure of the RVE remains unchanged under the applied macrostress $\boldsymbol{\Sigma} = \boldsymbol{\sigma}^0$.

To obtain the overall elastic compliance tensor $\bar{\mathcal{S}}$, in terms of the constant compliance of the matrix, \mathcal{S} , and the *constant* tensor \mathbb{H} , substitute (3.76), (3.88) and (3.95) into (3.78), and noting that the resulting equation must hold for any macrostress $\boldsymbol{\sigma}^0$, arrive at

$$\bar{\mathcal{S}} = \mathcal{S} + \mathcal{H} , \quad (3.96)$$

Note that in many situation, the tensor \mathcal{H} can be computer directly, using the (3.87).

3.3. Average stress for prescribed macrostrain

Suppose that the linear displacements $\mathbf{u}^0 = \mathbf{x} \cdot \boldsymbol{\varepsilon}^0$ (associated with the constant symmetric macrostrain $\mathbf{E} = \boldsymbol{\varepsilon}^0$) are prescribed on ∂V . The matrix of the RVE is assumed to be homogeneous, as marked before. *In the absence of cavities*, the corresponding average stress associated with the prescribed macrostrain, $\boldsymbol{\varepsilon}^0$, would be

$$\boldsymbol{\sigma}^0 = \mathcal{C} : \boldsymbol{\varepsilon}^0 . \quad (3.97)$$

Due to the presence of cavities, the actual field quantities are nonuniform. From the (3.6),

$$\boldsymbol{\varepsilon} = \langle \boldsymbol{\varepsilon} \rangle = \frac{1}{V} \int_V \boldsymbol{\varepsilon} dv = \frac{1}{V} \int_{\partial V} \frac{1}{2} (\mathbf{n} \otimes \mathbf{u} + \mathbf{u} \otimes \mathbf{n}) ds = \boldsymbol{\varepsilon}^0 \quad (3.98)$$

which is valid for any RVE of any material and microstructure. Note that the surface integral in (3.98) extends over the exterior boundary, ∂V , of the RVE only. It does *not* include the cavity boundaries $\partial\Omega$. Equation (3.98) is the direct consequence of the fact that the average strain for an RVE is given in terms of its boundary displacements which are prescribed here to be $\mathbf{u}^0 = \mathbf{x} \cdot \boldsymbol{\varepsilon}^0$.

In general, for a prescribed macrostrain, the average stress is not equal to $\boldsymbol{\sigma}^0$ but

$$\bar{\boldsymbol{\sigma}} = \langle \boldsymbol{\sigma} \rangle = \boldsymbol{\sigma}^0 + \bar{\boldsymbol{\sigma}}^c , \quad (3.99)$$

where $\boldsymbol{\sigma}^0$ is *defined* by (3.97), and $\bar{\boldsymbol{\sigma}}^c$ is the decrement in the overall stress due to the presence of cavities.

As in Subsection 3.1., the reciprocal theorem will be applied to calculate the average stress a in (3.99). To this end, a third set of boundary data defined by

$$\begin{aligned} \mathbf{u}^{(3)} &= \mathbf{n} \cdot \boldsymbol{\sigma}^0 & \text{on } \partial V \\ \mathbf{t}^{(3)} &= \mathbf{0} & \text{on } \partial\Omega. \end{aligned} \quad (3.100)$$

The displacement, strain, and stress fields associated with these boundary conditions are denoted by

$$\{\mathbf{u}^{(3)}, \boldsymbol{\varepsilon}^{(3)}, \boldsymbol{\sigma}^{(3)}\} = \{\mathbf{u}, \boldsymbol{\varepsilon}, \boldsymbol{\sigma}\} \quad (3.101)$$

which are actual fields, in general, different from those given by (3.82) for the boundary conditions (3.80). The actual tractions on the boundary of the RVE now are

$$\mathbf{t}(\mathbf{x}) = \mathbf{n}(\mathbf{x}) \cdot \boldsymbol{\sigma}(\mathbf{x}), \quad (3.102)$$

where \mathbf{x} is on ∂V . These tractions are required in order to impose the boundary displacements prescribed by (3.100).

Applying the reciprocal theorem to the two sets of loads, (3.79) and (3.100), it follows that

$$\int_{\partial V} \mathbf{t} \cdot (\mathbf{x} \cdot \delta \boldsymbol{\varepsilon}^0) ds = \int_{\partial V} (\mathbf{n} \cdot \delta \boldsymbol{\sigma}^0) \cdot (\mathbf{x} \cdot \delta \boldsymbol{\varepsilon}^0) ds - \int_{\partial \Omega} (\mathbf{n} \cdot \delta \boldsymbol{\sigma}^0) \cdot \mathbf{u} ds \quad (3.103)$$

which can be written as

$$\delta \boldsymbol{\varepsilon}^0 : \left\{ \int_{\partial V} \mathbf{t} \otimes \mathbf{x} ds - \int_{\partial V} \mathbb{C} : \{(\mathbf{x} \otimes \mathbf{n}) \cdot \boldsymbol{\varepsilon}^0\} ds + \int_{\partial \Omega} \mathbb{C} : (\mathbf{n} \otimes \mathbf{u}) ds \right\} = 0 \quad (3.104)$$

where, in using loading (3.81), the quantity $\delta \boldsymbol{\varepsilon}^0$ is regarded as a virtual spatially constant strain field with the corresponding stress field, $\delta \boldsymbol{\sigma}^0 = \mathbb{C} : \delta \boldsymbol{\varepsilon}^0$. Since $\delta \boldsymbol{\varepsilon}^0$ is an arbitrary symmetric tensor, the symmetric part of the quantity within the braces in (3.104) must vanish identically. Noting that the second integral within the parentheses can be expressed as

$$\frac{1}{V} \int_{\partial V} \mathbb{C} : \{(\mathbf{x} \otimes \mathbf{n}) \cdot \boldsymbol{\varepsilon}^0\} ds = \mathbb{C} : \{\mathbf{I} \cdot \boldsymbol{\varepsilon}^0\} = \boldsymbol{\sigma}^0, \quad (3.105)$$

and using the averaging procedure, it now follows that

$$\bar{\boldsymbol{\sigma}} = \frac{1}{V} \int_{\partial V} \mathbf{t} \otimes \mathbf{x} ds = \boldsymbol{\sigma}^0 - \mathbb{C} : \left\{ \frac{1}{V} \int_{\partial \Omega} \frac{1}{2} (\mathbf{n} \otimes \mathbf{u} + \mathbf{u} \otimes \mathbf{n}) ds \right\} \quad (3.106)$$

Comparison with (3.99) shows that the decremental stress $\bar{\boldsymbol{\sigma}}^c$ due to the presence of cavities, is given by

$$\bar{\boldsymbol{\sigma}}^c = -\mathbb{C} : \bar{\boldsymbol{\varepsilon}}^c \quad (3.107)$$

where $\bar{\boldsymbol{\varepsilon}}^c$ is the strain due to the presence of cavities given by (3.87), which now must be computed for the prescribed boundary displacements $\mathbf{u}^0 = \mathbf{x} \cdot \boldsymbol{\varepsilon}^0$.

3.4. Overall elasticity tensor for porous elastic solids

When the overall macrostrain is regarded prescribed, $\mathbf{E} = \boldsymbol{\varepsilon}^0$, designate the overall elasticity tensor of the porous RVE with a linearly elastic and homogeneous matrix, by $\bar{\mathcal{C}}$, and define it through

$$\bar{\boldsymbol{\sigma}} = \bar{\mathcal{C}} : \boldsymbol{\varepsilon}^0. \quad (3.108)$$

Substitution of (3.97), (3.107), and (3.108) into (3.99) then yields

$$(\bar{\mathcal{C}} - \mathcal{C}) : \boldsymbol{\varepsilon}^0 + \mathcal{C} : \bar{\boldsymbol{\varepsilon}}^c = \mathbf{0}. \quad (3.109)$$

For a given microstructure (i.e., for existing cavities with fixed shapes, sizes, and distribution), the response of the RVE is linear. Hence, the displacement field anywhere within the linearly elastic matrix of the RVE is a linear and homogeneous function of the prescribed overall constant strain $\boldsymbol{\varepsilon}^0$. Therefore, in line with results (3.91) and (3.92) for the case when the macrostresses were considered to be prescribed, at a typical point \mathbf{x} on the boundary of the cavities, $\partial\Omega$,

$$u_i(\mathbf{x}) = L_{ijk}(\mathbf{x}) \varepsilon_{jk}^0 \quad (3.110)$$

where $\mathbf{L}(\mathbf{x})$ is a third-order tensor-valued function with the symmetry property, $L_{ijk} = L_{ikj}$. Now, from the definition of $\bar{\boldsymbol{\varepsilon}}^c$, given by the (3.87),

$$\bar{\varepsilon}_{ij}^c = J_{ijkl} \varepsilon_{kl}^0, \quad (3.111)$$

where the *constant* fourth-order tensor, \mathbb{J} , is given by

$$J_{ijkl} \equiv J_{jikl} \equiv J_{ijlk} \equiv \frac{1}{V} \int_{\partial\Omega} \frac{1}{2} \{ n_i(\mathbf{x}) J_{jkl}(\mathbf{x}) + n_j(\mathbf{x}) J_{ikl}(\mathbf{x}) \} dS. \quad (3.112)$$

Hence, for an RVE with a linearly elastic matrix (whether homogeneous or not) containing cavities of arbitrary shapes and sizes, the following general result is obtained, when the overall macrostrains are regarded prescribed:

$$\bar{\boldsymbol{\varepsilon}}^c = \mathbb{J} : \boldsymbol{\varepsilon}^0. \quad (3.113)$$

To obtain an expression for the overall elastic moduli of the porous RVE, substitute (3.113) into (3.109) and, noting that the resulting expression must be valid for any constant symmetric macrostrain $\boldsymbol{\varepsilon}^0$, arrive at

$$\bar{\mathcal{C}} = \mathcal{C} - \mathcal{C} : \mathcal{J} . \quad (3.114)$$

It should be noted that in many practical problems the tensor \mathbf{J} , similarly to the tensor \mathcal{H} , can be calculated *directly* from (3.87), and therefore, the overall elastic moduli can be estimated from (3.114).

It may, however, be instructive to seek to construct the tensor \mathcal{J} in terms of the Green functions $\mathbf{G}(\mathbf{x}, \mathbf{y})$ and $\mathbf{G}^{-1}(\mathbf{x}, \mathbf{y})$.

To this end, for the linear displacements, $\mathbf{u}^0 = \mathbf{z} \cdot \boldsymbol{\varepsilon}^0$, *prescribed* on the outer boundary ∂V of the RVE, by remembering that the *resulting* tractions, $\mathbf{t}(\mathbf{y})$, may be written as

$$\mathbf{t}(\mathbf{y}) = \int_{\partial V} \mathbf{G}^{-1}(\mathbf{y}, \mathbf{z}) \cdot (\mathbf{z} \cdot \boldsymbol{\varepsilon}^0) d\mathbf{s} , \quad (3.115)$$

where the integration is taken with respect to \mathbf{z} over the outer boundary ∂V (excluding the traction-free cavity boundaries) of the RVE. Substituting (3.115) into (3.89), the displacement field for points on $\partial\Omega$ is obtained in terms of the prescribed macrostrain $\boldsymbol{\varepsilon}^0$, as

$$\mathbf{u}(\mathbf{x}) = \int_{\partial V} \mathbf{G}(\mathbf{x}, \mathbf{y}) \cdot \left\{ \int_{\partial V} \mathbf{G}^{-1}(\mathbf{y}, \mathbf{z}) \cdot (\mathbf{z} \cdot \boldsymbol{\varepsilon}^0) d\mathbf{s} \right\} d\mathbf{s} \quad (3.116)$$

where both the \mathbf{y} - and \mathbf{z} -integral are taken over ∂V . Noting that $\boldsymbol{\varepsilon}^0$ is a symmetric tensor, tensor \mathbf{L} in (3.110) may now be written in terms of \mathbf{G} and \mathbf{G}^{-1} , as

$$L_{ijk}(\mathbf{x}) = \int_{\partial V} G_{im}(\mathbf{x}, \mathbf{y}) \left\{ \int_{\partial V} \frac{1}{2} \left\{ G_{mj}^{-1}(\mathbf{y}, \mathbf{z}) z_k + G_{mk}^{-1}(\mathbf{y}, \mathbf{z}) z_j \right\} d\mathbf{s} \right\} d\mathbf{s} . \quad (3.117)$$

Therefore, from comparison of (3.113) with (3.117), a fourth-order tensor, $\mathbf{j}(\mathbf{x}, \mathbf{y})$, can be introduced as

$$j_{ijkl} = \int_{\partial V} \frac{1}{4} \left\{ n_i(\mathbf{x}) G_{jm}(\mathbf{x}, \mathbf{y}) G_{mk}^{-1}(\mathbf{y}, \mathbf{z}) z_l + n_i(\mathbf{x}) G_{jm}(\mathbf{x}, \mathbf{y}) G_{ml}^{-1}(\mathbf{y}, \mathbf{z}) z_k + \right. \\ \left. n_j(\mathbf{x}) G_{im}(\mathbf{x}, \mathbf{y}) G_{mk}^{-1}(\mathbf{y}, \mathbf{z}) z_l + n_j(\mathbf{x}) G_{im}(\mathbf{x}, \mathbf{y}) G_{ml}^{-1}(\mathbf{y}, \mathbf{z}) z_k + \right\} d\mathbf{s} , \quad (3.118)$$

where the integral is taken with respect to \mathbf{z} over ∂V . The constant tensor \mathcal{J} in (3.113) now becomes

$$\mathcal{J} = \frac{1}{V} \int_{\partial\Omega} \int_{\partial V} \mathbf{j}(\mathbf{x}, \mathbf{y}) ds ds, \quad (3.119)$$

where the \mathbf{y} -integration is over ∂V , and the \mathbf{x} -integration is over $\partial\Omega$.

CHAPTER IV

ISOTROPIC AND CUBIC POROUS MEDIA

1. Evaluation of the Elastic Moduli for Poroelastic Solids: Randomly arranged Microstructure

The micromechanical characterization of porous materials is of primary importance in the study of biomaterials, in many problems of tissue mechanics as well as in the application of engineering of materials.

In fact, porous media made by a solid matrix and isolated or linked voids – which determine the porosity of the medium – form the microstructure of a wide number of materials such as the geotechnical materials (soils and rocks), cellular conglomerates, ceramic materials, synthetic biomaterials or biological tissues (e.g. cancellous bone, soft tissue). The mechanical interpretation of the elastic and ultra-elastic behaviour of such materials requires the homogenization of the overall physic and geometrical properties inside RVE of the considered poro-elastic solid. In this way, it is then possible to establish the constitutive relationship for such solids, to analyze the structural response under specific load conditions as well as – in biomedical circles – to have mathematical models useful to simulate problems of permeability or drug delivery.

If the volume fraction is strongly variable inside the considered solid, it is not possible apply standard homogenization procedure which usually require periodic microstructure, namely constant porosity.

With specific reference to cancellous bone, many author determined the elastic moduli and the strength as function of the volume fraction by means of mechanical experimental tests on a large number of bone specimens taken *in situ*.

In particular, Rho (1995) – by means of experimental tests – obtained interpolation functions between the stiffness and the volume fraction of the bone that sometimes show a too high value of standard deviation. The dispersion of the results and the dependence upon the specific type of bone are the main limits of such experimental relations.

Besides, further studies are based on numerical approaches. Analyses based on Finite Element (FE) method are implemented on micro-models whose micro-architecture has been accurately reconstructed. Unfortunately, these kind of analysis do not furnish general relations between the elastic moduli and the density because of the dependence of the results upon the specific densitometry of the specimen.

2. Elastic moduli penalization law for Cubic/Isotropic Media

Determination of the elastic constant of porous material is a complex problem. The relations between elastic constants and apparent density obtained by fitting experimental data often show a not negligible dispersion of the results. It is probably due to the fact that being the density a scalar quantity, it is not able to describe other microstructural features such as the orientation. On the other hand, FEM-analyses of micro-models whose micro-architecture has been accurately reconstructed require too heavy computer's elaborations and, moreover, do not furnish general relationships between the elastic moduli and the density because of the dependence of the results upon the specific densitometry of the specimen.

In order to overcome these problems, many authors also employ analysis based on the finite element method on micro-models with a regularized micro-geometry, Wagner and Gibson (2000), Kouznetsova et al. (2001), González et al. (2004). This approach permits to simulate mechanical tests on three-dimensional RVE by introducing both material and geometrical non-linearity, in order to predict the elastic moduli of the heterogeneous media, the yield strengths as well as possible post-elastic stress-strain curves.

To the author knowledge, no explicit investigations have been performed in Literature for determining the overall elastic response of porous RVEs with wide variable volume fractions, i.e. RVEs characterized by the presence of voids – with eventual different sizes and shapes – whose percentage ranges from high porosity up to high matrix volume fraction.

In this chapter FE method is adopted with the aim of establishing a general relationship between averaged elastic moduli and matrix volume fraction for a copious amount of porous RVE materials, all exhibiting at least three planes of symmetry: this gives cubic anisotropy or isotropy, in terms of overall response. In particular, the geometrical evolution of the RVE porosity is obtained by means of three-dimensional periodic arrangement of voids, embedded in a linearly elastic isotropic solid matrix and spatially distributed so that cubic symmetry is reached too, exploring a number of cavity shapes. FE analyses are hence performed over the single porous RVEs, to obtain homogenized mechanical properties for both *centred on void* (CV) and *centred on matrix* (CM) models, fig. 4.1. The investigation is conducted on these two classes of RVEs, in order to highlight possible differences, in terms of homogenized elastic moduli, making variable the choice of the RVE position.

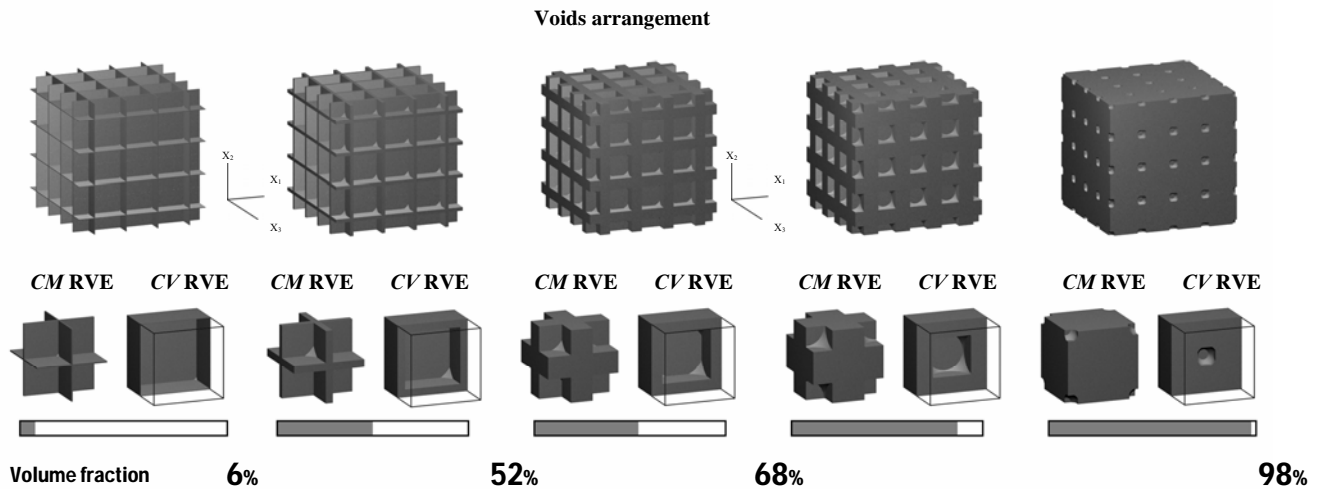


Fig. 4.1. 3D representation of \square CF - see further - porous RVE 4X4 matrix through increasing volume fraction sketches. Respective single RVE representation is also shown, both centred on matrix and centred on void case (middle section).

In particular, the upper and lower bounds of the effective elastic constants as a function of the volume fraction are evaluated, by considering displacement and traction-prescribed boundary conditions.

Following this way, several RVEs are built up increasing void sizes and elastic analyses are then performed over a wide range of porosity values, obtaining overall elastic moduli as function of RVE matrix volume fraction, γ . Thus, computational results are utilized for constructing a mathematical one-to-one relation between γ and overall elastic moduli. In order to relate volume fraction to moduli in a closed form, the corresponding set of data is compared to an analytical function. This law is based on the third polynomial regression and is solved through limit conditions defined to make it obeying to dilute and porous theories. Such theories, the first referred to the theory of dilute distribution of voids, Nemat-Nasser (1983), – valid in the case of high volume fraction – and the second to Flugge's theory, Flugge (1972), – in case of high

porosity – are defined in a narrow range of density values, for dilute analytical model is fit on almost dense materials as porous model is fit on highly porous ones. Chosen cavity type ensures a good comparison between FE data results and analytical function, its void expansion allows spanning from dilute FE models to porous ones, that is invoking dilute and Flugge theories in the same model, Flugge (1972). Such kind of cavity types will further defined as \square CF cavity, fig. 4.1.

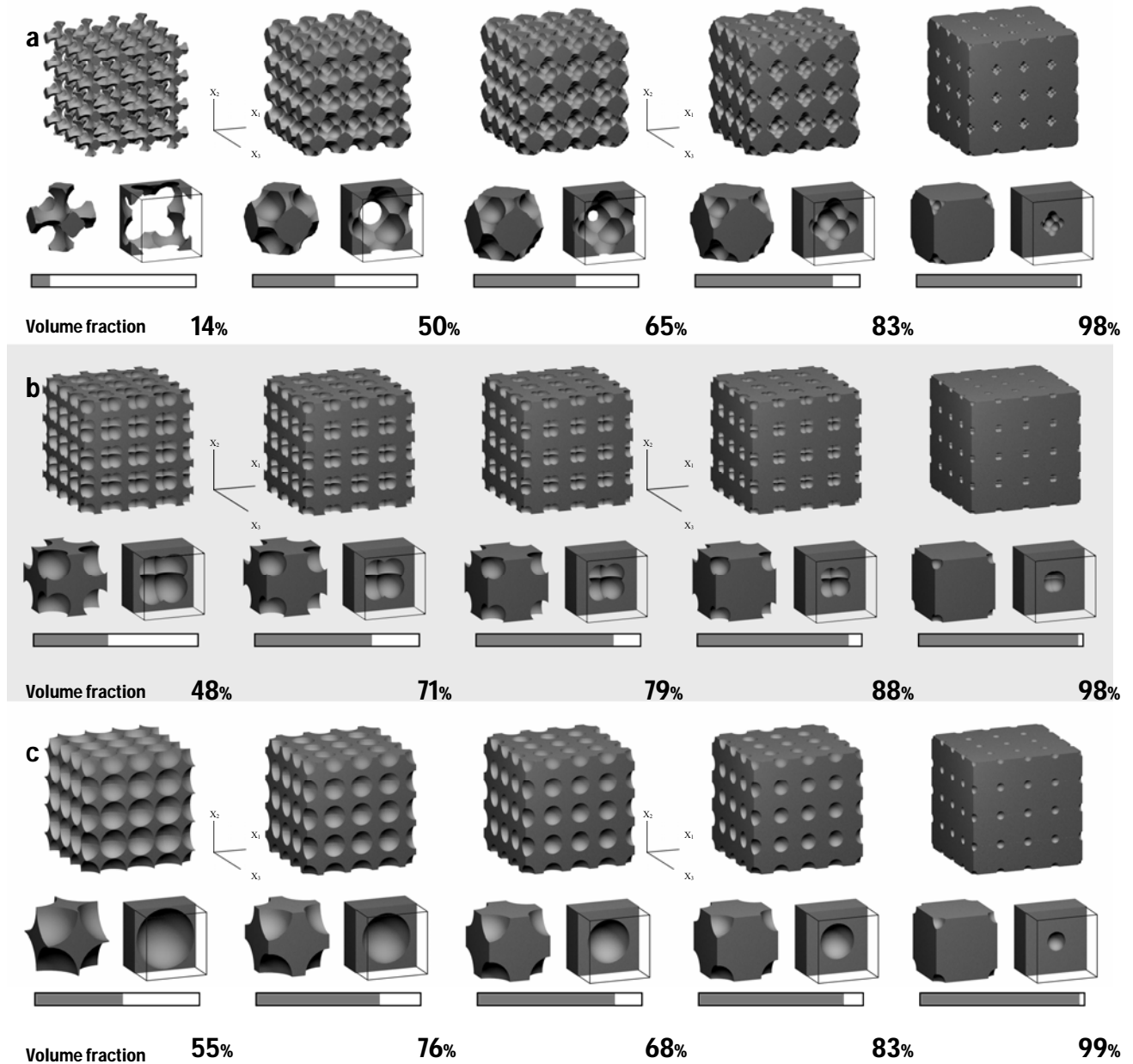


Fig. 4.2. 3d representation of more cavity types of porous RVE 4X4 arrays trough increasing volume fraction sketches: a) \square 7E, seven ellipsoides cavity type, b) \square 8S, eight spheres cavity type, c) \square SC, single sphere cavity type. Respective single RVE representation is also shown, both corner eroded and void centred case (middle section).

Moreover, in order to also evaluate the influence of cavity shapes on the overall mechanical properties of the porous material at a fixed value of the volume fraction, voids of three different shapes are considered: seven overlapping ellipsoidal voids (\square 7E cavity), eight overlapping

spherical voids (\square 8S cavity) and a sole centred spherical void (\square SC cavity), fig. 4.2. For reaching lowest matrix volume fractions, in \square 7E cavity type, voids are able to intersect cubic RVE sides. FE models are processed under tractions-prescribed boundary conditions as well as displacement ones. In this way, according to Voigt and Reuss theories, Voigt (1928), Reuss (1929), the upper and lower bounds of the effective elastic constants as a function of the volume fraction are evaluated.

2.1 Finite Element Analyses

2.1.a. Geometry material and mesh

Cubic and isotropic heterogeneous porous material is analyzed by meaning of homogenization criteria. For materials with periodic voids arrangement, such homogenization is based on RVE fixing, as RVE position, besides RVE size, sets how results are to be read.

To predict homogenized behaviour of a porous cubic symmetric material, a cubic cell RVE is chosen with faces oriented towards the material symmetry direction, i.e. parallel to the coordinate planes of a Cartesian system $\{x_1, x_2, x_3\}$, as a cubic symmetric cell is obtained. By the shape and distribution of voids investigated, two different type of cubic symmetric RVE are available: centred on void cubic cell (CV), and centred on matrix one (CM), fig. 4.1.

Both of them are modelled and analyzed through finite element method by tractions prescribed and displacement applied tests in a way to completely define elastic behaviour through volume fraction variation. Tests produce values of homogenized Young modulus, Poisson ratio and shear modulus, bulk modulus calculations are even performed as validation tests.

In case of \square CF type cell, results show difference in tractions and displacement for every tests but one: centred on matrix (CM) RVEs Young modulus calculation (i.e. uniaxial tests, see Appendix A.1). Testing \square CF CM cavity type, to obtain Young modulus density variation, no relevant differences are highlighted in case of tractions prescribed or displacement applied boundary condition, moreover results thoroughly match Young modulus density function obtained by CV RVE displacement tests, graph 4.1.

This trend is related to different distribution of boundary condition as consequence of different representative volume position. The box-like shape of the centred on void RVE, CV, ensures a better distribution of loads and a complete results data set, in a way to highlight the upper and lower values of Young modulus trend as Voigt and Reuss theories prescribe, Voigt (1928), Reuss (1929). As in CV RVE position pressure loads the whole RVE face for every volume fraction, resulting in a lower overall stiffness. On the contrary, for the orthogonal shell configuration of the centred on matrix RVE, CM, pressure stands on shells loading in plane, determining parallel behaviour of local matrix stiffness equal in series behaviour, that is Reuss calculations is equal to Voigt.

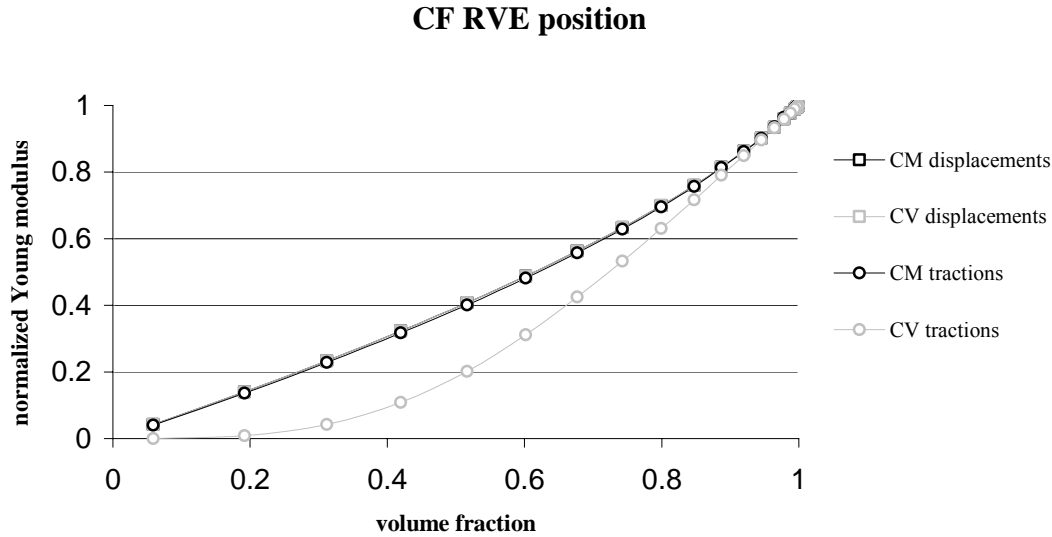
Furthermore, is worth to observe that \square CF RVE cavity types ensure a larger range of volume fraction than all other cavity types adopted, fig. 4.2.

Therefore, in order to estimate the influence of the volume fraction on the overall mechanical behaviour of the porous media, FE models of cubic cell porous RVE centred on void with such cavity type (\square CF CV RVE) are chosen to perform suitable computational analyses.

\square CF RVE model density varies within a characteristic voids length. Void shape consists in a smoothed edge cubical block and its diagonal can vary from $\frac{L}{20}$ to $\sqrt{3}L$, where L is the length of

RVE edge. Cavity type shows different shapes related to growing volumes, indeed RVE matrix volume fraction γ is defined in the range $[0.06, 1]$, porosity p is related as $p = 1 - \gamma$. A typical dilute porous material arrangement is obtained when matrix volume fraction is close to 1,

whereas a structure like orthogonal shell comes out as \mathcal{V} tends to 0, fig. 4.1. Therefore, *CF* cavity material model (\square *CF*) spans, through a single geometric parameter variation, from dilute porous material, whose analytical behaviour is described by Nemat-Nasser (1983), to tin wall porous model similar to one proposed in the Flugge studies, Flugge (1972).



Graph 4.1. Trend of Young modulus, normalized over matrix value, within volume fraction in case of \square *CF* CV porous RVE and \square *CF* CM porous RVE FE calculations (isotropic matrix properties: $E_0 = 17200$ MPa, $\nu_0 = 0.3$). Both displacements applied and tractions prescribed calculation are highlighted.

Material properties of matrix of cubic cell are modelled as linear, elastic and isotropic, characterized by the Young modulus $E_0 = 17200$ MPa and the Poisson's ratio $\nu_0 = 0.3$; the length of cubic cell edge is set equal to 1. Matrix elastic behaviour affects the overall porous RVE properties, values are chosen by human bone elastic average ones. Every value result presented in this work is given normalized over matrix parameters.

Mesh of 3D RVE models is performed through three dimensional isoparametric tetrahedral element with ten nodes, element is well suited to model irregular meshes as supports a quadratic displacement shape function.

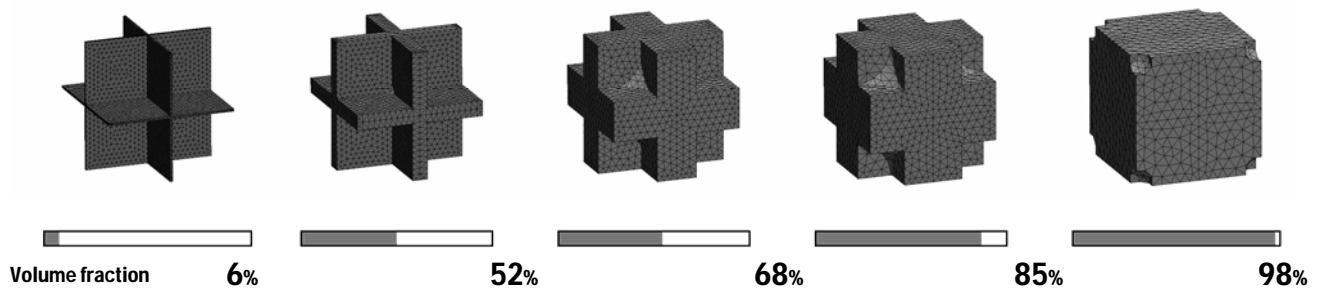


Fig. 4.3. 3d representation of \square *CF* porous CM RVE FE models through increasing volume fraction sketches.

Routine for the automatic generation of both geometric and mesh models is created. In particular, the algorithm allows the automatic generation of a wide number of porous FE models with progressively increasing voids dimension. Thus, a data set of results, large enough to draw with accuracy the relations between average mechanical properties and volume fraction, is achieved.

In figure 4.3 sketches of some FE meshes are shown; note that, to perform a better visualization, \square CF centred on matrix, instead of centred on void, cavity type is shown.

2.1.b. Boundary conditions and implementation

Several boundary conditions on RVE cell are considered in a way to define a suitable set of FE analyses. In particular, to explore the elastic behaviour of the porous material RVE, analyses are performed both applying uniform tractions and uniform displacement on cubic cell faces. Edges of cubic cell are parallel to the coordinate planes of a Cartesian system $\{x_1, x_2, x_3\}$ centred on cell. FE models are tested both under uniform tractions and uniform displacement applied normally to cell face of coordinates $\left(x_1, x_2, \frac{L}{2}\right)$. Moreover, porous cell models are even tested under pure shear uniform tractions and angular deflection applied parallel to RVE faces of coordinates $\left(x_1, x_2, \frac{L}{2}\right)$ and $\left(\frac{L}{2}, x_2, x_3\right)$, as well as loaded by hydrostatic pressure and uniform triaxial displacement, figure 4.4. For more details refer to Appendix A.1.

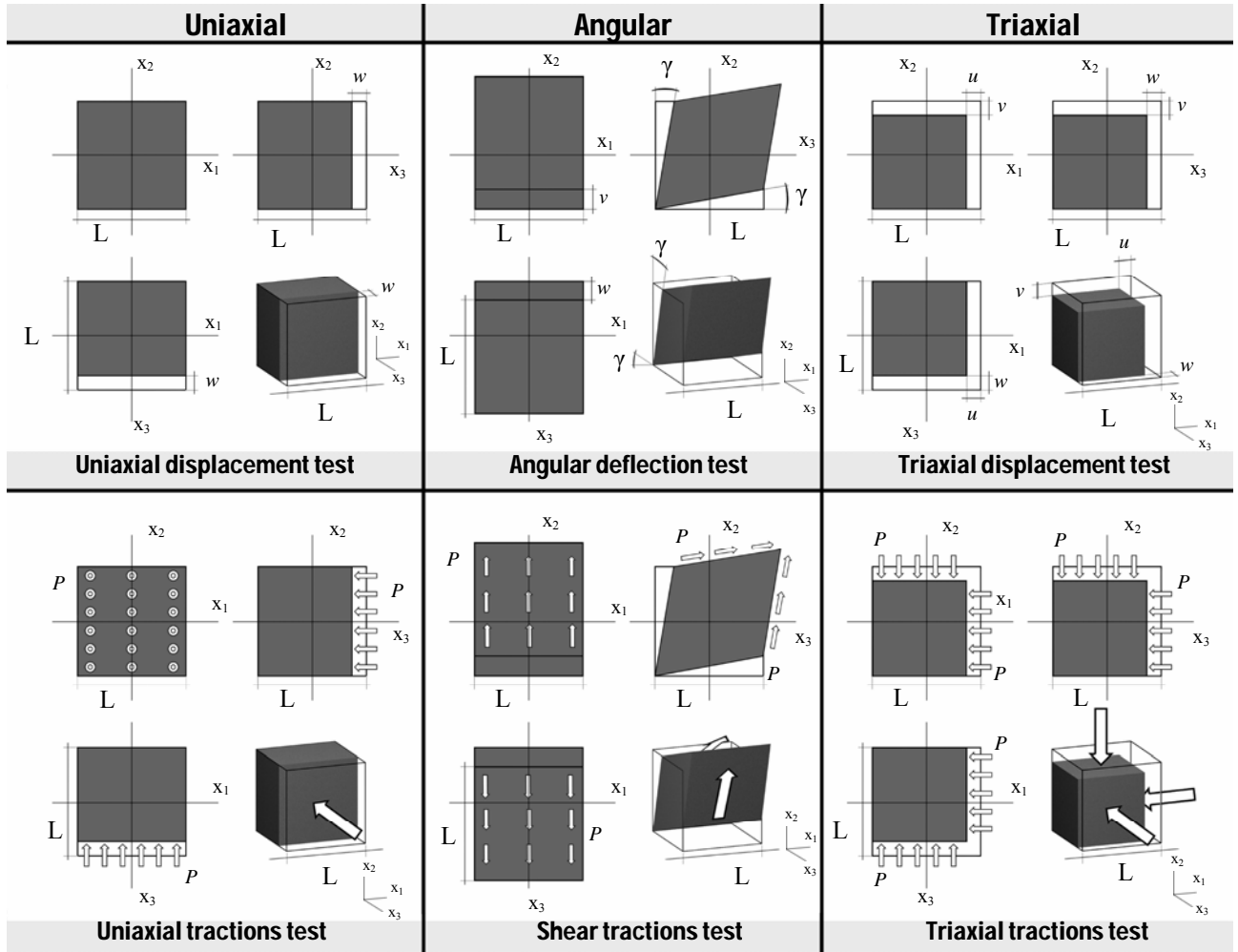
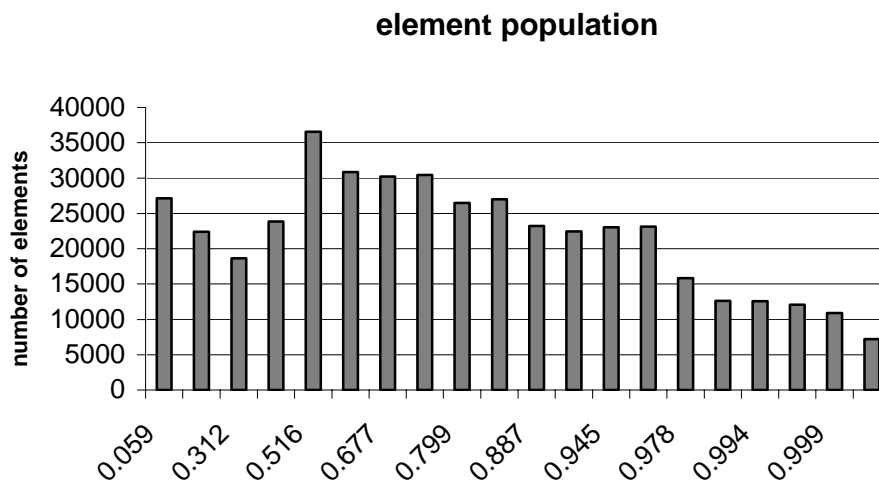


Fig. 4.4. RVE boundary conditions tests.

2.1.c. Model accuracy

Fine element local density defines fidelity both of geometrical and material model. FEM model mesh accuracy is generally intended to assure a high precision of performed analysis results and a good geometrical approximation. Mesh density upper bound is marked by solving process time, it is directly related to clock speed of implemented machine. Fixing results error tolerance and geometrical fidelity, finite element mesh is to be lower populated as possible, in way to obtain an easily handling model.

In this work an error tolerance percentage of 3% is assumed, model mesh precision were tested to ensure this accuracy level and it shows less than 35.600 elements for cases of highest complexity of cavity geometry. In any case theoretical density does not considerably differ from one computed on discrete model. So was able to perform a large number of analyses. Graph 4.2, shows element population of models of RVE *CM* with \square *CF* cavity type with different volume fractions.





Graph 4.2. *CM CF* RVE element population varying volume fraction.

RVE modelled porous geometry varies with a single geometrical parameter, in a way to vary the RVE porosity. For each geometrical parameter value a specific routine aimed to obtain local parametric meshing is generated. In no one case a wall of less than three finite elements thickness appears and the generally coarse mesh becomes automatically more and more fine whereas the cavity surface curvature drastically increase.

2.1.d. Cavities of different shapes



Porous RVE mechanical behaviour is generally also related to shape and direction of voids. To investigate this aspect three different cavity types more are used to model cubic cell porosity. Cubic symmetry is at least preserved over all three types, different volume fraction range is allowed for each case. As for previous cavity type, model density varies within a specific void size. Models reproduce a cubic cell with constant length edge, L , with different types of cavity. Such cavity types are: one centred spherical cavity (\square *SC*), eight centred overlapping spherical cavity with equal radius (\square *8S*), and finally seven centred overlapping ellipsoidal cavity of common dimensions (\square *7E*), fig. 4.2.

In the first model, \square *SC* type, a single spherical void is considered, its centre coincides with the centre of cubic cell and the radius rises from the minimum value of $\frac{L}{20}$ to the maximum value of

$\frac{L}{2}$, where L is the length of the RVE cubic cell side, model type shows a matrix volume fractions in the range $[0.55, 1]$, (see fig. 4.2a). In the second model,  8S type, eight overlapping spherical voids are considered. Every sphere has its centre located on one of the eight semi-diagonal of the cubic cell and passes for its centre, that is all the spheres have their centres decided by own radii (see fig. 4.2b), type shows matrix volume fractions in the range $[0.48, 1]$. The increasing sphere radius r must satisfy the inequality $r < \frac{L}{3.23}$ in order to avoid intersection between cubic cell surface and cavity. In the last cavity type,  7E type, the centre of each of the seven ellipsoidal cavities is placed at the centre of the cell, the major diameters of three of them lying on the three axes orthogonal to the cell faces, and the other four ellipsoids major diameters lie on the four RVE diagonals. The major ellipsoidal diameter varies between $\frac{L}{20}$ and $\frac{L}{1.21}$, for this cavity type intersections with cubic cell face are allowed, (see fig. 4.2c), as wider range of volume fraction is achieved, upper limit of ellipsoidal axes length value is imposed by model geometrical consistency. Other two diameters of the ellipsoidal cavities are equal and set to be half of the major one, cavity type shows matrix volume fractions in the range $[0.14, 1]$.

The matrix of every cubic cell is assumed to be linear, elastic and isotropic, characterized by Young modulus $E_0 = 17200 \text{ MPa}$ and the Poisson's ratio $\nu_0 = 0.3$; length of cubic cell edge is set equal to unit Matrix elastic behaviour affects the overall porous RVE properties, values are chosen by human bone elastic average ones. Both mesh and density varying model generation follow the procedure used to create the above CF cavity type FE model (sec. IV.2.1a). Modelled RVEs are numerical tested under conditions exposed in Appendix A.1. Every value result is give normalized over matrix parameters.

2.1.e. Homogenized elastic constant

Several numerical mechanical tests are performed using models based on  CF type RVE, shifting from shell like configuration (Flugge model) to matrix heterogeneous one (zero porosity material). Isotropic elastic behaviour of matrix is defined by $E_0 = 17200 \text{ MPa}$ and $\nu_0 = 0.3$. This kind of model spans in the range of quite all density spectrum, in way to describe its behaviour in a wide density spectrum for all the homogenized elastic characteristics. Model cavity type is defined by a centred on void RVE cell with above described  CF cavity form (par. IV 2.1.a), it gives a cubic symmetric RVE. Thus, to define its elastic behaviour, three elastic constants are needed.

Model is tested both under uniform tractions and uniform displacement apply normal to (x_1, x_2, L) face of the RVE cubic cell, see fig 4.4. Moreover, porous cells are even tested both under pure share uniform tractions and angular deflection parallel to a RVE face, and loaded by hydrostatic pressure as well as uniform triaxial displacement, see fig 4.4, as explained in Appendix A.1. These tests are aimed to obtain linear relation between average stresses and average deformations in way to define homogenized linear elastic properties of the porous RVE. Analyses performed under uniform displacement allow calculating the average stress tensor of the RVE. Average deformation tensor is directly deduced by uniform displacement applied at the RVE surface, thus, depending on displacement test kind, isotropic elastic constants, as first and second Lamé constant (as well as related Young modulus and bulk modulus), and anisotropic shear modulus of the porous RVE can be calculated. For more details refer to Appendix A.2. According to Voigt and Reuss theory numerical tractions prescribed and displacement defined tests give respectively upper and lower bound of the investigated elastic properties. Models are tested in the available volume fraction range by a lot of FE analyses. Both displacement imposed

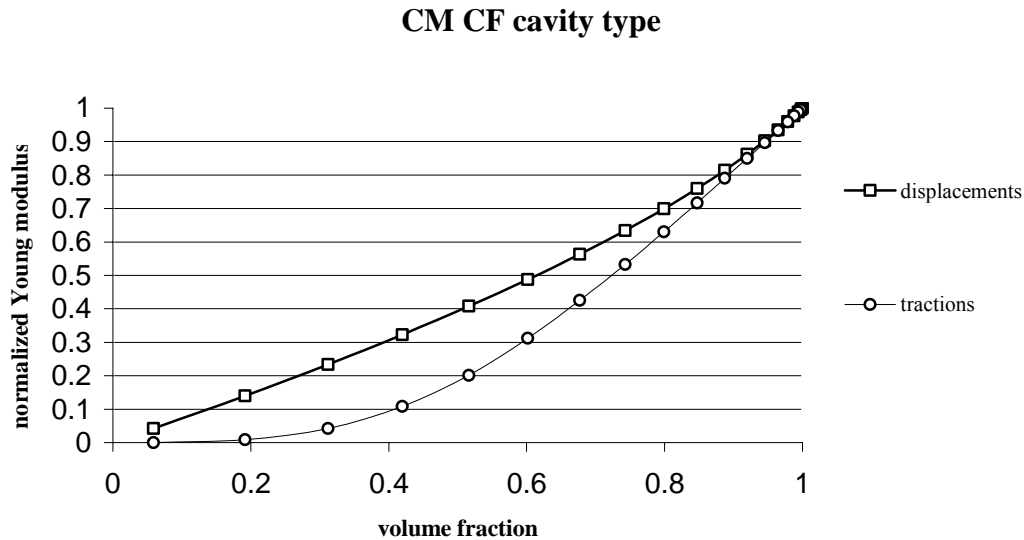
and tractions prescribed tests are performed whether to obtain elastic isotropic characterization or to define cubic constant. Totally 20 finite element porous RVE models are processed under 6 different load cases.

Isotropic constants

Two constants are needed to describe isotropic elastic behaviour for all of the porous RVE cavity types. In the follow E , Young modulus, and K , bulk modulus will be used. For more details refer to Appendix A.2

Young modulus

Isotropic elastic analyses, performed on \square CF CV porous RVE models, show how Young modulus varies within volume fraction graph 4.3. Moduli are normalized by defined value of matrix Young modulus. Graph shows how normalized modulus tends to unit value when matrix volume fraction is close to 1, whereas while volume fraction diminishes results give values gradually lower and lower. According to Voigt and Reuss theory results are greater in displacement tests then tractions prescribed ones.



Graph 4.3. Trend of Young modulus, normalized over matrix value, within volume fraction in case of \square CF CV porous RVE FE calculations (isotropic matrix properties: $E_0 = 17200$ MPa, $\nu_0 = 0.3$). Both displacements applied and tractions prescribed calculation are highlighted.

Figure 4.5 shows FE contour value ranges of results obtained through uniaxial displacement as well as tractions tests performed on \square CF porous RVE model for different volume fractions. Fe results are used in eqs. (7.1) and (7.4), see Appendix A.2, to calculate two Lamé constant that is Young modulus and Poisson ratio, eq. (7.7). To realize a better visualization, results attained to centred on void RVE position, in spite of centred on matrix, are highlighted.

Bulk modulus

RVE model, used in this work, shows a cubic anisotropy, this mean that first diagonal block of its constant elastic matrix coincides with isotropic one, in other word, even if model is not isotropic, bulk modulus density variation depends just by Young modulus and Poisson ratio variation. This evidence is remarked by correspondence between bulk calculations, by means of eq. (7.8), see

Appendix A.2, and tests results of both hydrostatic pressures prescribed and uniform displacement applied type, see figure 4.6, by means of eqs. (7.3) and (7.6), see Appendix A.2. Figure 7 shows FE contour value ranges of results obtained through triaxial displacement as well as idrostatic pressure tests performed on $\square CF$ porous RVE model for different volume fractions. Fe results are used in eqs. (7.3) and (7.6), see Appendix A.2, to calculate bulk modulus. To realize a better visualization, results attained to centred on void RVE position, in spite of centred on matrix, are highlighted.

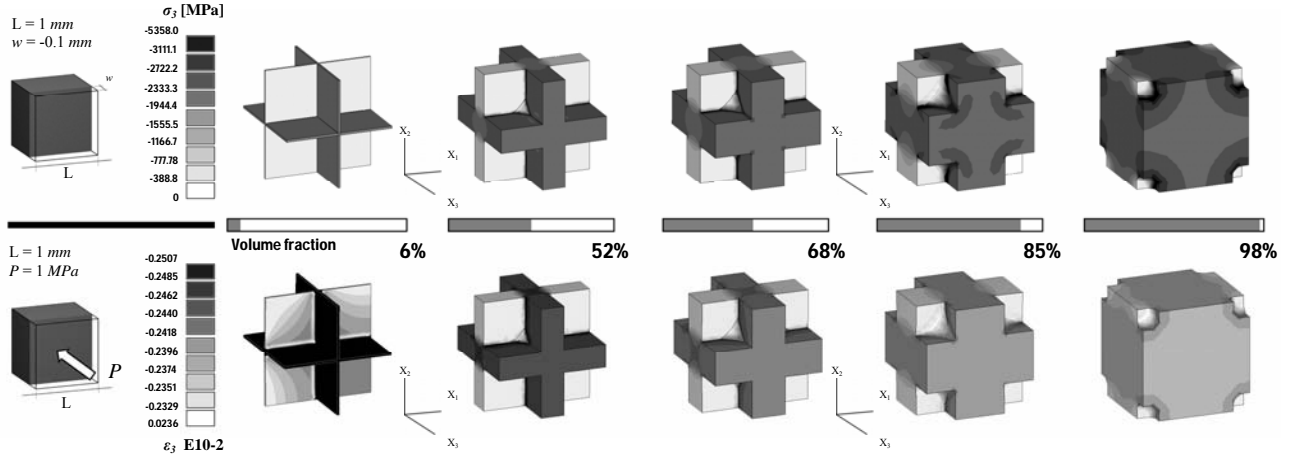


Fig. 4.5. F.E. results on CM RVE FE models trough increasing volume fraction sketches (isotropic matrix properties: $E_0 = 17200$ MPa, $\nu_0 = 0.3$). On top uniaxial displacement tests. On bottom uniaxial tractions tests.

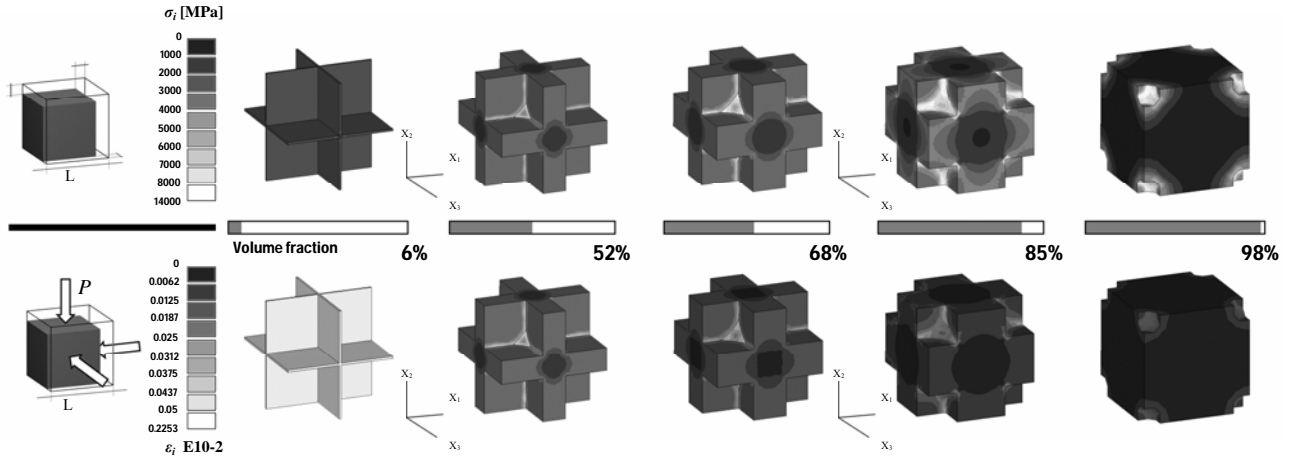


Fig. 4.6. F.E. results on CM RVE FE models trough increasing volume fraction sketches (isotropic matrix properties: $E_0 = 17200$ MPa, $\nu_0 = 0.3$). On top triaxial displacement tests. On bottom idrostatic pressure tests.

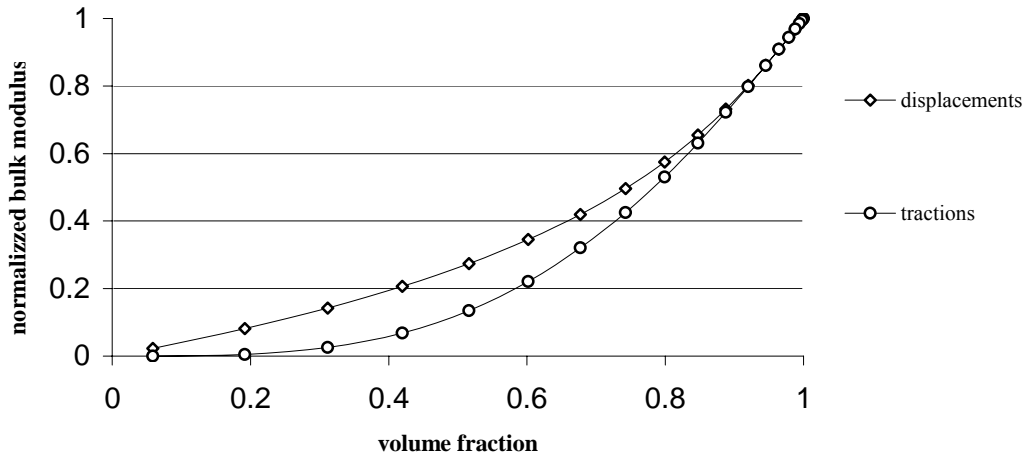
Graph 4.4, shows how normalized modulus tends to unit value when matrix volume fraction is close to 1, whereas while volume fraction diminishes results give values gradually lower and lower. According to Voigt and Reuss theory, results are greater in displacement tests then tractions prescribed ones. Values, as usual, are normalized by corresponding matrix bulk modulus value.

Anisotropic constants

Due to the cubic symmetry of the RVE, more numerical tests has been necessary for estimating the unique anisotropic constant, that is G' , the cubic shear modulus, in a way to completely define RVEs mechanical behaviour. A pure shear prescribed and angular deflection imposed test types are implemented. In both of case, elastic constant dependence by density is obtained trough

relation between homogenized stress and deformation, eqs. (7.2) and (7.5), see Appendix A.2,

CM CF cavity type



Graph 4.4. Trend of bulk modulus, normalized over matrix value, within volume fraction in case of \square CF CV porous RVE FE calculations (isotropic matrix properties: $E_0 = 17200$ MPa, $\nu_0 = 0.3$). Both displacements applied and tractions prescribed

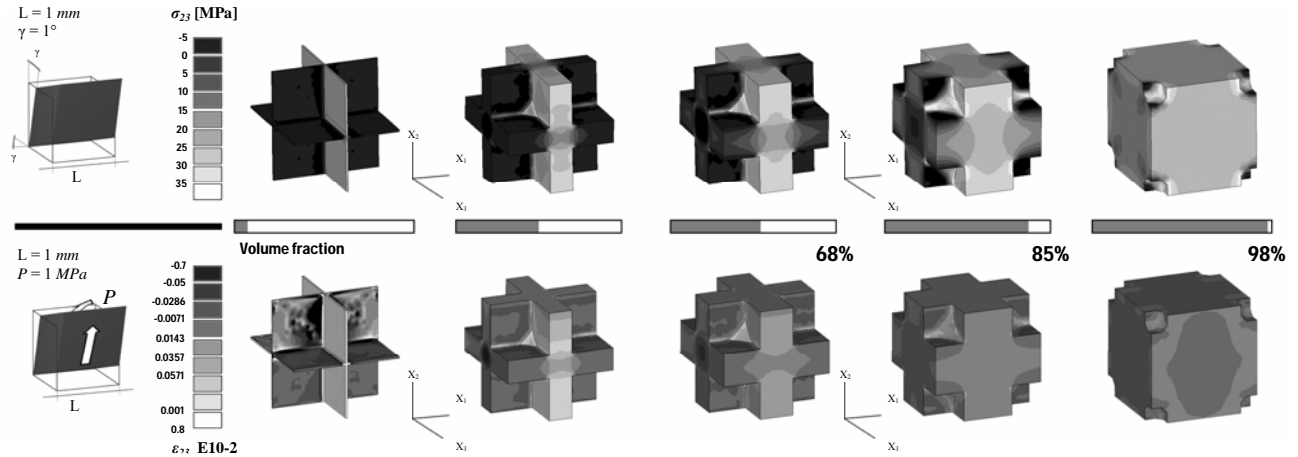
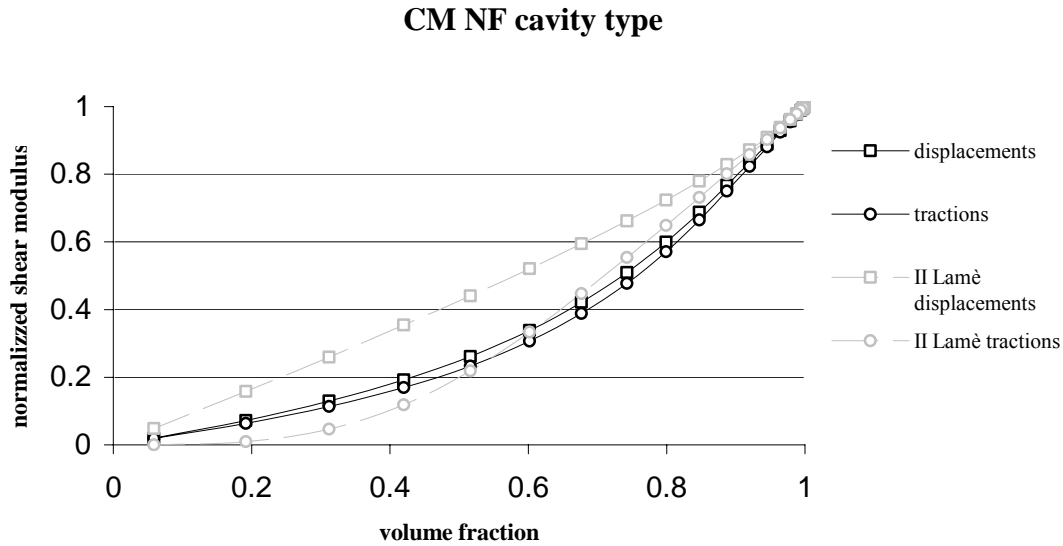


Fig. 8. F.E. results on CM RVE FE models through increasing volume fraction sketches (isotropic matrix properties: $E_0 = 17200$ MPa, $\nu_0 = 0.3$). On top angular displacement tests. On bottom shear tests.

Anisotropic shear modulus

For this cavity type model, \square CF CV porous RVE, numerical tests aim to obtain shear modulus density variation. Analyses show no great difference between tractions prescribed and displacement applied ones, graph 4.5. However, in both of case, normalized modulus rises with density from zero value to one. Values are normalized by correspond matrix one. In graph 4.5 is even represent second Lamé constant variation, normalized by its matrix value, and in case of displacement applied and tractions prescribed tests. As second Lamé constant and shear modulus coincide in case of isotropy, curve distance highlight model anisotropic order by density. Note that Voigt and Reuss evaluations bound a region of values where effective normalized II Lamé curve is defined as well as for normalized shear modulus one, thus, intersection between this regions do not means curves intersection. On the contrary, by isotropy of porous RVE in case of

matrix volume fraction equal to unit and close to zero, is to suppose that effective curve of II Lamé constant keep higher than displacement shear modulus for every value of volume fraction.



Graph 4.5. Trend of shear modulus, normalized over matrix value, within volume fraction in case of \square CF CV porous RVE FE calculations (isotropic matrix properties: $E_0 = 17200$ MPa, $\nu_0 = 0.3$). Trend of II Lamé constant, normalized over matrix value, is even shown. Both displacements applied and tractions prescribed calculation are highlighted

Figure 8 shows FE contour value ranges of results obtained through angular displacement as well as shear tests performed on \square CF porous RVE model for different volume fractions. Fe results are used in eq. (7.2), see Appendix A.2 to calculate cubic shear modulus. To realize a better visualization, results attained to centred on void RVE position, in spite of centred on matrix, are highlighted.

2.1.f. Cavity's shape influence

Numerical mechanical tests are performed on porous RVEs typified by three different cavity shapes, varying in the range of quite all density spectrum, in way to obtain a density function of all the homogenized elastic characteristics of porous RVEs. Isotropic elastic behaviour of matrix is defined by $E_0 = 17200$ MPa and $\nu_0 = 0.3$. Two of the three porous RVEs model types show a cavity geometry realized by spheres, one is a single centred sphere cavity, (\square SC), the other is a polar symmetric eight sphere union, (\square 8S), sec. IV.2.1.d, in both of case symmetry gives isotropic models, that is two constant only are needed to define elastic homogenized RVE properties. The third model cavity type is a seven centred polar symmetric ellipsoids, (\square 7E), see sec. 3.4, it results in a cubic symmetric RVE. Thus, to define its elastic behaviour, one more constant is needed.

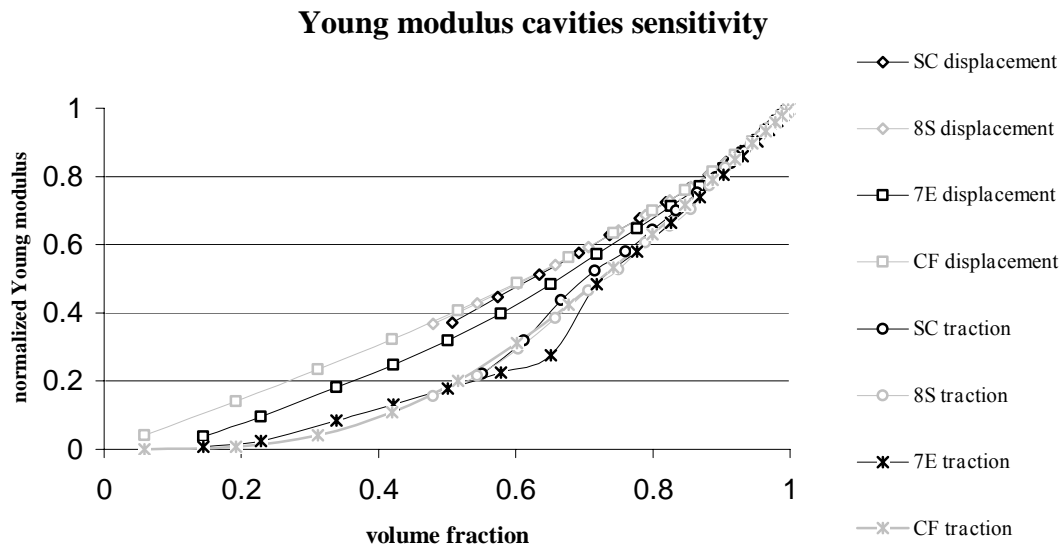
Each model is tested both under uniform tractions and uniform displacement normal to a face of the RVE cubic cell, i.e. uniaxial tests. Moreover, cubic symmetric RVE models are even tested both under pure share uniform tractions and angular deflection in a plane parallel to a RVE face. These tests are aimed to obtain the relation between average stresses and average deformations in way to define homogenized elastic properties of the porous RVE, following same procedure used above, see sec. A.1, A.2.

Each of three cavity types models are tested in the available volume fraction range by 20 analyses per type. Both displacement imposed and tractions prescribed tests are performed whether to

obtain elastic isotropic characterization or to define cubic constant. Totally 60 finite element porous RVE models are processed under 6 different load cases. All this data set is compared to one obtained through *CF* cavity centred on void RVE models tests in way to estimate cavity shape influence on elastic constants density trend.

Young modulus

Isotropic elastic analyses show how Young modulus varies within volume fraction for every cavity types, graph 4.6. Moduli are normalized by constant value of matrix Young modulus. Graphs show how normalized moduli tend to unit value when matrix volume fraction is close to 1, whereas while volume fraction diminishes results give values gradually lower and lower. This trend remain quite the same both for displacement and tractions prescribed tests, in graph 4.6 difference between this two calculation methods is highlighted; results, according to Voigt and Reuss theory, set tractions defined Young modulus always lower than displacement one. Different cavity types density range not allows comparing elastic behaviours on total span density value. However not relevant differences in Young modulus density function are detected both in displacement and tractions prescribed tests throughout different cavity shapes, graph 4.6.



Graph 4.6. Trend of Young modulus, normalized over matrix value, within volume fraction for every processed porous RVE cavity type FE calculations (isotropic matrix properties: $E_0 = 17200$ MPa, $\nu_0 = 0.3$). Both displacements applied and tractions prescribed calculation are highlighted

Bulk modulus

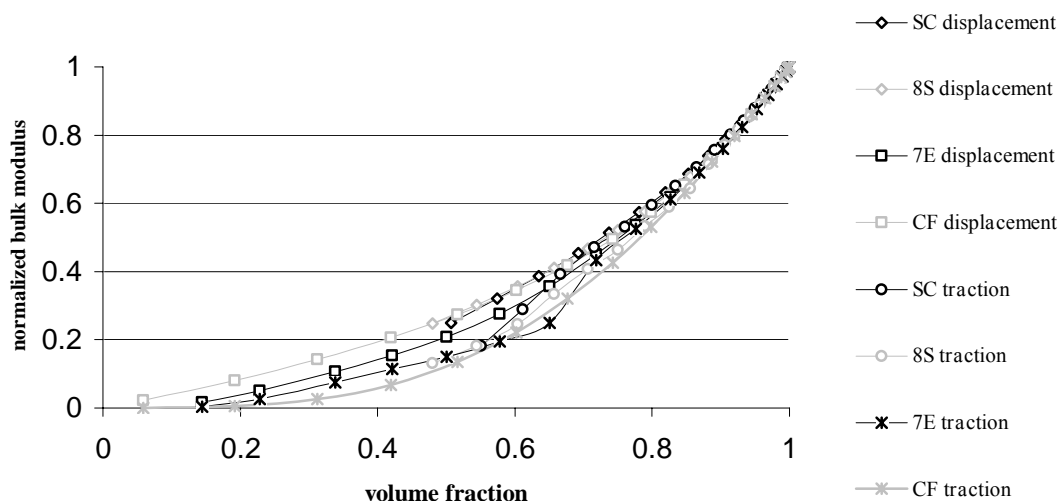
Same graphic comparison is performed to evaluate bulk modulus density varying shape sensitivity. Moduli are normalized by constant value of matrix bulk modulus. In graph 4.7 a regular trend is highlighted, where displacement applied tests values are greater than tractions prescribed ones. In both of case results are similar for every cavity types, and as density decreases values go from unity to zero.

Anisotropic shear modulus

Shape sensitivity valuation, is finally realized on anisotropic shear modulus density variation. In case of isotropic RVE models shear modulus and second Lamé constant agree. Same remark

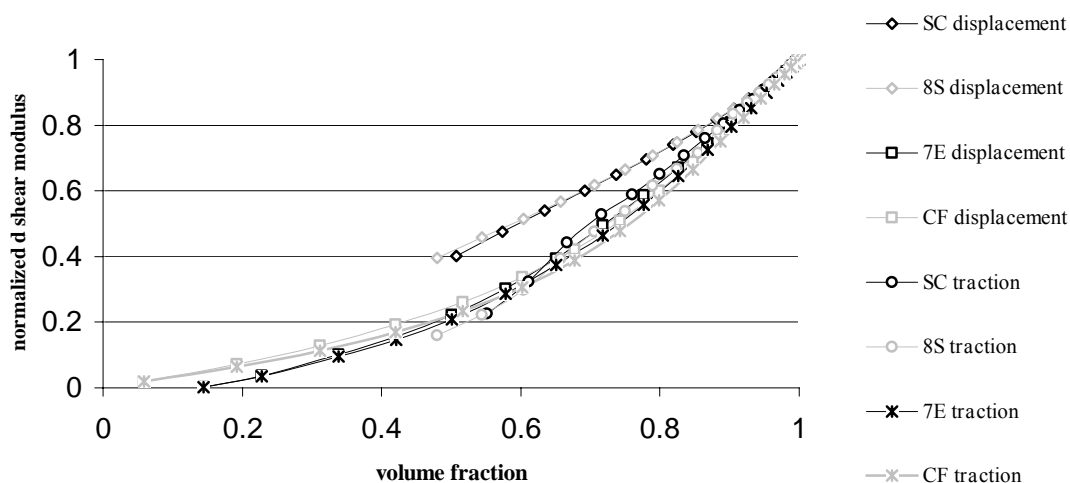
made in case of Young and bulk modulus can be used, graph. 4.8.

Bulk modulus cavities sensitivity



Graph 4.7. Trend of bulk modulus, normalized over matrix value, within volume fraction for every processed porous RVE cavity type FE calculations (isotropic matrix properties: $E_0 = 17200$ MPa, $\nu_0 = 0.3$). Both displacements applied and tractions prescribed calculation are highlighted

Shear modulus cavities sensitivity



Graph 4.8. Trend of shear modulus, normalized over matrix value, within volume fraction for every processed porous RVE cavity type FE calculations (isotropic matrix properties: $E_0 = 17200$ MPa, $\nu_0 = 0.3$). Both displacements applied and tractions prescribed calculation are highlighted

2.1.g. Algebraic formulation

Theory of elastic behaviour of solid containing a dilute distribution of microcracks, Nemat-Nasser (1983), provides a useful self-consistent evaluation of density moduli variation valid in a volume fraction range close to unit. Otherwise, Flugge bases his theory of elastic solid on a model realized through three dimensional orthogonal shell arrangement. This theory gives some equations, restricted to matrix volume fraction close to zero, to define elastic constant in every

isotropic porous material. Generally, in case of isotropic material, porous Young modulus normalized over matrix value can deduced as follow:

$$\frac{E}{E_0} = \begin{cases} \varphi_E(\gamma) & \gamma \rightarrow 0 \\ \eta_E(\gamma) & \gamma \rightarrow 1 \end{cases} \quad (4.1),$$

where E_0 is reference matrix Young modulus and γ is the matrix volumetric fraction, $\varphi_E(\gamma)$ and $\eta_E(\gamma)$ functions are exposed in table 4.1, is worth to note that both of them are related to matrix Poisson ratio ν_0 .

Theories based on dilute and Flugge models give also a density law to porous bulk modulus normalized over matrix value, in case of isotropic material. Such law it can deduce as follow:

$$\frac{K}{K_0} = \begin{cases} \varphi_K(\gamma) & \gamma \rightarrow 0 \\ \eta_K(\gamma) & \gamma \rightarrow 1 \end{cases} \quad (4.2),$$

where E_0 is reference matrix Young modulus and γ is the matrix volumetric fraction, $\varphi_K(\gamma)$ and $\eta_K(\gamma)$ functions are exposed in table 4.1, is worth to note that, even in this case, both of them are related to matrix Poisson ratio ν_0 .

Both laws (4.1) and (4.2) are valid just at the end of range of volume fraction. Such equations provide to draw overall elastic behaviour of porous isotropic material for matrix volume fraction close to unit and close to zero. Starting from these theories, a single density law can be deduced for every isotropic elastic constant. Equations (4.1) furnish four algebraic conditions, thus a third polynomial regression $\chi_E(\gamma)$ is used to approximate porous Young modulus density variation.

Four polynomial constants are deduced by following condition:

$$\begin{aligned} \chi_E(0) &= \varphi_E(0), & \frac{\partial \chi_E}{\partial \gamma}(0) &= \frac{\partial \varphi_E}{\partial \gamma}(0) \quad \text{by (4.1),} \\ \chi_E(1) &= \eta_E(1), & \frac{\partial \chi_E}{\partial \gamma}(1) &= \frac{\partial \eta_E}{\partial \gamma}(1) \quad \text{by (4.1).} \end{aligned}$$

This density function $\chi_E(\gamma)$ is consistent with theories above and is defined over all volume fraction range, it is defined as:

$$\chi_E(\gamma) = A_E + B_E \cdot \gamma + C_E \cdot \gamma^2 + D_E \cdot \gamma^3 \quad \gamma \in [0,1] \quad (4.3),$$

where A_E, B_E, C_E, D_E are polynomial constants, whose values area shown in table 4.1, constants depend on matrix mechanical behaviour.

That is porous Young modulus density variation, approximated to a third polynomial regression, in an isotropic material, is defined just through matrix isotropic elastic behaviour.

Due to basic theories restriction equation (4.3) is valid for porous material with isotropic matrix elastic behaviour and deduced values follow displacement calculation.

Through four algebraic condition deduced by equation (4.2), a third polynomial regression $\chi_K(\gamma)$ can be used to approximate porous bulk modulus density variation.

	Normalized Young modulus	Normalized bulk modulus
Flugge	$\varphi_E(\gamma) = \frac{2}{3} \cdot \frac{\nu_0 - 2}{\nu_0^2 + \nu_0 - 2} \cdot \gamma$	$\varphi_K(\gamma) = \frac{2}{3} \cdot \frac{1 - 2\nu_0}{1 - \nu_0} \cdot \gamma$
Dilute	$\eta_E(\gamma) = \frac{(8 + 15\gamma \cdot (1 - \nu_0) - 10\nu_0) \cdot (1 + 3\gamma \cdot (-1 + \nu_0) + \nu_0)}{10 + 6\gamma \cdot (-1 + \nu_0) \cdot (4 + \nu_0 \cdot (-6 + 5\nu_0)) - 2\nu_0 \cdot (11 + \nu_0 \cdot (-23 + 15\nu_0))}$	$\eta_K(\gamma) = \frac{1 + 3\gamma \cdot (1 - \nu_0) + \nu_0}{-2 + 4\nu_0}$
Polynomial constants	$A_E = 0$	$A_K = 0$
	$B_E = \frac{2(-1 + 2\nu_0)}{3(-2 + \nu_0 + \nu_0^2)}$	$B_K = \frac{2(-1 + 2\nu_0)}{3(-1 + \nu_0)}$
	$C_E = -\frac{22 + 17\nu_0 - 59\nu_0^2 - 9\nu_0^3 + 45\nu_0^4}{6(-7 + 5\nu_0) \cdot (-2 + \nu_0 + \nu_0^2)}$	$C_K = -\frac{-1 + 4\nu_0 + 5\nu_0^2}{6(-1 + \nu_0) \cdot (-1 + 2\nu_0)}$
	$D_E = -\frac{-50 + 17\nu_0 - 91\nu_0^2 - 21\nu_0^3 - 45\nu_0^4}{6(14 - 17\nu_0 - 2\nu_0^2 + 5\nu_0^3)}$	$D_K = -\frac{-1 - 2\nu_0 - \nu_0^2}{6(1 - 3\nu_0 + 2\nu_0^2)}$

Table 4.1. Porous material theories laws on overall mechanical behaviour, on top; polynomial approximation constants, on bottom.

To draw a whole density range porous bulk modulus function, four polynomial constant are deduced by following condition:

$$\begin{aligned} \chi_K(0) &= \varphi_K(0), & \frac{\partial \chi_K}{\partial \gamma}(0) &= \frac{\partial \varphi_K}{\partial \gamma}(0) \quad \text{by (4.2),} \\ \chi_K(1) &= \eta_K(1), & \frac{\partial \chi_K}{\partial \gamma}(1) &= \frac{\partial \eta_K}{\partial \gamma}(1) \quad \text{by (4.2).} \end{aligned}$$

This density function $\chi_K(\gamma)$ is consistent with theories above and is defined over all volume fraction range, it is defined as:

$$\chi_K(\gamma) = A_K + B_K \cdot \gamma + C_K \cdot \gamma^2 + D_K \cdot \gamma^3 \quad \gamma \in [0, 1] \quad (4.4),$$

where A_K, B_K, C_K, D_K are polynomial constants, whose values area shown in table 4.1, constants depend on matrix mechanical behaviour.

That is porous bulk modulus density variation, approximated to a third polynomial regression, in an isotropic material, is defined just through matrix elastic behaviour.

Owed to basic theories restriction equation (4.4) is valid for porous material with isotropic matrix elastic behaviour and deduced values follow displacement calculation. Moreover, due to bulk modulus sensitivity to Poisson ratio, eq. (7.8), see Appendix A.2.3, restriction has to be made: as

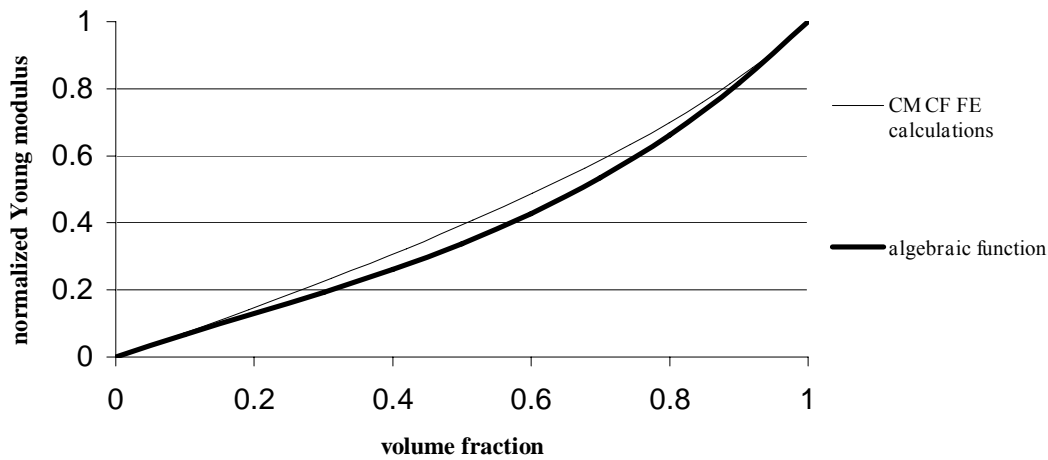
matrix material behaviour tends to uncompressible, i.e. $\nu_0 \rightarrow \frac{1}{2}$, bulk modulus diverges, in this case third polynomial approximation do not seems to match well, as shown in the next. Then

equation (4.4) is to intend for Poisson ratio defined in a range $[-1, \frac{1}{3}]$, in spite of this restriction,

it remains valid for almost all natural material.

This procedure allows to unify dilute and Flugge theories on isotropic porous material, in a way to draw an algebraic density law variation of normalized Young modulus and normalized bulk modulus, as all related isotropic elastic constant. FE tests results exposed above, sec. IV.2.1.e, are obtained for matrix Poisson ratio equal to 0.3, so comparison between FE displacement applied tests on \square CF porous RVE and such calculation can evaluates quality of algebraic approximations. To realize it, graphs 4.9 and 4.10 show how CF centred on void RVE Young and bulk moduli density functions match respective algebraic density functions, such relations are obtained using same matrix elastic properties used in FE displacement applied calculations, $E_0 = 17200 \text{ MPa}$ and $\nu_0 = 0.3$. Note that just displacement FE calculations are plotted, as algebraic functions are implemented on theories based on displacement evaluations.

algebraic validation



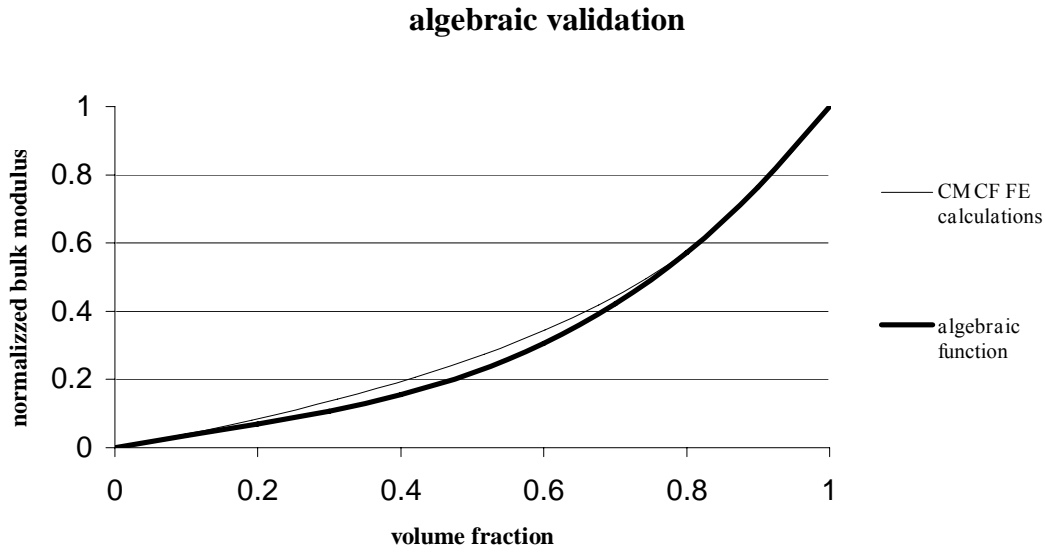
Graph 4.9. Algebraic Young modulus density function, normalized over matrix value. Normalized Young modulus variation within volume fraction in case of \square CF CV porous RVE FE calculations are even plotted as comparison (isotropic matrix properties: $E_0 = 17200 \text{ MPa}$, $\nu_0 = 0.3$).

Exponential Law Reduction

Usually in literature, is possible to find relation between elastic constant and volume fraction for porous media in exponential law form, Rho (1995), Zysset (1995). The simplest formula describes Young modulus penalization as a density law for a single phase material is:

$$\phi = \frac{E}{E_0} = \gamma^k \quad (4.5),$$

where E_0 is reference matrix Young modulus, γ is the matrix volumetric fraction and k is a constant.



Graph 4.10. Algebraic bulk modulus density function, normalized over matrix value. Normalized bulk modulus variation within volume fraction in case of \square CF CV porous RVE FE calculations are even plotted as comparison (isotropic matrix properties: $E_0 = 17200$ MPa, $\nu_0 = 0.3$).

The value of exponential constant k that best fit the third polynomial penalization law (4.3) is deduced by the meanings of minimization of the sum of the squared difference between the law (4.3) and (4.5) and their derivatives:

$$k = \text{Minimum} \left[\sqrt{\int_0^1 \frac{|\chi^2 - \phi^2|}{\chi^2} d\rho} - \sqrt{\int_0^1 \left| \frac{\partial \chi^2}{\partial \rho} - \frac{\partial \phi^2}{\partial \rho} \right| \frac{\partial \chi^2}{\partial \rho} d\rho} \right] = 1.37924 \quad (4.6),$$

the value found refers to lower local minimum, polynomial regression (4.3) and exponential law (4.5) for value of k above are plotted together in the graph 4.11.

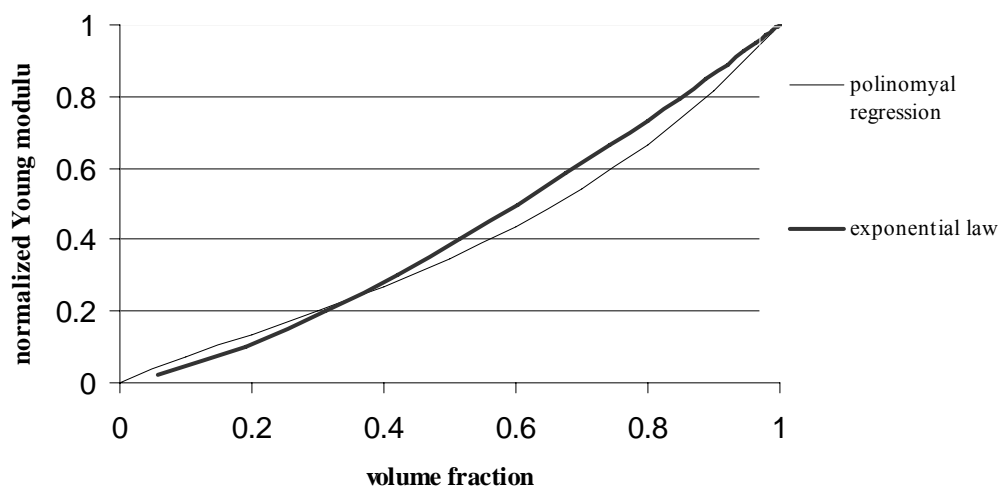
Poisson Ratio Sensitivity

Algebraic equation shown above, (4.3) and (4.4), permit to define overall mechanical behaviour starting from matrix material properties. Normalized over matrix porous Young modulus calculation depends on matrix Poisson ratio, as coefficients in table 4.1 shown. Such calculation has a low sensibility to Poisson ratio variation, as well as FE Young modulus density variation. In graph 4.12, equation (4.3) is plotted for different value of Poisson ratio varying in the range

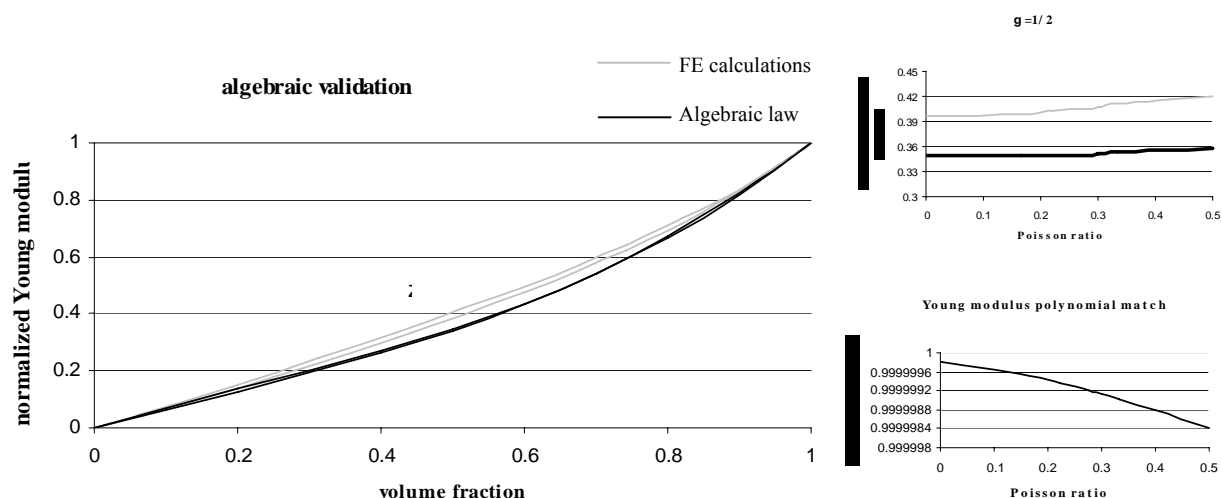
$]0, \frac{1}{2}[$, and relative FE displacement applied normalized Young modulus calculations is

compared. Poisson ratio range restriction is due to usually FE program conditions. By evidence Young modulus algebraic calculation resulting matching well FE tests in whole Poisson ratio range. To confirm such good agreement the square main root Poisson ratio variation is even shown.

algebraic comparison



Graph 4.11. Algebraic bulk modulus density function, normalized over matrix value. Normalized bulk modulus variation within volume fraction in case of \square CF CV porous RVE FE calculations are even plotted as comparison (isotropic matrix properties: $E_0 = 17200$ MPa, $\nu_0 = 0.3$).

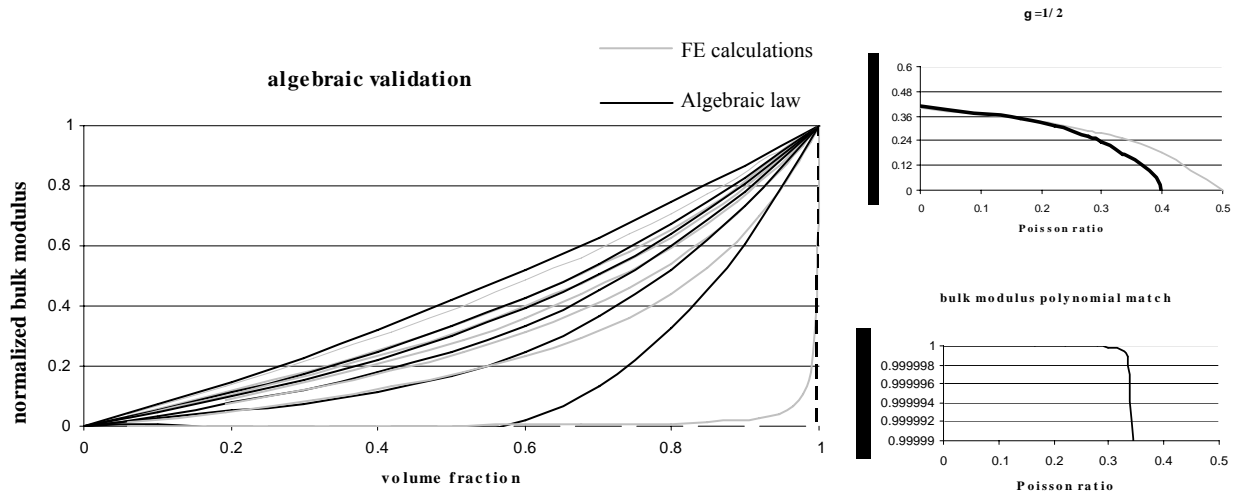


Graph 4.12. Algebraic Young modulus density function, normalized over matrix value, varying with Poisson ratio. Relative normalized Young modulus variation within volume fraction in case of \square CF CV porous RVE FE calculations are even plotted as comparison (isotropic matrix properties: $E_0 = 17200$ MPa, $\nu_0 \in]0, \frac{1}{2}[$). On the upper left curves for Poisson ratio equal to $\frac{1}{2}$, on the bottom left approximation level varying Poisson ratio.

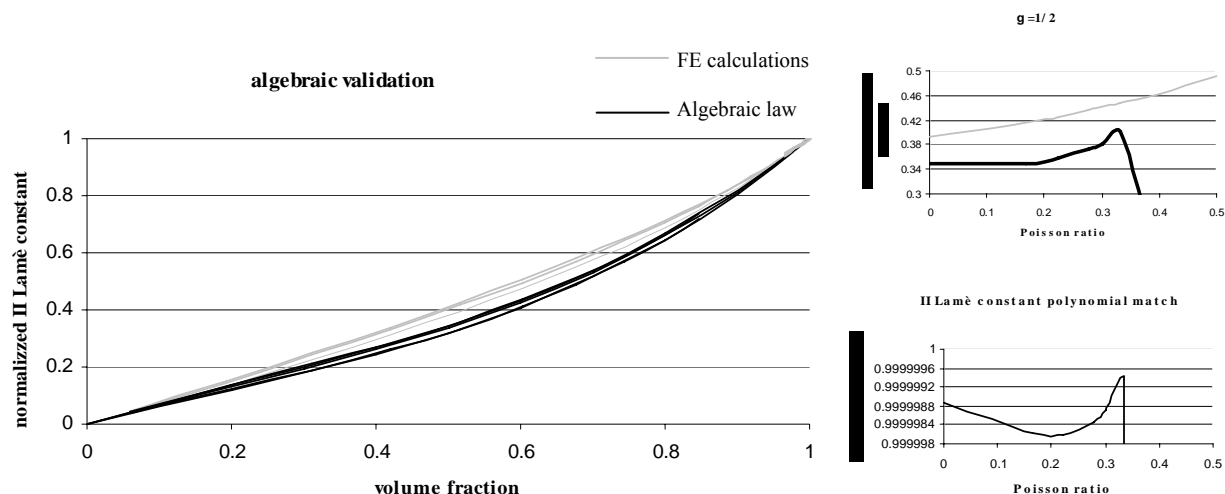
Normalized over matrix porous bulk modulus calculation even depends on matrix Poisson ratio, as coefficients in table 4.1 shown, but different considerations are to be made. As anticipated, in isotropic material, bulk modulus value shows divergence as Poisson ratio tends to 0.5, that is behaviour of incompressible material, this means a sensibility to Poisson ratio higher and higher as Poisson ratio get closer to 0.5, this results in a global softer behaviour while Poisson ratio increase. In graph 4.12, equation (4.4) is plotted for different value of Poisson ratio varying in the range of $]0, \frac{1}{2}[$, relative FE displacement applied normalized bulk modulus calculations are

even shown. By evidence bulk modulus algebraic calculation resulting matching well FE tests in Poisson ratio range of $]0, \frac{1}{3}]$, is worth to note that algebraic law differ more and more as matrix behaviour tends to uncompressible, to confirm Poisson ratio law restriction. Even in this case the square main root Poisson ratio variation is also shown. Such relations are plotted in graph 4.13 even for isotropic shear modulus, i.e. II Lamé constant. As in case of bulk modulus, algebraic third polynomial approximation is defined in Poisson ratio range of $] -1, \frac{1}{3}]$, for higher values law shows divergences and does not match FE analyses. Numerical calculations are performed using $\nu_0 \in]0, \frac{1}{2}[$, in this way isotropic shear modulus approximation law shows good agreement just for Poisson ration in the range $]0, \frac{1}{3}]$.

In conclusion, in this chapter, overall mechanical behaviour of porous media RVE has investigated, trend of isotropic elastic constants related to density variation in the range $[0, 1]$ has researched. Finite elements mechanical tests were performed using different types of cavities varying in size to allow density variation. Algebraic laws are used to describe constants penalization. Starting from algebraic solutions in case of strictly high and strictly low porosity a third polynomial regression, as unique algebraic law, has traced for each isotropic elastic constant (4.3) and (4.4), coefficients are shown in table 4.1 for normalized Young and bulk modulus. Approximation laws depends on mechanical behaviour of matrix, and match well FE calculations for Poisson range of $]0, \frac{1}{3}]$, for every density values.



Graph 4.13. Algebraic bulk modulus density function, normalized over matrix value, varying with Poisson ratio. Relative normalized bulk modulus variation within volume fraction in case of \square CF CV porous RVE FE calculations are even plotted as comparison (isotropic matrix properties: $E_0 = 17200$ MPa, $\nu_0 \in]0, \frac{1}{2}[$). On the upper left curves for Poisson ratio equal to $\frac{1}{2}$, on the bottom left approximation level varying Poisson ratio.



Graph 13. Algebraic II Lamé constant density function, normalized over matrix value, varying with Poisson ratio. Relative normalized isotropic shear modulus variation within volume fraction in case of \square CF CV porous RVE FE calculations are even plotted as comparison (isotropic matrix properties: $E_0 = 17200$ MPa, $\nu_0 \in]0, \frac{1}{2}[$). On the upper left curves for Poisson ratio equal to $\frac{1}{2}$, on the bottom left approximation level varying Poisson ratio.

CHAPTER V

ORTHOTROPIC POROUS MEDIA

1. Micromechanical Approach to Inhomogeneous and Anisotropic Materials

Advances in soil mechanics, tissue engineering, biomechanics, composites, porous and granular media and micro/nano-structured materials have motivated a significant and growing interest in the analysis of heterogeneous solids that often exhibit inhomogeneous and anisotropic mechanical features. As a consequence, recently, homogenization techniques and micro-mechanical approaches are widely presented in Literature, making reference to the *volume fraction* – as stereological measure of the inhomogeneities (voids, fraction of constituents in composites, isotropic damage variables) – and to second-order (or higher) *Fabric Tensors*, in order to take into account void (or matrix) orientations revealed at the micro-structure level of a selected Representative Volume Element material, with the aim of estimating its overall mechanical anisotropy.

Despite the use of Fabric Tensor approaches constitutes the sole mechanically consistent and effective way for determining the influence of RVE material microstructure in many engineering problems, several disadvantages and difficulties limit the actual use of this strategy and inhibit its implementation some fields, such as design of new materials or prediction of biological tissue remodelling phenomena.

In particular, the above mentioned disadvantages can be identified in two classes. The first one collects several aspects, say of practical order, related to the difficulty of estimating the quantities characterizing the Fabric point-by-point for a prescribed heterogeneous media, also if it presents periodical microstructure. Indeed – for example in a porous material – without considering the volume fraction, at least three second-order Fabric Tensor eigenvalues and the corresponding three eigenvectors (or equivalently principal axis Euler angles) have to be carried out for a selected RVE. This number significantly grows if the solid under analysis shows a not periodical structure.

Also, being the Fabric classically deduced by first constructing the Mean Intercept Length (MIL), the final interpolation of the density *rose diagrams* with an ellipse (or ellipsoid in 3D cases) requires other computational efforts and – at the authors knowledge – no automatic software or standard protocols exist in Literature for ensuring that two distinct operators obtain the same results.

The second class of disadvantages in the use of Fabric Tensor approaches can be traceable in order to the theoretical assessment of the method. Indeed, the following problems are still open issues: 1) the rational and geometrically consistent definition – for example in porous materials – of (RVE matrix or void) *orientation*; 2) the proof that the MIL, as well as other minor techniques, are actually able to trace anisotropy of a RVE with any oriented microstructure; 3) the possibility of obtaining closed-form elastic solutions for anisotropic materials from which to derive corresponding elastic moduli matching the Fabric Tensor-based ones; 4) the definition of a Fabric Tensor able to be frame-indifferent in cases of periodical media, that is measures of the anisotropy which do not depend on the choice of RVE “window” when the periodicity of the solid would allow to select any RVE box.

1.1 Second Order Fabric Tensor

A wide number of theoretical models were proposed in the literature to describe relationships between anisotropic porosity and elasticity. Some of them – for both isotropic and anisotropic materials – are briefly recalled in a review paper by Zysset (1995).

In particular, for orthotropic materials, a general approach was proposed by Cowin (1985) using a second-order positive definite fabric tensor. Starting from the notion that the matrix material of the porous elastic solid is isotropic and that the anisotropy of the porous elastic solid itself is only due to the geometry of microstructure represented by the fabric tensor, the stress tensor is assumed to be an isotropic function of the strain tensor and the fabric tensors as well as the volume fraction. Thus, based on this mathematical statement, expressions for the elastic constants in terms of invariants of the fabric tensor are developed as

$$\begin{aligned}
 C_{ijkh} = & a_1 \delta_{ij} \delta_{hk} + a_2 (M_{ij} \delta_{ij} + M_{hk} \delta_{hk}) + a_3 (\delta_{ij} M_{hq} M_{qk} + \delta_{hk} M_{iq} M_{qj}) + \\
 & + b_1 A_{ij} A_{hk} + b_2 (M_{ij} M_{hq} M_{qk} + M_{is} M_{sj} M_{hk}) + b_3 M_{is} M_{sj} M_{hq} M_{qk} + \\
 & + c_1 (\delta_{hi} \delta_{kj} + \delta_{ki} \delta_{hj}) + c_2 (M_{ih} \delta_{kj} + M_{hj} \delta_{ki} + M_{ik} \delta_{hj} + M_{kj} \delta_{hi}) + \\
 & + c_3 (M_{ir} M_{rh} \delta_{kj} + M_{rj} M_{hr} \delta_{ki} + M_{ir} M_{rk} \delta_{hj} + M_{kr} M_{rj} \delta_{ih})
 \end{aligned} \quad (0.1)$$

where M_{ij} denote the components of the fabric tensor while $a_1, a_2, a_3, b_1, b_2, b_3, c_1, c_2$ and c_3 are functions of γ and $Tr\mathbf{M}$, $Tr\mathbf{M}^2$ and $Tr\mathbf{M}^3$.

It is also shown that the representation (5.1) for the fourth rank elasticity tensor may represent at least the orthotropy and the material symmetry is governed by the fabric tensor. In fact, expanding (5.1) in indicial notation in the coordinate system that diagonalized the fabric tensor ($M_{12} = M_{13} = M_{23} = 0$), only nine components of the elastic tensor are non-zero and are function of the nine coefficient $a_1, a_2, a_3, b_1, b_2, b_3, c_1, c_2, c_3$ and of the three eigenvalues of \mathbf{M} , M_{11}, M_{22} and M_{33} .

Moreover, by setting $M_{22} = M_{33}$, it is shown that the corresponding material symmetry is the transverse isotropy, being only five elastic constant independent. In the same way, when the eigenvalues of \mathbf{M} are all equal ($M_{11} = M_{22} = M_{33}$) the corresponding material symmetry is the isotropy.

Using this approach, more specific models were derived by Turner and Cowin (1987) to uncouple the effects of volume fraction and fabric and by Zysset and Curnier, Zysset (1995), to ensure positive definiteness of the elasticity tensor a priori.

In particular, Turner and Cowin (1987) proposed a model where the fabric data are normalized with $Tr\mathbf{M} = I$. By using the decomposition of the fabric tensor

$\mathbf{M} = \sum_{i=1}^3 m_i \mathbf{M}_i = \sum_{i=1}^3 m_i (\mathbf{m}_i \otimes \mathbf{m}_i)$, where m_i are strictly positive eigenvalues and \mathbf{m}_i the normalized eigenvectors, the compliance and stiffness tensor are

$$\mathbb{D}(\gamma, \mathbf{M}) = \sum_{i=1}^3 \frac{1}{\varepsilon_i(\gamma, m_i)} \mathbf{M}_i \otimes \mathbf{M}_i - \sum_{\substack{i,j=1 \\ i \neq j}}^3 \frac{\nu_{ij}(\gamma, m_i, m_j)}{\varepsilon_i(\gamma, m_i)} \mathbf{M}_i \otimes \mathbf{M}_j + \sum_{\substack{i,j=1 \\ i \neq j}}^3 \frac{1}{2\mu_{ij}(\gamma, m_i, m_j)} \mathbf{M}_i \bar{\otimes} \mathbf{M}_j \quad (0.2)$$

$$\mathbb{C}(\gamma, \mathbf{M}) = \sum_{i=1}^3 \lambda_{ii}(\gamma, m_i) \mathbf{M}_i \otimes \mathbf{M}_i + \sum_{\substack{i,j=1 \\ i \neq j}}^3 \lambda_{ij}(\gamma, m_i, m_j) \mathbf{M}_i \otimes \mathbf{M}_j + \sum_{\substack{i,j=1 \\ i \neq j}}^3 2\mu_{ij}(\gamma, m_i, m_j) \mathbf{M}_i \bar{\otimes} \mathbf{M}_j \quad (0.3)$$

where the constants are expanded in polynomial series of the volume fraction and the fabric eigenvalues up to the order two:

$$\begin{aligned}
\frac{I}{\varepsilon_i(\gamma, m_i)} &= k_1'(\gamma) + 2k_6'(\gamma) + (k_2'(\gamma) + 2k_7'(\gamma))II + 2(k_3'(\gamma) + 2k_8'(\gamma))m_i + (2k_4'(\gamma) + k_5'(\gamma) + 4k_9'(\gamma))m_i^2, \\
-\frac{v_{ij}(\gamma, m_i, m_j)}{\varepsilon_i(\gamma, m_i)} &= k_1'(\gamma) + k_2'(\gamma)II + k_3'(\gamma)(m_i + m_j) + k_4'(m_i^2 + m_j^2) + k_5'(\gamma)m_im_j, \\
\frac{I}{2\mu_{ij}(\gamma, m_i, m_j)} &= 2k_6'(\gamma) + 2k_7'(\gamma)II + 2k_8'(\gamma)(m_i + m_j) + 2k_9'(m_i^2 + m_j^2), \quad i, j = 1, 2, 3, \quad i \neq j, \\
II &= m_2m_3 + m_3m_1 + m_1m_2, \\
k_i'(\gamma) &= k_{i1}' + k_{i2}'\gamma^{-2}
\end{aligned} \tag{0.4}$$

and

$$\begin{aligned}
\lambda_{ii}(\gamma, m_i) &= k_1(\gamma) + 2k_6(\gamma) + (k_2(\gamma) + 2k_7(\gamma))II + 2(k_3(\gamma) + 2k_8(\gamma))m_i + (2k_4(\gamma) + k_5(\gamma) + 4k_9(\gamma))m_i^2, \\
\lambda_{ij} &= k_1(\gamma) + k_2(\gamma)II + k_3(\gamma)(m_i + m_j) + k_4(m_i^2 + m_j^2) + k_5(\gamma)m_im_j, \\
2\mu_{ij} &= 2k_6(\gamma) + 2k_7(\gamma)II + 2k_8(\gamma)(m_i + m_j) + 2k_9(m_i^2 + m_j^2), \quad i, j = 1, 2, 3, \quad i \neq j, \\
II &= m_2m_3 + m_3m_1 + m_1m_2, \\
k_i(\gamma) &= k_{i1} + k_{i2}\gamma^{-2}.
\end{aligned} \tag{0.5}$$

The positive definiteness conditions of these compliance and stiffness tensors depend on the volume fraction and fabric and cannot be expressed in terms of the parameters of the model.

Zysset and Curnier, Zysset (1995), proposed a general approach analogous to Cowin's one but their fabric data are normalized with $Tr\mathbf{M} = 0$. By assuming that the elastic free energy is an isotropic function of strain tensor and fabric tensor, they derived the associated elasticity as function of both the volume fraction and the invariants of the fabric noticing that the resulting material symmetry is restricted to orthotropy that may degenerate into transverse isotropy when two eigenvalues of the second rank tensor are identical and into isotropy when the second rank fabric tensor vanishes. Moreover, basing on an invariance principle of the constitutive law with respect to normalization of the microstructural property, the elasticity model is described by two independent elastic constants, an exponent and two fabric data – a scalar and a second order tensor. The obtained constitutive law is invertible and thermodynamically admissible under trivial conditions.

It was later formulated an extension of this model that may degenerate at least into a cubic symmetry model when the eigenvalues of the fabric tensor coincide, Zysset (1998). The resulting compliance and stiffness tensor are

$$\mathbb{D}(\gamma, \mathbf{M}) = \sum_{i=1}^3 \frac{I}{\varepsilon_0 \gamma^k m_i^{2l}} \mathbf{M}_i \otimes \mathbf{M}_i - \sum_{\substack{i,j=1 \\ i \neq j}}^3 \frac{\nu_0}{\varepsilon_0 \gamma^k m_i^l m_j^l} \mathbf{M}_i \otimes \mathbf{M}_j + \sum_{\substack{i,j=1 \\ i \neq j}}^3 \frac{I}{2\mu_0 \gamma^k m_i^l m_j^l} \mathbf{M}_i \underline{\otimes} \mathbf{M}_j \tag{0.6}$$

$$\mathbb{C}(\gamma, \mathbf{M}) = \sum_{i=1}^3 (\lambda_0 + 2\mu_0) \gamma^k m_i^{2l} \mathbf{M}_i \otimes \mathbf{M}_i + \sum_{\substack{i,j=1 \\ i \neq j}}^3 \lambda_0' \gamma^k m_i^l m_j^l \mathbf{M}_i \otimes \mathbf{M}_j + \sum_{\substack{i,j=1 \\ i \neq j}}^3 2\mu_0 \gamma^k m_i^l m_j^l \mathbf{M}_i \underline{\otimes} \mathbf{M}_j \tag{0.7}$$

Due to the strictly positive volume fraction and fabric eigenvalues, the positive definiteness conditions reduce to those for cubic symmetry $\varepsilon_0 > 0$, $\frac{1}{2} < \nu_0 < -1$, $\mu_0 > 0$. In fact, this generalized model degenerates into isotropic symmetry if and only if the fabric tensor coincides with the identity tensor $\mathbf{M} = \mathbf{I}$ and the following relationship holds $\mu_0 = \frac{\varepsilon_0}{2(1+\nu_0)}$ or $\lambda_0 = \lambda_0'$.

This latter condition was enforced a priori in the original Zysset-Curnier model.

2. Compliance Penalization Law for Orthotropic Porous Media

Spatial arrangement of voids affects the overall behaviour of porous media. Anisotropic distribution of the matrix reflects on anisotropic mechanical response. To detect such relation more than a single scalar quantity, as density, is needed. To set global parameters able to describe quantity and distribution of porosity in the solid, orthotropic porous RVE models are adopted.

To the author knowledge, no explicit investigations have been performed in Literature for determining the overall elastic response of orthotropic porous RVEs with wide variable volume fractions, i.e. RVEs characterized by the presence of voids whose percentage ranges from high porosity up to high matrix volume fraction.

In this chapter FE method is adopted with the aim of establishing a general relationship between averaged elastic moduli and matrix volume fraction for orthotropic porous RVE materials, all exhibiting a parallelepiped cavities: this gives an orthotropic overall response. In particular, the geometrical evolution of the RVE porosity is obtained by means of three-dimensional periodic arrangement of voids, embedded in a linearly elastic isotropic solid matrix and spatially distributed. FE analyses are hence performed over the single porous symmetrical 1/8 RVEs, to obtain homogenized mechanical properties, fig. 5.1. The investigation is conducted on centre of void RVEs type, according with remarks presented in the previous chapter.

Following this way, several RVEs are built up increasing void sizes and elastic analyses are then performed over a wide range of porosity values, obtaining overall elastic moduli as function of RVE matrix volume fraction, γ . Thus, computational results are utilized for constructing a mathematical one-to-one relation between γ and overall elastic moduli. In order to relate volume fraction to moduli in a closed form, the corresponding set of data is compared to analytical expressions presented in literature.

2.1 Finite Element Analyses

2.1.a. Geometry material and mesh

Orthotropic heterogeneous porous material is analyzed by meaning of homogenization criteria. To predict homogenized behaviour of such type of porous material, a cubic cell RVE is chosen with faces oriented towards the material symmetry direction, i.e. parallel to the coordinate planes of a Cartesian system $\{x_1, x_2, x_3\}$. It show density varying thorough a characteristic cavity length and are modelled and analyzed trough finite element method by tractions prescribed tests in a way to completely define elastic behaviour through volume fraction variation related to anisotropic order. Tests produce values of homogenized Young modulus, Poisson ratio and shear modulus in every coordinate direction.

Orthotropic isotropic RVE cavity shape consists in a parallelepiped block, parallel to RVE faces,

define by $a \times \left(\frac{l}{2} - 2a \right) \times \left(\frac{l}{2} - 1.5a \right)$ dimensions respectively along x_1 , x_2 and x_3

directions. Cavity type shows different shapes related to growing volumes, indeed RVE matrix volume fraction γ is defined in the range $[0.169, 1.00]$, porosity p is related as $p = 1 - \gamma$.

Thus a generic orthotropic porous RVE is obtained. Material properties of matrix of cubic cell are modelled as linear, elastic and isotropic, characterized by the Young modulus $E_0 = 20000 \text{ MPa}$

and the Poisson's ratio $\nu_0 = \frac{1}{3}$; length of cubic cell edge is set equal to 20 mm. Matrix elastic

behaviour affects the overall porous RVE properties, values are chosen by human bone elastic average ones. Every value result presented in this work is given normalized over matrix parameters. Such RVE has three plane of symmetry, coincident with coordinate planes, and is tested under symmetric boundary conditions, thus, in a way to realize better performing models, just 1/8 of RVE is modelled.

Mesh of 3D RVE models is performed through three dimensional isoparametric brick element with 20 nodes, element is well suited to realized a regular mesh and in no one case model presents a wall thickness divided in less than three element.

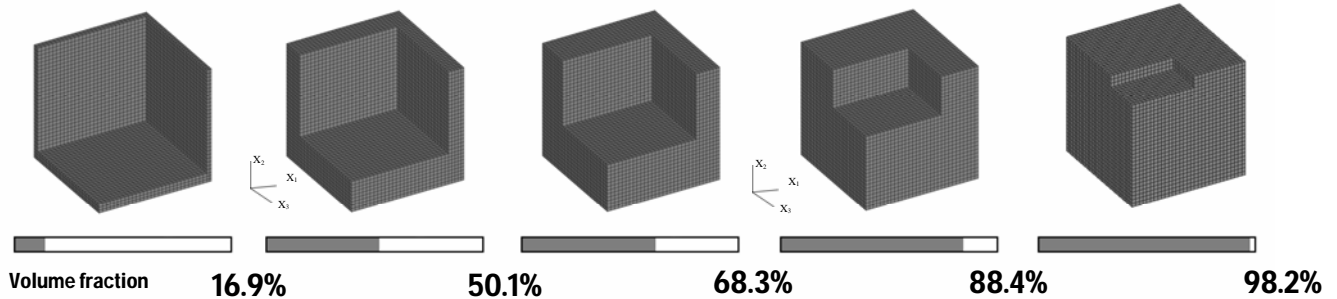


Fig. 5.1. 3d representation of orthotropic porous CV RVE 1/8 FE models trough increasing volume fraction sketches.

Routine for the automatic generation of both geometric and mesh models is created. In particular, the algorithm allows the automatic generation of a wide number of porous FE models with progressively increasing voids dimension. Thus, a data set of results, large enough to draw with accuracy the relations between average mechanical properties and volume fraction, is achieved. In figure 5.1 sketches of some FE meshes are shown; note that, thanks to symmetric load and geometry, just $\frac{1}{8}$ of the RVE is modelled, the positive x and negative y and z.

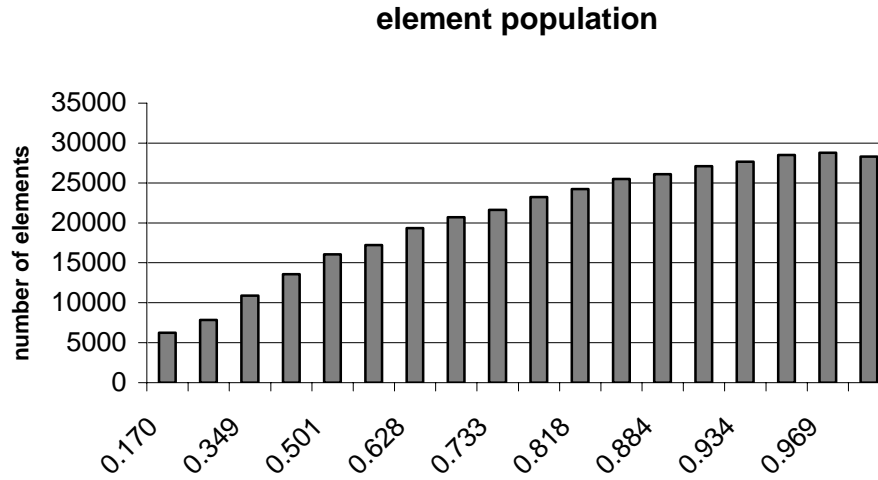
2.1.b. Boundary conditions and implementations

Three boundary conditions on RVE cell are considered in a way to define a suitable set of FE analyses. In particular, to explore the elastic behaviour of the transversal porous material RVE, analyses are performed applying uniform tractions on cubic cell faces in each of three coordinate directions. Edges of cubic cell are parallel to the coordinate planes of a Cartesian system $\{x_1, x_2, x_3\}$ centred on cell. FE models are tested under uniform tractions applied normally to cell face of coordinates $\left(x_1, x_2, -\frac{L}{2}\right)$, $\left(x_1, -\frac{L}{2}, x_3\right)$ and $\left(\frac{L}{2}, x_1, x_2\right)$, see figure 4.4. For more details refer to Appendix A.1

2.1.c. Model accuracy

Fine element local density defines fidelity both of geometrical and material model. FEM model mesh accuracy is generally intended to assure a high precision of performed analysis results and a good geometrical approximation. Mesh density upper bound is marked by solving process time, it is directly related to clock speed of implemented machine. Fixing results error tolerance and geometrical fidelity, finite element mesh is to be lower populated as possible, in way to obtain an easily handling model.

In this work an error tolerance of 3% is assumed, model mesh precision were tested to ensure this accuracy level and it shows 28320 elements for the zero porosity model. Isoparametric 20 nodes brick elements are used thus model density always match theoretical density. A large number of analyses were performed. Graph 5.1, shows element population of different orthotropic models with different volume fractions.



Graph 5.1. 1/8 RVE element population varying volume fraction.

RVE modelled porous geometry varies with a single geometrical parameter, in way to define varying RVE porosity. For each parameter value a specific routine aimed to obtain local parametric meshing is generated. In no one case a wall of less than two finite elements thickness appears and the regular shape of the cavities is well modelled through brick elements.

2.1.d. Homogenized elastic constant

Several numerical mechanical tests are performed using orthotropic RVE/8 models, shifting from shell like configuration (Flugge transversally isotropic model) to matrix heterogeneous isotropic one (zero porosity material). Isotropic elastic behaviour of matrix is defined by

$E_m = 20000 \text{ MPa}$ and $\nu_m = \frac{1}{3}$. This kind of model spans in the range of quite all density

spectrum, in way to describe the material behaviour of all the homogenized elastic characteristics in a wide density range. Models are tested under axial uniform tractions apply normal to

$\left(x_i, x_j, \frac{L}{2}\right)$ face of the RVE cubic cell in each of three coordinate directions, see fig. 4.4. These

tests are aimed to obtain linear relation between average stresses and average deformations in way to define homogenized linear elastic properties of the porous RVE.

Analyses performed under uniform tractions allow calculating the average deformation tensor. Average stress tensor is directly deduced by uniform tractions applied on the RVE surface, thus, due to axial traction test in each of coordinate directions, nonzero compliance constants D_{ijj} of the porous RVE are calculated. For more details refer to Appendix A.2.2.

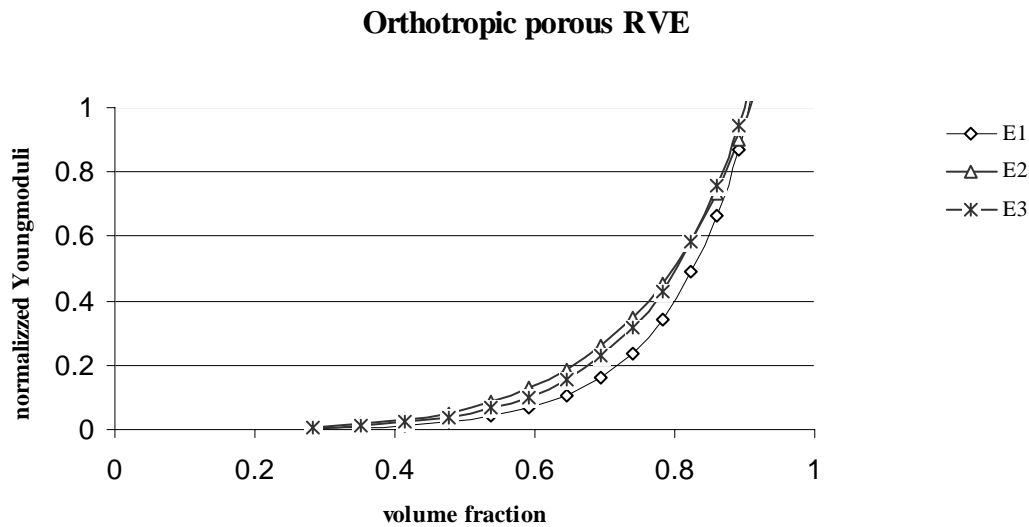
Totally 18 finite element porous RVE models are processed under 3 different load cases.

Orthotropic elastic constants

Nine constants are needed to describe orthotropic elastic behaviour for the porous RVEs. In the follow D_{ijj} , nonzero compliance constants will highlighted, as well as related Young moduli in the three coordinate directions. For more details refer to Appendix A.2.3.

Orthotropic Young moduli

Orthotropic elastic analyses, performed on porous RVE models, show how Young moduli in the three coordinate directions vary within volume fraction graph 5.2. Moduli are normalized by defined value of matrix Young modulus. Graph shows how normalized modulus tends to unit value when matrix volume fraction is close to 1, whereas while volume fraction diminishes results give values gradually lower and lower. The parallelepiped cavity shape change sides ratios during its volume increasing, as consequence change direction of higher rigidity for different volume fraction values. Porous models vary from dense matrix isotropic configuration to transversally isotropic shell configuration, anisotropy of the model is driven by cavity shape morphing, different order of orthotropy are investigated such procedure leads to some intermediate transversally isotropic condition as it appears by intersection between Young moduli curves in the graph.



Graph 5.2. Trend of Young moduli, normalized over matrix value, within volume fraction for porous orthotropic RVE FE calculations (isotropic matrix properties: $E_0 = 20000$ MPa, $\nu_0 = 0.3$). Results refer to tractions prescribed calculation.

Figure 6 shows FE contour value ranges of results obtained through tractions tests performed on porous RVE model for different volume fractions. Fe results are used in eq. 7.7, see Appendix A.2.2, to calculate elastic compliance constants. The models reproduce only the 1/8 symmetric part of the RVE.

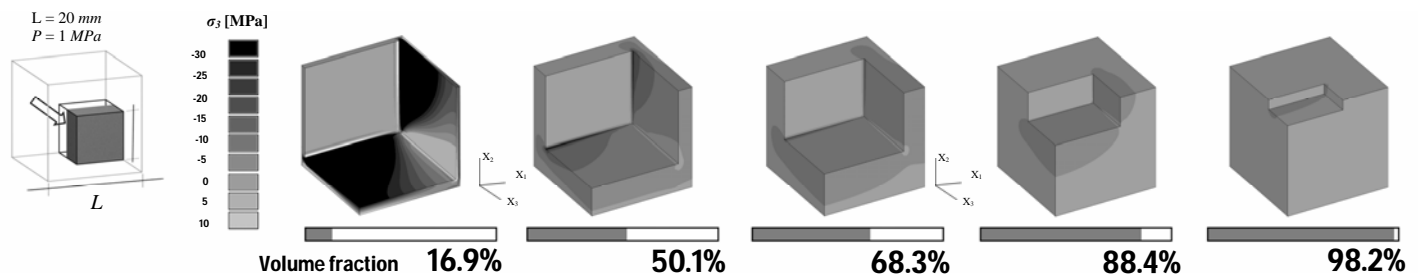
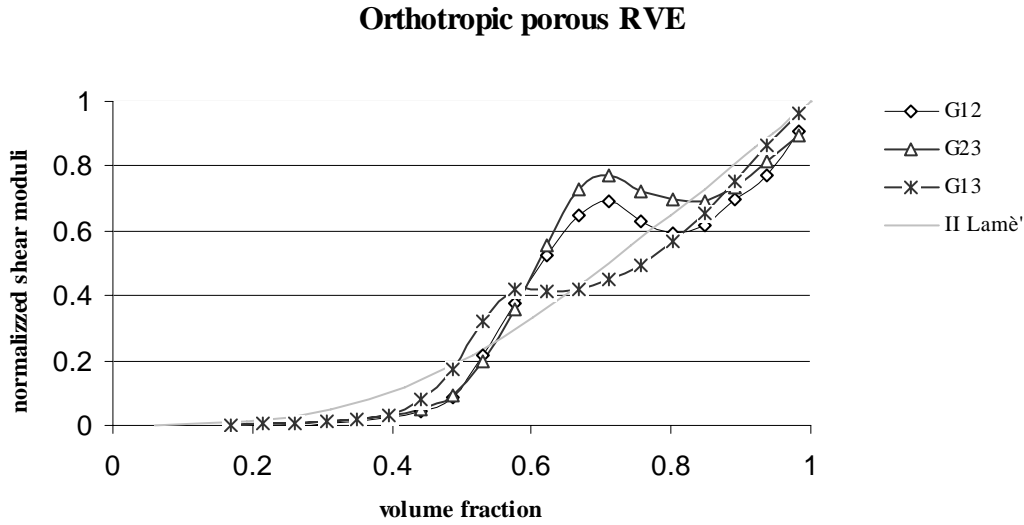


Fig. 5.2. F.E. results on CM RVE FE models through increasing volume fraction sketches (isotropic matrix properties: $E_0 = 20000$ MPa, $\nu_0 = 0.3$). Results refer to tractions prescribed calculation.

Orthotropic Shear Moduli

Due to the orthotropy of the porous RVE, more numerical tests has been necessary for estimating the orthotropic shear modulus, in a way to completely define RVEs mechanical behaviour. Pure shear prescribed test types are implemented. Elastic constant dependence by density is obtained trough relation between homogenized stress and deformation, eq. 7.7, see Appendix A.2.2.



Graph 5.3. Trend of shear moduli, normalized over matrix value, within volume fraction for porous orthotropic RVE FE calculations (isotropic matrix properties: $E_0 = 20000$ MPa, $\nu_0 = 0.3$). Results refer to tractions prescribed calculation.

For such model, numerical tests aim to obtain shear modulus density variation. In graphic 5.3 normalized shear moduli rise with density from null value to unit. Values are normalized by correspond matrix one. The parallelepiped cavity shape change sides ratios during its volume increase, as consequence change direction of plane of higher shear rigidity for different volume fraction values. In the graphic is also represent second Lamé constant variation, normalized by its matrix value, in case of tractions prescribed tests. As second Lamé constant and shear modulus coincide in case of isotropy, curve distance highlight model anisotropic order by density.

2.1.e. Fitting Zysset Parameters

Theory of Zysset on second order fabric tensor (1995), see sec. V.1.1, prescribes a relation between elastic compliance constants and volume fraction for porous media. Such model is directly related to a second order measure of the spatial porosity distribution as well as volume fraction, in compact:

$$D_{ijjj} = \frac{1}{E_0 \cdot \gamma^k} \cdot \frac{1}{m_i^v m_j^v} \quad i, j = [1, 2, 3] \quad (0.8),$$

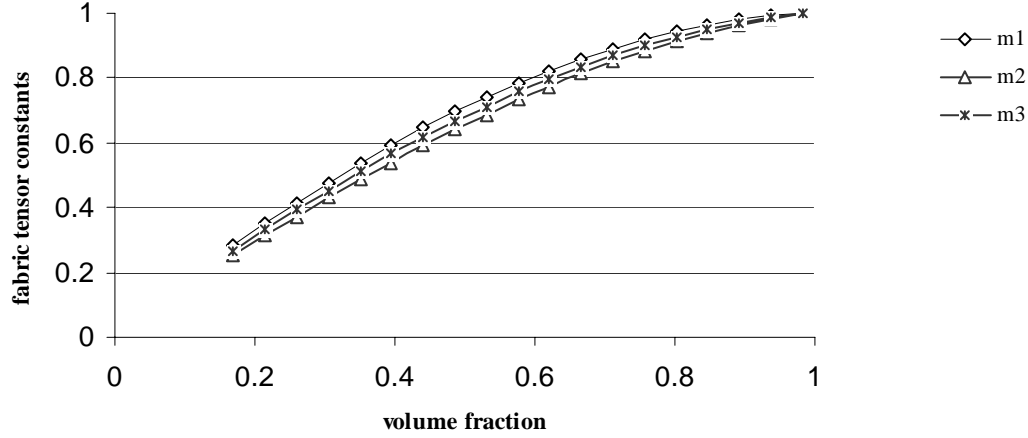
where E_0 is reference matrix Young modulus, γ is the matrix volumetric fraction, m_i is the fabric tensor constant and k and v are constants.

$D_{ijjj}(\gamma)$ elastic compliance constants deduced through FE analyses performed on orthotropic porous RVE are used as benchmarks to set the best value for k and v exponential parameters appear in Zysset formula (5.8). It has been assumed that Fabric tensor constants are related to principal inertia values of porous media in a way:

$$m_i = 1 - 2 \frac{I_i}{I_1 + I_2 + I_3}; \quad i = [1, 2, 3] \quad (0.9)$$

where I_1 , I_2 and I_3 are Inertia in x_1 , x_2 and x_3 direction respectively.

Orthotropic porous RVE



Graph 5.4. Trend of fabric tensor constants within volume fraction for porous orthotropic RVE FE calculations.

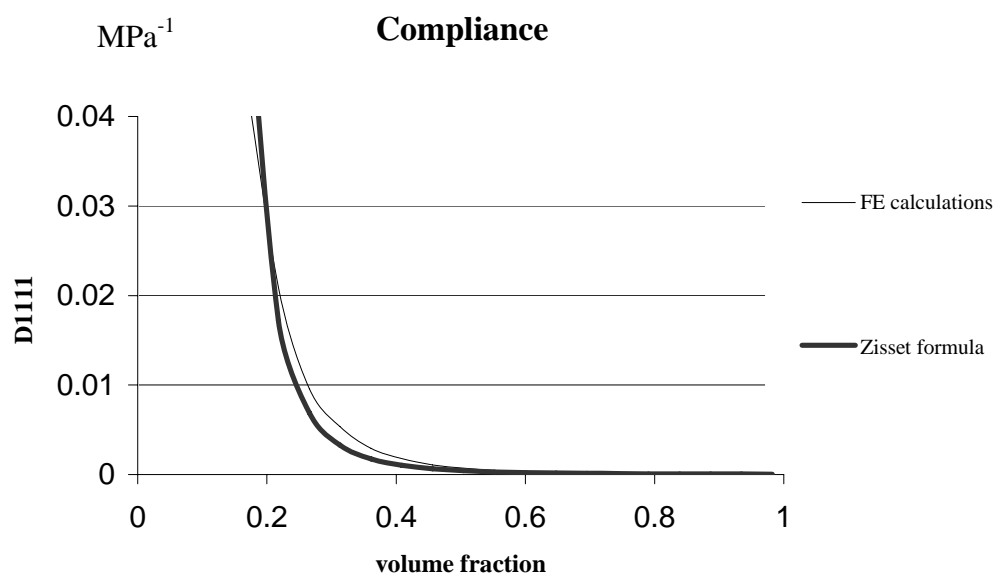
In the formula (5.8) as exponent k for volume fraction, the value calculated in the previous chapter par IV.2.1.g has used. The value of exponential constant ν in (5.8) is deduced by the meanings of minimization of the sum of the squared difference between the FE compliance volume fractions variations and the law and their derivates:

$$v_{ijj} = \underset{\downarrow}{\text{Minimum}} \left[\sqrt{\int_0^1 \frac{|D_{ijj}^{FE\ 2} - D_{ijj}^{Z\ 2}|}{D_{ijj}^{FE\ 2}} d\rho} - \sqrt{\int_0^1 \left| \frac{\partial D_{ijj}^{FE\ 2}}{\partial \rho} - \frac{\partial D_{ijj}^{Z\ 2}}{\partial \rho} \right| / \frac{\partial D_{ijj}^{FE\ 2}}{\partial \rho}} d\rho \right] \quad (0.10),$$

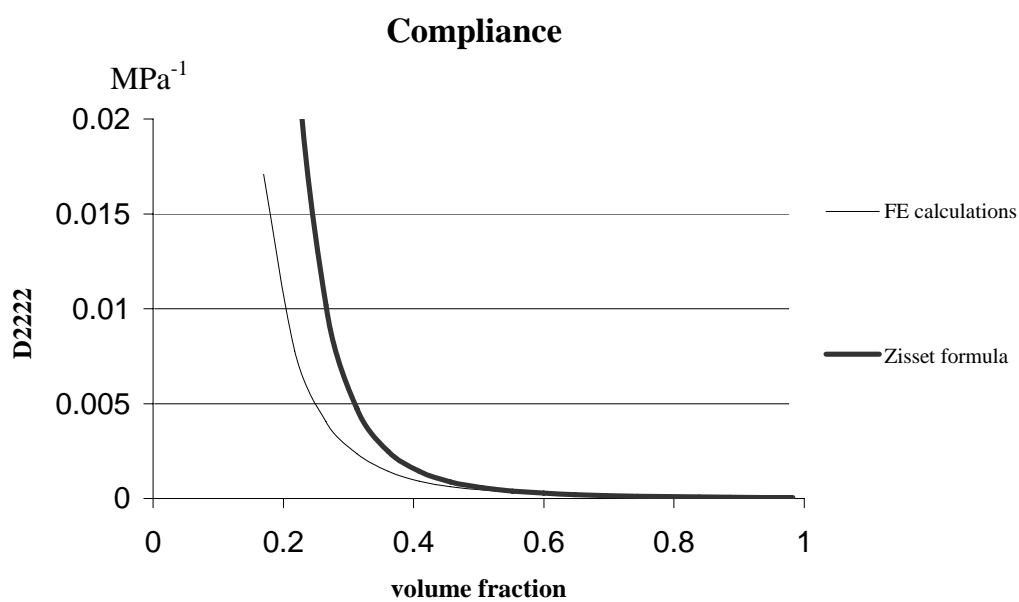
$$\nu = 1.8$$

where D_{ijj}^{FE} is the generic compliance constant deduced by FE calculations and D_{ijj}^Z is the respective constant calculated through Zysset equation (5.8). Each compliance constant defines a different value of ν , the value 1.8 found refers to the mean value. Graphs 5.6-5.8, below show how Zysset formula with settings derived from (5.9) and (5.10) matches the orthotropic FE porous RVE

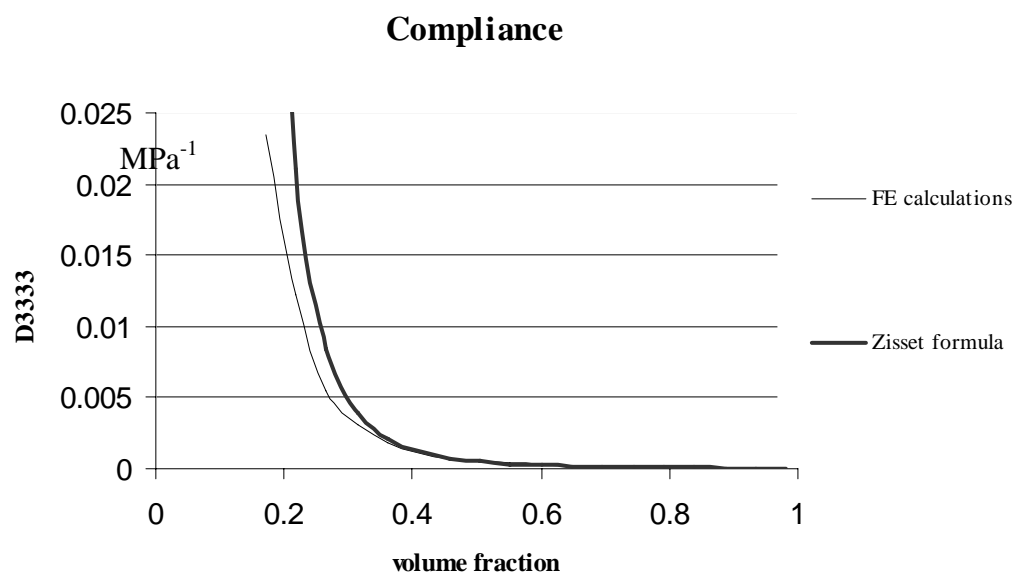
calculations



Graph 5.6. Trend of D1111 within volume fraction for porous orthotropic RVE FE calculations (isotropic matrix properties: $E_0 = 20000 \text{ MPa}$, $\nu_0 = 0.3$). Results refer to tractions prescribed calculation



Graph 5.7. Trend of D2222 within volume fraction for porous orthotropic RVE FE calculations (isotropic matrix properties: $E_0 = 20000 \text{ MPa}$, $\nu_0 = 0.3$). Results refer to tractions prescribed calculation.



Graph 5.8. Trend D_{3333} within volume fraction for porous orthotropic RVE FE calculations (isotropic matrix properties: $E_0 = 20000 \text{ MPa}$, $\nu_0 = 0.3$). Results refer to tractions prescribed calculation.

CHAPTER VI

TRANSVERSELY ISOTROPIC MEDIA

1. Homogenized Behavior of Fiber Composite Material

In this chapter results on numerical analyses on behavior of fiber composites are presented. Composites show transversely isotropic mechanical behavior and its analysis represent one of the most used and complex application of the theory of homogenization of porous materials. Indeed such heterogeneous material systems are widely present in many engineering fields of application as well as in natural material and biological tissues, therefore outlining their properties is a challenge that modern design techniques cannot miss.

Materials come in a variety of forms with a very wide range of properties. Rarely, however, does a single material suffice to provide the perfect balance of properties required for a particular application. As a practical expedient, it has been found, mixtures of materials often provide an advantageous blend of properties. It is perhaps inevitable that engineering science would be called on to explain accidental discoveries and empirical results. More importantly, engineering science is being utilized to gain a fundamental understanding of materials behavior in heterogeneous systems, so that further improvements can be achieved. Ultimately, of course, only a rigorous discipline of heterogeneous material behavior can provide the key to optimizing material utilization. Two examples will help provide the motivation and thrust for the further developments. Many polymers in homogeneous form are glassy and brittle. It was found by trial and error, in a chemical laboratory, that a uniform dispersion of rubber spheres can greatly improve the impact sensitivity of the material. A significant proportion of the glassy polymers now manufactured contain the rubber “toughening” agent, as a means of upgrading the material behavior. The Second example is that of fiber reinforced composite materials. Some fibers are composed of materials that are not even available in bulk form, or, if available, the fiber form has completely different and improved properties from those of the bulk form. In either case it has been found to be of great advantage to retain the material in fiber form, and bind the fibers together with a compliant matrix phase. In composite form the system still retains many of the properties associated with the unique fiber form of material. These examples are typical of the kinds of systems that may be considered in heterogeneous material combinations. It must be kept in mind that combinations of materials that enhance a particular property often involve the degradation of another property. Therefore, all relevant properties must be considered and tradeoffs must often be made.

1.1 Composite Cylinder Model

In the follow a method, Christensen (1979), to determine the effective moduli of heterogeneous media made of matrix and cylindrical inclusions has reported as a good analytical benchmark to evaluate mechanical properties in fiber composite materials. Usually the use of fiber reinforced materials has a very direct rationale to improve both the stiffness and strength properties and how much stiffening effect can be achieved is shown. As first approach these type of inclusion can be obtained as limiting cases of prolate and ellipsoids, or even as cases in which the ratios of the maximum to the minimum dimension of the ellipsoids are very large. In a further approach the

cylindrical inclusions are taken to be of infinite extent. This simply means that the fibers are idealized as uniform cylinders of infinite length.

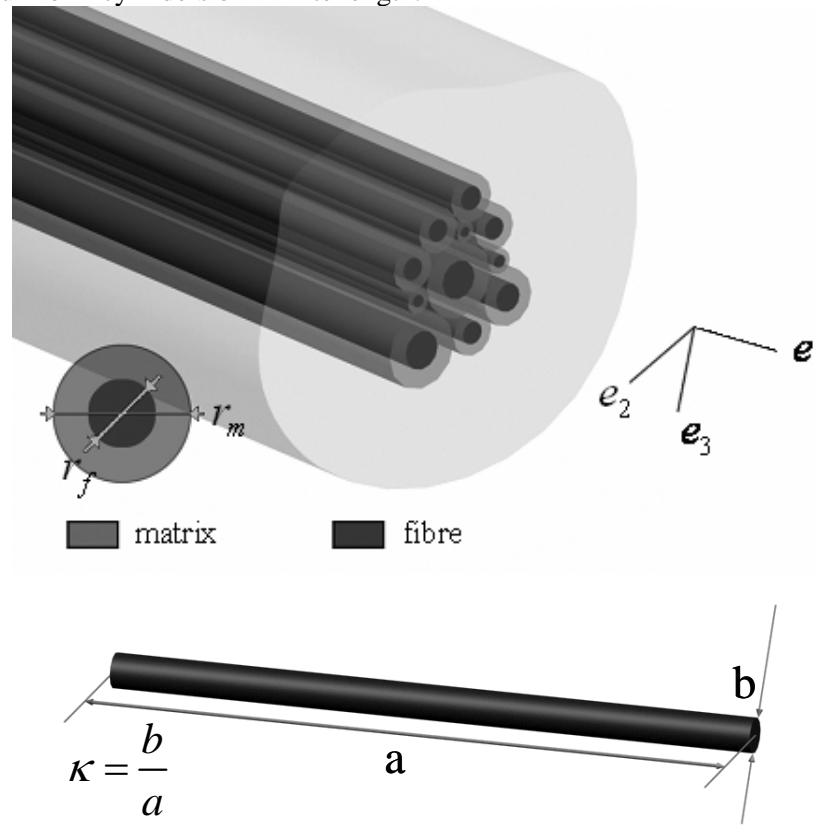


Figure 6.1. Heterogeneous fiber composite media.

Objective of the method is to characterize the effective stiffness properties of the heterogeneous fiber composite media. Consider for example systems of aligned fibers. As long as the fibers are randomly positioned in space, the media can be ideates as being effectively homogeneous. Further, media of this type, as shown in fig. 6. 1, have symmetry properties in the plane normal to that of the fiber direction. Such media are characterized as being transversely isotropic. Such module type properties are those of the equivalent homogeneous characterization of the heterogeneous media. Transversely isotropic media needs five independent parameters to be characterized on the mechanical point of view. The objective is to obtain an analytical representation for the five properties in terms of the fiber phase properties, the matrix phase properties, and the volume concentration of each phase.

A geometric model of the composite material must be introduced to accomplish this task. The most commonly used model is that of the composite cylinders model, introduced by Hashin and Rosen (1964). This model is a three-dimensional composite spheres model. The fiber phase is taken to be composed of infinitely long circular cylinders embedded in a continuous matrix phase. The model is shown in fig. 6.1. With each individual fiber of radius a , there is associated an annulus of matrix material of radius b . Each individual cylinder combination of this type is referred to as a composite cylinder, and the absolute values of radii a and b vary with each composite cylinder such that a volume filling configuration is obtained. The ratio of radii a/b , let it κ , is, however, required to be constant for all composite cylinders. Naturally, the absolute size of the individual cylinders must vary, down to infinitesimal. The utility of this model results from the fact that the analysis of an individual composite cylinder will suffice to determine four of the five effective moduli for the representative volume element.

1.1.a. Uniaxial modulus

The initial objective is to determine the effective uniaxial modulus E_{11} . To this Christensen report:

$$E_{11} = cE_f + (1-c)E_m + \frac{4c(1-c)(\nu_f - \nu_m)^2 \mu_m}{\frac{(1-c)\mu_m}{\kappa_f + \frac{\mu_f}{3}} + \frac{c\mu_m}{\kappa_m + \frac{\mu_m}{3}} + 1} \quad (6.1)$$

where E is the Young modulus, ν the Poisson's ratio, μ the shear modulus and c the fiber volume fraction, m and f subscripts refer to matrix and fiber properties respectively.

The result is the effective uniaxial modulus for a single composite cylinder. It remains to show that it is, in fact, the proper result for the representative volume element. Namely, the theorem of minimum potential energy can be used to show that the result is a lower bound for the corresponding result of the representative volume element. Alternatively, rather than imposing displacement boundary conditions, stresses can be imposed, and an upper and for E_{11} can be found through the use of the theorem of minimum complementary energy. In so doing, it is found that the upper and lower bounds coincide, thus providing the exact solution, which then is given by.

1.1.b. Other properties

The problem just outlined also provides a solution for the effective Poisson's ratio ν_{12} , where axis 1 is in the fiber direction and $\frac{\nu_{12}}{\nu_{21}}$. In the context of the present problem ν_{12} related to composite material properties through:

$$\nu_{12} = c\nu_f + (1-c)\nu_m + \frac{c(1-c)(\nu_f - \nu_m) \left(\frac{\mu_m}{\kappa_m + \frac{\mu_m}{3}} - \frac{\mu_m}{\kappa_f + \frac{\mu_f}{3}} \right)}{\frac{(1-c)\mu_m}{\kappa_f + \frac{\mu_f}{3}} + \frac{c\mu_m}{\kappa_m + \frac{\mu_m}{3}} + 1} \quad (6.2)$$

It is interesting to note that the formula for E_{11} is very closely approximated by the rule of mixtures, simply by neglecting the last term in. To a lesser extent the formula is also approximated by the rule of mixtures. On the other hand, the remaining three effective properties have values not well approximated by the rule of mixtures.

In an entirely similar manner to that just considered, two more problems can be posed to give exact solutions for the plane strain bulk modulus K_{23} and shear modulus in the fiber direction μ_{12} . It is found that

$$K_{23} = K_m + \frac{\mu_m}{3} + \frac{c}{\frac{1}{\kappa_f - \kappa_m + \frac{(\mu_f - \mu_m)}{3}} + \frac{1-c}{\kappa_m + \frac{4\mu_m}{3}}} \quad (6.3)$$

$$\frac{\mu_{12}}{\mu_m} = \frac{\mu_f(1+c) + \mu_m(1-c)}{\mu_f(1-c) + \mu_m(1+c)} \quad (6.4)$$

These problems are equally simple to that outlined in the derivation of E_{11} and ν_{12} , in the sense that only one displacement component is involved in the field variable solutions. The explicit formulas were derived by Hill (1964) and Hashin (1966).

The remaining property to be determined is μ_{23} , the transverse shear modulus. Displacement type problem can be posed to determine the upper bound for μ_{23} and a stress type problem to determine the lower bound. As shown by Hashin and Rosen (1964), the bounds do not coincide, except at very low and very high volume fractions. At author knowledge no exact analytical solution for μ_{23} has been presented.

1.1.c. A model for the transverse shear of a fibre system

Specifically, it has proved to be very difficult to determine the transverse shear modulus for the composite cylinders model. Accordingly, a model is introduced that is intimately related to the composite cylinders model, but one for which we can determine the transverse shear modulus.

It is considered the composite cylinders model of Fig. 3.1, replacing all but a single composite cylinder by equivalent homogeneous media, as down in Fig. 3.1. A state of shear deformation is imposed on the representative volume element, and by meanings of energetic criteria it follows:

$$\frac{\mu_{22}}{\mu_m} = 1 + \frac{c}{\frac{\mu_f}{\mu_f - \mu_m} + \frac{\kappa_m + \frac{7\mu_m}{3}}{2\kappa_m + \frac{8\mu_m}{3}}} \quad (6.5)$$

Relation yields the solution for the transverse shear modulus μ_{23} for the model of fig. 6.1, in terms of the properties and volume fractions of each phase. It is reassuring and useful that the solution for μ_{23} is independent of any of the other effective properties.

It should be noted that the composite cylinders model allow the full range for the fiber phase, $0 \leq c \leq 1$.

1.2 Finite Length Fiber Effects

The effective properties obtained in the preceding sections all assumed a condition of infinitely long cylinders. However, fiber composites are increasingly being used in forms involving so-called chopped fibers. Under this condition the fibers have finite aspect ratio, and is expect that under this condition the reinforcing properties of the fibers would be degraded. Christensen, provides a quantification of the reinforcing effect. However attention is restricted to a dilute condition in which there is no interaction between fibers. The effective properties derived in the preceding sections had no restriction to dilute conditions, and in accordance with the geometry of the composite cylinder model the full volume fraction range for fiber phase $0 \leq c \leq 1$ was possible.

The derivation to be given follows that of Russel (1973), which in turn is based on the results obtained by Eshelby (1957).

The problem solved is that of an ellipsoidal inclusion embedded in an infinite matrix phase, which is subjected to conditions of uniform deformation at large distance from the inclusion.

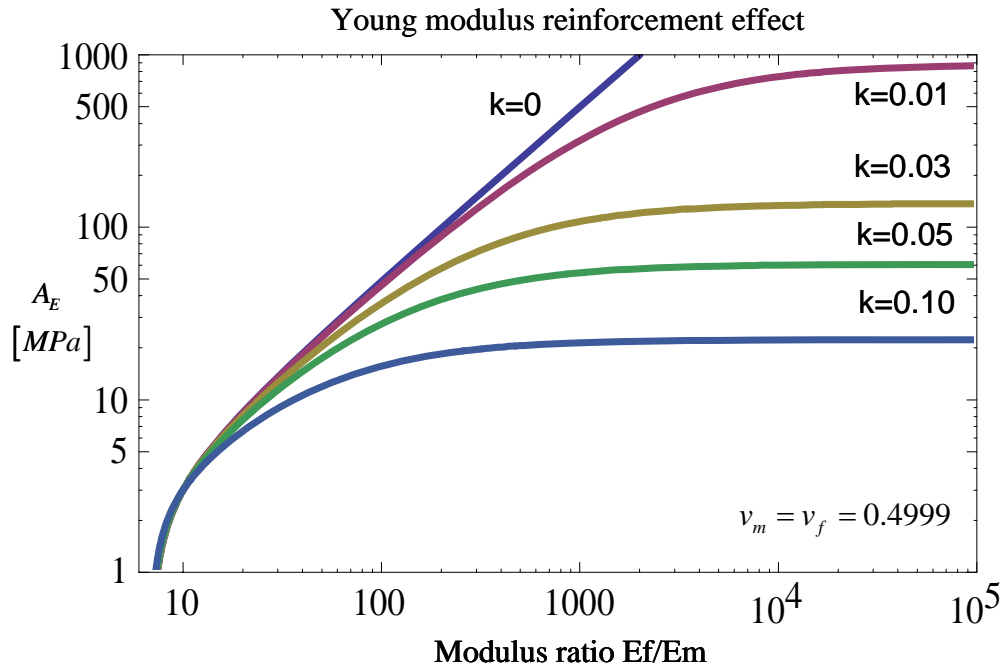
From this solution it is possible to determine the effective properties of the heterogeneous medium. Since the interest is focused on finite bench fiber system, the ellipsoid can take the form of a slender prolate ellipsoid. The effective properties are determined as a function of the aspect ratio of the ellipsoid, as well as the properties of the two phases. In the follow relation for homogenized Young modulus is highlighted:

$$\frac{E_{11}}{E_m} = 1 + c \left[\frac{\frac{E_f}{E_m} - 1 + \frac{2(\nu_f - \nu_m)^2}{(1 + \nu_m) + \left(\frac{E_m}{E_f}\right)(1 + \nu_m)(1 - 2\nu_f)}} \right] \quad (6.6)$$

This solution show the strong dependent the effective property E_{11} has on the aspect ratio of the inclusion $\kappa = \frac{b}{a}$... Writing in the form

$$\frac{E_{11}}{E_m} = 1 + cA \quad (6.7)$$

the form of A is shown in graph 6.1 as a function of κ and $\frac{E_f}{E_m}$.



Graph 6.1. Trend of Young modulus reinforcement effect A on matrix fibers Young modulus ratio, varying fibers aspect ratio.

The particularly interesting range of $10 \leq \frac{E_f}{E_m} \leq 10^3$ covers many fiber composites of practical interest. In this range there is a strong dependence of E_{11} on the aspect ratio κ . For example, for $\frac{E_f}{E_m} = 200$, with $\kappa = 0.01$ the factor A in eq. (6.7) has a value of about 82% of the infinitely long case, whereas at $\kappa = 0.1$, A retains only about 11% of its value at the infinitely long case. These

results, of course, apply only to the dilute suspension case. In the nondilute case the degrading effect of a finite κ value would probably be less severe, but still qualitatively the same as that shown. Clearly, the fibers must be very long in comparison to the diameter, or significant stiffness effect is sacrificed.

2. Design in Composite Material

As exposed before, composite material is formed by the combination of two or more distinct materials to form a new material with enhanced properties. For example, rocks are combined with cement to make concrete, which is as strong as the rocks it contains but can be shaped more easily than carving rock. While the enhanced properties of concrete are strength and ease of fabrication, most physical, chemical, and processing-related properties can be enhanced by a suitable combination of materials. The most common composites are those made with strong fibers held together in a binder. Particles or flakes are also used as reinforcements, but they are not as effective as fibers.

The oldest composites are natural: wood consists of cellulose fibers in a lignin matrix, and human bone can be described as fiber like osteons embedded in an interstitial bone matrix. While manmade composites date back to the use of straw-reinforced clay for bricks and pottery, modern composites use metal, ceramic, or polymer binders reinforced with a variety of fibers or particles. For example, fiberglass boats are made of a polyester resin reinforced with glass fibers. Sometimes composites use more than one type of reinforcement materials in which case they are called hybrids. For example, consider reinforced concrete, a particle-reinforced composite (concrete) that is further fiber reinforced with steel rods. Sometimes different materials are layered to form an enhanced product, as in the case of sandwich construction where a light core material is sandwiched between two faces of stiff and strong materials.

Fiber reinforcement is preferred because most materials are much stronger in fiber form than in their bulk form. In the case of glass, this is attributed to the sharp reduction in the number of defects in the fibers compared with those in bulk glass.

Property	E-Glass/ Epoxy	S-Glass/ Epoxy	E-Glass/ Isophthalic Polyester	Kevlar 49/ Epoxy	Carbon/ Epoxy AS4/3501-6	Carbon/ Epoxy T800/3900-2	Carbon/ Epoxy IM7/8551-7	Carbon/ PEEK AS4/APC2	Carbon/ Polyimide AS4/ AvimidK-III
Density [g/cc]	2.076	1.993	1.85	1.380	1.58	—	—	1.6	—
Longitudinal Modulus E_1 [GPa]	45	55	37.9	75.8	142	155.8	151	138	110
Transverse Modulus E_2 [GPa]	12	16	11.3	5.5	10.3	8.89	9.0	10.2	8.3
Inplane Shear Modulus G_{12} [GPa]	5.5	7.6	3.3	2.07	7.2	5.14	5.6	5.7	—
Poisson's Ratio ν_{12}	0.19	0.28	0.3	0.34	0.27	0.3	0.3	0.3	—
Longitudinal Tensile Strength F_{1t} [MPa]	1020	1620	903	1380.0	1830	2698	—	2070	—
Transverse Tensile Strength F_{2t} [MPa]	40	40	40	34.5	57	—	—	86	37
Inplane Shear Strength F_6 [MPa]	60	60	40	44.1	71	—	—	186	63
Longitudinal Compressive Strength F_{1c} [MPa]	620	690	357	586.0	1096	1691	—	1360	1000
Transverse Compressive Strength F_{2c} [MPa]	140	140	68	138.0	228	—	—	—	—
Intralaminar Shear Strength (F_4 or F_5) [MPa]	60	80	76	48.69	—	—	—	150	—
Longitudinal Tensile Strain ϵ_{1t} [%]	2.3	2.9	2.4	1.8	1.29	1.68	1.64	1.45	—
Longitudinal CTE α_1 [$10^{-6}/^\circ\text{C}$]	3.7	3.5	6.5	−2.0	−0.9	—	—	0.5	—
Transverse CTE α_2 [$10^{-6}/^\circ\text{C}$]	30	32	22	60	27	—	—	30	—
Longitudinal moisture expansion β_1	0	0	0	0.01	0	0.0095	—	—	—
Transverse moisture expansion β_2	0.2	0.2	0.2	0.2	0.2	0.321	—	—	—
Fiber Volume Fraction V_f [%]	60	60	50	60	60	—	57.3	61	—
Void Content V_v [%]	—	—	2.0	—	—	—	0.1	—	0.5
Fiber Misalignment Ω [deg]	—	—	3.53	—	—	—	—	—	—

Table 6.1. Typical properties of unidirectional composites.

The high strength of polymeric fibers, such as aramid, is attributed to the alignment of the

polymer chains along the fiber as opposed to the randomly entangled arrangement in the bulk polymer. Crystalline materials, such as graphite, also align along the fiber length, increasing the strength. Whiskers, which are elongated single crystals, are extremely strong because the dislocation density of a single crystal is lower than in the polycrystalline bulk material.

The main factors that drive the use of composites are weight reduction, corrosion resistance, and part-count reduction. Other advantages that motivate some applications include electromagnetic transparency, wear resistance, enhanced fatigue life, thermal- acoustical insulation, low thermal expansion, low or high thermal conductivity, etc.

Weight reduction provides one of the more important motivations for use of composites in transportation in general and aerospace applications in particular. Composites are lightweight because both the fibers and the polymers used as matrices have low density. More significantly, fibers have higher values of strength-weight and stiffness-weight ratios than most materials, as shown in table 6.1.

However strong fibers cannot be used alone (except for cables), because fibers cannot sustain compression or transverse loads. A binder or matrix is thus required to hold the fibers together. The matrix also protects the fibers from environmental attack. Therefore, the matrix is crucial in determining the corrosion resistance of the composite. Because of the excellent resistance to environmental and chemical attack of polymer matrices and most fibers, composites have conquered large markets in the chemical industries, displacing conventional materials such as steel, reinforced concrete, and aluminum. This trend is expanding into the infrastructure construction and repair markets as the resistance to environmental degradation of composites is exploited.

Since polymers can be molded into complex shapes, a composite part may replace many metallic parts that would otherwise have to be assembled to achieve the same function. Part-count reduction often translates into production, assembly, and inventory savings that more than compensate for higher material cost. Since the fibers cannot be used alone and the strength and stiffness of polymer are negligible when compared with the fibers, the mechanical properties of composites are lower than the properties of the fibers. Still, composites are stiffer and stronger than most conventional materials when viewed on a per unit weight basis, as shown in table 6.1, Barbero (1999), by the data of unidirectional composites. The reduction from fiber to composite properties is proportional to the amount of matrix used.

Since the fibers do not contribute to the strength transversely to the fiber direction, and the strength of the matrix is very low, it becomes necessary to add layers with various orientations to face all the applied loads. One way to achieve this is to create a laminate, stacking layers with various orientations. Although such a laminate can handle multidirectional loads, the strength and stiffness per unit weight of the laminate on a given direction are lower than the corresponding values for a unidirectional composite.

Composite materials are formed by the combination of two or more materials to achieve properties (physical, chemical, etc.) that are superior to those of the constituents. The main components of composite materials are fibers and matrix. The fibers provide most of the stiffness and strength, and the matrix binds the fibers together providing load transfer between fibers and between the composite and the external loads and supports.

The design of a structural component using composites involves concurrently material design and structural design (e.g., the geometry). Unlike conventional materials (e.g., steel), the properties of the composite material can be designed simultaneously with the structural aspects. Composite properties (e.g., stiffness, thermal expansion, etc.) can be varied continuously over a broad range of values, under the control of the designer.

Although micromechanics can predict very well stiffness of a material, it is not as accurate at predicting strength. Therefore, experimental data of strength is very valuable in design. For this reason, manufacturers and handbooks tend to report composite properties rather than fiber and matrix properties separately. The problem is that the reported properties correspond to a myriad

of different reinforcements and processing techniques, which makes comparison among products every difficult. Typical properties of unidirectional composites are listed in table 6.1, Barbero (1999).

Fiber	Modulus [Gpa]	Tensile Strength (*) [GPa]	Compression Strength [GPa]	Elongation [%]	Density [gr/cc]	Longitudinal Thermal Expansion [$10^{-6}/^{\circ}\text{C}$]	Transverse Thermal Expansion [$10^{-6}/^{\circ}\text{C}$]	Poisson Ratio	Thermal Conduct [W/m $^{\circ}\text{C}$]	Maximum Operating Temperature [$^{\circ}\text{C}$]	Resistivity [micro ohm-m]
E-Glass	72.345	3.45	—	4.4	2.5–2.59	5.04–5.4	—	0.22	1.05	550	—
S-Glass	85	4.8	—	5.3	2.46–2.49	1.6–2.9	—	0.22	1.05	650	—
C-Glass	69	3.31	—	4.8	2.56	6.3	—	—	1.05	600	—
D-Glass	55	2.5	—	4.7	2.14	3.06	—	—	—	477	—
Carbon											
T300	230	3.53	—	1.5	1.75	–0.6	7–12	0.2	3.06	—	18
M50	490	2.45	—	0.5	1.91	—	—	—	54.43	—	8
AS2	227	2.756	—	1.3	1.8	—	—	—	8.1–9.3	—	15–18
AS4-D	241	4.134	—	1.6	1.77	–0.9	—	—	8.1–9.3	—	15–18
IM6	275.6	5.133	—	1.73	1.74	—	—	—	8.1–9.3	—	15–18
HMS4	317	2.343	—	0.8	1.8	—	—	—	64–70	—	9–10
UHM	441	3.445	—	0.8	1.85	—	—	—	6.5	—	120
P55	379	1.9	—	0.5	2	–1.3	—	—	120	—	8.5
P100	758	2.41	—	0.32	2.16	–1.45	—	—	520	—	2.5
Kevlar 29	62	3.792	—	—	1.44	—	—	—	—	—	—
Kevlar 49	131	3.62	0.72	2.8	1.45	–2	59	0.35	0.04	160 (#)	—
Kevlar 149	179	3.62	0.69	1.9	1.47	—	—	—	—	—	—
Technora H	70	3	0.6	4.4	1.39	–6	59	0.35	—	160 (#)	—
Boron	400	2.7–3.7	6.9	0.79	2.57	4.5	0.2	0.2	38	315 (#)	—
SCS-6	427	2.4–4	—	0.6	3	4–4.8	—	0.2	10	—	—
Nextel 720	260	2.1	—	—	3.4	6	—	—	—	1200 (#)	—

Table 6.2. Laminate properties of general purpose polyester resin reinforced with stitched layers of E-glass reinforcement.

The design of composites can be done using composite properties, such as those given in table 6.1, provided experimental data are available for all types of fiber-matrix combinations to be used in the laminate. While using experimental composite properties eliminates the need for micromechanical modeling, it requires a large investment in generating the experimental data. Furthermore, a change of matrix material later in the design process invalidates all the basic material data used and requires a new experimental program for the new matrix. Most of the time, experimental material properties are not available for the fiber-matrix-process combination of interest. Then fiber and matrix properties, which are readily available from the material supplier, or can be measured with a few tests, are used in micromechanics to predict layer properties. This is often done when new materials are being evaluated or in small companies that do not have the resources to generate their own experimental data. Then the accuracy of micromechanics results can be evaluated by doing a few selected tests. The amount of testing will be determined by the magnitudes of the project and the availability of resources, and in some cases testing may be deferred until the prototype stage.

Once the properties of individual layers are known, the properties of a laminate can be obtained by combining the properties of the layers that form the laminate (see table 6.1). Note, however, that the effect of changing the matrix or the manufacturing process is unknown and any such change would require repeating the whole experimental program. The cost of experimentation is likely to limit the number of different laminates for which data are available. When laminate properties are not available from an experimental program, they can be generated using micromechanics and macromechanics.

2.1 Materials: Fibers and Matrix

Fibers are used in composites because they are lightweight, stiff, and strong. Fibers are stronger than the bulk material that constitutes the fibers. This is because of the preferential orientation of molecules along the fiber direction and because of the reduced number of defects present in a fiber as opposed to the bulk material. Whereas the tensile strength of bulk E-glass is low (1.5–5.8 GP, Gauthier (1995)), the same material reaches 72.3 GPa in fiber form, mainly because of the

reduction in the number and size of surface defects. Fibers are used as continuous reinforcements in unidirectional composites by aligning a large number of them in a thin plate or shell, called lamina, layer, or ply. A unidirectional lamina has maximum stiffness and strength along the fiber direction and minimum properties in a direction perpendicular to the fibers. When the same properties are desired in every direction on the plane of the lamina, randomly oriented fibers are used. The resulting composite has the same properties in every direction on the plane of the lamina, and it is weaker in the thickness direction. The creep properties of the composite are dominated by the matrix. Composites reinforced with chopped fibers, whiskers (elongated single crystals), or particles may experience large creep deformations, even at room temperature. This is the main reason for using continuous fibers for structural applications. By choosing fibers with very low creep compliance (e.g., carbon or glass), polymer matrix composites (PMC) can be made as creep resistant as necessary. The most common fibers used in composites are glass, carbon, and organic (Kevlar). Boron, Silicon carbide (SiC), alumina, and other fibers are used in specialized applications. Choosing which type of fiber to use depends on the mechanical and environmental properties desired and the cost of the fiber, see table 6.2.

Most fibers can be obtained in the form of prepreg tape in which the fibers are held together by an epoxy resin and a fiberglass backing. Because the making of the prepreg tape, i.e. matrix preimpregnated into the fibers, introduces additional labor, the cost of prepreg tape is usually 75-100% higher than the cost of the fibers, the fabrication methods using prepreg tape are slow and labor intensive. Therefore, most of the new applications of composites use fibers in their simplest, unprocessed forms. For example, protrusion and filament winding use roving or tow and resin to produce the final product without intermediate operations. Woven or stitched fabrics facilitate the fabrication of laminates in resin transfer molding (RTM) and other processes, while adding only 20-40% to the cost of the reinforcement.

Composites are reinforced either with continuous fibers, discontinuous fibers, or particles. Continuous fibers are long fibers that usually attain maximum values in properties such as strength and stiffness due to their controlled anisotropy and low number and size of surface defects. In continuous fiber reinforced composites, the load is assumed to be carried mostly by the fibers oriented along the direction of the load. Discontinuous fibers are short fibers obtained by chopping continuous fibers or produced directly as short fibers to reduce the cost. Other short fiber forms include milled fibers and whiskers, whiskers are elongated single crystals with very high strength. The aspect ratio (length over diameter, L/D) significantly affects the properties of short fiber composites. The orientation of short fibers cannot be controlled easily and they are assumed to be randomly oriented unless special provisions are taken to control the fiber orientation. Composites made with short fibers arranged randomly have nearly isotropic properties in the plane of the laminate. Perhaps the main disadvantage for structural applications is that short fiber composites do not reduce the creep of polymer matrices as effectively as continuous reinforcement. Furthermore, short fiber composites usually have lower strength than continuous fiber composites.

A **strand**, **tow**, or **end** is an untwisted bundle of continuous filaments (fibers) used as a unit. All fibers in a strand are produced at the same time, from a single furnace, and spun together. A **yarn** is a twisted strand. A **roving** is a collection of parallel continuous strands. Rovings are produced by winding together the number of single strands needed to achieve the desired yield. **Yield** is the length of yarn or roving contained in a unit weight of a package. The most common units for yield are yards per pound (yd/lb). The metric denomination is TEX and it is given g/km. TEX is the weight in grams per 1000 meters of roving. Therefore, TEX is inversely proportional to yield

$$\text{TEX}[\text{g/km}] = \frac{496238}{\text{YELD}[\text{yd/lb}]}$$

The higher the TEX number of a roving, the larger the cross-sectional area occupied by the fibers. This can be computed as

$$A[\text{cm}^2] = 10^{-5} \frac{\text{TEX}[\text{g/km}]}{\rho_f[\text{g/cm}^3]}$$

where the brackets indicate the units of each quantity in the equation and ρ_f is the density of the fibers. The area of a roving is useful for the computation of fiber volume fraction of composites. The term **tow** is commonly used with carbon fibers, where the filament count is the number of fibers in a tow. The K-number, used for carbon fibers, represents the number of fibers in a tow in thousands. The K-number is related through the fiber diameter and the density to the TEX (and yield) as

$$\text{TEX} = \frac{\pi d_f^2}{4} \rho_f K$$

with TEX in [g/km], K in thousands, ρ_f in [g/cc], and d_f in microns. However, this equation does not give accurate TEX results if the K-number or the fiber diameter are only approximate. For accurate prediction of the weight or volume fraction in the composite, it is advisable to request the TEX value directly from the manufacturer or to measure it. Also, it must be noted that's variability of 6% in TEX is not unusual, even within the same material lot.

A direct-draw roving is wound into a spool directly from the furnace with the required numbers of strands to achieve the desired yield. An indirect-draw roving is formed in a secondary operation to increase the yield by rewinding several direct-draw rovings into one. In each roving, the fibers wound on the outside of the spool are longer than the ones on the inside. When the roving is unwound to fabricate the composite, not all the fibers have the same length, which creates microcatenary. An indirect-draw roving has in general more microcatenary than a direct-draw roving because several direct-draw rovings are rewound to obtain the higher yield. To measure the microcatenary, a length of roving (about 2.5 m) is stretched between two supports and the fibers are loosely separated by hand. The shorter fibers will be stretched and the longer fibers will hang in a catenary shape because of gravity. Microcatenary results in misalignment in the composite, which is adverse to the compressive strength of the material. Rovings are used directly in protrusion and filament winding without intermediate operations, thus reducing the cost of the final part. Common fiberglass rovings have yields between 56 and 259 yd/lb (TEX between 8861 and 1985 g/km). Carbon fibers are commonly packaged in 3K to 36K tows (TEX 198 to 2290). The matrix material holds the fibers together, thus transferring the load between fibers and between the composite and the supports. It also protects the fibers from the environment and mechanical abrasion and carries some of the loads, particularly transverse stress and interlaminar shear stress. Some properties of the composite, such as transverse stiffness and strength, are matrix dominated. They affect the matrix selection more than fiber dominated properties. Furthermore, matrix dominated properties depend strongly on the operating temperature.

Matrix materials can be polymers, metals, or ceramics. Polymer matrices are the most common because they add a crucial advantage to composites, which is the ease of fabrication of very complex parts with low tooling cost and low capital investment. In fact, manmade composites have their roots in fiber-reinforced plastics. Unreinforced plastics provide cost savings in tooling and through part integration, and unlimited freedom for esthetic design, but suffer from creep problems. Reinforcing plastics with fibers virtually eliminates the creep problem and opens another dimension for material and structural concurrent design, which is the continuous and virtually unlimited variation of mechanical properties under the designer's control. Since polymer matrix composites (PMCS) are the most commonly used type of composite material. The matrix of PMCS is a polymer that can be either a thermoset or a thermoplastic. Various terms are used in the marketplace to refer to PMC. Advanced composite materials (ACMs) usually refer to more expensive and high performance composites targeted to aerospace applications, mostly carbon-

epoxy and carbon-thermoplastic systems. Fiber-reinforced plastics (FRPs) usually refer to less expensive materials targeted to consumer goods and mass markets, including fiberglass-polyester systems. However, the distinction is no longer clear since many new materials marketed as FRP systems also have high performance and particularly performance-cost ratios that exceed those of some materials labeled as ACMs. Other designations attempt to differentiate the fiber type used. For example, GRP and GFRP both refer to glass-fiber-reinforced plastics, and CFRP refers to carbon-reinforced plastics. Sometimes the term RP (reinforced plastic) is used when the term composite may be confusing. This is the case in the area of the civil construction market, where composite construction means structures made of steel structural shapes and reinforced concrete used together, notably for bridge construction. The first steps of the design process of composites are the selection of a few candidate matrices and a few candidate processing methods. The selection of a matrix is guided by the mechanical properties, the corrosion resistance, and the flammability of the polymer matrix in the composite. The corrosion resistance of the resulting composite is dominated by the matrix. Even though carbon fibers are chemically inert, if the matrix degrades, the integrity of the composite will be severely compromised. Therefore, a proper resin selection must be made at the beginning of the design process. Some properties such as transverse stiffness and strength are dominated by the matrix, with the fibers having little influence. Furthermore, not every resin can be processed by every processing technique. Quite the contrary, resins are available in families of products, each member of the family targeting a specific processing technique. Therefore, the resin and the processing technique are selected simultaneously. Selecting candidate processing methods must be done at the beginning of the design process for several reasons. First, processing methods impose constraints on the design process by limiting parameters like the fiber volume fraction and fiber orientations. Second, the production rate and cost are controlled by the processing technique. Third, every production technique imposes some limit on part size and complexity, which in turn are related to the resin system used: the lower the viscosity of the resin, the larger and thicker a part can be. In summary, the designer will try to select a few candidate resin systems that meet the mechanical, corrosion, flammability, and processing requirements at the minimum cost possible.

2.2 Chirality in Trigonal Material

The classification of the types of linear elastic material symmetries by the number and orientation of the normals to the planes of material symmetry is fully equivalent to the crystallographic method using group theory, Chadwick (2001) (see also Cowin (1987) and (1995)).

Triclinic material symmetry has no planes of mirror symmetry. The monoclinic crystal system has exactly one plane of reflective symmetry. Trigonal symmetry has three planes of mirror symmetry. The normals to these three planes all lay in one plane and make angles of sixty degrees with one another. Since the negative of a plane of symmetry is also the normal to a plane of symmetry, it is easy to see that trigonal symmetry is a three-fold symmetry. The triclinic, monoclinic and trigonal symmetries are the only three of the eight elastic symmetries that, in their canonical symmetry coordinate system retain cross-elastic constants connecting normal stresses (strains) to shear strains (stresses) and vice versa. In the 6 by 6 matrix of elastic coefficients these cross-elastic constants appear in the lower and upper right 3 by 3 submatrices (6.8). In Cowin (2002) it was pointed out that these three elastic symmetries are the only elastic symmetries of the eight linear elastic symmetries that permit directions that are not normals to planes of reflective symmetry. Every direction in triclinic symmetry is a direction in which a normal to the plane of material symmetry is *not* permitted. Every direction that lies in the single symmetry plane in monoclinic symmetry is a direction in which a normal to the plane of material symmetry is *not* permitted. The only direction in trigonal symmetry in which a normal to the plane of material symmetry is not permitted is the direction normal to a plane of three-fold symmetry. As shown in

Cowin (2002) there are *not* other such directions.

A representation for the elastic compliance matrix in the Voigt notation, Voigt (1928), for a material with trigonal symmetry is

$$\begin{bmatrix} c_{ij} \end{bmatrix} = \begin{bmatrix} c_{11} & c_{12} & c_{13} & c_{14} & 0 & 0 \\ c_{12} & c_{11} & c_{13} & -c_{14} & 0 & 0 \\ c_{13} & c_{13} & c_{33} & 0 & 0 & 0 \\ c_{14} & -c_{14} & 0 & c_{44} & 0 & 0 \\ 0 & 0 & 0 & 0 & c_{44} & c_{14} \\ 0 & 0 & 0 & 0 & c_{14} & \frac{1}{2}(c_{11} - c_{12}) \end{bmatrix} \quad (6.8)$$

Other equivalent representations of the elastic compliance matrix in the Voigt notation for trigonal symmetry are possible 8. An interesting aspect of trigonal symmetry is the chiral and symmetry-breaking character of the cross-elastic constant c_{14} . Note that c_{14} is not constrained to be of one sign; the sign restriction on c_{14} from the positive definiteness of strain energy is

$$-\sqrt{\frac{c_{44}(c_{11} - c_{12})}{2}} < c_{14} < \sqrt{\frac{c_{44}(c_{11} - c_{12})}{2}} \quad (6.9)$$

If c_{14} vanishes, the elastic compliance matrix (6.8) becomes that for hexagonal or transversely isotropic symmetry. Hexagonal symmetry is a six-fold symmetry with seven planes of mirror symmetry. Six of the normals to these seven planes all lie in the seventh plane and make angles of thirty degrees with one another. Transversely isotropic symmetry is characterized by a single plane of isotropy. A plane of isotropy is a plane of mirror symmetry in which every vector is itself a normal to a plane of mirror symmetry. Since a plane of isotropy is also a plane of symmetry, there are an infinity plus one planes of symmetry associated with transverse isotropy. The elasticity matrix associated with the hexagonal symmetry and the elasticity matrix associated with transversely isotropic symmetry are identical (they are given by (6.8) with $c_{14} = 0$) and therefore, for this purposes, they are identical.

A simple thought model is possible for the visualization of the symmetry-breaking character of the elastic constant c_{14} . This constant could be described as a chiral constant, chiral being a word coined by Kelvin, Thompson (1904).

(“I call any geometrical figure, or group of points, *chiral*, and say it has *chirality* if its image in a plane mirror, ideally realized, cannot be brought to coincide with itself.”) and used in describing architecture and the structure of molecules. It means that a structure cannot be superposed on its mirror image, that the structure has a handedness, McManus (2002). For example, helical spirals are chiral; they are either left-handed or right-handed. Consider a composite material constructed of an isotropic matrix material reinforced by only right-handed spiral helices whose long axes are all parallel. These helical spirals may be either touching or separated by a matrix material. It’s possible to demonstrate that the symmetry-breaking elastic constant in trigonal symmetry is proportional to the angle of the helical structure of the material, if the material has a helical structure.

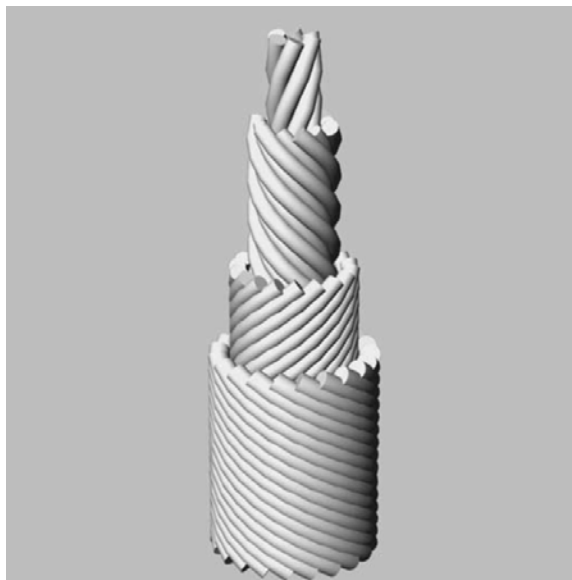


Figure 6.2. A composite structure composed from sets of left- and right-handed helically wound fibrous laminae that are in the form of concentric coaxial cylinders; the fibers of each lamina or component cylinder are characterized by a different helical angle. The angle of the helices of- ten rotates regularly from one cylinder to the next. This type of structure is called “helicoidal” and described as a cylinder made of “twisted plywood”.

The association of the micro geometric chiral character of C_{14} with a helix is not a unique association. The basic property of C_{14} is its symmetry-breaking character, and it may be associated with structural gradients in the material Cowin (2002).

Lakes, in his work, Lakes (2001), uses a different criterion for chirality in elastic symmetry. The present criterion is the non-existence of a plane of mirror symmetry Cowin (2002); hence exposed “chiral” character is possible in the traditional triclinic, monoclinic and trigonal elastic symmetries. This criterion is consistent with the generally employed definition of chiral due to Kelvin. Lakes, on the other hand, requires the non-existence of a center of symmetry as his criterion for “chirality” in elastic symmetry, and since there are no linear elastic materials without a center of symmetry, suggests the use of Cosserat elasticity to model material “chirality”. A center of symmetry is three mutually perpendicular planes of symmetry, thus Lakes (2001), uses a different and stronger criterion for chirality than the one reported here. In the next section, examples of chiral materials and locally chiral components in globally non-chiral composites are described.

2.2.a Chiral Materials and Locally Chiral Components in Globally Non-chiral Composites

Chiral materials that form chiral and non-chiral structures are employed by man and by nature. A typical such structure is illustrated in figure 6.2. The structure is a set of concentric coaxial cylinders, each lamina or cylinder characterized by a different helical angle. The angle of the helices often rotates regularly from one cylinder to the next. This type of structure is called helicoidal, NEVILLE (1985), and described as a cylinder made of “twisted plywood”. The helical fibers may or may not be touching. The examples of this structure in nature are numerous, Neville (1993), and include fish scales and plant stem walls. Man also uses cylinders made of “twisted plywood” to create structures.

Chiral materials that form chiral structures occur in nature. The horns of many animals are chiral. Perhaps the most famous is the tusk of the narwhal (in the Middle Ages the tusk of the narwhal was thought to be the horn of the mythical unicorn). This whale is edentulous except for the upper

lateral incisors. The right incisor normally remains embedded in the jaw, but in adult males the left tooth forms a tusk, which can in large specimens reach a length of 2.4 m, and have a diameter of 8 cm at the point of eruption. (In the year 2000, a nine-pound, a foot long narwhal tusk from Resolute Bay was offered for sale on the Web for \$25,000 (Canadian)). The chiral or twisted helical structure and mechanical properties of one tusk are described in Baer (1992).

D'Arcy Thompson (1942), suggested that the fluid drag due to the rotational motion about the long axis of the body in the narwhal swimming pattern was the mechanism that forced the chiral structure on the growing tusk and Gould concurred, Gould (1976). However, a more reasonable rationale and mechanism for the chiral structure was suggested in a short two page article in the journal *Arctic*, Kingsley (1988). Normally the tusk is imprinted with the curvature of the bone socket as it erupts or extrudes itself from a bone socket. However, if the tusk slowly twists in the socket as it grows, the imprinted curvature will be neutralized or averaged and the tusk will grow straight with the spiral structure.

A second example of a natural chiral structure occurs in trees, both hardwoods and softwoods, due to a combination of genetic and environmental factors, Noskowlak (1963). As can be seen from a well-illustrated Website, Cherkaev, the wood fibers spiral around the trunk. The spiral structure in trees causes a practical problem with telephone and power poles, Lowery (1967). Changes in the moisture content of the wood of the pole causes the pole to twist after it has been employed as part of a transmission network.

2.3 Trigonal Effects in Reinforcing Fibers

Composite overall mechanical behavior can be predicted throughout meaning of homogenization theory using different approach, such as the composite cylinders model, Hashin and Rosen (1964), introduced before, or by an easier way using the rule of mixtures. In any case the trigonal properties of the reinforcing fibers do not affect the homogenized model. Analytical solutions can cut down on the number of design cycles and can be used to optimize designs. Before the mechanical response of an assemblage of cord- rubber layers can be understood, the mechanics of a single unidirectional lamina must be understood. The mechanics of this lamina should be based on the mechanics of its constituents, cord and matrix. Investigators have steered away from analytical models for cord composites because of the difficulty in analyzing the cord mechanics. Many investigators who have tried to predict the behavior of cord composites analytically have typically ignored the mechanics of the cord, and treated the cord-rubber lamina as an orthotropic material, Gough (1968) and Tangorra (1969) developed expressions for the elastic constants of a single unidirectional ply based on the methods of analyzing plywood. They neglected the flexural stiffness of the cords and treated them as unidirectional load carrying members, with no transverse properties. They ignored the tension-twisting coupling of the cord, Akasaka and Hirano (1972) further simplified the Gough-Tangorra relations by utilizing the large difference in moduli, and the fact that for most applications, the cord volume fraction is small. Once the elastic constants are known for a single ply, the constants for a ply, or series of plies at arbitrary orientations, can be determined using classical lamination theory (Jones, 1975) if lamination theory is appropriate. Shield and Costello (1993) have investigated the appropriateness of lamination theory for cord composites when the cord-matrix modulus ratios are very large, By modeling the cord composite as orthotropic a part of the mechanical response of the cord is neglected, If the cord is treated as a single body it exhibits extension-twisting coupling; when a cord is pulled on, it also rotates, Costello (1990) has developed both a general theory and a linear theory for the response of a cord that exhibits this behavior. This coupling between extension and rotation will also be apparent in the general lamina response, therefore, it may not be appropriate to classify the lamina as orthotropic.

In a way to compute the trigonal effect of the twisted fibers on the homogenized composite

material a model for the prediction of mechanical properties in twisted wire will introduce. Starting from Costello analytical linear approach, Costello (1990), a nonlinear analytical model is realized, as shown in the following.

Simple straight strand

A simple straight strand is made of a straight centre wire surrounded by several helical wires. G. A. Costello (1990) realizes a model of such kind of strand based on the meanings of thin wire mechanics. Thin wire is a wire in which the maximum characteristic length of the cross section is small compared to wire length and radius curvature of the wire center line.

Equilibrium equations

Forces on wire cross section can be easily computed in the *principal torsion-flexural coordinate system* $\{x,y,z\}$, Love (1944), where the z axes is tangent to wire centerline and centered on it; N and N' are the components of shearing force in x and y directions, respectively, T is the axial tension in the wire, G and G' are the components of bending moment in x and y directions, respectively, H is the twisting moment in the wire; external loads are defined as X , Y , and Z as components of external load per centerline wire unit length in the x , y , and z directions, respectively, K , K' , and Θ are the components of external moment per centerline wire unit length in the x , y , and z directions, respectively; wire geometric configuration is completely shown through center line position, κ and κ' as the components of curvature in the x and y directions, respectively, and t as the twist per unit length of the wire.

Wire equations of equilibrium in $\{x,y,z\}$ coordinate system are defined as:

$$\begin{aligned} \frac{dN}{ds} - N'\tau + T\kappa' + X &= 0 & \frac{dG}{ds} - G'\tau + H\kappa' - N + K &= 0 \\ \frac{dN'}{ds} - T\kappa + N\tau + Y &= 0 & \frac{dG'}{ds} - H\kappa + G\tau + N + K' &= 0 \\ \frac{dT}{ds} - N\kappa' + N'\kappa + Z &= 0 & \frac{dH}{ds} - G\kappa' + G'\kappa + \Theta &= 0 \end{aligned} \quad (6.10)$$

Such equations define a set of non linear equations and are valid for large deflections. Hence relations between loads and deformations can be written as follow:

$$\begin{aligned} T &= AE\xi_f & G &= EI_x(\kappa - \kappa_0) \\ H &= C(\tau - \tau_0) & G' &= EI_y(\kappa' - \kappa'_0) \end{aligned} \quad (6.11)$$

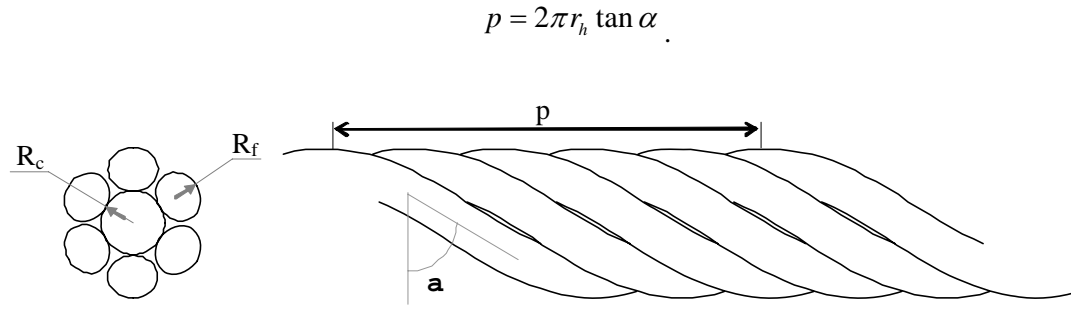
where E is elasticity modulus, C torsional rigidity of the material, I_x and I_y cross sectional moment of inertia about the x and y axes, respectively, A wire cross sectional area and ξ_f axial wire deformation.

Geometry

Geometry model prescribes a central filament of radius R_c surrounded by m helical wires of same radius R_f . Helix radius of the external filaments path is defined as:

$$r_h = R_c + R_f,$$

α is the helix angle and pitch is related in the way:



Cross section and front of a straight strand with 6 external filament.

Core radius, radius and number of external filaments, such as helix angle determine if surrounding filament touch the core or, touching each other, do not. Core touching condition is given by:

$$R_f \sqrt{1 + \frac{\tan^2 \left(\frac{\pi - \pi}{2m} \right)}{\sin^2(\alpha)}} < R_c + R_f \quad (6.12)$$

Axial response of a single helical filament

For a single helical filament in the simple straight strand model subject to axial load, the wire axial tension T is assumed constant along the length of the wire, with no bending moment acting, that is, $K = K' = 0$.

Equilibrium equations become:

$$\begin{aligned} N'\tau + T\kappa' + X &= 0 & -G'\tau + H\kappa' - N &= 0 \\ Y &= 0 & N &= 0 \\ Z &= 0 & \Theta &= 0 \end{aligned} \quad (6.13)$$

Prescribing a small variation of helix filament angle as $|\Delta\alpha| \ll 1$, following solutions, for deformed helix configuration, can be written as:

$$\begin{aligned}
\frac{G'}{ER_f^3} &= \frac{\pi}{4} R_f \Delta \kappa' & \frac{N'}{ER_f^2} &= \frac{H}{ER_f^2} \frac{\cos^2(\alpha)}{r_h} - \frac{G'}{ER_f^2} \frac{\sin(\alpha)\cos(\alpha)}{r_h} \\
\frac{H}{ER_f^3} &= \frac{\pi}{4(1+\nu)} R_f \Delta \tau & \frac{T}{ER_f^2} &= \pi \xi_f \\
\frac{X}{ER_f} &= \frac{N'}{ER_f} \frac{\sin(\alpha)\cos(\alpha)}{r_h} - \frac{T}{ER_f} \frac{\cos^2(\alpha)}{r_h}
\end{aligned} \tag{6.14}$$

such relations gives deformed filament loads condition as function of $\Delta \kappa'$, $\Delta \tau$, and \mathbf{x}_f , that is function of $\Delta \alpha$ as, by geometrical remarks, for $|\Delta \alpha| \ll 1$:

$$\begin{aligned}
\Delta \kappa' &= -\frac{2 \sin(\alpha) \cos(\alpha)}{r_h} \Delta \alpha + \nu \frac{R_c \xi_c + R_f \xi_f}{r_h} \frac{\cos^2(\alpha)}{r_h} & \xi_f &= \xi_c - \frac{\Delta \alpha}{\tan(\alpha)} = \varepsilon - \frac{\Delta \alpha}{\tan(\alpha)} \\
\Delta \tau &= \frac{1 - 2 \sin^2(\alpha)}{r_h} \Delta \alpha + \nu \frac{R_c \xi_c + R_f \xi_f}{r_h} \frac{\sin(\alpha) \cos(\alpha)}{r_h} & \tau &= \frac{\xi_f}{r_h \tan(\alpha)} - \frac{\Delta \alpha}{r_h} + \nu \frac{R_c \xi_c + R_f \xi_f}{r_h^2}
\end{aligned} \tag{6.15}$$

where ε is the strand axial deformation and τ is the filament angle twist per unit length in the strand.

Projecting wire forces on strand axial directions, both axial force and moment can be computed as:

$$\begin{aligned}
F &= T \sin(\alpha) + N' \cos(\alpha) \\
M &= H \sin(\alpha) + G' \cos(\alpha) + T r_2 \cos(\alpha) - N' r_2 \sin(\alpha)
\end{aligned} \tag{6.16}$$

Hence for a helical filament in a straight strand, equations above allow to bind loads to strand deformations as ε and τ , starting from initial configuration. Axial-twisting coupling can be highlight trough relation:

$$\begin{bmatrix} F \\ M \end{bmatrix} = \begin{bmatrix} C_1 & C_2 \\ C_3 & C_4 \end{bmatrix} \begin{bmatrix} \varepsilon \\ \beta \end{bmatrix} \tag{6.17}$$

where β , positive when twisting, is the rotational strain of the strand defined as:

$$\beta = (R_c + 2R_f) \tau \tag{6.18}$$

Load deformation laws are based on initial configuration of the strand, defined through R_c , R_f and α , and assumed stress free.

2.3.a. Numerical models

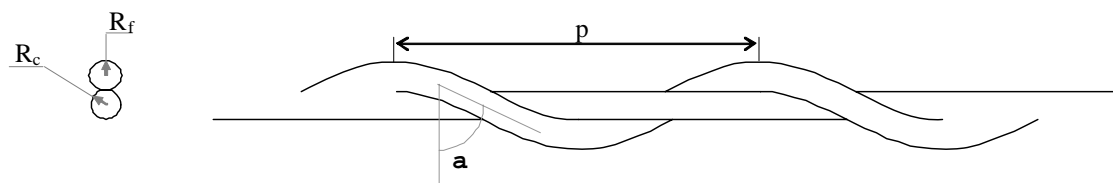
Simple straight strand

A simple straight numerical model is implemented to deduce axial response under both displacements imposed and tractions prescribed conditions.

Single filament

Numerical results upon a simple straight strand with a single helical filament are exposed. Both external and core filament are considered isotropic, homogeneous and linearly hyperelastic with Young modulus equal to 2500 MPa and Poisson ratio of 0.3. Geometrical strand configuration at zero stress, say it B_0 , is highlighted in the following table.

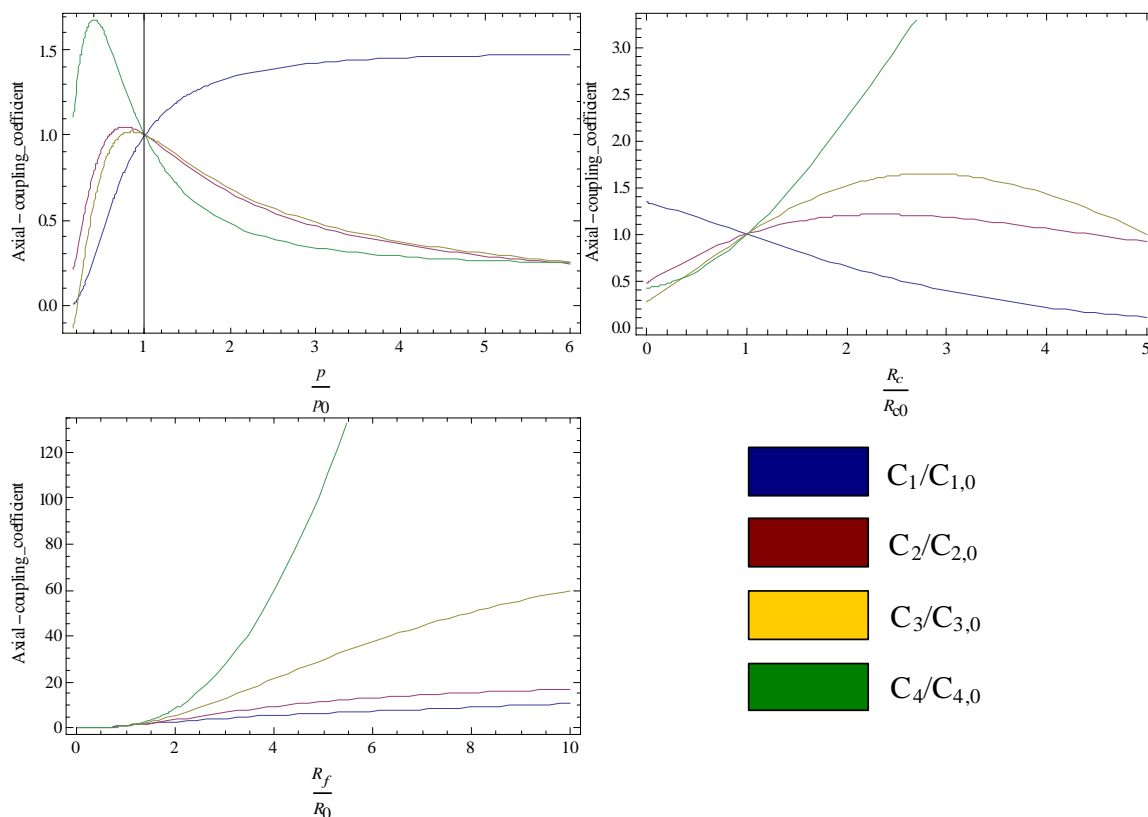
R_c	R_f	p	α
mm	mm	mm	°
2	2	50	63.3134



Cross section and front of a straight strand with a single external filament.

Thanks to Costello theory is possible to deduce mechanical behavior of such kind of strand.

Applying load conditions not so far from initial configuration as to ensure $|\Delta\alpha| \ll 1$, the four coefficients of axial-twisting coupling can be determined.



Graph 6.2. Axial-Torsional coupling coefficients on strand parameters configuration variation.

Axial-twisting coupling

Is remarkable at this point, to investigate how the coefficient of the axial-twisting coupling matrix varies changing initial configuration B_0 . Graphs below show the four coefficient dependence on filament radius, core radius, and helical filament pitch; each value is normalized on respective value in B_0 configuration.

Strand performances

To better understand material performances on helical wire configuration in a straight strand, its mechanical behavior is compared to behavior of the same filament used in the strand configuration, i.e. same length and sectional cross area, in a straight cylinder configuration. Performance of such cylinder configuration, say it reference configuration, made of the same material used for the wire, is investigated under same loads, F and M axial and torsional load, respectively, and same displacement applied on helical configuration, say ΔL and $\Delta \theta$ axial and torsional displacements, respectively. Hence reference stiffness coefficients of bulk configuration can define direct relations between forces and strand deformations:

$$\begin{aligned} F_R = C_{R1} \varepsilon &= \pi R_f^2 E \varepsilon \sin(\alpha) & , \Delta L_R = \Delta L \\ M_R = C_{R2} \beta &= G_s \frac{\pi R_f^4}{2(R_c + R_f)} \beta \sin(\alpha) & , \Delta \theta_R = \Delta \theta \end{aligned} \quad (6.19)$$

in case of displacements applied conditions,

$$\begin{aligned} \Delta L_R = \frac{F}{C_{R1}} &= \frac{F}{\pi R_f^2 E \sin(\alpha)} & , F_R = F \\ \Delta \theta_R = \frac{2M}{C_{R2}} &= \frac{2M(R_c + R_f)}{\pi R_f^4 G_s \sin(\alpha)} & , M_R = M \end{aligned} \quad (6.20)$$

in case of tractions prescribed conditions, for a unit length strand,

where E and G_s are material Young modulus and shear modulus, respectively, and ε and β are strand deformations; equivalently for the strand cylindrical core:

$$F_c = C_{C1} \varepsilon = \pi R_c^2 E \varepsilon \quad M_c = C_{C2} \beta = G_s \frac{\pi R_c^4}{2R_f} \beta \quad (6.21)$$

Note that values of $\frac{C_{R1}}{\sin(\alpha)}$ and $\frac{C_{R2}}{\sin(\alpha)} R_c + R_f$ represent the effective axial and torsional

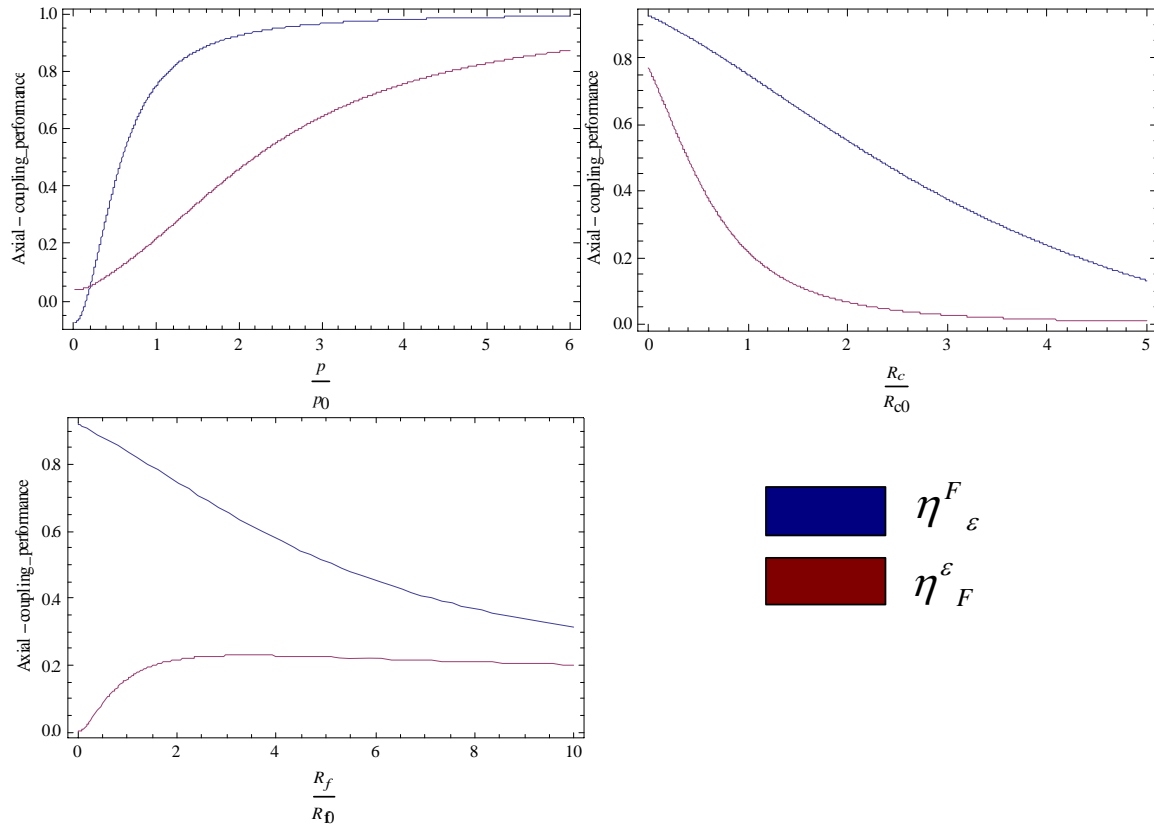
stiffness, respectively, in the reference configuration. To evaluate stiffness variation using a wire in simple straight strand more than reference configuration, is essential to define test boundary condition. Hence axial-torsional coupling gives, for the same strand, different values of stiffness whether displacements or tractions are applied, more than in no coupling configurations. In the following table calculation of performances for a helical filament in a straight strand referred to straight cylinder behavior are shown varying boundary conditions.

Voigt	$\varepsilon \neq 0 \quad \beta = 0$	$\varepsilon = 0 \quad \beta \neq 0$
Yield	$\eta^F_\varepsilon = \frac{F}{F_R} = \frac{C_1}{C_{R1}}$	$\eta^M_\beta = \frac{M}{M_R} = \frac{C_4}{C_{R2}}$
Reuss	$F \neq 0 \quad M = 0$	$F = 0 \quad M \neq 0$
Yield	$\eta^\varepsilon_F = \frac{\Delta L_R}{\Delta L} = \frac{1}{\frac{D_1}{C_{R1}}}$	$\eta^\beta_M = \frac{\Delta \theta_R}{\Delta \theta} = \frac{1}{\frac{D_4}{C_{R2}}}$

Table 6.3. Axial and Torsional stiffness performances.

Following graphs show the strand performances, as defined in upper table, varying strand configuration with filament radius, core radius, and helical filament pitch.

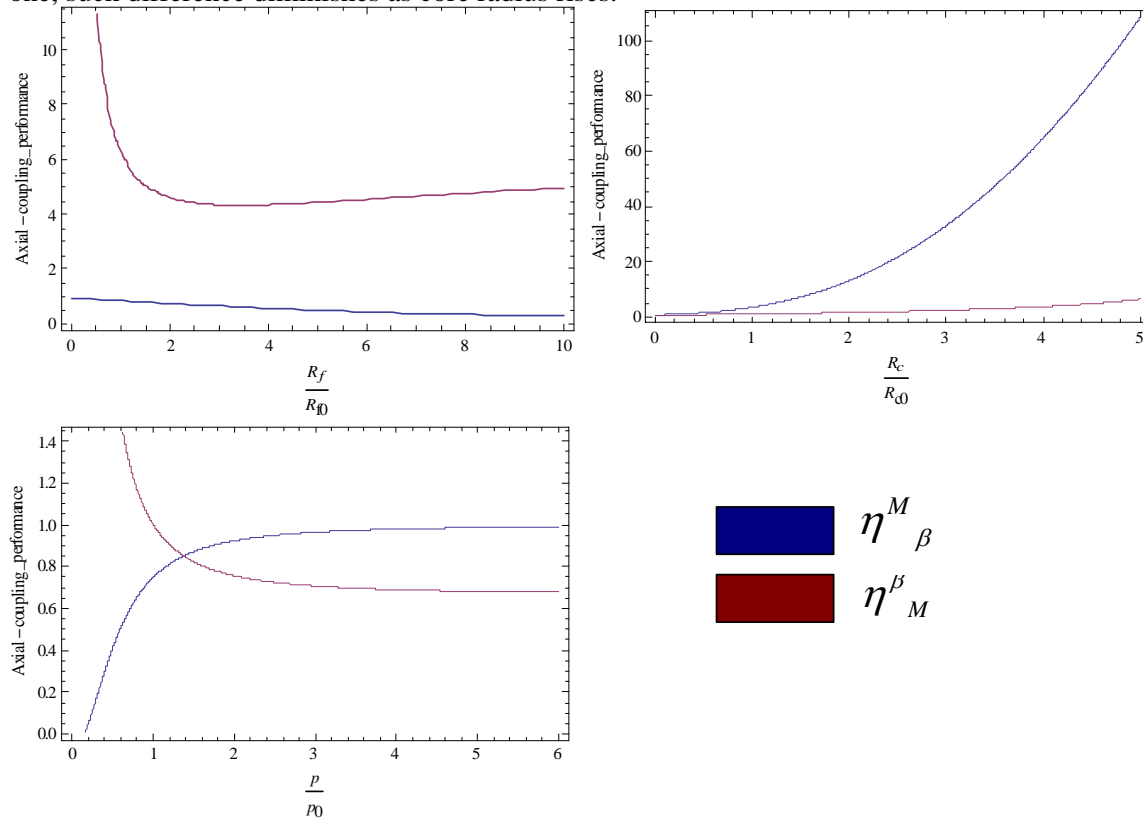
Axial stiffness performances η^F_ε and η^ε_F , to displacements and tractions prescribed test, respectively, by varying strand configuration results always less than unit, Reuss calculations appears always below Voigt calculations as theory prescribes. This behaviour affirms that using a wire in strand configuration, is less axially stiffness than same wire in straight cylindrical configuration.



Graph 6.3. Axial stiffness performances on strand parameters configuration variation.

This trend derives from wire wrapping. In case of displacements prescribe conditions, to stretch an helical wire wrapped around a core in axial direction of a length ΔL , the wire is both axially stretched and straightened, that is applied displacement derives from axial as well as bending and torsional stiffness, last terms need less energy to stretch the wire in axial strand direction. On the contrary in straight cylindrical wire axial displacement is linked just too axial stiffness, and a higher work has necessary to cover ΔL . Same considerations can follow considering compliance instead of stiffness in case of tractions prescribe conditions. In core radius varying graphs, appears a null value convergence, it is for helix angle tends to increase as core radius rises, hence work spent to unwrapping the helix increases. In pitch varying graphs, appears a unit value convergence, it is for strand configuration tends to straight cylindrical configuration while helical pitch increases, hence straighten work diminishes.

Torsional stiffness performances η^M_β and η^β_M , related to displacements and tractions prescribed test, respectively, by varying strand configuration results in different values, Reuss calculations appears always below Voigt calculations as theory prescribes but in case of low pitch varying curves. Whether torsional performance ratio is higher than unit or not, in case of displacements prescribe conditions, depends on entity of axial wire stretch produced by applied strand torsion $\Delta\theta$. If angular displacement causes a high axial wire stretch, depending on strand configuration, ratio results greater then one as axial deformation needs a greater energy than torsional deformation. In case of high pitches, for example, where wire tends to straight, angular torsion cause a negligible wire axial stretch and ratio tends to unit. Is worth to observe that in case of tractions prescribed conditions for high value of the helix pitch, ratio tends to a value less than one, such difference diminishes as core radius rises.



Graph 6.3. Torsional stiffness performances on strand parameters configuration variation.

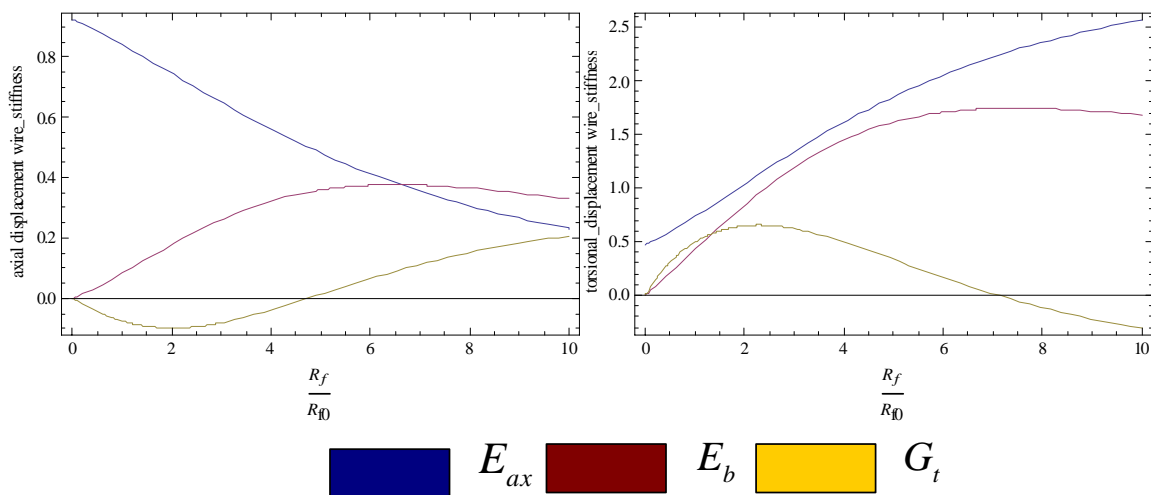
In a way to better compare stiffness in strand configuration to stiffness in reference configuration, stresses generated in the wire are calculated. Axial tests, for both displacements and tractions

applied conditions, generate in the wire cross sectional area of reference configuration only stresses in axial directions, σ_R^{ax} , as well as torsional tests generate in the cross sectional area only shear stress, σ_R^s . Such load conditions, instead, cause in wire cross sectional area of straight strand configuration both shear stress due to torsional stretch, σ^t , and normal stresses due to axial, σ^{ax} , and bending wire stretch, σ^b . Is, hence, possible to define stiffness moduli both in reference and strand configuration as shown in the table below.

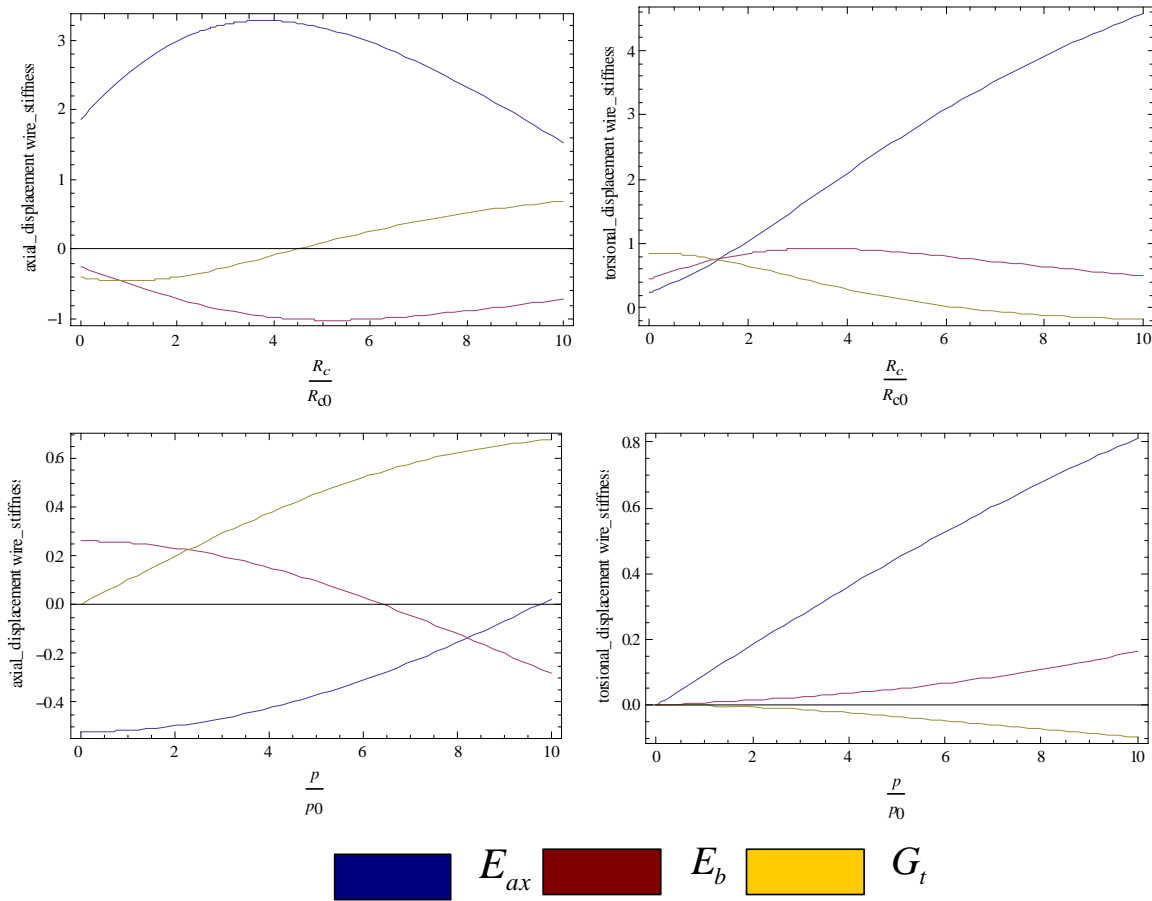
	Young modulus		Shear modulus
reference configuration	E		G_s
	Axial modulus	Bending modulus	Torsional modulus
straight strand configuration b=0	$E_{ax} = \frac{\sigma^{ax}}{\varepsilon}$	$E_b = \frac{\sigma^b}{\varepsilon}$	$G_t = \frac{\sigma^t}{\varepsilon} (R_c + R_f)$
straight strand configuration e=0	$E_{ax} = \frac{\sigma^{ax}}{\beta}$	$E_b = \frac{\sigma^b}{\beta}$	$G_t = \frac{\sigma^t}{\beta} (R_c + R_f)$

Table 6.4. Elastic constant calculations.

in case of tractions prescribed conditions, where E and G_s are material Young modulus and shear modulus, respectively, and ε and β are strand deformations; following graphs shown such entities normalized respect to respective reference moduli, as they varying with strand configuration properties. Tests are realized applying small deformations.



Graph 6.4. Elastic constants trend on strand parameters configuration variation.



Graph 6.5. Elastic constants trend on strand parameters configuration variation.

Constitutive behavior

Let's now introduce a non linear extension to Costello wire theory to a single straight strand in B_0 configuration, see table.

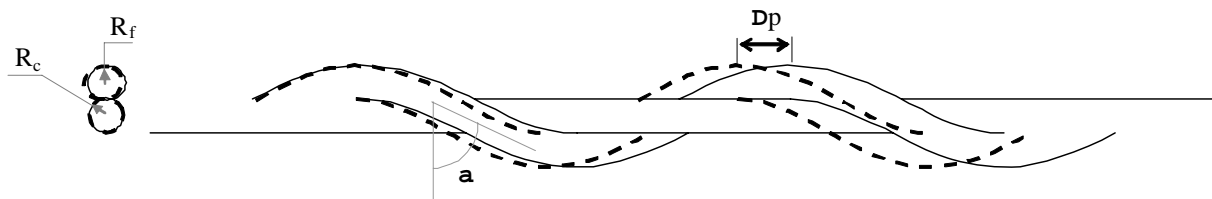
R_c	R_f	p	α
mm	mm	mm	°
2	2	50	63.3134

As load condition both axial and rotational deformation ε_1 , β_1 respectively, are applied separately to the strand, see table. Axial force and torsional moment on the external wire in the strand direction are computed as follow:

ε_1	$\Delta\alpha_{\varepsilon_1}$	β_1	$\Delta\alpha_{\beta_1}$	$\begin{bmatrix} F \\ M \end{bmatrix} = \begin{bmatrix} 21023.6 & 7183.24 \\ 38981.6 & 18729.1 \end{bmatrix} \begin{bmatrix} \varepsilon_1 \\ \beta_1 \end{bmatrix}$
	rad	rad	rad	
0.01	5.06E-03	0.1	5.16E-02	

such prescribe deformations cause a new geometric configuration of the strand, say it B_1 , as following table shown:

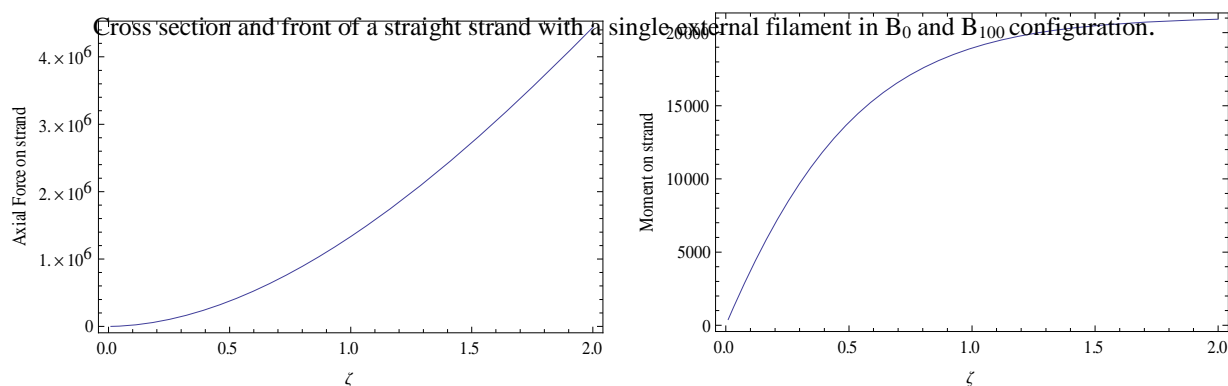
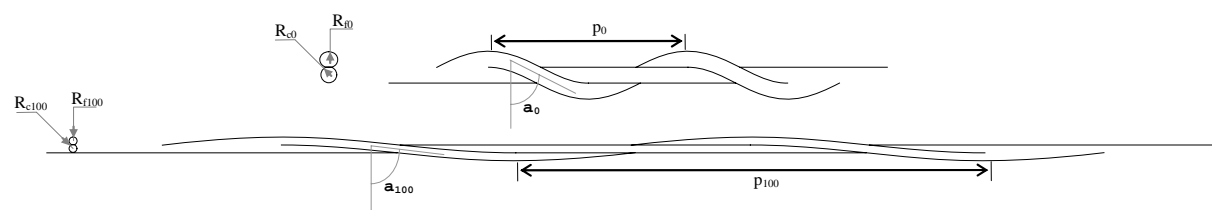
R_c	R_f	p	α
mm	mm	mm	°
1.99	1.98	44.6832	60.6438



Cross section and front of a straight strand with a single external filament in B_0 configuration. Dashed lines refer to deformed strand B_1 configuration.

Costello model prescribes to apply small load starting from initial configuration, as in the case of B_0 strand configuration subject to ε_1 , β_1 deformations. Such loads lead to new strand geometry B_1 , see table before. Starting from this deformed configuration is possible to apply another admissible load step that will produce another configuration, say B_2 , where apply another load step, and so on. Computing total forces acting on strand as sum of the forces acting in the previous calculations is possible to draw force-deformation curve. Non linear mechanical behavior of simple straight strand with one external helical filament is exposed in the following.

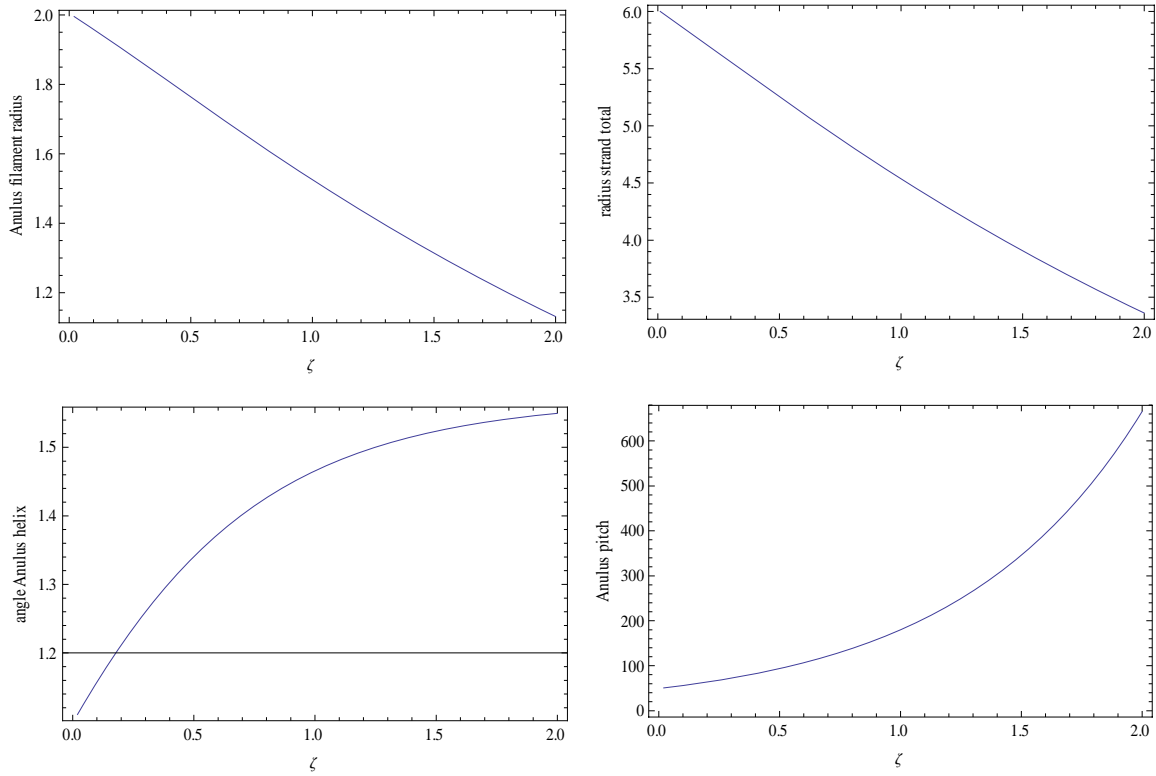
Starting from strand configuration shown above, B_0 , with zero stress, strand is stretched till a 200% deformation is achieved, no strand rotation is allowed, $\beta = 0$ and 200 load step analyses are performed. In the follow cross sectional area and front of the strand are shown for B_0 and B_{100} configuration, that is configuration of the strand for no deformation and for 100% axial deformation.



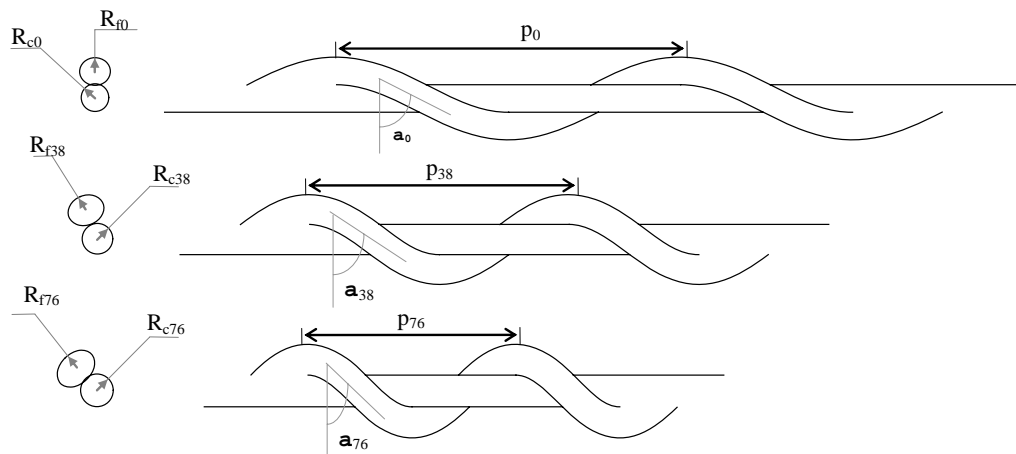
Graph 6.6. Strand mechanical response on axial deformation.

In following graphs, loads on total strand are computed. Due to axial-twisting coupling behavior of the strand, applying an axial deformation, means to generate in the strand both axial force reaction and torsional moment.

Curves of axial force on the strand, such as torsional moment, as strand deformation rises, are plotted. Graphs below show how strand configuration varies along the analyses.

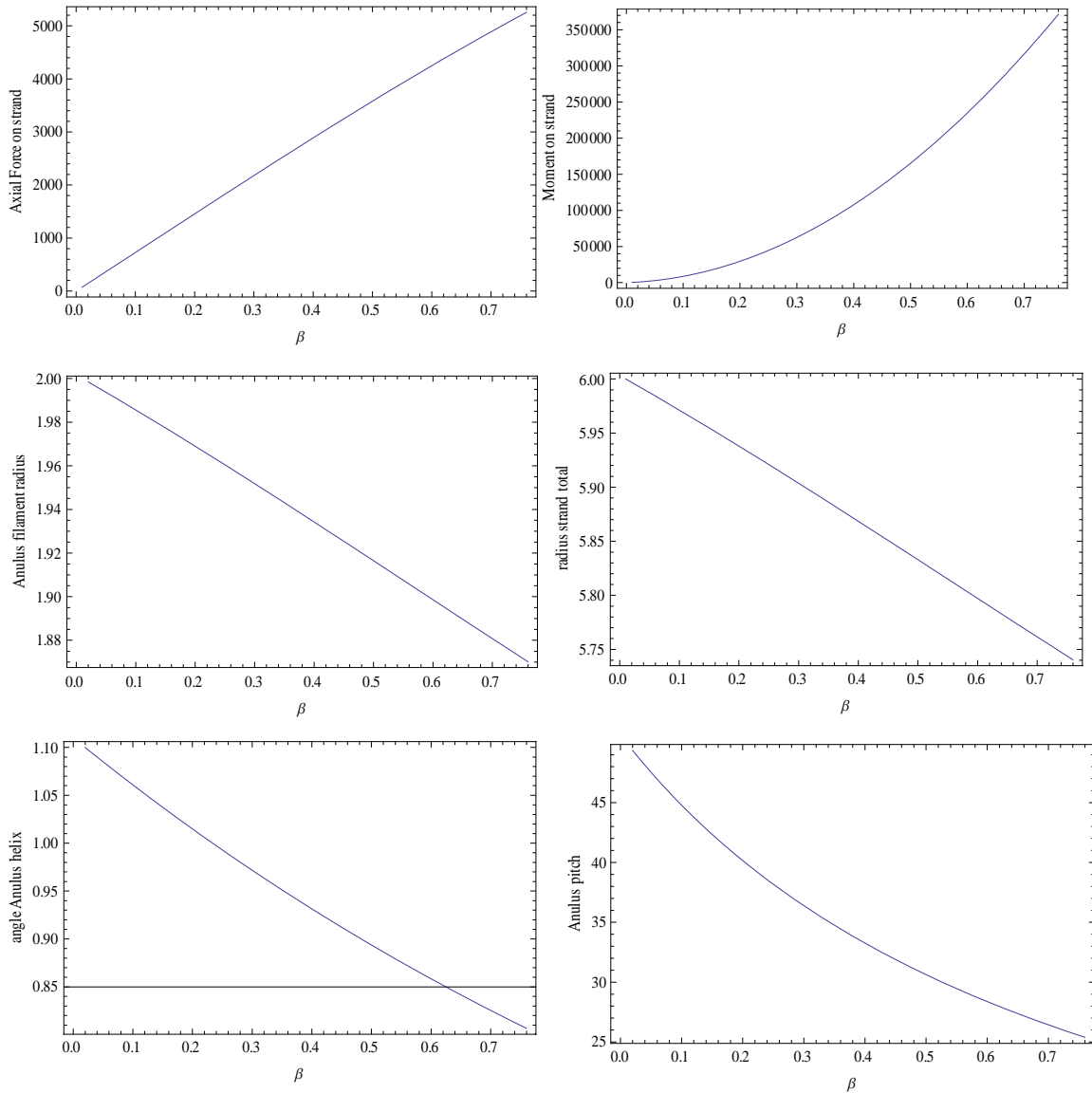


Graph 6.7. Strand parameters configuration on axial deformation.

Cross section and front of a straight strand with a single external filament in B_0 , B_{38} and B_{76} configuration.

$$\varepsilon = 0 \quad \beta \neq 0$$

Starting from strand configuration shown above, B_0 , with zero stress, strand is twisted of total 43° , no strand axial deformation is allowed, $\varepsilon = 0$, and 76 load step analyses are performed. In the follow image cross sectional area and front of the strand are shown for B_0 , B_{38} and B_{76} configuration, that is configuration of the strand for no deformation and for 21.5° and 43° twisting. In following graphs, loads on total strand are computed. Due to axial-twisting coupling behavior of the strand, applying an axial rotation, means to generate in the strand both axial force reaction and torsional moment. Curves of axial force on the strand, such as torsional moment, as strand deformation rises, are plotted. Other graphs show how strand configuration varies along the analyses. Single filament straight strand response to tractions prescribes tests will be investigated further.

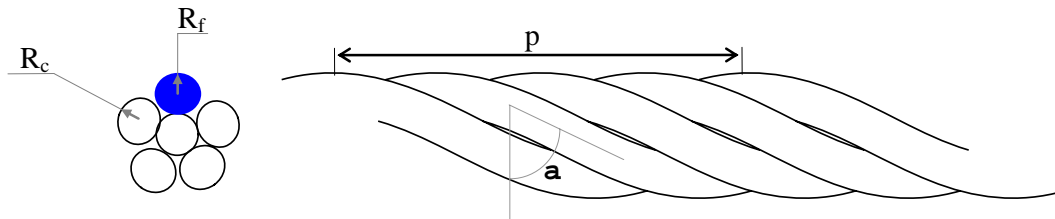


Graph 6.8. Strand mechanical response and parameters configuration on torsional deformation. $\varepsilon = 0$ $\beta \neq 0$

Single anulus

Numerical results upon a simple straight strand with a single anulus of filaments are exposed. As in previous case, core and external filaments are considered isotropic, homogeneous and linearly hyperelastic with Young modulus equal to 2.5 MPa and Poisson ratio of 0.3. Geometrical strand configuration at zero stress, say it B_{A0} , is highlighted in the following table.

R_c	R_f	p	α	n_f
mm	mm	mm	°	
2	2	50	63,3134	5



Cross section and front of a straight strand with a five filament external anulus.

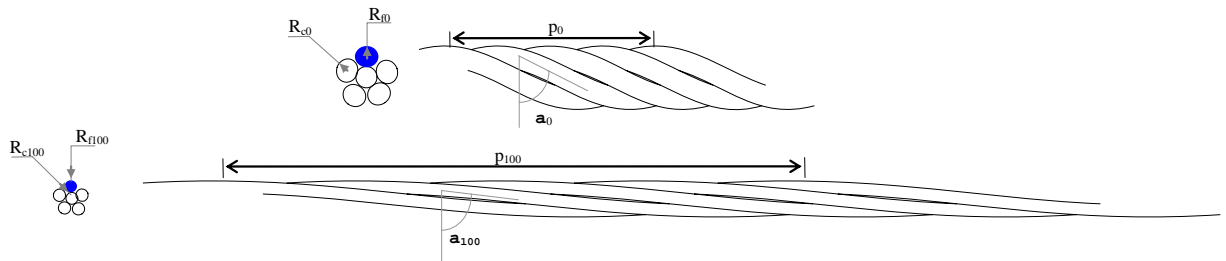
where n_f is the number of filaments in the anulus. Such integer is defined, in zero stress configuration, as the highest number of filaments filling the anulus in a way that they do not touch each other, that is each filament touches just only the core. This condition is expressed with inequality:

$$R_f \sqrt{1 + \frac{\tan^2\left(\frac{\pi}{2} - \frac{\pi}{m}\right)}{\sin^2(\alpha)}} < R_c + R_f \quad (6.22)$$

Anulus mechanical behavior is direct related to behavior of one of its single filament, see before. Hence, for the anulus, each of the four axial-twisting coupling constant values n_f times the value calculated for a single filament. While performance ratios have the same value.

Constitutive behavior

As done for single filament straight strand, nonlinear elastic behavior of a single anulus straight strand is investigated.

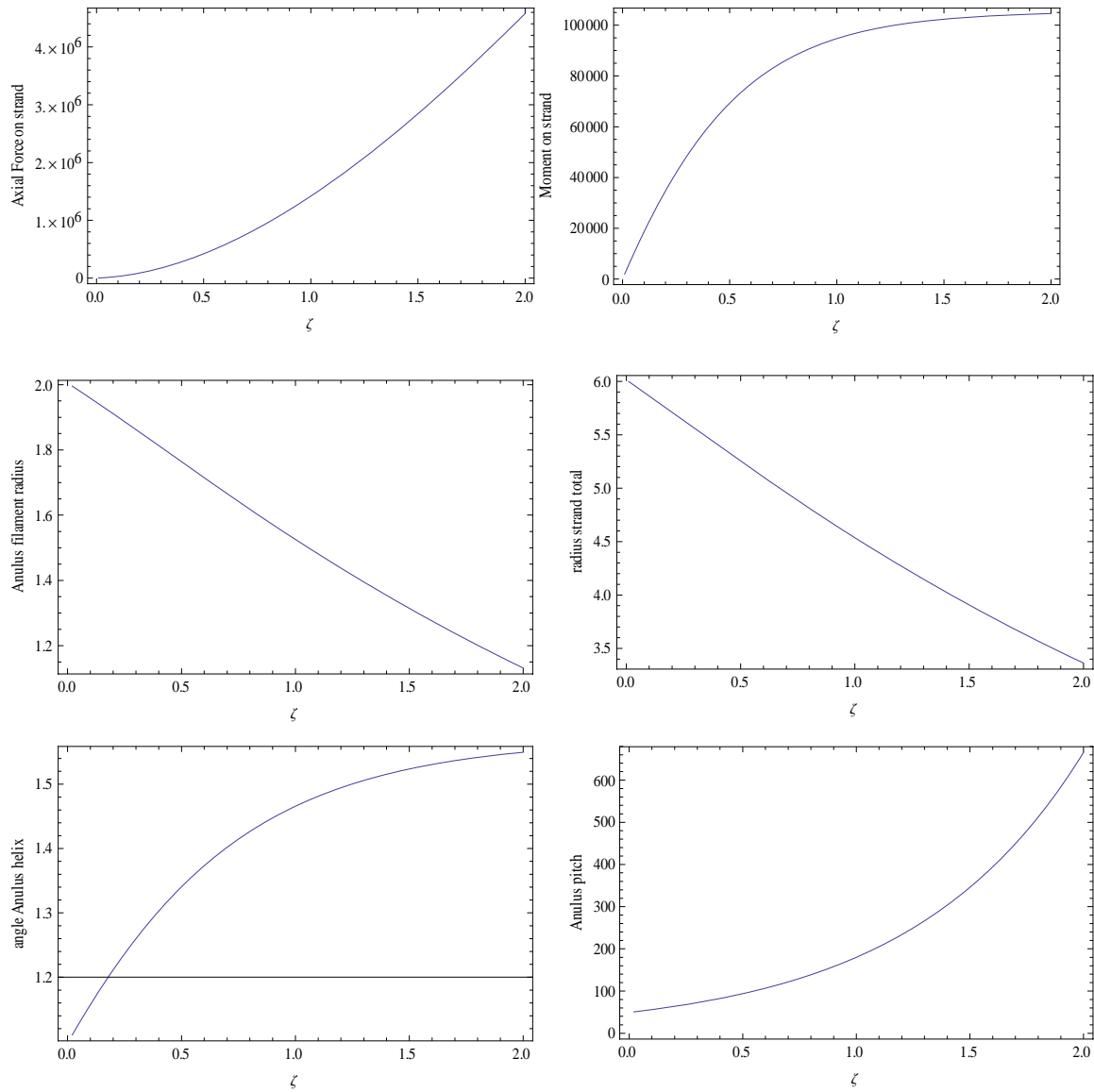


Cross section and front of a straight strand with a with a five filament external anulus in B_{A0} and B_{A100} configuration.

$$\varepsilon > 0 \quad \beta = 0$$

Starting from strand configuration shown above, B_{A0} , with zero stress, strand is stretched till a 200% deformation is achieved, no strand rotation is allowed, $\beta = 0$, and 200 load step analyses are performed. In the follow cross sectional area and front of the strand are shown for B_{A0} and B_{100} configuration, that is configuration of the strand for no deformation and for 100% axial deformation.

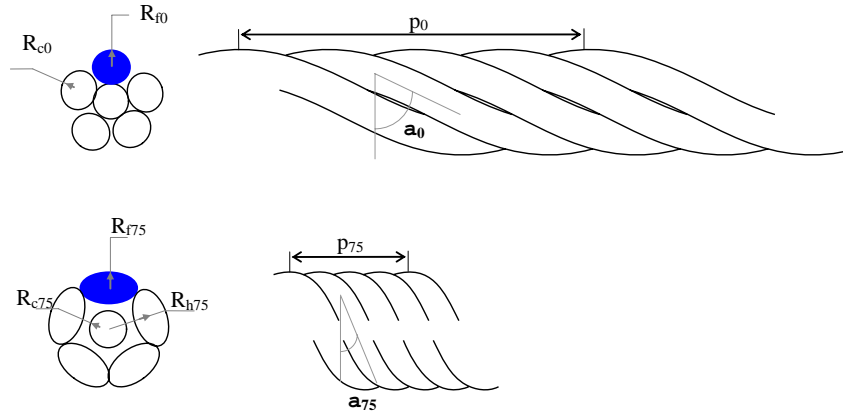
As the annulus is a sum of five filaments, and a filament in B_{A0} has the same configuration of the wire in B_0 , total axial and torsional load of the strand results n_f times the value obtained for B_0 initial configuration. While deformation of the wire remain exactly the same, as graphs below shown.



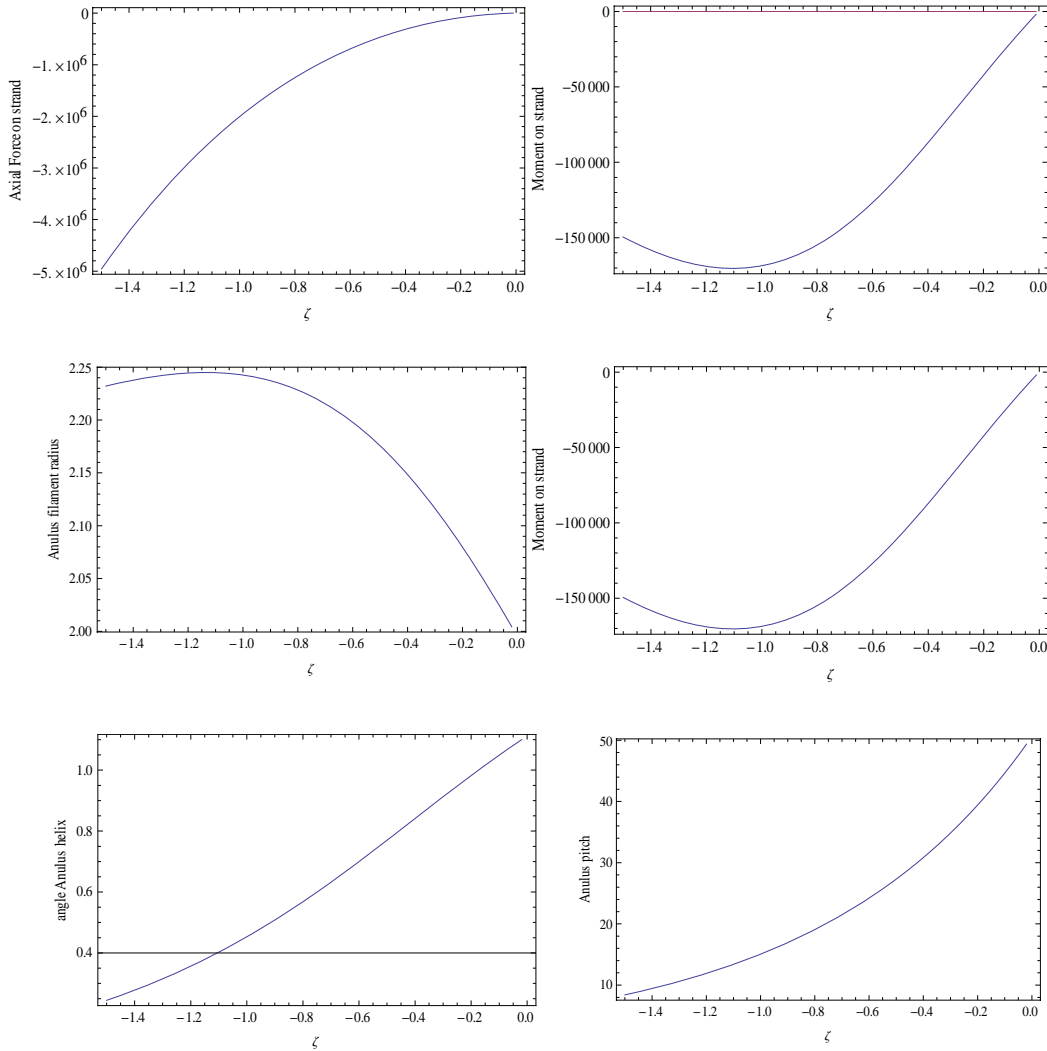
Graph 6.9. Strand mechanical response and parameters configuration on axial deformation. $\varepsilon > 0 \quad \beta = 0$

$$\varepsilon < 0 \quad \beta = 0$$

Relevant differences can occur, between single filament and single anulus straight strand configuration, when the strand is subject to compression $\varepsilon < 0$.



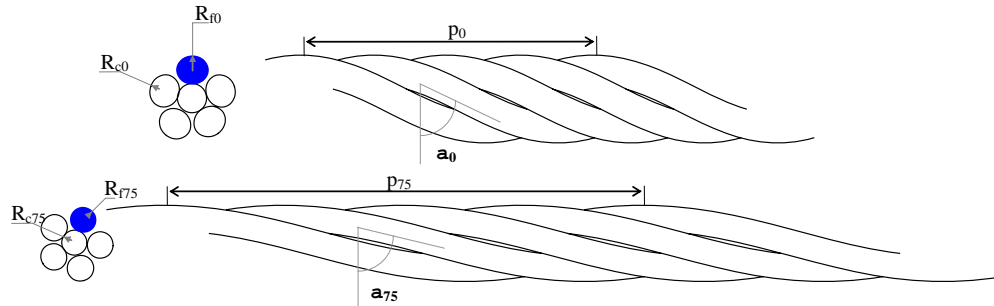
Cross section and front of a straight strand with a five filament external anulus in B_{A0} and B_{A75} configuration.



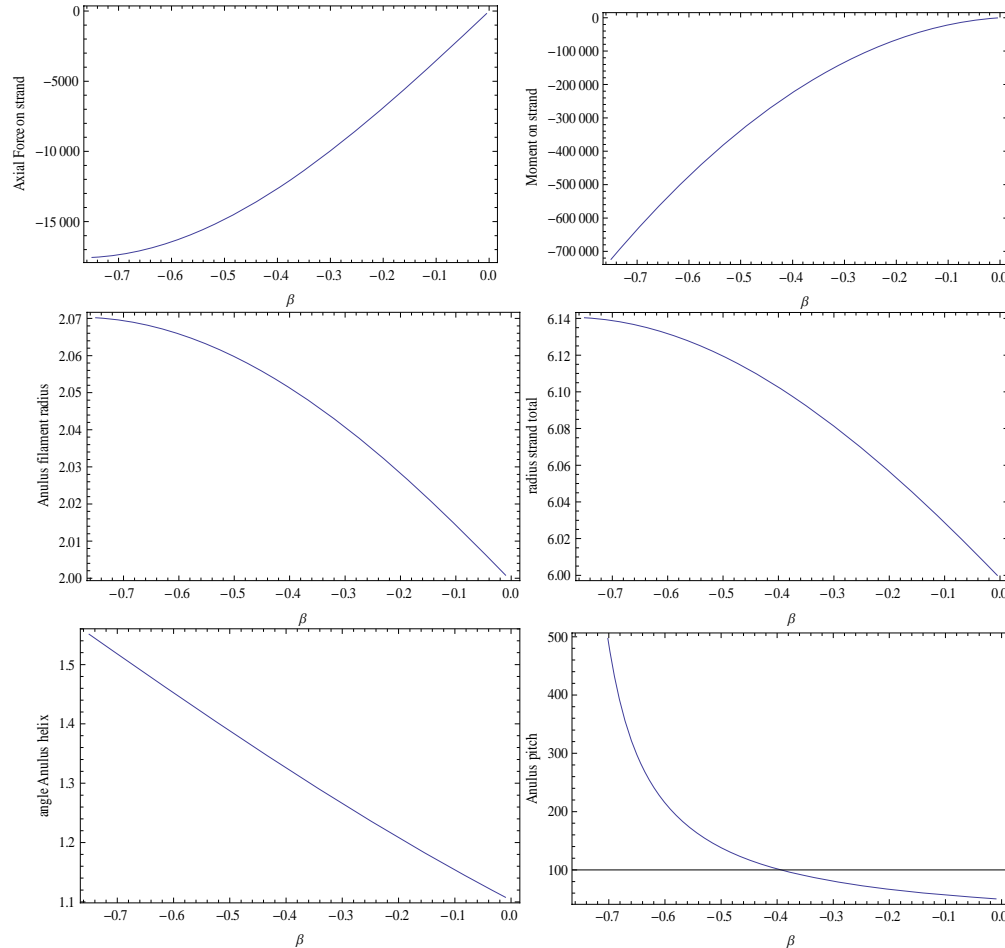
Graph 6.10. Strand mechanical response and parameters configuration on axial deformation. $\varepsilon < 0 \quad \beta = 0$

Since compression causes the helix angle decreasing, hence happen that anulus wire touch each other and core detaching occurs. In this case wire helical radius R_h results greater than sum of core and filament radius, as in B_0 configuration, and wire mechanics changes. In the rope mechanics this event is called bird caging. Starting from strand configuration shown above, B_{A0} , with zero stress, strand is compressed till a 150% deformation is achieved, no strand rotation is allowed, $\mathbf{b}=0$, and 150 load step analyses are performed. In the follow cross sectional area and front of the strand are shown for B_{A0} and B_{75} configuration, that is configuration of the strand for no deformation and for 75% axial deformation.

$$\varepsilon = 0 \quad \beta < 0$$



Cross section and front of a straight strand with a five filament external anulus in B_{A0} and B_{A75} configuration.



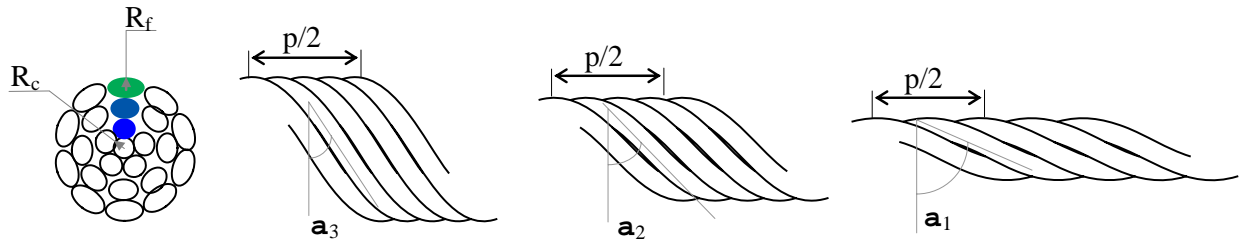
Graph 6.11. Strand mechanical response and parameters configuration on torsional deformation. $\varepsilon = 0 \quad \beta < 0$

Starting from strand configuration shown above, B_{A0} , with zero stress, strand is untwisted of total 43° , no strand axial deformation is allowed, $\varepsilon = 0$, and 150 load step analyses are performed. In the follow image cross sectional area and front of the strand are shown for B_{A0} and B_{A75} configuration, that is configuration of the strand for no deformation and for 21.5° untwisting. In following graphs, loads on total strand are computed. Due to axial-twisting coupling behavior of the strand, applying an axial rotation, means to generate in the strand both axial force reaction and torsional moment. Curves of axial force on the strand, such as torsional moment, as strand deformation rises, are plotted and compared to behavior of reference configuration. Other graphs show how strand configuration varies along the analyses. Is worth to observe that for a $\beta < 0$ test bird caging can occurs.

Multi anuli

Numerical results upon a simple straight strand with three anuli of filaments are exposed. As in previous case, core and external filaments are considered isotropic, homogeneous and linearly hyperelastic with Young modulus equal to 2.5 MPa and Poisson ratio of 0.3. Geometrical strand configuration at zero stress, say it B_{M0} , is highlighted in the following table.

R_c	R_f	p	α_1	n_{f1}	n_{f2}	n_{f3}
mm	mm	mm	°			
2	2	50	63,3134	5	8	10



Cross section and front of a straight strand with three external anulus.

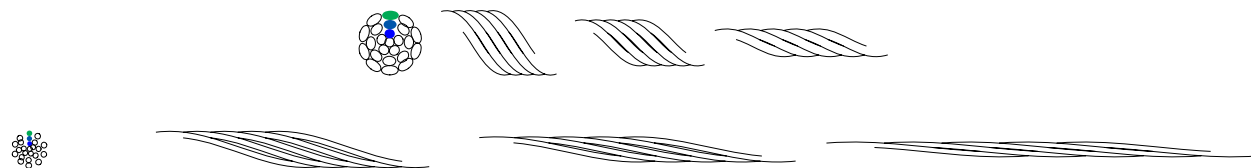
where n_i is the number of filaments in the i^{th} anulus, and α_i is the helix angle in the i^{th} anulus, in no stress configuration, numbered form inner to outer.

Constitutive behavior

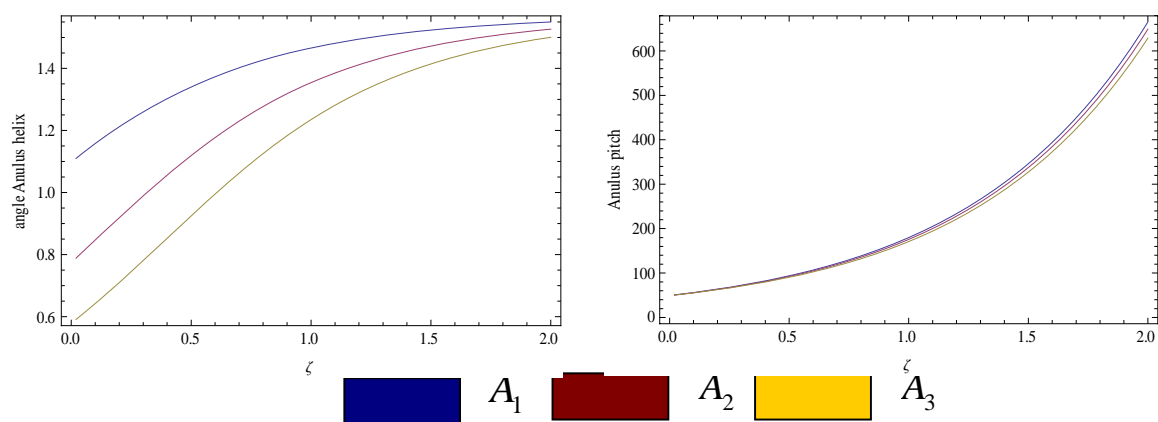
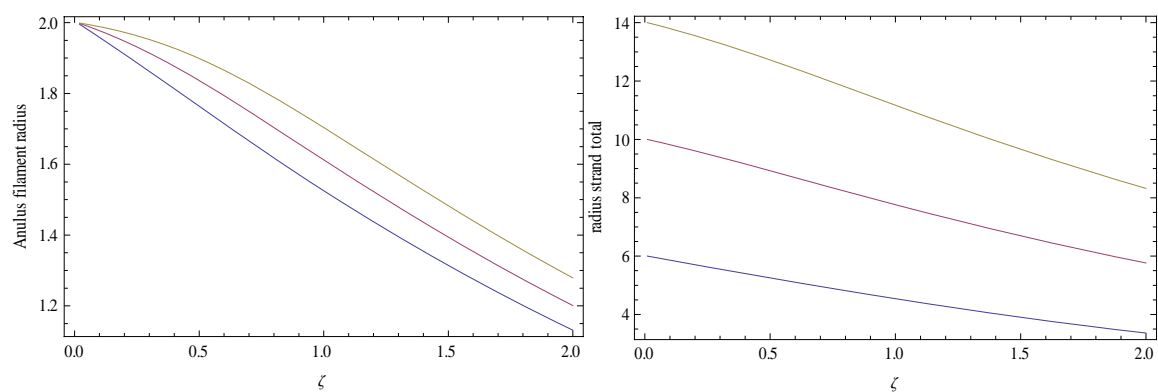
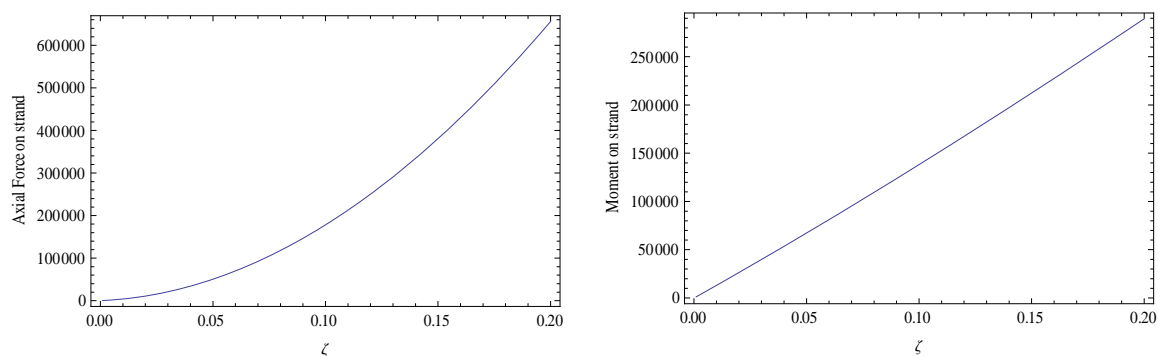
As done for single anulus straight strand, nonlinear elastic behavior of a multi anuli straight strand is investigated.

$$\varepsilon > 0 \quad \beta = 0$$

Starting from strand configuration shown above, B_{M0} , with zero stress, strand is stretched till a 200% deformation is achieved, no strand rotation is allowed, $\beta = 0$, and 200 load step analyses are performed. In the follow cross sectional area and front of the strand are shown for B_{M0} and B_{M100} configuration, that is configuration of the strand for no deformation and for 100% axial deformation.



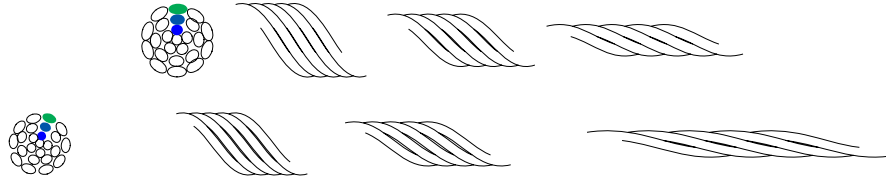
Cross section and front of a straight strand with three external anulus in B_{M0} and B_{M100} configuration.



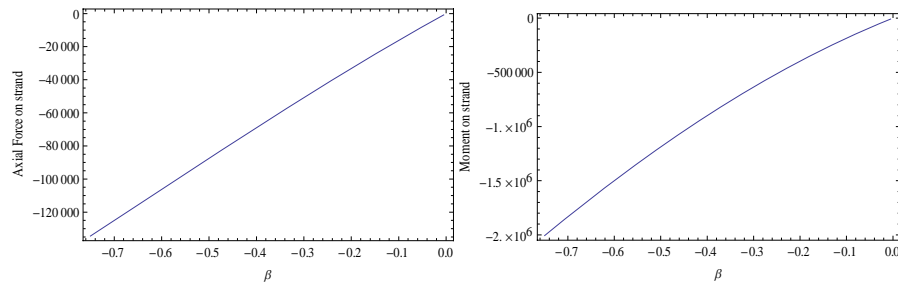
Graph 6.13. Strand parameters configuration on axial deformation. $\varepsilon > 0$ $\beta = 0$

$$\varepsilon = 0 \quad \beta < 0$$

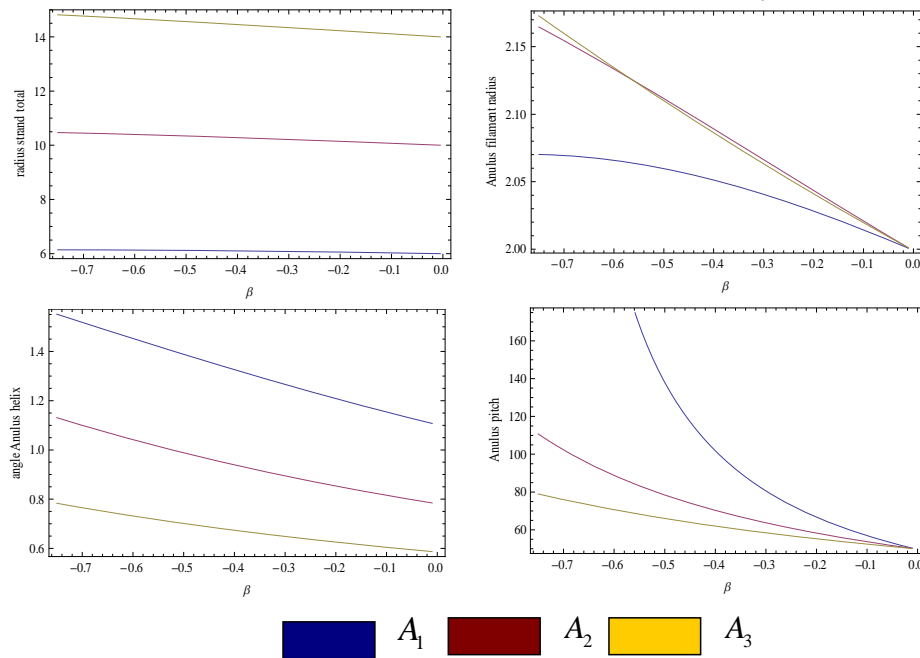
Starting from strand configuration shown above, B_{M0} , with zero stress, strand is untwisted of total 43° , no strand axial deformation is allowed, $\varepsilon = 0$, and 150 load step analyses are performed. In the follow image cross sectional area and front of the strand are shown for B_{M0} and B_{M75} configuration, that is configuration of the strand for no deformation and for 21.5° untwisting. In following graphs, loads on total strand are computed. Is worth to observe that even in this case for a $\beta < 0$ test bird caging can occurs.



Cross section and front of a straight strand with a five filament external anulus in B_{M0} and B_{M75} configuration.



Graph 6.14. Strand mechanical response on torsional deformation. $\varepsilon = 0 \quad \beta < 0$



Graph 6.15. Strand parameters configuration on torsional deformation. $\varepsilon = 0 \quad \beta < 0$

2.3 Axial-twisting effects on composites materials

The axial-twisting effects of reinforcing fibers are computed in the analysis of composite material by Costello, Shield and Costello (1994), using the Kirchhoff plate theory as reported in the following. Fiber properties are evaluated through the meaning of linear theory for the response of a cord, it's easy to extend such study taking in account the cord behavior as non linear by the approach exposed before.

To include these effects Costello developed a more general theory.

Classical lamination theory is based on some approximations that are not necessary when considering cord composites. In classical lamination theory, the exact distribution of the cord in the ply is not taken into account. With typical fiber composites this is a benefit, because the exact location of the reinforcement is not known. However, in cord composites the cords are purposefully placed carefully in the matrix, and their location is known. Typically, the cords are all evenly spaced at specific heights through the thickness of the plate. The cord is al so much larger than a typical fiber in a fiber composite.

Fibers are usually several orders of magnitude smaller than the thickness of the ply while the cords are on the order of the thickness of the ply.

Starting from Costello cord theory a model for non linear analysis of axial-coupling response in the helical arrangement of the fiber cords is developed. Than equilibrium formulation will be presented for the analysis of cord composite.

For this theory the action o f the cords will be smeared out over the layer containing the cords, but acting at the exact height that they are placed in the ply. Three specific problems was solved using this method: (1) the solution to the axial tension problem along the cord axis, (2) the solution of the axial tension problem perpendicular to the cord axis, and (3) the Solution to the pure shear problem, thus the effective moduli in the 1 and z-directions can be predicted as well as the amount of extension-twisting coupling .The Courier series solution to the general loading case of a simply supported plate as given in Kittredge (1991).

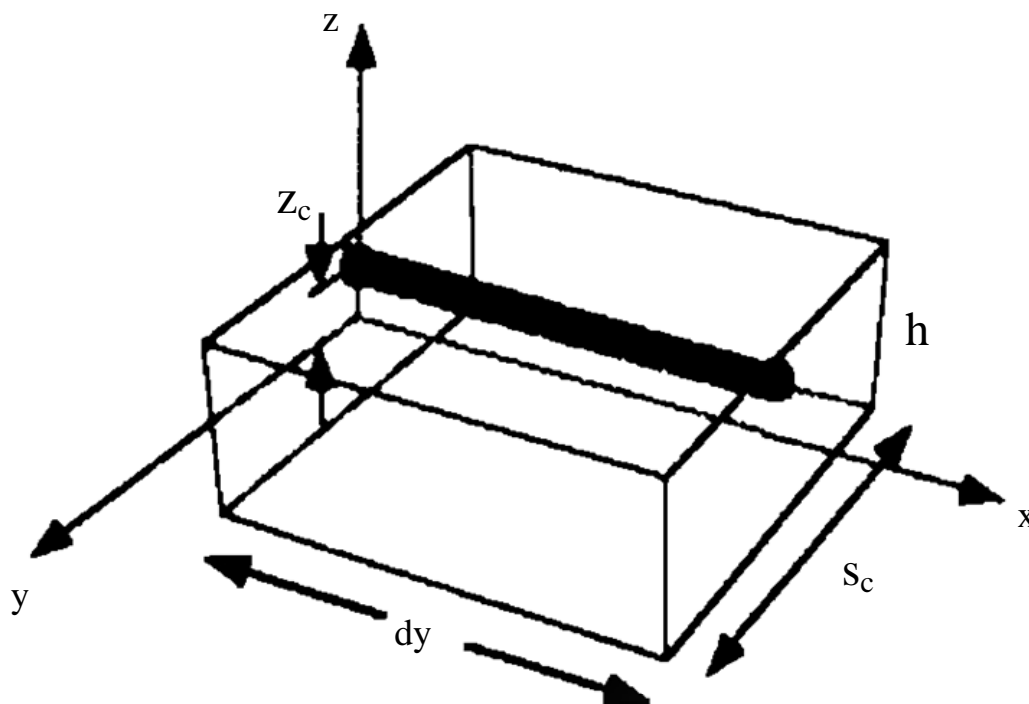


Fig. 6.2. Cord element.

Steel cord-rubber composites have a characteristic large stiffness ratio mismatch. The stiffness ratio, E_{cord} / E_{matrix} , can range from 58 for vulcanized rubber to between 3000-50,000 for synthetic rubbers. With this large mismatch between the moduli, the shear in the plate cannot be ignored for most loading situations. However, the Kirchhoff theory is a reasonable approximation in cases where the ends of the plate are constrained to remain normal and plane, or if the cords are close to the middle surface. Hence the Kirchhoff theory is a reasonable approximation for problems involving uniaxial tension with the cords along the neutral surface. The matrix material is considered to be linear elastic. This approximation is valid, because the rubber typically sees small strains due to the presence of the much stiffer cords. No viscoelastic properties are taken into account. The cords are treated as unimodular, having the same response in tension as in compression. The bimodular property of the cords has been dealt with elsewhere in the literature (Prakash et al, 1992). The results are compared with the results of Gough and Tangorra, as well as Akasaka and Hirano, to evaluate the suitability of these theories.

The formulation will be based upon the equilibrium of a small element of the plate. The in-plane and out-of-plane plate equations for an infinitesimal element of lengths of lengths dx and dy and height h can be derived by summing forces and moments on the element in the x , y , and z directions. If the changes in force and moment resultants across the element are represented by a first-order Taylor series, the usual plate equilibrium equations arise:

$$\frac{\partial N_x}{\partial x} + \frac{\partial N_{yx}}{\partial y} + p_x = 0 \quad (6.23),$$

$$\frac{\partial N_{xy}}{\partial x} + \frac{\partial N_y}{\partial y} + p_y = 0 \quad (6.24),$$

$$N_{xy} = N_{yx},$$

$$\frac{\partial Q_x}{\partial x} + \frac{\partial Q_y}{\partial y} + p_z = 0 \quad (6.25),$$

$$\frac{\partial M_x}{\partial x} + \frac{\partial M_{yx}}{\partial y} - Q_x = 0 \quad (6.26),$$

and

$$\frac{\partial M_{xy}}{\partial x} + \frac{\partial M_y}{\partial y} - Q_x = 0 \quad (6.27).$$

Equations 4-6 can be combined to yield the plate equation

$$\frac{\partial^2 M_x}{\partial x^2} + \frac{\partial^2 (M_{xy} + M_{yx})}{\partial x \partial y} + \frac{\partial^2 M_y}{\partial y^2} + p_z = 0 \quad (6.28).$$

While these equations were derived for an infinitesimal plate element, one approximation is to extend their use to an element that has finite length in one dimension. Consider the cord composite plate element shown in fig 6.2. The x -direction lines up with the cord direction and the element has finite length, S_c , in the y -direction, where S_c is the perpendicular spacing between the cords. The thickness of the element is h . The cord is a simple strand and is on the

middle surface. As an approximate solution, one can enforce the plate eqs. (6.23) - (6.25) and (6.28) derived above on this element. However, some of the assumptions made when deriving those equations may be violated. For example, because of the finite length, a first-order Taylor series approximation may not be accurate enough. Also, because of the finite length, it may be possible for the element in fig. 6.2 to have a moment resultant in the z -direction, due to the variation of σ_x with y over the length s_c . This model with the above approximations is identical with that for an infinitesimal element with the contributions of the cord smeared out along the plane containing the cord, In an element of width dy , there would be dy/s_c cords distributed across the element, and hence the contribution of the cords to the resultants acting on this element would be found by multiplying the resultants of a single cord by dy/s_c .

The theory exposed uses the Kirchhoff theory approximations, The displacements along the x and y -directions are assumed to be linear functions of the thickness coordinate z ; the transverse displacement is assumed to be constant through the thickness of the plate; hence

$$\begin{aligned} u(x, y, z) &= U(x, y) - z \frac{\partial W}{\partial x} \\ v(x, y, z) &= V(x, y) - z \frac{\partial W}{\partial y} \end{aligned} \quad (6.29)$$

and

$$w(x, y, z) = W(x, y)$$

where U, V , and W are the displacement of a point (x, y) on the middle surface.

The constitutive equations for a plate element of the composite are deduced by taking into account the contribution from the matrix plus a contribution from the cord. The matrix resultant contributions can be found by considering an equivalent element made entirely of the matrix material. The loss in stiffness of the matrix due the loss of volume of the matrix (the volume occupied by the cords) is neglected. The components of the resultants due to the matrix are given by

$$\begin{aligned} M_{xm} &= \int_{-h/2}^{h/2} \sigma_x z dz = -D_m \left(\frac{\partial^2 W}{\partial x^2} + \nu_m \frac{\partial^2 W}{\partial y^2} \right), \\ M_{ym} &= \int_{-h/2}^{h/2} \sigma_y z dz = -D_m \left(\frac{\partial^2 W}{\partial y^2} + \nu_m \frac{\partial^2 W}{\partial x^2} \right) \\ M_{xym} &= M_{yxm} = \int_{-h/2}^{h/2} \tau_{xy} z dz = -(1 - \nu_m) D_m \frac{\partial^2 W}{\partial xy} \\ N_{xm} &= \int_{-h/2}^{h/2} \sigma_x dz = C_m \left(\frac{\partial U}{\partial x} + \nu_m \frac{\partial V}{\partial y} \right) \end{aligned}$$

$$N_{ym} = \int_{-h/2}^{h/2} \sigma_y dz = C_m \left(\frac{\partial V}{\partial y} + \nu_m \frac{\partial U}{\partial x} \right), \quad (6.30)$$

and

$$N_{xym} = \int_{-h/2}^{h/2} \tau_{xy} dz = \frac{1-\nu_m}{2} C_m \left(\frac{\partial U}{\partial y} + \frac{\partial V}{\partial x} \right),$$

where $C_m = \frac{E_m h}{1-\nu_m^2}$, $D_m = \frac{E_m h^3}{12(1-\nu_m^2)}$, E_m is the modulus of elasticity of the matrix

material and ν_m is the Poisson's ratio for the matrix material.

The resultant contributions due to the cord are based on the Costello theory cord assumptions. The cord is assumed to be able to transmit only a force in the x -direction, a twisting moment in the y - z plane. Hence

$$M_{yc} = M_{yxc} = N_{yc} = N_{xyc} = 0 \quad (6.31).$$

The only nonzero resultant contributions are due to the bending moment M_b , the twisting moment M_t , and the axial force F .

$$\begin{aligned} M_{xc} &= \frac{M_b}{s_c} = \frac{-E_c R^4 c_5}{s_c} \frac{\partial^2 W}{\partial x^2}, \\ M_{xyc} &= \frac{-M_t}{s_c} = \frac{-E_c R^3}{s_c} \left[c_3 \frac{\partial U}{\partial x} + c_4 R \frac{\partial^2 W}{\partial x \partial y} \right] \\ N_{xyc} &= \frac{F}{s_c} = \frac{A_c E_c}{s_c} \left[c_1 \frac{\partial U}{\partial x} + c_2 R \frac{\partial^2 W}{\partial x \partial y} \right] \end{aligned} \quad (6.32)$$

Note that equation (6.32) adds in-plane coupling to eq. (6.28).

The complete resultants are expressed by

$$M_x = M_{xm} + M_{xc},$$

$$M_y = M_{ym},$$

$$M_{xy} = M_{xym} + M_{xyc}$$

$$M_{yx} = M_{xym},$$

$$N_x = N_{xm} + N_{xc},$$

$$N_y = N_{ym}, \quad (6.33)$$

and

$$N_{xy} = N_{xym}.$$

It is evident from eqs. (6.33) that $M_{xy} \neq M_{yx}$, which is a usual assumption in plate and lamination theory (Jones 1975).

Equations (6.30)-(6.33) can be substituted into equations (6.23), (6.24) and (6.28), resulting in the equations of equilibrium in terms of the displacement:

$$C_m + \frac{c_1 A_c E_c}{s_c} \frac{\partial^2 U}{\partial x^2} + C_m \frac{1 - \nu_m}{2} \frac{\partial^2 U}{\partial y^2} + C_m \frac{1 + \nu_m}{2} \frac{\partial^2 V}{\partial x \partial y} + \frac{c_2 A_c E_c R}{s_c} \frac{\partial^3 W}{\partial x^2 \partial y} + p_x = 0 \quad (6.34)$$

$$C_m + \frac{1 - \nu_m}{2} \frac{\partial^2 V}{\partial x^2} + C_m \frac{\partial^2 V}{\partial y^2} + C_m \frac{1 + \nu_m}{2} \frac{\partial^2 U}{\partial x \partial y} + p_y = 0 \quad (6.35)$$

and

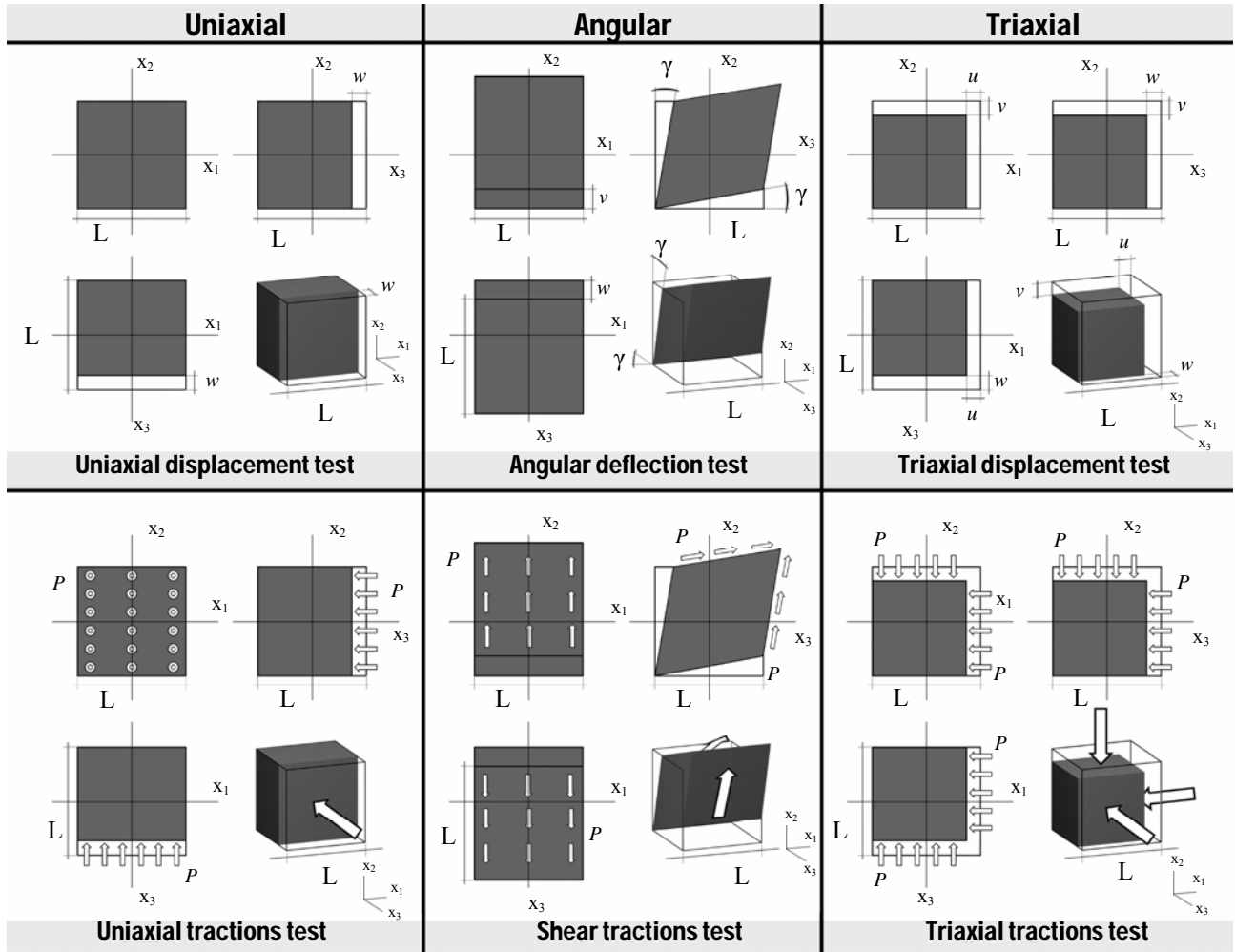
$$\left(D_m + \frac{c_5 E_c R^4}{s_c} \right) \frac{\partial^4 W}{\partial x^4} - \left(2D_m + \frac{c_4 E_c R^4}{s_c} \right) \frac{\partial^4 W}{\partial x^2 \partial y^2} - D_m \frac{\partial^4 W}{\partial y^4} - \frac{c_3 E_c R^4}{s_c} \frac{\partial^3 U}{\partial x^2 \partial y} + p_z = 0 \quad (6.36).$$

Again is evident from eqs. (6.34) and (6.36) that coupling exists between extension and twisting through the $\partial^3 U / \partial^2 x \partial y$ term in the last equation.

Appendix

A.1 FE test boundary conditions

To draw mechanical behavior of porous RVE both displacement and tractions are applied over cubic cell faces. Every analysis is performed considering RVE material as linearly elastic, thus stress-strain conditions due to every value of displacement or tractions follow same laws.



FigA.1. RVE boundary conditions tests.

A.1.1 Displacement FE test conditions

Performing displacement FE tests, displacement, applied on boundary of cubic cell, can be expressed as function of vector $\mathbf{u} = [u_1 \ u_2 \ u_3]^T$ and defined as:

in case of uniaxial tests,

$$\begin{cases} u_1\left(-\frac{L}{2}, x_2, x_3\right) = u_1\left(\frac{L}{2}, x_2, x_3\right) \\ u_2\left(x_1, -\frac{L}{2}, x_3\right) = u_2\left(x_1, \frac{L}{2}, x_3\right) \\ u_3\left(x_1, x_2, -\frac{L}{2}\right) - w = u_3\left(x_1, x_2, \frac{L}{2}\right) \end{cases} \quad (7.1),$$

where w is the uniform displacement applied on $\left(x_1, x_2, \frac{L}{2}\right)$ face in x_3 direction, see figure A.1;
in case of angular deflection,

$$\begin{cases} u_1\left(-\frac{L}{2}, x_2, x_3\right) = u_1\left(\frac{L}{2}, x_2, x_3\right) \\ u_2\left(x_1, -\frac{L}{2}, x_3\right) - w = u_2\left(x_1, \frac{L}{2}, x_3\right) \\ u_3\left(-\frac{L}{2}, x_2, x_3\right) - v = u_3\left(\frac{L}{2}, x_2, x_3\right) \end{cases} \quad (7.2),$$

where v and w are the uniform displacement applied respectively on $\left(x_1, x_2, \frac{L}{2}\right)$ face in x_2
direction, and on $\left(x_1, \frac{L}{2}, x_3\right)$ face in x_3 direction, as $\gamma = \arctan\left(\frac{v}{L}\right) = \arctan\left(\frac{w}{L}\right)$ is the
applied angular deflection, see figure A.1;
in case of triaxial tests,

$$\begin{cases} u_1\left(-\frac{L}{2}, x_2, x_3\right) - u = u_1\left(\frac{L}{2}, x_2, x_3\right) \\ u_2\left(x_1, -\frac{L}{2}, x_3\right) - v = u_2\left(x_1, \frac{L}{2}, x_3\right) \\ u_3\left(x_1, x_2, -\frac{L}{2}\right) - w = u_3\left(x_1, x_2, \frac{L}{2}\right) \end{cases} \quad (7.3),$$

where $u = v = w$ is the triaxial uniform displacement, see figure A.1.

A.1.2 Traction FE test conditions

Performing traction FE tests, tractions prescribed on boundary of cubic cell can be expressed as function of the tensile vector $\mathbf{t} = [t_1 \ t_2 \ t_3]^T$ while boundary constraints can be expressed as displacement vector $\mathbf{u} = [u_1 \ u_2 \ u_3]^T$, in a way to define displacement and tensile vectors as :
in case of uniaxial tests,

$$\begin{cases} u_1\left(x_1, x_2, -\frac{L}{2}\right) = u_1\left(x_1, x_2, \frac{L}{2}\right) \\ u_2\left(x_1, -\frac{L}{2}, x_3\right) = u_2\left(x_1, \frac{L}{2}, x_3\right) \\ u_3\left(-\frac{L}{2}, x_2, x_3\right) = u_3\left(\frac{L}{2}, x_2, x_3\right) \end{cases}, \quad t_3\left(x_1, x_2, \frac{L}{2}\right) = P \quad (7.4),$$

where P is the normal pressure applied on $\left(x_1, x_2, \frac{L}{2}\right)$ face, see figure A.1;

in case of shear tests,

$$\begin{cases} u_1\left(x_1, x_2, -\frac{L}{2}\right) = u_1\left(x_1, x_2, \frac{L}{2}\right) \\ u_2\left(x_1, -\frac{L}{2}, x_3\right) = u_2\left(x_1, \frac{L}{2}, x_3\right) \\ u_3\left(-\frac{L}{2}, x_2, x_3\right) = u_3\left(\frac{L}{2}, x_2, x_3\right) \end{cases}, \quad \begin{cases} t_2\left(x_1, x_2, \frac{L}{2}\right) = P \\ t_3\left(x_1, \frac{L}{2}, x_3\right) = P \end{cases} \quad (7.5),$$

where P is the tangential pressure applied on $\left(x_1, x_2, \frac{L}{2}\right)$ and $\left(x_1, \frac{L}{2}, x_3\right)$ faces, see figure A.1;

in case of idrostatic pressure,

$$\begin{cases} u_1\left(-\frac{L}{2}, x_2, x_3\right) = u_1\left(\frac{L}{2}, x_2, x_3\right) \\ u_2\left(x_1, -\frac{L}{2}, x_3\right) = u_2\left(x_1, \frac{L}{2}, x_3\right) \\ u_3\left(x_1, x_2, -\frac{L}{2}\right) = u_3\left(x_1, x_2, \frac{L}{2}\right) \end{cases}, \quad \begin{cases} t_1\left(\frac{L}{2}, x_2, x_3\right) = P \\ t_2\left(x_1, \frac{L}{2}, x_3\right) = P \\ t_3\left(x_1, x_2, \frac{L}{2}\right) = P \end{cases} \quad (7.6),$$

where P is the pressure applied, see figure A.1.

Note that the effective value of pressure applied on face with emerging cavities, that is every *CM* cavity types or \square 7E CV cavity types (see par. IV.2.1.d for description), is $P' = P \cdot a_p$ where a_p is ratio between effective porous cell emerging area and RVE face area, in a way to perform FE tractions prescribe tests under an uniform load.

A.2 Elastic constant calculation

A.2.1 Voigt calculation

In case of uniaxial displacement, in a coordinate system parallel to cubic edges, constants for cubic symmetry material, are defined by the meaning of:

$$\left\langle \begin{bmatrix} \sigma_1 \\ \sigma_2 \\ \sigma_3 \\ \tau_{12} \\ \tau_{23} \\ \tau_{13} \end{bmatrix} \right\rangle = \begin{bmatrix} \lambda + 2G & \lambda & \lambda & 0 & 0 & 0 \\ \lambda & \lambda + 2G & \lambda & 0 & 0 & 0 \\ \lambda & \lambda & \lambda + 2G & 0 & 0 & 0 \\ 0 & 0 & 0 & 2G' & 0 & 0 \\ 0 & 0 & 0 & 0 & 2G' & 0 \\ 0 & 0 & 0 & 0 & 0 & 2G' \end{bmatrix} \cdot \left\langle \begin{bmatrix} 0 \\ 0 \\ \varepsilon_3 \\ 0 \\ 0 \\ 0 \end{bmatrix} \right\rangle \quad (7.1),$$

where λ and G are respectively first and second Lamé constants and, defying l as RVE cubic cell edge length, $w = \langle \varepsilon_3 \rangle \cdot l$ is the applied displacement over $\left(x_1, x_2, \frac{L}{2}\right)$ cubic cell face in x_3

direction, see figure A.1;

in case of angular deflection for cubic symmetry material:

$$\left\langle \begin{bmatrix} \sigma_1 \\ \sigma_2 \\ \sigma_3 \\ \tau_{12} \\ \tau_{23} \\ \tau_{13} \end{bmatrix} \right\rangle = \begin{bmatrix} \lambda + 2G & \lambda & \lambda & 0 & 0 & 0 \\ \lambda & \lambda + 2G & \lambda & 0 & 0 & 0 \\ \lambda & \lambda & \lambda + 2G & 0 & 0 & 0 \\ 0 & 0 & 0 & 2G' & 0 & 0 \\ 0 & 0 & 0 & 0 & 2G' & 0 \\ 0 & 0 & 0 & 0 & 0 & 2G' \end{bmatrix} \cdot \left\langle \begin{bmatrix} 0 \\ 0 \\ 0 \\ 0 \\ \varepsilon_{23} \\ 0 \end{bmatrix} \right\rangle \quad (7.2),$$

where G' is the shear modulus, $\gamma = 2 \cdot \langle \varepsilon_{23} \rangle$ is applied angular deflection in the x_2, x_3 plane, see figure A.1;

in case of uniform triaxial displacement:

$$K = \frac{\langle \sigma_1 \rangle + \langle \sigma_2 \rangle + \langle \sigma_3 \rangle}{3} \cdot \frac{1}{3 \langle \varepsilon \rangle} \quad (7.3),$$

where k is the bulk modulus and $\langle \varepsilon \rangle \cdot l = \langle \varepsilon_1 \rangle \cdot l = \langle \varepsilon_2 \rangle \cdot l = \langle \varepsilon_3 \rangle \cdot l$ is uniform displacement applied normally over faces $\left(\frac{L}{2}, x_2, x_3\right)$, $\left(x_1, \frac{L}{2}, x_3\right)$ and $\left(x_1, x_2, \frac{L}{2}\right)$ of the RVE cubic cell, see figure A.1. Equations (7.1), (7.2) and (7.3) can be used in case of isotropic material behaviour taking the assumption $G' = G$.

A.2.2 Reuss calculation

Analyses performed under uniform tractions allow to calculate the average deformation tensor. Average stress tensor is directly deduced by uniform tractions applied on the RVE surface, thus, depending on tractions test kind, elastic constants of the porous RVE, as Young modulus, Poisson ratio, anisotropic shear modulus and bulk modulus, are calculated. In case of normal tractions, constants for cubic symmetry material, are defined by the meaning of:

$$\begin{aligned} \left\langle \begin{bmatrix} \varepsilon_1 \\ \varepsilon_2 \\ \varepsilon_3 \\ \varepsilon_{12} \\ \varepsilon_{23} \\ \varepsilon_{13} \end{bmatrix} \right\rangle &= \begin{bmatrix} \frac{1}{E} & -\frac{\nu}{E} & -\frac{\nu}{E} & 0 & 0 & 0 \\ -\frac{\nu}{E} & \frac{1}{E} & -\frac{\nu}{E} & 0 & 0 & 0 \\ -\frac{\nu}{E} & -\frac{\nu}{E} & \frac{1}{E} & 0 & 0 & 0 \\ 0 & 0 & 0 & \frac{1}{2G'} & 0 & 0 \\ 0 & 0 & 0 & 0 & \frac{1}{2G'} & 0 \\ 0 & 0 & 0 & 0 & 0 & \frac{1}{2G'} \end{bmatrix} \cdot \left\langle \begin{bmatrix} 0 \\ 0 \\ \sigma_3 \\ 0 \\ 0 \\ 0 \end{bmatrix} \right\rangle \end{aligned} \quad (7.4),$$

where E and ν are respectively Young modulus and Poisson ratio and $t = \langle \sigma_3 \rangle$ is the applied tractions over $\left(x_1, x_2, \frac{L}{2}\right)$ cubic cell face along x_3 direction, see figure A.1; in case of shear tractions for cubic symmetry material:

$$\left\langle \begin{bmatrix} \varepsilon_1 \\ \varepsilon_2 \\ \varepsilon_3 \\ \varepsilon_{12} \\ \varepsilon_{23} \\ \varepsilon_{13} \end{bmatrix} \right\rangle = \begin{bmatrix} \frac{1}{E} & -\frac{\nu}{E} & -\frac{\nu}{E} & 0 & 0 & 0 \\ -\frac{\nu}{E} & \frac{1}{E} & -\frac{\nu}{E} & 0 & 0 & 0 \\ -\frac{\nu}{E} & -\frac{\nu}{E} & \frac{1}{E} & 0 & 0 & 0 \\ 0 & 0 & 0 & \frac{1}{2G'} & 0 & 0 \\ 0 & 0 & 0 & 0 & \frac{1}{2G'} & 0 \\ 0 & 0 & 0 & 0 & 0 & \frac{1}{2G'} \end{bmatrix} \cdot \left\langle \begin{bmatrix} 0 \\ 0 \\ 0 \\ 0 \\ \tau_{23} \\ 0 \end{bmatrix} \right\rangle \quad (7.5),$$

where $t = \langle \tau_{23} \rangle$ is applied pure shear tractions over $\left(x_1, \frac{L}{2}, x_3\right)$ and $\left(x_1, x_2, \frac{L}{2}\right)$ cubic cell faces respectively parallel to x_3 and x_2 axes, see figure A.1; in case of hydrostatic pressure:

$$K = \frac{P}{3} \cdot \frac{1}{\langle \varepsilon_1 \rangle + \langle \varepsilon_2 \rangle + \langle \varepsilon_3 \rangle} \quad (7.6),$$

where P is hydrostatic applied pressure, see figure A.1. Equations (7.4), (7.5) and (7.6) can be used in case of isotropic material behaviour taking the assumption $G' = G$. In case of normal tractions in x_3 direction, for orthotropic RVEs constants are defined by the meaning of:

$$\begin{aligned}
\begin{pmatrix} \varepsilon_1 \\ \varepsilon_2 \\ \varepsilon_3 \\ \varepsilon_{12} \\ \varepsilon_{23} \\ \varepsilon_{13} \end{pmatrix} &= \begin{bmatrix} \frac{1}{E_1} & -\frac{\nu_{12}}{E_1} & -\frac{\nu_{13}}{E_1} & 0 & 0 & 0 \\ -\frac{\nu_{21}}{E_2} & \frac{1}{E_2} & -\frac{\nu_{23}}{E_2} & 0 & 0 & 0 \\ -\frac{\nu_{31}}{E_3} & -\frac{\nu_{32}}{E_3} & \frac{1}{E_3} & 0 & 0 & 0 \\ 0 & 0 & 0 & \frac{1}{2G_{12}} & 0 & 0 \\ 0 & 0 & 0 & 0 & \frac{1}{2G_{23}} & 0 \\ 0 & 0 & 0 & 0 & 0 & \frac{1}{2G_{13}} \end{bmatrix} \cdot \begin{pmatrix} \sigma_1 \\ \sigma_2 \\ \sigma_3 \\ \tau_{12} \\ \tau_{23} \\ \tau_{13} \end{pmatrix} \quad (7.7);
\end{aligned}$$

by the meaning of matrix symmetry:

$$\frac{\nu_{12}}{E_1} = \frac{\nu_{21}}{E_2}, \quad \frac{\nu_{13}}{E_1} = \frac{\nu_{31}}{E_3}, \quad \frac{\nu_{23}}{E_2} = \frac{\nu_{32}}{E_3} \quad (7.8),$$

where E_i and ν_{ij} are respectively Young modulus in i direction and Poisson ratio in j direction in plane of normal i , and $t = \langle \sigma_3 \rangle$ is the applied tractions over $\left(x_1, x_2, -\frac{L}{2}\right)$ cubic cell face along x_3 direction, see figure A.1.

A.2.3 Isotropic constants unification

In case of Voigt calculation, finite element analysis gives as result the RVE average stress tensor, it allows direct calculation of the Lamé constant (sec. A.2.1 (7.1)). Furthermore in case of Reuss calculation RVE average deformation tensor is obtained; starting from imposed average stress tensor Young modulus and Poisson ratio are directly calculated (sec. A.2.2 (7.4)). The two couples of elastic constant are related by the laws:

$$\begin{cases} \lambda = \frac{\nu \cdot E}{(1+\nu) \cdot (1-2\nu)} \\ G = \frac{E}{2(1+\nu)} \end{cases}, \quad \begin{cases} E = \frac{G(3\lambda + 2G)}{\lambda + G} \\ \nu = \frac{\lambda}{2\lambda + G} \end{cases} \quad (7.9),$$

both of them can equivalently characterize RVE isotropic elastic behaviour, in case of Voigt calculation as well as in case of Reuss calculation. Moreover another fundamental elastic properties characterization is given by Poisson ratio, this constant is directly related to isotropic elastic material constants by the law:

$$K = \frac{E}{3(1-2\nu)} \quad (7.10),$$

such relation make possible a comparison between elastic behavior by means of (7.4), (7.5) and bulk modulus values obtained by means of (7.6), (7.10). Finally results show a perfect matching.

References

- Alshits, V.I., Kirchner, O.K., 2001. Cylindrically anisotropic, radially inhomogeneous elastic materials. *Proc. R. Soc., A* 457, 671-693, London.
- Akasak, T., Hirano, M., 1972. Approximate Elastic Constant of Fiber Reinforced Rubber Sheet and its Composite Laminate. *Fukugo Zairyo (Composite Materials & Structures)*. **1**: 70-76.
- Barber, J.R., 1992. *Elasticity*. Dordrecht, Boston, London, Kluwer Academic Publishers.
- Barbero, E.J., 1999. *Introduction to Composite Material Design*. Taylor & Francis, New York.
- Baer, E., Hiltner, A., Morgan, R., 1992. Biological and synthetic hierarchical composites. *Physics Today*. **Oct.**: 60-67
- Boehler, J.P., 1987. *Application of Tensor Functions in Solid Mechanics*. Springer, Wien.
- Bojarski, B., Iwaniec, T., 1983. Analytical foundations of the theory of quasi conformal mappings in R^n . *Annales Academiae Scientiarum, Ser. A.I. Mathematica*, **8**, 257-324.
- Brear, K., Kingsley, M.C.S., Ramsey, M., 1983. The mechanical design of the tusk of the narwhal (Monodon monoceros: Cetecea). *J. Zoology* 230, **41**: 1-423.
- Budiansky, B., O'Connell, R.J., 1976. Elastic Moduli of a Cracked Solid. *Int. J. Solid Structure*, **12**: 81-97.
- Budiansky, B., 1965. On the elastic moduli of some heterogeneous materials. *Journal of the Mechanics and Physics of Solids* 13, 223-227
- Bunge, G., 1970. *Texture Analysis in Material Science – Mathematical Methods*. Butterworth, London.
- Cauchy, A.L., 1923. Recherches sur l'équilibre et le mouvement intérieur des corps solides ou fluides, élastiques ou non élastiques. *Bulletin de la Société Philomatique*, 9-13 (Oeuvres (2) 2, pp. 300-304, Gauthier-Villars, Paris, 1889).
- Cauchy, A.L., 1927a. De la pression ou tension dans un corps solide, *Exercices de Mathématiques* 2, 42-56 (Oeuvres (2) 7, pp. 60-93, Gauthier-Villars, Paris, 1889).
- Cauchy, A.L., 1927b. Sur les relations qui existent dans l'état d'équilibre d'un corps solide ou fluide (Oeuvres (2) 7, pp. 141-145, Gauthier-Villars, Paris, 1889).
- Cauchy, A.L., 1928. Sur les equations qui experiment les conditions d'équilibre ou les lois du mouvement intérieur d'un corps solide, élastique (Oeuvres (2) 8, pp. 195-226, Gauthier-Villars, Paris, 1890).
- Chadwick, P., Vianello, M., Cowin, S.C., 2001. A new proof that the number of linear elastic symmetries is eight. *Journal of the Mechanics and Physics of Solids* **49**: 2471-2492.
- Cherkhev, A., www.math.utah.edu/~cherk/spiral-trees/story.html.
- Choquet-Bruhat, Y., Dewitt-Morette, C., Dillard-Bleick, M., 1977. *Analysis Manifolds and Physics*. North-Holland, Amsterdam.
- Christensen, R.M., 1979. *Mechanics of Composite Materials*. Wiley-Interscience, New York.
- Christensen, R.M., Lo, K.H., 1979. Solutions for effective shear properties in three phase sphere and cylinder models. *Journal of the Mechanics and Physics of Solids* 27, 315-330.
- Chung, M.Y., Ting, T.C.T., 1995. Line forces and dislocations in angularly inhomogeneous anisotropic piezoelectric wedges and spaces. *Philos. Mag. A* 71, 1335-1343.
- Cohen, I., Bergman, D.J., 2003a. Clausius-Mossotti-type approximation for elastic moduli of a cubic array of spheres. *Physical Review B* 68, 24104.
- Cohen, I., Bergman, D.J., 2003b. Effective elastic properties of periodic composite medium. *Journal of the Mechanics and Physics of Solids* 51, 1433-1457.
- Cohen, I., 2004. Simple algebraic approximations for the effective elastic moduli of cubic array of spheres. *Journal of the Mechanics and Physics of Solids* 52, 2167-2183.
- Costello, G.A., 1990. *Theory of Wire Rope*. Springer-Verlag, New York.
- Cowin, S.C., 1985. The Relationship between the Elasticity Tensor and the Fabric Tensor, *Mechanics of Materials* **4**: 137-147.
- Cowin, S.C., 1986. Wolff's law of trabecular architecture at remodelling equilibrium. *Journal of Biomechanical Engineering*, **108**: 83-88.
- Cowin, S.C., 1987. Torsion of cylinders with shape intrinsic orthotropy. *J. Appl. Mech.*, **109**, 778-782.
- Cowin, S.C., 1994. Optimization of the strain energy density in linear anisotropic elasticity. *Journal of Elasticity* **34**: 45-68.
- Cowin, S.C., 1995. On the minimization and maximization of the strain energy density in cortical bone tissue. *Journal of Biomechanics* **28**: 445-447.
- Cowin, S.C., 1997. Remarks on coaxiality of strain and stress in anisotropic elasticity. *Journal of Elasticity* **47**: 83-84.
- Cowin, S.C., Mehrabadi, M.M., 1987. On the identification of material symmetry for anisotropic elastic materials. *Quarterly Journal of Mechanics and Applied Mathematics* **40**: 451-476.
- Cowin, S.C., Mehrabadi, M.M., 1992. The structure of the linear anisotropic elastic symmetries. *Journal of the Mechanics and Physics of the Solids* **40**: 1459-1471.

- Cowin, S.C., Mehrabadi, M.M., 1995. Anisotropic symmetries in linear elasticity. *Applied Mechanics Review* **48**: 247-285.
- Cowin, S.C., Yang, G., 2000. Material symmetry optimization by Kelvin modes. *J. Eng. Math* **37**: 27-43.
- Cowin, S.C., 2002. Elastic symmetry restrictions from structural gradients. In: P. Podio-Guidugli and M. Brocato (eds), *Rational Continua, Classical and New - A Collection of Papers Dedicated to Gianfranco Capriz on the Occasion of his 75th Birthday*. Springer, Berlin
- Cox, S., Lipton, R., 1996. Extremal eigenvalue problems for two-phase conductors. *Arch. Rational Mech. Anal.* **136**: 101-118.
- Curran, D.R., Seaman, L., Shockey, D.A., 1987. Dynamic Failure of Solids. *Physics Reports*, Nos. 5&6, **147**: 253-388.
- D'Arcy Thompson, W., 1942. *On Growth and Form*, Cambridge Univ. Press, Cambridge.
- Eshelby, J.D., 1957. The determination of the elastic field of an ellipsoidal inclusion, and related problems. *Proc. R. Soc. Lond.*, **A241**: 376.
- Euler, L., 1757. Continuation des recherches sur la théorie du mouvement des fluids, *Hist. Acad. Berlin*, 316-361.
- Euler, L., 1771. Sectio tertia de motu fluidorum lineari potissimum aquae. *Novi Comm. Petrop.* 15: 219-360.
- Federer, H., 1969. *Geometric measure theory*, Springer-Verlag, New York.
- Flugge, W., 1972. *Tensor Analysis and Continuum Mechanics*, Springer-Verlag Berlin Heidelberg New York.
- Forte, S., Vianello, M., 1996. Symmetry classes for elasticity tensor. *Journal of Elasticity* **43**: 81-108.
- Fraldi, M., Cowin, S.C., 2004. Inhomogeneous elastostatic problem solutions constructed from stress-associated homogeneous solutions. *Journal of the Mechanics and Physics of Solids*, **52**, 2207-2233.
- Fraldi, M., Guarracino, F., 2001. On a general property of a class of homogenized porous media. *Mech. Res. Comm.*, **28**, 2, 213-221.
- Francfort, G.A., Murat, F., 1986. Homogenization and optimal bounds in linear elasticity. *Archive for Rational Mechanics and Analysis* **94**, 307-337
- Gauthier, M. M., 1995. *Engineered Materials Handbook*. Desk Ed., ASM International, Metals Park, OH
- Germain, P., 1972. *Mécanique des milieux Continus*. Tome I, Masson, Paris.
- Giangreco, E., 2003. *Ingegneria delle strutture*. UTET, 2 vol.
- Gonzáles, C., Segurado, J., Llorca, J., 2004. Numerical simulation of elasto-plastic deformation of composites: evolutions of the stress microfields and implications for homogenization models. *J. Mechanics and Physics of Solids* **52**, 1573-1593.
- Goodman, J., Khon, R.V., Reyna, L.: Numerical study of a relaxed variational problem from optimal design. *Comput. Methods Appl. Mech. Eng.* **57**:107-127.
- Gough, V.E., 1968. *Stiffness of Cord Wire Rope*. Springer-Verlag, New York.
- Gould, S.J., 1976. D'Arcy Thompson and the science of form. *Topics in the Philosophy of biology*. D. Reidel, Dordrecht, pp. 66-97.
- Gurtin, M. E., 1972. *The Linear Theory of Elasticity*, Handbuch der Physik, Springer, Berlin.
- Gurtin, M.E., 1981. *An introduction to continuum Mechanics*. Academic Press, New York.
- Harrigan, T.P., Mann R.W., 1984. Characterization of microstructural anisotropy in orthotropic materials using a second rank tensor. *Journal of Material Science*, **19**: 761-767.
- Hashin, Z., Shtrikman, S., 1963. A variational approach to the theory of the elastic behaviour of multiphase materials. *J. Mech. Phys. Solids* **11**: 127-140.
- Hashin, Z., Rose, B.W., 1964. The elastic moduli of fiber-reinforced materials. *J. Appl. Mech. Phys.* **31**: 223. .
- Hashin, Z., 1965. On elastic behaviour of fiber reinforced materials of arbitrary transverse phase geometry. *Journal of the Mechanics and Physics of Solids* **13**, 119-134.
- Hashin, Z., 1966. A variational approach to the theory of the elastic behaviour of multiphase materials. *J. Mech. Phys. Solids* **11**: 127-140.
- Hashin, Z., 1966. Viscoelastic fiber reinforced materials. *AIAA J.* **4**: 1411
- He, Q.-C., Curnier, A., 1995. A more fundamental approach to damaged elastic stress-strain relations. *International J. of Solids and Structures*, **32**: 1433-1457.
- Hearmon, R.F.S., 1961. *An introduction to applied anisotropic elasticity*. Oxford University Press, Oxford.
- Hill, R., 1964. Theory of mechanical properties of fiber-strengthened materials: I. Elastic behavior. *J. Mech. Phys. Solids*, **12**, 199.
- Hill, R., 1965a. A self-consistent mechanics of composite materials. *J. Mech. Phys. Solids*, **12**, 213-22.
- Hill, R., 1967. The essential structure of constitutive laws for metal composites and polycrystals. *J. Mech. Phys. Solids*, **15**, 79-95.
- Horii, H., Nemat-Nasser, S., 1983. Overall moduli of solids with microcracks: Load-induced anisotropy. *J. Mech. Phys. Solids*, Vol. **31**, 155-177.
- Huo, Y.Z., Del Piero, G., 1991. On the completeness of crystallographic symmetries in the description of symmetries of the elastic tensor. *Journal of Elasticity* **25**: 203-246.
- Ilankamban, R., Krajcinovic, D., 1987. A Constitutive theory for Progressively Deteriorating Brittle Solids. *Int. J. Solids Structures*, **23**, 1521-1534.
- Jones, R.M., 1975. *Mechanics of Composite Materials*. McGraw-Hill, New York.

- Jones, M.N., 1985. Spherical Harmonics and Tensors for Classical Field Theory. Wiley, New York.
- Kanatani, K., 1984. Distribution of directional data and fabric tensors. *Int. J. Engng Sci.* **22**, 149-164.
- Kartvelishvili, V.M., Kobelev, V.V., 1984. Rational schemes for reinforcing laminar plates from composite materials. *Prikladnaja Matematika I Mekhanika* **48**: 68-80. Traslated in: *Journal of Applied Mathematics and Mechanics* **48**: 40-49.
- Kingsley, M.C.S., Ramsay, M.A., 1988. The spiral tusk of the narwhal. *Arctic* **41**: 236-238.
- Kittredge, C.A., 1991. Static Response of Cord Composite Plates. *Ph.D. Thesis*, University of Illinois at Urbana-Champaign.
- Kouznetsova, V., Brekelmans, W.A.M., Baaijens, F.P.T., 2001. An approach to micro-macro modeling of heterogeneous materials. *Computational Mechanics* **27**, 37-48.
- Krajcinovic, D., 1996. Damage Mechanics. North-Holland.
- Lakse, R.S., 2001. Elastic and viscoelastic behavior of chiral materials. *Internet. J. Mech. Sci.* **43**: 1579-1589.
- Lelong-Ferrand, J., 1963. Géométrie Différentielle. Masson, Paris.
- Lekhnitskii, S.G., 1963. Theory of elasticity of an anisotropic elastic body, Holden Day Inc., San Francisco.
- Lekhnitskii, S.G., 1981. Theory of elasticity of an anisotropic elastic body, Mir Publisher, Moscow.
- Lemaitre, J., 1986. Local Approach of Fracture, *Eng. Fracture Mech.*, **25**: 523-537.
- Lemaitre, J., 1992. A Course on Damage Mechanics, Springer- Verlag, Berlin, Germany.
- Lemaitre, J., Chaboche, J.L., 1978. Aspect Phenomenologique de la Rupture par Endommagement, *J. Mech. Applique*, **2**: 317-365.
- Lemaitre, J., Dufailly, J., 1987. Damage measurement. *Engng Fracture Mech.*, **28**, 643-661.
- Lions, J.L., 1985. Les Methodes de l'Homogeneisation: Theorie et Applications en Physique, Saint Germain Paris, Eyrolles Ed.
- Love, A.E.H., 1994. A treatise on the mathematical theory of elasticity, fourth ed. Dover, New York.
- Lowery, D.P., Erickson, E.C.O., 1967. The effect of spiral grain on pole twist and bending strength. U.S. Department of Agriculture, U.S. Forest Service Research Paper INT-35
- Lubarda, V., Krajcinovic, D., 1993. Damage Tensors and the Crack Density Distribution, *Int. J. Damage Mech.*, **48**: 2859-2877.
- Malliavin, P., 1972. Géométrie Différentielle Intrinsèque. Hermann, Paris
- Mandel, J., 1971. Plasticité classique et viscoplasticité. Springer-Verlag, Vienna (CISM Lecture Notes, Udine, Italy).
- Marcus, M., Mizel, V.J. 1973. Transformations by functions in Sobolev spaces and lower semicontinuity for parametric variational problems, *Bull. Amer. Math. Soc.* **79**, 790-795.
- Mehrabadi, M.M., Cowin, S.C., 1990. Eigentensors of linear anisotropic elastic materials. *Quarterly Journal of Mechanics and Applied Mathematics* **43**: 15-41.
- Marsden, J.E., Hughes, T.J.R., 1983. Mathematical foundations of elasticity. Prentice-Hall, Englewood Cliffs.
- Maugin, G.A., 1993. Material inhomogeneities in elasticity. Chapman & Hall.
- McLaughlin, R., 1977. A study of the differential scheme for composite materials. *International Journal of Engineering Science* **15**, 237-244.
- McManus, C., 2002. Left Hand, Right Hand - The Origins Asymmetry in Brains, Bodies, Atoms and Cultures. Harvard, Cambridge, MA.
- Milton, G.W., 1988. Variational bounds on the effective moduli of anisotropic composites. *Journal of the Mechanics and Physics of Solids* **36**, 597-629.
- Milton, G.W., Cherkaev, A. V., 1995. Which elasticity tensor are realizable? *J. Eng. Mat. Tech.* **117**: 483-493.
- Mori, T., Tanaka, K., 1973. Average stress in the matrix and average elastic energy of materials with misfitting inclusions. *Acta Metallogr.* **21**, 571-574. *Acta Metallurgica Materialia*.
- Nadeau, J.C., Ferrari, M., 1998. Invariant tensor-to-matrix mappings for evaluation of tensorial expressions. *Journal of Elasticity*, **52**: 43-61.
- Nemat-Nasser, S., Taya, M., 1981. On effective moduli of an elastic body containing periodically distributed voids. *Quarterly of Applied Mathematics* **39**, 43-59.
- Nemat-Nasser, S., Iwakuma, T., Hejazi, M., 1982. On composite with periodic structure. *Mechanics of Materials* **1**, 239-267.
- Nemat-Nasser, S., Horii, H., 1993. Micromechanics: Overall properties of heterogeneous materials. North-Holland.
- Neville, A.C., 1985. Molecular and mechanical aspects of helicoid development in plant cell walls. *BioEssays* **3**: 4-8.
- Neville, A.C., 1993. *Biology of fibrous Composites*. Cambridge Univ. Press, Cambridge.
- Ni, Y., Chiang, M.Y.M., 2007. Prediction of the elastic properties of the heterogeneous materials with complex microstructures. *Journal of the Mechanics and Physics of Solids* **55**, 517-532.
- Noll, W., 1959. The foundation of classical mechanics in the light of recent advances in continuum mechanics, in *The axiomatic method, with Special Reference to Geometry and Physics*, pp. 266-281, North Holland, Amsterdam.
- Noskowlak, A.F., 1963. Spiral grain in trees: A review. *Forest Products J.* **13**: 266-275.
- Nunan, K.C., Keller, J.B., 1984. Effective elasticity tensor of a periodic composite. *Journal of the Mechanics and Physics of Solids* **32**, 259-280.

- Nye, J.F., 1957. Physical properties of crystals. Their Representation by tensors and matrices. Oxford University Press, Oxford.
- Odgaard, A., Kabel, J., van Rietbergen, B., Dalstra, M., Huiskes, R., 1997. Fabric and elastic principal directions of cancellous bone are closely related. *J. Biomechanics* **30**, 5: 487-495.
- Onat, E.T., 1984. Effective properties of elastic materials that contain penny shaped voids. *Int. J. Engng Sci.* **22**, 1013-1021.
- Onat, E.T., Leckie, F.A., 1984. Representation of mechanical behaviour in the Presence of Changing Internal Structure. *J. Appl. Mech.*, **55**: 1-10.
- Prakash, A., Conway, T., Costello, G.A., 1992. Compression of a Cord. *ASME J. of App. Mech.* **59**:S213-S216.
- Rado, T., Reichelderfer, P.V., 1955. Continuous transformations in analysis. Springer- Verlag, Berlin.
- Reuss, A. (1929). "Berechnung der Fließgrenze von Mischkristallen auf Grund der Plastizitätsbedingung für Einkristalle". *ZAMM* **9**: 49-58.
- Rho, J.Y., Hobatho, M.C., Ashman, R.B., 1995. Relation of mechanical properties to density and CT number in human bone. *Med. Eng. Phys.*, **17**: 347-355.
- Russel, W.B., 1973. On the effective moduli of composite materials: effect of fiber length and geometry at dilute concentrations. *Z. Angew. Math. Phys.* **24**: 581.
- Sangani, A.S., Lu, W., 1987. Elastic coefficients of a composite containing spherical inclusions in a periodic array. *Journal of the Mechanics and Physics of Solids* **35**, 1-21.
- Schwartz, L., 1967. Cours d'Analyse. Hermann, Paris.
- Sevostianov, I., Kachanov, M., 1999. Compliance tensors of ellipsoidal inclusions. *International Journal of Fracture* **96**: L3-L7.
- Sgarra, C., Vianello, M., 1997a. Directions of coaxiality between pure strain and stress in linear elasticity. *Journal of Elasticity* **46**: 263-265.
- Sgarra, C., Vianello, M., 1997b. Rotations which make strain and stress coaxial. *Journal of Elasticity* **47**: 217-224.
- Shield, C.K., Costello, G.A., 1992. The Effect of Wire Rope Mechanics on the Mechanical Response of Cord Composite Laminates – An Energy Approach. *ASME J. of App. Mech.* **60**.
- Shield, C.K., Costello, G.A., 1994. The Effect of Wire Rope Mechanics on the Material Properties of Cord Composites: An Elasticity Approach. *ASME J. of App. Mech.* **60**.
- Sirotin, Y., Chaskolkaia, M., 1984. Fondements de la physique des cristaux. Éditions Mir, Moscow.
- Smith, K.T., 1983. Primer of Modern Analysis, Second Edition, Springer-Verlag, New York.
- Smith, G.F., Rivlin, R.S., 1958. The strain energy function for anisotropic elastic materials. *Transaction of American Mathematical Society* **88**, 175-193.
- Suquet, P., 1981a. Sur les equations de la plasticité: existence et régularité des solutions. *J. Mécanique*, **20**, 3-40.
- Sutcliffe, S., 1992. Spectral decomposition of the elasticity tensor. *Journal of Applied Mechanics*, Transactions of the ASME **59**: 762-773.
- Tangorra, G., 1969. Fiber-Reinforced Oriented Rubber Sheets. *Proceedings of Int. Rubber Conference*, Moscow 459-466.
- Theocaris, P.S., Sokolis, D.P., 2000a. Invariant elastic constants and eigentensors of orthorhombic, tetragonal, hexagonal and cubic crystalline media. *Acta Crystallographica Sect. A* **56**: 319-331.
- Theocaris, P.S., Sokolis, D.P., 2000b. Spectral decomposition of the compliance fourth-rank tensor for orthotropic materials. *Archives of Applied Mechanics* **70**: 289-306.
- Ting, T.C.T., 1996. Anisotropic elasticity- Theory and applications. Oxford.
- Torquato, S., 1997. Effective stiffness tensor of composite media: I. Exact series expansions. *Journal of the Mechanics and Physics of Solids* **45**, 1421-1448.
- Torquato, S., 1998. Effective stiffness tensor of composite media: II. Applications to isotropic dispersions. *Journal of the Mechanics and Physics of Solids* **46**, 1411-1440.
- Torquato, S., Gibiansky, L.V., Silva, M.J., Gibson, L.J., 1998. Effective mechanical and transport properties of cellular solids. *Int. J. Mech. Sci.* **40**: 71-82.
- Thompson, W. (Lord Kelvin), 1904. *Baltimore Lectures on Molecular Dynamics and the Wave Theory of Light*. London.
- Tözeren, A., Skalak, R., 1989. Does fabric tensor exist for a fabric?, *Journal of Material Science*, **24**, 1700-1706.
- Truesdell, C., Noll, W., 1965. The non-linear field theories of mechanics. *Handbuch der Physik*, vol. III/3, Springer, Berlin.
- Truesdell, C., Toupin, R.A., 1960. The Classical Field Theory. *Handbuch der Physik*, vol. III/1, Springer, Berlin.
- Turner, C.H., Cowin, S.C., 1987. Dependence of elastic constants of an anisotropic porous material upon porosity and fabric. *Journal of Material Science*, **22**, 3178-3184.
- Vianello, M., 1996a. Coaxiality of strain and stress in anisotropic linear elasticity. *Journal of Elasticity* **42**: 283-289.
- Vianello, M., 1996b. Optimization of the stored energy and coaxiality of strain and stress in finite elasticity. *Journal of Elasticity* **44**: 193-202.
- Vilenkin, N.J., 1969. Fonctions Spéciales et Théorie de la Représentation des Groupes. Dunod, Paris.

- Vodopyanov, S.K., Goldshtein, V.M., Reshetnyak, Yu. G., 1979. On geometric properties of function with generalized first derivatives. *Russian Math. Surveys* **34**, 19-74.
- Voigt W., 1928. Lehrbuch der Kristallphysik. Leipzig: B.G. Teubner Verlag.
- Wagner, L.D., Gibson, L.J., 2000. The mechanical behaviour of interpenetrating phase composites - I: modelling. *International Journal of Mechanical Science* 42, 925-942.
- Walpole, L.J., 1984. Fourth-rank tensors of the thirty-two crystal classes: multiplication tables. *Proceedings of the Royal Society of London A* 391: 149-179.
- Wang, Y.,U., Jin, Y.M.M., Khachaturyan, A.G., 2002. Phase field microelasticity theory and modeling of elastically and structurally inhomogeneous solid. *Journal of Applied Physics* 92, 1351-1360.
- Willis, J., R., 1977. Bounds and self-consistent estimate for the overall moduli of anisotropic composites. *Journal of the Mechanics and Physics of Solids* 25, 185-202.
- Wong, T.-f., 1985. Geometric Probability Approach to the Characterization and Analysis of Microcracking in Rocks, *Mech. of Materials*, **4**: 261-276.
- Zheng, Q.S., Du, D.X., 2001. An explicit and universally applicable estimate for the effective properties of multiphase composites which accounts for inclusion distribution. *Journal of the Mechanics and Physics of Solids* 49, 2765-2788.
- Zysset, P.K., Curnier, A., 1995. An alternative model for anisotropic elasticity based on fabric tensors, *Mech. of Materials*, **21**: 243-250.